Université catholique de Louvain (UCL)
Institute of Condensed Matter and Nanosciences (IMCN)

# Challenges in Cocrystallization of Chiral Compounds:

## Cocrystals of Amino Acids and Profens

*Thèse présentée en vue de l'obtention du grade de docteur en Sciences par*

Natalia Tumanova

Promoteur: Prof. Tom Leyssens

Louvain-la-Neuve

September 2017

# JURY MEMBERS

**Professor Y. Filinchuk**
Université catholique de Louvain

**Professor G. Hautier**
Université catholique de Louvain

**Dr. F. Emmerling**
BAM Federal Institute for Materials Research and Testing
Berlin (Germany)

**Professor J. Wouters**
Université de Namur

**Professor J. Devaux (President)**
Université catholique de Louvain

**Professor T. Leyssens (Supervisor)**
Université catholique de Louvain

# ACKNOWLEDGMENTS

In 2012, my husband and I moved to Belgium to start a new chapter in our life, him as a postdoc in the Y. Filinchuk's group, me, well… looking for a job… Out of pure coincidence, the research done in the Tom Leyssen's group (whose lab was just next door to the Yaroslav's) perfectly matched my background and he invited me to start a PhD project in his group.

I am deeply grateful to you, Tom: you helped me to develop my scientific personality, independent and critical thinking, and research skills. Without your advices, guidance, patience, encouragement, this work would not have been possible. I am thanking you for having confidence in me and in my research ideas during all these years and for giving me freedom to pursue the scientific project I like, a luxury not all PhD students have. I also want to thank you for all the scientific conferences you gave me the opportunity to visit, owing to which I met many interesting people and learned many new things from the leading scientists. Doing my PhD in your group has been a great experience for me that I will always appreciate and remember.

Finding funding for my PhD project was not an easy task, I would like to thank all the professors who sacrificed their valuable time to do FRIA trainings with me: Prof. Sophie Hermans, Prof. Istvan Marko, Prof. Olivier Riant, Prof. Raphaël Robiette, Prof. Daniel Peeters.

My special thanks go to Prof. J. Wouters for allowing me to use their diffractometers for powder and single-crystal characterization and for his interesting ideas about amino acids at the initial step of my project.

It is my great pleasure to thank Prof. Allan Myerson from the MIT (Boston, USA) for kindly inviting me for a two-month research stay. I thank him and all the members of his group for a warm welcome. My special thanks to Cameron Weber, Kyungju Park, and Tsai-ta Christopher Lai for their help and valuable advices on the MagLev project.

I take this opportunity to thank Dr. Franziska Emmerling for her kind invitation to spend a one-month research stay in her group at BAM (Berlin, Germany) and for allocating some of her beam time for my experiments. I would like to thank her group for a warm welcome during my research stay and especially Franziska Fischer and Lisa Batzdorf for their help with sample measurements and data treatment.

I am deeply indebted to Prof. Yaroslav Filinchuk for sharing with me his beam time at synchrotron sources; without those data, this research would not have been possible. I am thanking Fabrice Morelle and Voraksmy Ban for measuring some of my samples when I could not go to synchrotron myself.

I sincerely thank Dr. Koen Robeyns for the meticulous reading and corrections of my articles and for doing his best without any complain when working with my small and bad-quality crystals.

I'm grateful to Dr. J. Hautier for sharing his knowledge about DFT with me and helping me to apply it to my systems. I also would like to thank Dr. David Waroquiers and Dr. Guodong Yu from Dr. J. Hautier's group for kindly permitting me to use their compilation of VASP for DFT calculations. I highly appreciate advices from Dr. Radovan Cerny concerning the structure solution from PXRD and from Dr. Jacco van de Streek concerning DFT calculations for molecular crystals.

I thank Lisa Baulard for her help in preparing solutions for single crystal growth and Pascal Van Velthem for his help with the treatment of thermal analysis data.

I would like to thank François Billard for introducing me to the IMCN volleyball team. Thank you, my volley buddies, for our Wednesday competitions which made working hours more fun.

I express my sincere gratitude to all my friends and colleagues; it was a great pleasure to work in such a warm and friendly atmosphere. I sincerely thank Fanny and Géraldine for the pleasant time spent together at the lab and at the conferences and Bram, Ricky, Jean-Baptiste, Vanessa, Xavier, Gabriel, Yurii, Chloé, Fabrice, Voraksmy, … for being such nice and supportive co-workers all the time.

I am thanking our secretaries, Jacqueline Boniver, Chantal Delaet, and Aurore Becquevort for their help with administrative issues.

This acknowledgment would be incomplete without mentioning my girlfriends from the Limal-Ottignies volleyball club. Being a part of our team meant a lot to me. Our trainings together and competitions helped me to keep my spirits up during all these years in Belgium. Merci Sophie, Chiara, Géraldine, Anaëlle, Clairette, Antoinette, Justine, Jennifer, Valérie, Mireille, Diana, Marie, Marine, Julie, Nelle, Marina pour tous les bons moments passés ensemble.

Огромное спасибо всем моим друзьям, кто поддерживал меня и из России, и в Бельгии. Спасибо мои любимые и драгоценные подружки, Таня, Даша, Алена, Лера, Катя, Алина за вашу поддержку и отзывчивость. Мое особенное спасибо Лене за наши женские посиделки и шоппинги, которые были так необходимы в трудные моменты. Паша и Леся, спасибо за вашу дружбу и поддержку.

I am deeply thankful to my husband Nikolay Tumanov. Kolya, I cannot thank you enough for always been there for me, for your constant support no matter what, for your patience, for believing in me, for helping me to overcome difficult times during these years and always, for loving me for who I am, my negative and positive sides. And, since you also happened to be an expert in X-ray crystallography, I would like to thank you as my colleague and advisor, who patiently taught me a great deal about crystallography, who measured samples for me at synchrotron sacrificing your sleeping hours during nights, who helped me a lot with technical issues and the preparation of figures for this work. This work, literally, would not have been possible without you.

Я бы хотела выразить глубокую благодарность моей семье и, особенно, родителям за веру в меня и поддержку. Мама и папа, я вас очень люблю.

I want to thank my son Maxime, even though he does not understand it yet, for putting a new meaning into my life, for the happiness he is bringing every day and, of course, for his profound sleeps that liberated me from my mummy duties and allowed finishing this work.

Finally, I would like to thank again Dr. Franziska Emmerling, Prof. Geoffroy Hautier, Prof. Yaroslav Filinchuk, Prof. Johan Wouters, and Prof. Jacques Devaux for accepting to be my jury members and for the time they have taken to read my thesis.

# LIST OF PUBLICATIONS

1. Tumanova N., Tumanov N., Robeyns K., Wouters J., and Leyssens T., Structural insight into cocrystallization with zwitterionic co-formers: cocrystals of S-naproxen. *CrystEngComm* (**2014**), 16**,** pp. 8185-8196. DOI: 10.1039/C4CE00353E

2. Leyssens T., Tumanova N., Robeyns K., Candoni, N., and Veesler, S., Solution cocrystallization, an effective tool to explore the variety of cocrystal systems: caffeine/dicarboxylic acid cocrystals. *CrystEngComm* (**2014**), 16, pp. 9603-9611. DOI: 10.1039/C4CE01495B

3. Matheys C., Tumanova N., Leyssens T., and Myerson A., Magnetic Levitation as a Tool for Separation: Separating Cocrystals from Crystalline Phases of Individual Compounds. *Cryst. Growth Des.* **(2016)**, 16, pp. 5549−5553, DOI: 10.1021/acs.cgd.6b01018

4. Tumanova N., Payen R., Springuel G., Norberg B., Robeyns K., le Duff S., Wouters J., and Leyssens T., Cocrystallization out of the blue: DL-mandelic acid/ethyl-DL-mandelate cocrystal. *J. Mol. Struct.* **(2017)**, 1127, pp. 397-402. DOI: 10.1016/j.molstruc.2016.07.109

# SUMMARY

Cocrystals are of interest to pharmaceutical industry as they allow varying pharmacological properties of drugs, *e.g.*, improving bioavailability, dissolution rate, hygroscopicity, stability, etc., without changing the chemical nature of the active pharmaceutical ingredient (API). Moreover, owing to some specific properties, cocrystals can also be used in other crystallization applications, for instance, as a purification tool or for chiral resolution. Since a substantial part of drugs is chiral, the question how they respond to cocrystallization with chiral or nonchiral co-formers is a hot topic for pharmaceutical industry.

In this work we focus on amino acids as potential co-formers for chiral drugs, , studying the fundamental aspects of cocrystallization, *i.e.* how the zwitterionic nature of amino acids affects the structural aspects of cocrystallization, the role of chirality and its influence on the cocrystallization outcome, as well as some related challenging aspects of cocrystal synthesis and characterization.

Working on naproxen/proline cocrystals, we established that amino acids are the most efficient co-formers when cocrystallized with compounds that contain a carboxylic group. Among obtained cocrystals, both diastereomeric pairs of cocrystals (naproxen/alanine and naproxen/tryptophan) and enantiospecific cases (naproxen/tyrosine) were encountered. From the structural point of view, amino acids in cocrystals tended to form head-to-tail chains via strong charge-assisted hydrogen bonds typical of pure amino acid crystals. The presence of strong charge-assisted hydrogen bonds had a significant effect on the cocrystal structures providing them with higher melting points as compared to the pure drugs. This property of amino acids may be used to increase the stability of drugs with low melting points.

In the second part of this work, we studied profoundly flurbiprofen/proline system through cocrystallizing various combinations of enantiopure as well as racemic forms of the initial compounds. Flurbiprofen is a non-steroidal anti-inflammatory drug used to treat acute or chronic painful condition. Proline is an amino acid widely used as a coformer for various applications, e.g. for modifying the properties of APIs, chiral resolution, creation of amino acid derived semiconductor, etc. We discovered an extreme complexity for the flurbiprofen/proline system: depending on the enantiopure or racemic forms used and cocrystallization conditions, the system exhibited polymorphism (up to 4 polymorphs for only one combination), was prone to forming cocrystal solvates and stoichiometrically diverse cocrystals (1 : 1, 2 : 1, 1 : 2, and even 1 : 3 flurbiprofen : proline). Cocrystallization in this system often yielded a mixture of various phases, whose identification required the combination of different cutting-edge techniques, including *in-situ* ball-milling, X-ray diffraction upon varying temperature, structure solution from powder and single-crystal X-ray diffraction data. We established the conditions under which various cocrystal forms emerged. Exploring the structural peculiarities of the obtained phases helped us to clarify important aspects of cocrystallization that involves chiral co-formers as well as the issues related to the zwitterionic nature of amino acids.

The results of this work can be of interest to pharmaceutical industry as they deal with real drugs and important aspects of cocrystallization and chirality essential for the development of various pharmaceutical applications of cocrystals.

# ABBREVIATIONS

| | |
|---|---|
| API | Active Pharmaceutical Ingredient |
| CSD | Cambridge Structural Database |
| DFT | Density Functional Theory |
| DSC | Differential Scanning Calorimetry |
| FDA | Food and Drug Administration |
| GI | Gastrointestinal Tract |
| GRAS | Generally Recognized as Safe |
| NSAID | Non-Steroidal Anti-inflammatory Drug |
| PXRD | Powder X-ray Diffraction |
| SS-NMR | Solid-State Nuclear Magnetic Resonance |
| TGA | Thermogravimetric Analysis |
| vdW | van der Waals interactions |

# PREFACE: Outlining the Goals

Cocrystals are of great interest to pharmaceutical industry as they can provide an efficient way to modify the pharmacological properties of drugs, such as bioavailability, dissolution rate, hygroscopicity, etc. without changing the drug's chemical nature.[1–3] Chirality introduces a selectivity aspect into cocrystallization: chiral active pharmaceutical ingredients may respond differently when cocrystallized with chiral co-formers. The latter can be used to develop chiral resolution techniques based on cocrystallization which may become an alternative to expensive chiral chromatography or other resolution approaches.[4–6] Thus, designing cocrystals involving chiral drugs or developing other chiral cocrystallization-based applications requires knowledge and understanding of how chiral co-formers respond to cocrystallization and how the outcome can be controlled.

As was mentioned above APIs used in the form of cocrystals may exhibit improved pharmacological performance. The use of amino acids as co-formers for various cocrystallization purposes may have the following advantages:

1) amino acids are natural to the body and, besides the possibility of improving the pharmacological properties, they can be safely left in the final pharmaceutical form if cocrystallization is used as a separation or purification tool,
2) amino acids have both carboxylic and amino groups prone to hydrogen bonding,
3) amino acids are chiral (except glycine) and thus allow us to study chirality aspects in cocrystal formation.

These were the reasons why our primary focus was set on applying amino acids as co-formers.

The work described in this thesis represents a fundamental research in the field of chiral cocrystallization with zwitterionic co-formers. The thesis is based on two articles: one that focuses on the cocrystals of naproxen and amino acids, and another that is dedicated to the flurbiprofen/proline system. The aforementioned articles are integrated into the thesis as Chapters 2 and 3, respectively.

The **first set of questions** raised in this thesis concerns amino acids being applied as zwitterionic co-formers:

- What sort of APIs do amino acids tend to cocrystallize with?
- How do amino acids behave when cocrystallized with APIs, taking into account the zwitterionic nature of the former?
- What properties of APIs can be changed through cocrystallization with amino acids?
- Under which conditions can various cocrystals be obtained, including polymorphs, stoichiometrically diverse forms or solvates/hydrates and can the outcome be controlled?
- What are the challenges when producing cocrystals with amino acids?

The **second important question** intends to clarify how chirality affects the outcome of cocrystallization reactions.

Finally, the **third question** addresses characterization methods with respect to our cocrystals: which methods are the most powerful and how they can be combined when dealing with

complicated cases. The main focus is set on the X-ray diffraction techniques and, especially, on the structure determination from powder X-ray diffraction data as it is considered more challenging than single-crystal methods.

By going through the results obtained, I will provide answers to these questions and briefly outline them in the Conclusions chapter.

The thesis will open with the introduction (Chapter 1). I will first introduce some important concepts that are particularly relevant to this work, i.e., some terminology used in solid-state chemistry to describe crystalline compounds, and chirality, which is of great importance in chemistry and biology. Second, I will talk about cocrystals in more detail, which will include methods for their production and application in pharmacy and other domains. Third, I will describe physicochemical methods that are used to characterize cocrystals, putting emphasis on X-ray diffraction techniques as it is the main tool used in this work; other methods will be mentioned briefly. In the final subsection, I will outline some fundamentals of Density Functional Theory (DFT) and discuss how DFT can complement experimental data in the case of cocrystals.

The first article integrated as Chapter 2, which has been published by our group in 2014, deals with the structural aspects of cocrystallization involving zwitterionic co-formers. Within the research presented in that contribution, we performed cocrystal screening for a series of active pharmaceutical ingredients that have different functional groups (naproxen, oxiracetam, dyprophilline and levetiracetam) in order to test the cocrystallization ability of amino acids with various APIs. Among all the APIs, only naproxen yielded cocrystals, which we structurally characterized. Enantiopure S-naproxen formed a diastereomeric pair of cocrystals with D- and L-alanine as well as with D- and L-tryptophan, whereas in the case of tyrosine it exhibited enantiospecific behavior producing a cocrystal with D- but not the L-enantiomer. We also performed an extensive search in the Cambridge Structural Database, in order to understand with which compounds amino acids tend to cocrystallize..

Amino acids in the solid form are zwitterionic and are characterized by the presence of strong charge-assisted N-H…O hydrogen bonds formed in a head-to-tail manner between carboxylate and amino groups. Although both the carboxylate and the amino group are prone to hydrogen bonding with various functional groups, in order to form a cocrystal the target compound should contain functional groups capable of forming hydrogen bonds strong enough to counterbalance charge-assisted hydrogen bonding in the crystal lattices of individual amino acids. Among the studied APIs, only naproxen provided efficient bonding in cocrystals. This fact led us to the conclusion that amino acids are effective cocrystal formers with carboxylic acids and most likely fail when dealing with other compounds.

Working on the first article, we found that amino acids are effective carboxylic acids; this is why for further research, we selected another representative of the profen family of drugs – flurbiprofen. Preliminary screening made for a series of amino acids and flurbiprofen yielded cocrystals only with proline. Thus, the second article deals with flurbiprofen/proline system. When studying this system, we focused on the chirality aspect of cocrystallization. Combining various combinations of enantiopure and racemic flurbiprofen and proline we discovered 17 cocrystals, including polymorphs, stoichiometrically diverse forms, and solvates. The use of various

characterization techniques helped us to untangle complicated cases when cocrystal mixtures were concerned. All the results and conclusions are extensively described in chapter 3 and are not repeated here for the sake of brevity.

The Conclusions and Perspectives chapter will outline the most important findings and the value of these results for the field of cocrystallization.

Appendices A and B provide the supplementary information for the Chapters 2 and 3, respectively.

# TABLE OF CONTENTS

JURY MEMBERS ..... i
ACKNOWLEDGMENTS ..... iii
LIST OF PUBLICATIONS ..... v
SUMMARY ..... vii
ABBREVIATIONS ..... ix
PREFACE: Outlining the Goals ..... xi
TABLE OF CONTENTS ..... xv
CHAPTER 1 | General Introduction ..... 1
1.1 Solid State: Defining Terminology ..... 1
1.2 Chirality and chiral drugs ..... 3
1.3 Cocrystals and Cocrystallization ..... 4
1.3.1 Application in pharmacy ..... 5
1.3.2 Cocrystals screening ..... 7
1.4 Characterization methods ..... 9
1.4.1 X-ray crystallography ..... 9
1.4.2 Raman and Infrared (IR) Spectroscopy. ..... 18
1.4.3 Thermal analysis: Differential Scanning Calorimetry (DSC) and Thermogravimetric Analysis (TGA). ..... 19
1.4.4 Solid-state nuclear magnetic resonance (SS-NMR). ..... 20
1.5 Density Functional Theory: A tool to complement experimental data ..... 20
CHAPTER 2 | Structural insight into cocrystallization with zwitterionic co-formers: cocrystals of S-naproxen ..... 25
2.1 Introduction ..... 27
2.2 Experimental ..... 28
2.3 Results and discussion ..... 32
2.3.1 S-Naproxen/L-alanine and S-naproxen/D-alanine ..... 33
2.3.2 S-Naproxen/D-tryptophan monohydrate ..... 36
2.3.3 S-Naproxen/D-tyrosine ..... 37
2.3.4 Comparison with known structures from the CSD ..... 38
2.4 Conclusions ..... 41
CHAPTER 3 | Opening Pandora's Box: Chirality, Polymorphism, and Stoichiometric Diversity in Flurbiprofen/Proline Cocrystals ..... 43
3.1 Inroduction ..... 45

3.2 Experimental section ..... 47
3.3 Results and discussion ..... 58
3.3.1 R-flurbiprofen/L-proline ..... 59
3.3.2 R-flurbiprofen/D-proline ..... 64
3.3.3 R-flurbiprofen/DL-proline ..... 65
3.3.4 RS-flurbiprofen/L-proline (RS-flurbiprofen/D-proline) ..... 68
3.3.5 RS-flurbiprofen/DL-proline ..... 72
3.4 Structural Analysis ..... 76
3.5 DFT: Analysis of Calculated Energies ..... 80
3.6 Conclusions ..... 84
CONCLUSIONS AND PERSPECTIVES ..... 85
REFERENCES ..... 89
APPENDIX A | Supporting information for Chapter 2 ..... 101
APPENDIX B | Supporting information for Chapter 3 ..... 109

# CHAPTER 1 | General Introduction

## 1.1 Solid State: Defining Terminology

'A material is a **crystal** if it has essentially a sharp diffraction pattern. The word 'essentially' means that most of the intensity of the diffraction is concentrated in relatively sharp Bragg peaks, besides the always present diffuse scattering'. This definition appears on the website of the International Union of Crystallography and includes aperiodic crystals, which have a sharp diffraction pattern but no long-range order[7]. Leaving beyond the scope aperiodic crystals, crystals in this work are periodic, which means they exhibit an ordered, three-dimensionally periodic spatial atomic structure. A **crystal structure** is described by the dimensions of the unit cell, the coordinates, and the nature of every atom in the unit cell. This information is supplemented by specifying the space group symbol, which includes information about the crystal system, the point group, and the lattice type.

Multicomponent crystalline systems had been known long before the term "***cocrystal***" was widely introduced[8]. Our intuition prompts us that cocrystals may be considered the crystals that contain two or more sorts of molecules. During the last years, along with the "term" cocrystal, such crystals have been referred to in literature as "molecular complexes", "molecular adducts", or other related terms.[9] The term "cocrystal" has been already used in 1968 to describe a multicomponent crystal containing pyrimidine and purine[10] and during 1990s the term has been widely used in crystal engineering and among crystallographers. However, some scientists still considered it too vague and ambiguous.[11–15] To date, it seems a consensus on this topic has been reached and the official definition for ***cocrystal***, as cited on the website of the International Union of Crystallography, is the following: '*Solid consisting of a crystalline single-phase material composed of two or more different molecular and/or ionic compounds generally in a stoichiometric ratio, which are neither solvates nor simple salts'*.[16] ***Pharmaceutical cocrystals*** are comprised of an active pharmaceutical ingredient (API) and a certain ***co-crystal former*** (or ***co-former***), which should be non-toxic (GRAS – Generally Recognized as Safe[17]).

As other crystalline compounds, cocrystals can exhibit polymorphism and form solvates and hydrates. ***Polymorphism*** is the phenomenon when the same chemical compound exhibits different crystal structures. Due to the differences in the arrangement of molecules, physicochemical properties of polymorphs may differ significantly, which is especially important for pharmaceutical industry as it may affect dissolution rate, solubility, bioavailability, stability, etc.[18]

When solvent molecules are incorporated into a crystal structure, we talk about a ***solvate*** or a ***hydrate*** (if the solvent is water). As well as polymorphs, solvated and unsolvated crystalline compounds can have significantly different physicochemical properties. Moreover, due to a potential volatility of solvent, solvated (hydrated) forms may be less stable than their unsolvated (unhydrated) analogs; evaporation of solvent molecules from the crystal may result in the rearrangement of molecules, which in its turn, may lead to formation of a different crystal structure or may even turn the compound amorphous, which would significantly alter compound properties.[19] A schematic representation that highlights the difference between aforementioned solid forms is given in Fig. 1.1.

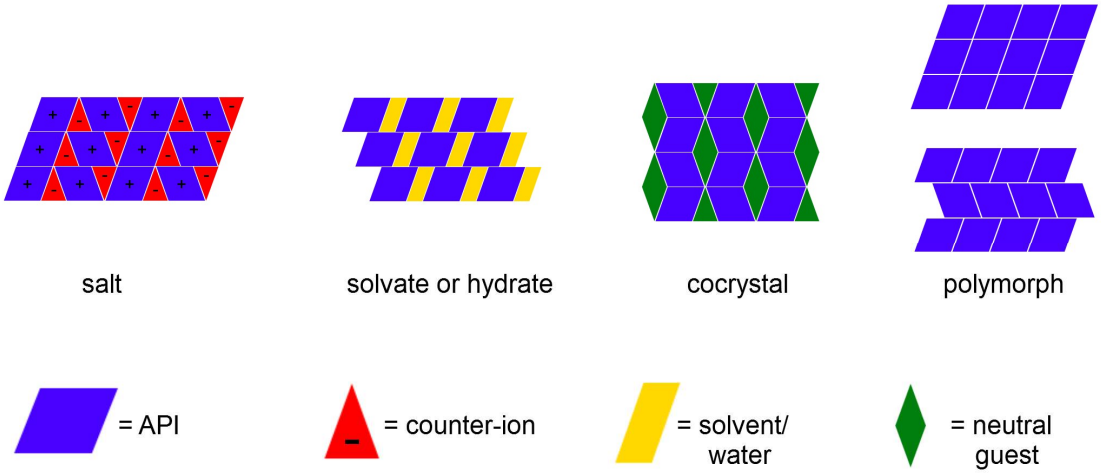


**Figure 1.1.** Schematic representation of various solid forms.

A great majority of organic substances form so-called "***molecular crystals***", with cocrystals not being an exception. In molecular crystals, molecules usually connect via noncovalent interactions: ***hydrogen bonding*** and ***van der Waals interactions***.

***Van der Waals interactions*** represent attractive or repulsive forces between molecules (or between parts of the same molecule) that cannot be considered covalent bonds, hydrogen bonds or the electrostatic interaction of ions or of ionic groups with one another or with neutral molecules. Van der Waals interactions include dipole-dipole, dipole-induced dipole and London (instantaneous induced dipole-induced dipole) forces.[20] Van der Waals forces are non-directional and, in structures in which they prevail, result in close packing – the molecules/atoms pack as closely as possible to one another[21]. An example of van der Waals forces in molecular crystals is the π-π stacking which is often observed between aromatic rings.

***Hydrogen bonds*** occur between pairs of atoms of highly electronegative elements, such as fluorine, oxygen, or nitrogen, in which one serves as a hydrogen donor and another as a hydrogen acceptor[22]. Thus, hydrogen bonds represent an electrostatic interaction, which is stronger than van der Waals interactions but weaker than covalent or ionic bonds. Hydrogen bonds are directional, with the hydrogen bond angle tending towards 180°; however, the latter is not always possible in crystal structures as they, in terms of interactions, are a compromise between many intermolecular interactions of different strengths, angular preferences, and distance characteristics. The distances of hydrogen bonds strongly depend on the nature of atoms involved.

Although, in the majority of cases hydrogen atom is situated closer to one of the atoms involved in hydrogen bonding, there are examples when the hydrogen atom is equidistant from the both atoms, *e.g.*, in crystals $KHF_2$ the hydrogen bond appears to be symmetrical[21]. The position of hydrogen atom within a hydrogen bond gives rise to the salt-cocrystal debate. Crystals in which molecular components are charged, *i.e.* hydrogen is completely shifted towards the acceptor, are generally recognized as ***salts***, in contrast to cocrystals in which the components are usually neutral. However, this distinction is not always straightforward as the position of hydrogen atom may vary from the aforementioned extremes. In the context of the latter, the concept of ***salt-cocrystal continuum*** was introduced in order to include all the cases[23,24].

## 1.2 Chirality and chiral drugs

An object is considered ***chiral*** if it is not superimposable on its mirror image. On the contrary, ***achiral*** objects are identical to their mirror images. A chiral molecule and its mirror image constitute ***enantiomeric pair*** of isomers (also called ***enantiomers***), whose physicochemical properties are the same, except when probed asymmetrically, for instance, by plane-polarized light or when used with reactants that also contain chiral centers. Chiral compounds crystallize in chiral space groups, which exclude the centers of inversion and mirror plane. The majority of chiral compounds possess an ***asymmetric carbon atom***, but other atoms such as sulfur, phosphorus, nitrogen can also act as asymmetric centers.

***Diastereomers*** constitute a different type of stereoisomers. This phenomenon occurs when chiral compounds differ by the configurations of one or more (but not all) chiral centers. These stereoisomers are not the mirror images of one another.

Since chiral molecules exhibit optical activity, when polarized light passes through them, the plane of polarization when viewed along the axis toward the source is rotated in a clockwise (to the right) or counter-clockwise (to the left) direction. A right-handed rotation is called ***dextrorotary*** (*d*- or '+') and a left-handed rotation is ***levorotary*** (*l*- or '–').

The second widely used naming convention for chiral molecules is based on the ***Cahn-Ingold-Prelog priority rules***, which rank the priority of the groups attached to a stereocenter. After the substituents have been assigned their priorities, the molecule is oriented in space so that the group with the lowest priority is pointed away from the observer. If the order of priorities goes in the clockwise direction the R-(rectus) descriptor is assigned to the chiral center, and if the direction is counter-clockwise, the S-(sinister) descriptor.

The third naming convention is based on the ***relative configuration*** principle. According to this convention, two enantiomers (denoted as L- and D-) of glyceraldehyde are used as a template. Chiral molecules are compared to glyceraldehyde enantiomers and are assigned L- or D-descriptor by analogy.

The two last convention schemes are not related to the actual optical activity of enantiomers and thus do not indicate which enantiomer is dextrorotatory or levorotatory. In this work, for convenience, R and S descriptors are used for flurbiprofen and D and L descriptors, for amino acids.

When a compound contains equal amounts of both enantiomers, it is called a ***racemate***. Since the enantiomers rotate polarized light in opposite directions, the net optical rotation for a racemate is zero. Racemates can crystallize as **conglomerates**, which represent a mechanical mixture of both enantiomers. The melting point for a conglomerate coincides with its eutectic point and is always lower than that of pure enantiomers. Only around 10 % of racemic compounds are conglomerates.

The majority of racemates crystallize as ***racemic compounds***, in which only one type of crystals that contain equal amounts of both enantiomers is formed. The melting point of a racemic compound corresponds to a peak on the phase diagram, and it can be higher or lower than that of pure enantiomers.[25]

Unlike synthesized chiral products, all natural compounds are found only under single enantiomeric form; for instance, all natural amino acids are levorotatory, whereas all natural sugars are dextrorotatory. Most enantiomers of racemic drugs exhibit different biological activity, such as pharmacology, toxicology, pharmacokinetics, metabolism, etc. The latter depends on whether or not the three-dimensional structure of the drug molecule allows interaction with a target receptor. Enantiomer that has higher pharmacological activity is usually referred as ***eutomer*** and the one that is less bioactive is called ***distomer***.[26]

Depending on the biological activity, racemic drugs can be divided into three main groups. In the drugs from the first group, one enantiomer exhibits higher bioactivity, whereas the second enantiomer is less active, can be toxic or may have other desired or undesired pharmacological effect. The drugs from the second group exhibit similar pharmacodynamics and thus are equally active. The third group includes drugs that can undergo chiral inversion *in vivo*. Non-steroidal anti-inflammatory drugs (NSAID) from the profen group, e.g. ibuprofen, ketoprofen, fenoprofen belong to the third type as they undergo chiral inversion in the body. Flurbiprofen is another representative of this family of drugs: its S-enantiomer appears to exhibit better anti-inflammatory activity, while both enantiomers may have analgesic effect as well.[27]

In theory, drugs made of single biologically active isomers should provide a better control over the therapeutic action, which may help to reduce drug dosage and avoid unwanted side effects. However, in practice, producing pure enantiomeric drugs may require more sophisticated approaches, *e.g.* expensive chiral resolution techniques or laborious asymmetric synthesis. Albeit the mentioned difficulties, marketing of enantiopure drugs is nowadays preferred over the racemates[26].

## 1.3 Cocrystals and Cocrystallization

Cocrystallization has been studied extensively during recent years from both the fundamental and application points of view. Fundamental aspects of cocrystallization mostly deal with structural peculiarities that predispose compounds to cocrystal formation, involving analysis of functional groups and their ability to form hydrogen bonds, with packing being also one of the factors responsible for polymorphism in cocrystals; identifying stable synthons (*e.g.*, between an amide and carboxyl groups) serve as guidelines in designing cocrystals.[28–34] In the context of applications, cocrystals are considered good alternatives to existing pharmaceutical formulations, as they may help to improve pharmacological properties of drugs, *e.g.*, bioavailability, dissolution rate, hygroscopicity.[1–3] Recent works also show that cocrystals can be applied for separation, purification, or chiral resolution[4,35–39]. Although cocrystal studies have already uncovered some of the thermodynamic and kinetic factors driving cocrystal formation[40–44], cocrystallization still remains poorly predictable; polymorphism issues may also be underestimated, as recent works report that cocrystal systems may be extremely complex[45,46]. Work presented in this thesis concerns cocrystals of APIs with amino acids, thus below I will be talking mostly about pharmaceutical cocrystals, albeit potential applications of cocrystals go far beyond pharmacy, *e.g* as molecular semiconductors or optical materials.[47–49]

### 1.3.1 Application in pharmacy

Cocrystals have found their special niche in pharmacy due to their ability to alter physicochemical properties without changing the nature of the active pharmaceutical ingredient (API) and thus, possibly preserving or even improving its biological activity. To date salt formation is considered one of the primary solid-state approaches to modify physicochemical properties of a drug; as a result, over 50% of APIs on the market are salts[50]. However, in order to form a salt, an API has to possess easily ionizable functional groups (basic or acidic), which is not always the case. Cocrystals, on the other hand, offer a possibility of producing molecular crystals which are held together only by weak interactions (hydrogen bonding or vdW interactions), which becomes a good alternative for drugs that cannot be turned into salts; it should be ensured that cocrystal formers are nontoxic and compatible with the API. Cocrystallization may have a significant effect on the performance of a drug. Below we will outline several important physicochemical properties that can be altered by cocrystallization, such as melting point, stability, solubility, and bioavailability.

**Melting point.** One of the physicochemical properties of APIs that can be easily altered by cocrystallization is its melting point. N. Schultheiss & A. Newman[3] has conducted a survey on 50 cocrystals, in which reported cocrystal melting points were compared to those of pure cocrystal constituents (API or co-former). They have found that a half of cocrystals (51 %) had melting points between those of API and co-former, 39 % melted at lower temperatures than the API or co-former, only 6 % had higher temperatures, and 4% had the same melting point as either the API or co-former. Thus, it shows that cocrystallization is a viable option when one needs to adjust the melting point of a particular API which may be critical for drug development: when the melting point is too high it may be associated with a low solubility of the drug[51], while melting points that are too low may hinder processing, drying, and stability.

**Stability.** The second important parameter to be accounted for during the development of a new drug is stability. Stability is a general term that describes how a particular compound depending on its nature and characteristics behaves under various conditions, e.g. how it responds to humidity, elevated temperatures, solution.

Moisture sorption/desorption studies can help to evaluate *water uptake* when a compound is exposed to various levels of relative humidity[52]. If water uptake is too high, then phase transformations, for example, a formation of hydrate may be suspected, which is crucial for further stages of drug development. Cocrystals respond differently to humid conditions[53–55]: depending on the nature, they may well be resistant to hydration[54] or may dissociate resulting in the emergence of hydrates[53].

Thermal studies, such as DSC, TGA, variable temperature PXPD can provide valuable information on possible phase transformations, degradation, polymorphism. This information may help to predict long-term stability of a drug, select right drying conditions, and provide a better understanding of the solid-state system, thereby leading to the development of more robust compounds and production procedures[56,57].

When cocrystals are in question, *solution stability* is of great importance not only for development processes but also for understanding drug behavior in the GI tract. Solution stability in this case is

defined as the ability of the cocrystal components to stay in solution and not readily crystallize. Depending on the medium, dissociation of the cocrystal may be immediately followed by precipitation of one of its pure constituents or hydrates[53] if water is used, which is crucial for drug development procedure. Moreover, in the body, dissociation and recrystallization of the cocrystal as well as other solution chemistry aspects such as ionization or complexation may significantly affect the bioactivity and thus have to be thoroughly studied at early stages of drug development[58–60].

**Solubility.** One of the main advantages of cocrystals is that they may improve the solubility of poorly soluble drugs. When collecting solubility data, one can measure *kinetic solubility*; it has approximate values and usually based on one measurement at one time point. It is not known for sure whether equilibrium has been reached. Measuring *equilibrium solubility* requires several time points to ensure solution has reached equilibrium which appears as a plateau in the concentration data. How fast a drug dissolves is crucial for its biological effect: it is highly desired that the drug should dissolve while it is in the gastrointestinal tract since longer dissolution time may result in less absorption. In the case of cocrystals, the solubility data collected should be examined with great caution: due to possible phase changes related to solution stability, the measured data may have nothing to do with the cocrystal itself but with one of its constituents. Cocrystal examples studied[59–61] show that some cocrystals indeed can exhibit better solubility; however, for those APIs that are also able to form salts, salts tend to have a higher solubility value as compared to that of cocrystals[3].

**Bioavailability** is one of the main pharmacokinetic properties of drugs. Bioavailability represents the fraction of an administered drug dose that reaches the systemic circulation[62]. It is highly associated with solubility. For cocrystals, reported animal bioavailability data[58,63] indicate that, in some cases, cocrystals indeed improve the bioavailability of poorly soluble drugs; however, the *in vitro/in vivo* correlation is not always straightforward due to the aforementioned dissociation problem.

To date, FDA (US Food and Drug Administration) applies no official guidance on the classification of pharmaceutical cocrystals. However, according to their recommendations, cocrystals are classified as dissociable "API-excipient" molecular complexes (with the neutral guest compound, or co-former, being the excipient), in which the molecular association of API and its excipient occurs within the crystal lattice. Excipients are generally inactive substances included into drug formulations for various purposes, *e.g.* long-term stabilization, therapeutic enhancement through facilitation of drug absorption, reduction of viscosity, improvement of solubility, etc. Excipients can be useful in manufacturing processes as well by proving better powder flowability.[64] When claiming a cocrystal form, one should prove that API and co-former are both neutral and that their dissociation occurs prior to reaching the target biological site. Thus, cocrystals are not regarded as new APIs so far.[65] However, the latter may change with more data on cocrystal formation and their behavior *in vivo* and *in vitro* becoming available.

**Toxicity caused by cocrystal formation *in vivo*.** As was shown above, cocrystallization may be an efficient way to alter physicochemical properties of a particular drug without changing its chemical integrity. However, an unexpected cocrystallization of otherwise non-toxic molecules *in vivo* can be also fatal. One of such examples is cocrystallization of melamine and cyanuric acid,

which was found to cause renal failures in cats and dogs: formation of insoluble melamine/cyanuric acid cocrystals was catalyzed by acidic nature of the urine. Thus, these two compounds, not showing any severe adverse effects when administered separately, proved to be lethal in combination[19,66]. This study highlights that detailed examination of solid-state characteristics of individual crystalline compounds done separately is not enough to assume their safety when they are put together into one formulation; one should thoroughly study not only the effect of each compound in the formulation, but also their combined bioactivity *in vivo*.

### 1.3.2 Cocrystals screening

Methods to produce cocrystals include mechanochemical treatment, melt or solution crystallization[67–69], more exotic supercritical fluid-based techniques[70]. I will describe in more detail a mechanochemical approach and, more precisely, liquid-assisted grinding, as it is the main technique used to prepare cocrystals in this work. In addition, I will outline some aspects of solution cocrystallization as the latter is mainly applied at industrial scale.

**Liquid-assisted grinding.** Mechanochemical methods and especially liquid-assisted grinding proved highly efficient for cocrystal screening.[44,55,71–73] A typical reaction can be performed by mixing two or more solid compounds together, adding a small amount of solvent (~10-20 μL per ~100 mg of solid) and grinding it. Grinding can be done simply by hand or using different kinds of mills. Despite extensive use of this technique, the mechanism of such transformations is not well understood, partially due to the difficulties of directly observing them at microscopic or molecular levels. Another difficulty arises from a lack of temperature control of mechanochemical reactions.

In contrast to solution-based reactions in which molecules move freely to react, in solid-solid transformations most of the molecules are found within the interior of material and are relatively immobile. Thus, any mechanism that might explain a high-yield reaction should address the question of mass transport of material from the reactant to the solid phase. Mechanisms presented to date, all suggest the formation of an intermediate bulk phase (a vapor, a liquid, an amorphous solid) that provides enhanced mobility and/or higher energy of reactant molecules in comparison with their starting crystalline forms.[44] Liquid-phase mediated reaction can be one of the most efficient, in which mass transport is ensured via convection and/or diffusion.

According to the one of the theories, added liquid in liquid-assisted grinding reactions acts as a solvent for one or more of the reactant solids, allowing transport of molecules via an intermediate solution phase by convection and/or diffusion: which of the two mechanisms predominates depends on the ratio of liquid to solid in the reaction mixture. Since the percentage of liquid in a typical liquid-assisted grinding reaction is quite small, the role of diffusion should prevail, as the latter is inversely dependent on the particle size; whereas entrapment of the liquid within the paste formed by the ground reactants may prevent efficient convection.[74–77]

*In-situ* monitoring of mechanochemical reactions has gained popularity in recent years to provide a direct observation of the reaction pathway.[78–81] In this thesis, via studying profen/amino acid cocrystals, I will provide another example of how this method can be successfully applied to monitor reaction outcome. A short desctription of a typical setup for *in-situ* ball-milling

experiments, along with some technical issues of the technique will be given below in the Characterization Methods section.

**Solution cocrystallization.** Albeit a great success of mechanochemical methods for cocrystal production, their use remains limited to laboratory scales as obtaining pure material by grinding at large scales is still challenging. When working in solution, cocrystallization obeys all the mechanisms involved in crystallization of mono-component crystals, but the relative solubilities of the initial cocrystal formers become of crucial importance. The choice of solvent determines whether the system will behave congruently or incongruently. In the solvents in which both components have relatively similar solubilities, system exhibits congruent behavior, whereas when the solubilities differ significantly, the behavior is incongruent. Construction of ternary phase diagrams helps to identify the system's behavior; the schematic representation of the phase diagrams for the congruent and incongruent systems is given in Fig. 2. Ternary phase diagrams for cocrystals represent thermodynamic pathway and are constructed at a certain fixed temperature; the concentrations are usually expressed in molar fractions, but weight fractions can also be used. Thus, if the system is congruent, the region corresponding to cocrystal formation is right in the middle of the phase diagram (for 1 : 1 cocrystals) and thereby the cocrystal can be obtained from the equimolar ratio of cocrystal formers; whereas in the case of the incongruent behavior, the cocrystal region is shifted from the center depending on the relative solubilities of the initial cocrystal formers.[19,40,82,83]

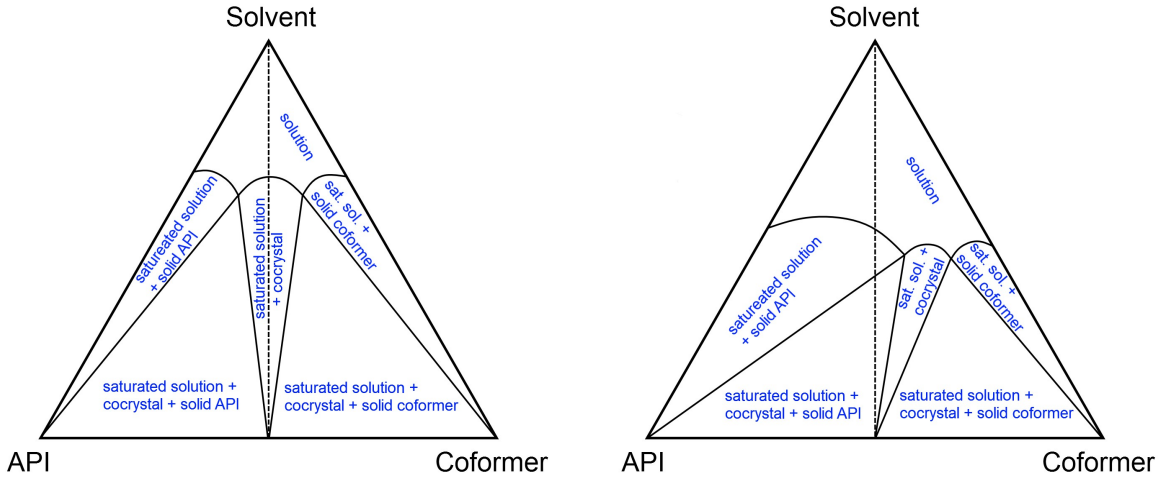


**Figure 1. 2.** Ternary phase diagrams representing the congruent (left) and incongruent (right) behavior in solution.

When developing cocrystal applications in solution, *e.g.*, as a tool for chiral resolution or purification, even more advanced quaternary phase diagrams, which account for more components in solution, may become necessary.[39,41]

## 1.4 Characterization methods

### 1.4.1 X-ray crystallography

X-ray crystallography is a central technique in structural physics, chemistry, materials science, which is used to determine the arrangement of atoms, molecules, or ions within a crystalline solid. X-rays are electromagnetic radiation with the wavelength of the order of 1 Å, which is comparable to atomic spacing, and when they hit crystalline materials diffraction phenomenon occurs: when a regular array of scatters is irradiated with X-rays, each of them produces spherical waves which either cancel one another through destructive interference or add to one another constructively. Bragg's law gives a condition on the scattering angle, θ, for the constructive interference:

$$2d\sin\theta = n\lambda,$$

where $d$ is the interplanar distance, $n$ is a positive integer, and λ is the wavelength.

X-rays can be generated by bombarding a metal with high-energy electrons, for instance copper or molybdenum anodes most commonly used in laboratory X-ray generators; in this case, the characteristic wavelengths of metals are used. Synchrotron radiation on the other hand offers a broad spectrum of wavelengths; X-rays are emitted by electrons accelerated in magnetic field. Synchrotron radiation provides better resolution and brilliance than laboratory diffractometers and thus helps to deal with weakly diffracting samples, complex structures, or other related problems. In comparison with the laboratory X-ray sources, structure determination from powder synchrotron X-ray diffraction data is easier as peaks are better resolved, which facilitates indexing and further steps of structure solution procedure.

In this work, both laboratory and synchrotron X-ray sources were used. Synchrotron source was used for *in-situ* analysis upon variable temperature, including structure solution and *in-situ* ball-milling experiments; whereas laboratory X-ray sources were used for single-crystal structure solution when single crystals were available or for simple phase identification when working with powders.

Below I will describe the basics of structure solution from single-crystal as well as powder X-ray diffraction data, concluding with some remarks on the application of these methods.

#### *1.4.1.1 Structure determination from single-crystal X-ray diffraction data*

X-rays interact with electrons in the material: when the incoming X-ray beam hits material, electrons start oscillating in its electric field radiating electromagnetic waves at the same frequency as the incoming beam. Thus, as a result of diffraction experiment, we should obtain an electron density distribution map from which the structure can be modelled. The main steps of single-crystal structure solution are summarized in Fig. 3

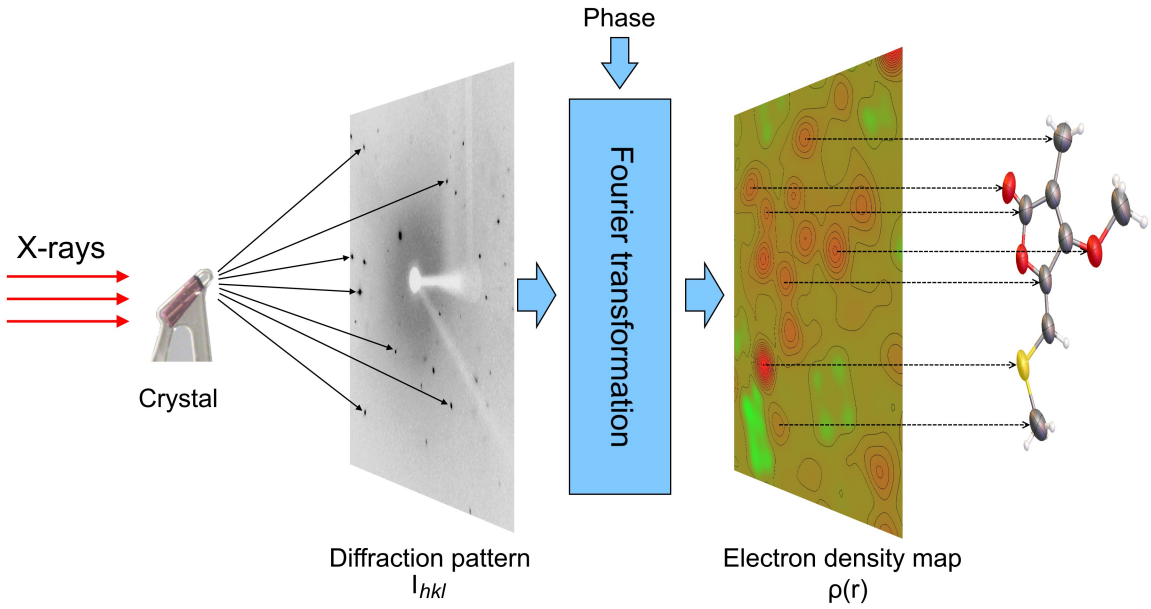


**Figure 1.3.** Summary of single-crystal X-ray diffraction analysis.

When a material is subjected to X-rays, it produces a diffraction pattern through constructive and destructive interference. The intensity of the peaks observed is determined by the atomic arrangement within the unit cell as follows:

$$I_{hkl} \sim | F_{hkl} |^2$$

where $F_{hkl}$ is the structure factor defined as:

$$F_{hkl} = \sum_{j=1}^{n} f_j \exp[2\pi i(hx_j + ky_j + lz_j)]$$

where ($x_j$, $y_j$, $z_j$) are the fractional coordinates that give the position of the $j$-th atom; $hkl$ are the Miller indices; $f_j$ is the scattering factor of the $j$-th atom; and $n$ is the total number of atoms in the unit cell. Since $F_{hkl}$ is the complex number, it can be represented as follows:

$$F_{hkl} = |F_{hkl}|e^{i\varphi_{hkl}}$$

which means that each structure factor represents a diffracted beam with an amplitude $| F_{hkl} |$ and a relative phase $\varphi_{hk}$ .

The electron density can be expressed in terms of the structure factors as:

$$\rho(xyz) = \frac{1}{V}\sum_{hkl} F_{hkl} \exp[-2\pi i(hx+ky+lz)]$$

Thus, providing the knowledge of the structure factors, one can find the electron density using the Fourier transform. However, diffraction experiment gives only the values of $| F_{hkl} |^2$, but phases remain unknown. The latter give rise to the so-called phase problem, solving which is the main difficulty in single-crystal X-ray diffraction. There are several approaches to solve the phase

problem, including the most commonly used for small molecules direct methods, which were applied in this work. Other approaches are omitted, as they are not relevant to this work.

In direct methods, the possible phase angles are guessed directly by the crystallographer (using available crystallographic software). The methods should satisfy two conditions: (1) the value of the electron density is never negative and (2) the highest values of the electron density are observed at and near atomic positions and have nearly zero values everywhere else.

Once the initial structural model is found, one can move to the next step, which is structure refinement. Structure refinement is performed using the least-squares minimization procedure to improve structural model.

For chiral molecules, single-crystal X-ray diffraction may help to find the absolute configuration from the contribution of anomalous scattering. Anomalous scattering can be observed for relatively heavy atoms at certain wavelengths due to X-ray absorbance.

In the case when no anomalous scattering occurs, the scattering factor of the *j*-th atom has only the real part contribution, $f_j = f_{0j}$. The intensities of the two mirror reflections constituting the Friedel pair, *hkl* and $\bar{h}\bar{k}\bar{l}$, are the same and the reflections are indistinguishable, since

$$F^*_{hkl} = F_{\bar{h}\bar{k}\bar{l}}$$

and, consequently, as $I \sim F \cdot F^* \sim |F|^2$,

$$I_{hkl} = I_{\bar{h}\bar{k}\bar{l}}$$

However, in the case of anomalous scattering,

$$f_j = f_{0j} + f'_j + if''_j$$

where $f'_j$ and $if''_j$ are the contributions of anomalous scattering, $F_{hkl}$ is not equal anymore to $F^*_{hkl}$; and thereby the intensities of the mirror reflections are no longer equal. Anomalous scattering depends on the atom type and the wavelength used. Low-energy X-rays are more sensitive to anomalous scattering, for instance, if a studied compound contains oxygen, its absolute configuration can be determined using copper radiation. In the case of anomalous scattering, the diffraction pattern is treated similarly to twin crystals: it is considered to contain reflections from the two mirror structures. Refinement of the absolute configuration is introduced via the so-called Flack parameter, $x$, which is introduced as follows:

$$|F|^2 = (1 - x)|F|^2_{hk} + x|F|^2_{\bar{h}\bar{k}\bar{l}}$$

If $x = 0$, our structure has the right chirality, if $x = 1$, the structure has to be inverted, and if $0 < x < 1$ then the crystal in a racemic twin, *i.e.*, the crystal contains blocks of both enantiomers.[84–86]

Hence, single-crystal X-ray diffraction analysis is a powerful technique irreplaceable in solid-state characterization. Owing to modern computer technologies and the development of algorithms for structure solution, one can treat simple cases almost automatically using the crystallographic software without any need for the deep knowledge of crystallography. However, understanding

general concepts of structure solution helps critical assessment of the result and is essential when dealing with complicated structures.

### *1.4.1.2 Structure determination from powder X-ray diffraction data*

Crystal structure determination from powder X-ray diffraction data is much more complicated and time consuming than from single crystals. The main difficulty comes from the fact that the 3D diffraction pattern observed from single crystals becomes reduced to one dimension in the case of polycrystalline materials.

In 1980s, finding an unknown structure from powder X-ray diffraction data was considered possible only for simple systems. However, development of new algorithms (including global optimization approaches), powerful computers, and high-resolution instruments in recent decades allowed solving complicated structures with more than 120 non-hydrogen atoms per unit cell[87].

The main stages of structure determination from powder X-ray data are outlined in the Scheme below:

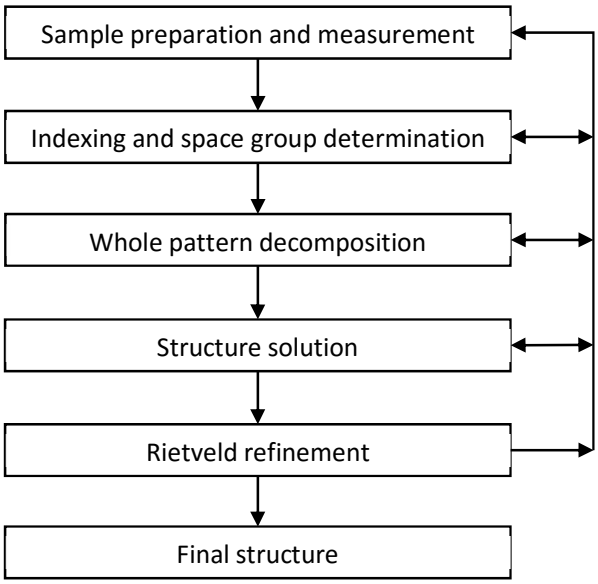


However, finding the correct crystal structure is not always straightforward and often requires going back to the previous step instead of the next one. These steps will be discussed below in more detail.

**Sample preparation**

Sample production and preparation can be performed in various ways. The main requirement is that the sample should contain uniformly distributed crystallites similar in size and ideally in shape. The occasional appearance of large crystallites (of single crystal size) may cause strong not averaged single peaks in the diffraction pattern, which may introduce error into the integrated intensities. The shape is important as it may cause preferred orientation effect, which in its turn affects the peak intensities as well.

**Determination of unit cell parameters and space group (indexing)**

The result of a diffraction experiment can be represented as a table of $2\theta_i$ and $y_i$ values, where $2\theta_i$ is the scattering angle and $y_i$ is the measured intensity corresponding to that angle. These data can also be represented graphically.

Appearance of peaks results from constructive interference of scattered waves, which obeys the Bragg's law:

$$2d\sin\theta = n\lambda,$$

where θ is the scattering angle, $d$ is the interplanar distance, $n$ is a positive integer, and λ is the wavelength.

The peak search can be done automatically using standard crystallographic software. The peak positions are associated with the Miller planes, each characterized by a set of three integer values, $h\ k\ l$, known as Miller indices. Using the Bragg's law, from a series of $2\theta_i$ values at which the intensity maxima are observed we obtain a series of $\{d\}$ values which are in their turn are associated with the unit cell parameters, $a$, $b$, $c$, α, β, γ, via the following relation:

$$d_{hkl} = \frac{1}{\left(h^2a^{*2} + k^2b^{*2} + l^2c^{*2} + 2\text{hla}^*b^*\cos\gamma^* + 2hlb^*c^*\cos\beta^* + 2\text{klb}^*c^*\cos\alpha^*\right)^{\frac{1}{2}}}$$

where $a^*$, $b^*$, $c^*$, α*, β*, γ* are the reciprocal unit cell parameters. The procedure of finding $a$, $b$, $c$, α, β, γ and $hkl$ that satisfy the aforementioned equation for the entire set of $\{d\}$ values is called indexing.

In practice, the procedure of automatic indexing may become complicated since some of the weak peaks may not be included into the set of $\{d\}$ values or some of the strong peaks belonging to a different phase may be included mistakenly; overlap of the peaks also introduces ambiguity into the determination of their maxima. Working with the diffraction patterns from bulky organic compounds may be challenging due to a large number of overlapping peaks and may become even more complicated if the sample contains impurities.

There are multiple computer programs for automatic indexing, such as ITO[88], TREOR[89], DICVOL[90]. Each program has its own unique indexing algorithm, and thus in some cases only one of them is capable of finding the right solution. In this work we have used either DICVOL or an algorithm implemented in the FOX[91] program for structure solution that is analogous to DICVOL.

Whether the indexing result is reliable can be decided from its figure of merit value, which takes into account the discrepancy between the experimental and calculated values, as well as the volume of unit cell. When other parameters are equal, the choice of the unit cell with the smallest volume is preferred.

If wrong unit cell parameters are taken, further structure solution may not lead to a reasonable structure. However, if the unit cell parameters are reliable and only the space group is missing, the latter can determined by checking all possible space groups. The space group is found from the systematic absences. For example, disappearance of all the $0k0$ ($k$ is even) in the monoclinic system may indicate the presence of the $2_1$ axis and, thus, $P2_1$ group should be chosen instead of $P2$. It is easier to find systematic absences at low angles, whereas at high angles it becomes less

straightforward due to peak overlap. The majority of organic molecular crystals crystallize in one of the following space groups: $P2_1/c$, $P\text{-}1$, $P2_12_12_1$, $P2_1$, and $C2/c$; remembering this fact reduces significantly time needed for space group search. In the case of chiral compounds, the space groups that contain the centers of inversion or mirror plane should also be excluded. To date, several probabilistic approaches to determine the space group have been developed[92,93]. They provide a list of possible space groups whose reliability can be concluded from the figure of merit value associated with each group.

**Whole pattern decomposition**

When the diffraction pattern is successfully indexed, one can move to the next step, which is whole pattern decomposition, i.e., extraction of integrated intensities for individual reflections. Since in structure determination from powder diffraction data one is dealing with the 1D diffraction pattern and thus overlapping reflections, the obtained intensities may be ambiguous.

Calculated intensity, $y_{ci}$, in each point is related to the structural factor, $F_{hkl}$, as follows:

$$y_{ci} = s\sum_{hkl}(LPA)_{hkl}Y_{hkl}m_{hkl} \mid F_{hkl} \mid^2 \varphi(2\theta_i - 2\theta_{hkl}) + y_{bi}$$

where:
$s$ is the scale factor, which is a multiplier required to normalize experimentally observed integrated intensities with absolute calculated intensities;
$hkl$ are Miller indices;
$L_{hkl}$ is the Lorentz factor which is defined by the geometry of diffraction;
$P_{hkl} = \frac{1+\cos^2 2\theta}{2}$ is the polarization factor which accounts for partial polarization of the scattered electromagnetic wave;
$A_{hk}$ is the absorption correction coefficient;
$Y_{hkl}$ is the preferred orientation correction coefficient;
$m_{hkl}$ is the multiplicity factor which accounts for the number of symmetrically equivalent reflections;
$F_{hkl}$ is the structural factor;
$\varphi$ is the profile function that describes the peak shape;
$2\theta_i$ is the scattering angle in the *i*-th point;
$2\theta_{hkl}$ is the scattering angle for reflection *hkl*;
$y_{bi}$ is the background intensity in the *i*-th point.
In the whole pattern decomposition procedure, the equation above is used to minimize the following functional $S_y$:

$$S_y = \sum_{i}^{N} w_i(y_{oi} - y_{ci})^2 \rightarrow min$$

where
$N$ is the number of points measured;
$w_i$ is the weight factor which is usually determined as follows: $w_i = 1/y_{oi}^2$
$y_{oi}$ is the observed intensity in the i-th point,

$y_{ci}$ is the calculated intensity in the i-th point.
The integrated intensity $I_{hkl}$ is associated with $F_{hkl}$, as follows:

$$I_{hkl} \sim |F_{hkl}|^2$$

In this minimization procedure, the $|F_{hkl}|^2$ parameter is treated simply as a variable. A set of obtained $\{|F_{hkl}|^2\}$ values is used for structure determination, which will be described in the following section.

The least-squares minimization approach to find a set of indexed intensities was first suggested by Pawley[94] for evaluating the correctness of the chosen unit cell and space group. Another iterative least-squares method was suggested by Le Bail[95]. These two methods are generally implemented into various crystallographic software packages, including FullProf[96], Fox[91], and TOPAS[97] programs used in this work.

**Structure solution**

After finding a set of $\{|F_{hkl}|^2\}$ values, one can move to the next step, which is structure solution. Application of direct methods (also known as reciprocal space methods) used in single-crystal structure solution to powder diffraction data is limited only to simple cases when the number of atoms in the unit cell is small and reflections almost do not overlap. However, in the majority of cases, such simplicity is hardly attainable; this is why treating powder data requires a different approach.

In the recent years, global optimization approaches[98] belonging to the class of direct-space methods has become a powerful tool for structure determination from powder X-ray diffraction data. These methods require knowledge about possible structural fragments of studied materials, for instance, in the case of cocrystals, one need to know their initial constituents and the stoichiometry. Let us consider an example of a 2 : 1 flurbiprofen/proline cocrystal: atoms, bond lengths, bond angles are known in flurbiprofen and proline molecules and thus can be fixed, whereas their position, orientation and certain torsion angles are unknown and can be varied. This approach significantly reduces the number of varied parameters as compared with the single-crystal experiment and thus computational costs. Further reduction of variable parameters can be reached by making certain functional groups rigid, e.g. benzene ring, carboxyl and carboxylate, etc. A careful treatment of varied parameters increases the chances of obtaining a reliable solution.

There are two main global optimization algorithms implemented into crystallographic software: simulated annealing[99] and parallel tempering[100]. Both of them belong to the Monte-Carlo based methods[101]. Despite these methods do not guarantee finding the global minimum, they allow working with a relatively large number of parameters at affordable computational cost.

A simplified description of the algorithm implemented in these methods is as follows. Let us assume, we want to find the minimum for a function $R(P)$, where $P$ represents a number of parameters: $P = \{p_1, p_2, \ldots, p_n\}$. As long as the minimized function depends on $|F_{hkl}|^2$, it is valid for the method; parameters $P$ can include translation or orientation parameters for one or several fragments, torsion angles, bond lengths, atomic coordinates, etc. In the first iteration, all parameters are assigned some random values, $P_0 = \{p_1^{(0)}, p_2^{(0)}, \ldots, p_n^{(0)}\}$, from which $R(P_0)$ is

calculated. Then, a series of parameters $P_{test}$ is generated in the iterative manner through addition of a random increment to the *P* parameter from the previous iteration step:

$$p_{j,test}^{(i)} = p_j^{(i-1)} + r_j \Delta p_j$$

where $r_j$ is a random number, $|r_j| \leq 1$; $\Delta p_j$ is a specified maximum increment. For each $P_{test}$ value, the corresponding $R(P_{test})$ and $\Delta = R(P_{test}) - R(P_{i-1})$ are calculated. If $\Delta \leq 0$, then $P_{test}$ is taken as $P_i$; if $\Delta \geq 0$, then $P_{i-1}$ with the probability of $1 - \exp(-\Delta/T)$ and $P_{test}$ with the probability of $\exp(-\Delta/T)$ are taken as $P_i$, with the $P_{test}$ resulting in a higher *R*-factor than $P_{i-1}$. The latter offers an opportunity to avoid being trapped in a local minimum. The parameter *T* can be considered analogous to temperature; it decreases to 0 with respect to a certain specified function of time. Instead of a single chain of configurations with decreasing temperature used in simulated annealing, in parallel tempering, a small number of parallel optimizations, each with a different temperature, are made.

Global optimization results in a series of solutions. Which solution to choose can be decided by looking at the $\chi^2$ and GoF (goodness of fit) values, which are calculated as follows for each solution (as defined in the FOX program):

$$\chi^2 = \sum_i^N \frac{(y_{oi} - y_{ci})^2}{\sigma^2(y_{oi})}$$

$$GoF = \frac{\chi^2}{N}$$

where N is the number of parameters, $y_{oi}$ is the observed intensity in the i-th point, $y_{oi}$ is the calculated intensity in the i-th point, and $\sigma(y_{oi})$ is the standard deviation for the observed intensity in the i-th point. The best solution usually has the lowest $\chi^2$ and *GoF* values; however, the right solution is not always the one with the lowest $\chi^2$ and *GoF* values. Thus, all obtained solutions should be critically examined and only those that have chemical sense are taken into consideration.

**Rietveld refinement**

When a potential structural model is found, the next step is the refinement of this model, which can be done by the Rietveld method. Rietveld refinement relies on the least-squares minimization approach, matching the experimental diffraction pattern to the calculated one.

Powder diffraction pattern from a crystalline compound is composed of individual reflections, each with its own intensity, position and half width. As was already noted in the section that describes indexing procedure, each peak can be assigned with Miller indices, *hkl*.

Rietveld method uses the same formula for $y_{ci}$ as in the whole pattern decomposition procedure, which is then applied to minimize the functional $S_y$. But in contrast to whole pattern decomposition where only $|F_{hkl}|^2$ played the role of a variable parameter, in Rietveld refinement, one starts with a particular structural model and thus parameters included into the structural factor, such as atomic coordinates, thermal parameters, occupation, unit cell parameters can be varied additionally to the profile parameters, parameters characterizing absorption or preferred orientation, etc.

Preferred orientation, introduced as $Y_{hkl}$ in the equation for $y_{ci}$ may have a significant impact on the integrated intensities. In a powder sample, all crystallites are generally assumed to be randomly (isotropically) distributed, hence the atomic planes with various *hkl* indices evenly contribute to the intensity. This can be easily imagined if all crystallites are ball-shaped. However, in a real sample, crystallites may be needle or plate-shaped and thus they may tend to pack in a certain preferred manner. Plates may result in the appearance of the preferred orientation that coincides with the normal to the plate surface; in the case of needles, preferred orientation may appear along the needle axis. The effects of preferred orientation can result in a fact that diffraction from certain atomic planes will produce a higher contribution to the overall intensity as compared with other planes; and thus, the relative values of the integrated intensities will be ambiguous. In simple cases, preferred orientation can be accounted for by using the March-Dollase approach[102], which requires specifying the axis of preferred orientation. More complicated cases can be modeled through application of spherical harmonics.

Reflection profile, introduced as $\varphi$ parameter in in the equation for $y_{ci}$, depends on the instrumental as well as on the sample (absorption, particle size effect, defects) characteristics. Profile can be described using the Lorentz or Gaussian functions, as well as their combinations, for instance, Thompson-Cox-Hastings pseudo-Voigt function[103] (TCHZ) used in this work.

The quality of Rietveld refinement can be estimated on the basis of $\chi^2$ and GoF values already mentioned above. Additionally, several *R*-factors should be examined[103]:

$$R_{Bragg} = \frac{\sum_{hk} \left| |F_{o,\,hkl}| - |F_{c,\,hkl}| \right|}{\sum_{hkl} |F_{o,\,hk}|}$$

$$R_p = \frac{\sum_i^N (y_{oi} - y_{ci})^2}{\sum_i^N {y_{oi}}^2}$$

$$R_{wp} = \frac{\sum_i^N w_i (y_{oi} - y_{ci})^2}{\sum_i^N w_i {y_{oi}}^2}$$

$$w_i = 1/\sigma_i^2(y_{oi})$$

$R_{Bragg}$ is the discrepancy between the observed and calculated structural factors. $R_p$ and $R_{wp}$ are the discrepancies between the observed and calculated profiles. $R_{wp}$ accounts for the weights of the intensities.

### *1.4.1.3 In-situ ball-milling*

As was mentioned above in the section that concerned liquid-assisted grinding, mechanochemistry proved highly efficient for cocrystal synthesis. However, understanding the mechanisms of mechanochemical transformations is far from being straightforward due to difficulties in direct observation of material transformations at microscopic or molecular levels. *In-situ* monitoring of ball-milling reactions via simultaneous X-ray diffraction data collection provides a unique opportunity to follow the reactants transformations. The technique can be coupled with Raman spectroscopy to gain additional information.[78,80,81,104–106]

The experimental setup includes a milling device placed in front of the X-ray beam, and the entire milling container (jar) is probed with synchrotron radiation. Due to the scattering of the X-rays from the walls of the jar, the resultant diffraction pattern has a high background. The diffraction peaks are also much broader than in a usual synchrotron experiment since a larger sample area is probed.

The material from which the jars are made should satisfy the following requirements: (1) robust enough to withstand the mechanochemical treatment; (2) should produce as low background as possible and no diffraction peaks; (3) resistant to solvents if liquid-assisted grinding is concerned; (4) should be inert and not interfere with the reaction. Various types of plastic can be used for this purpose; one of the most widely applied materials is poly(methyl methacrylate), also known by the trade names Perspex or Plexiglas.

Recently new designs for the geometry of the jar have been suggested, which make possible thinner walls of the jars, thereby providing better quality diffraction data (reduced background, narrower peaks).[107]

Hence, structure solution from powder X-ray diffraction data becomes more and more routine in solid-state characterization field. Single-crystal diffraction experiment produces 3D diffraction pattern which *a priori* contains more information than the 1D diffraction pattern in powder diffraction; this fact significantly increases the reliability of the resultant structure in comparison with the powder one. However, obtaining single crystals good enough for single-crystal analysis is not always possible, and in those cases, powder diffraction may become the only option to find the structure. Powder diffraction methods give access to studying materials under non-ambient conditions, for example, when a starting single crystal due to some phase transformations turns into a polycrystalline material, which is no longer valid for single-crystal analysis. Powder X-ray diffraction is crucial when studying multiphase samples; if all the phases are known, simple Rietveld refinement can help one to estimate the relative amounts of each phase in the sample, providing the diffraction data are of sufficient quality. In this work, powder synchrotron X-ray diffraction helped us to identify unknown phases that were accessible only in a polycrystalline state and to perform *in-situ* experiments essential for understanding our systems.

### 1.4.2 Raman and Infrared (IR) Spectroscopy.

Vibrational spectroscopy is widely used in chemistry to characterize materials. In IR spectroscopy, infrared radiation is absorbed at certain resonant frequencies that match vibrational modes of organic molecules. For routine measurements of organic compounds, usually the mid-infrared region, 4000–400 $cm^{-1}$, is used.[108] Raman spectroscopy relies on inelastic light scattering. Raman effect is observed when excited molecule returning from so-called virtual state emits a photon with lower (Stokes scattering) or higher (Anti-Stokes scattering) energy than the initial laser photons.[109]

Thus, IR and Raman spectroscopy have different selection rules rendering these techniques complementary to each other: to be IR active, a vibrational mode should exhibit a change in the electric dipole moment, whereas Raman activity depends on the polarizability.

When applied to cocrystals, IR spectroscopy is often used to see if proton transfer occurred as it can distinguish between neutral carboxyl group and carboxylate anion. Neutral carboxyl group produces a strong C=O stretching band around 1700 $cm^{-1}$ and a weaker C-O stretch around 1200 $cm^{-1}$, whereas carboxylate anion displays two closely situated C-O stretches between 1000 and 1400 $cm^{-1}$.[110] It should be mentioned that whether we have a cocrystal or salt can be directly decided from single-crystal X-ray diffraction data since the bond distances in protonated and deprotonated carboxyl group differ.

Spectroscopic data can be treated as unique fingerprints of compounds. Simple comparison of the spectra of initial compounds and presumably formed cocrystal may give an indication of cocrystal formation. However, since spectroscopic data give only vibrational modes of functional groups present, it is not always straightforward to distinguish between a simple physical mixture of initial co-formers and cocrystal. Another disadvantage is that spectroscopy does not provide the exact structure. Thus, IR and Raman spectroscopy are usually used as a complementary technique in characterization of cocrystals, with diffraction methods being of the primary choice.

### 1.4.3 Thermal analysis: Differential Scanning Calorimetry (DSC) and Thermogravimetric Analysis (TGA).

Thermal analysis is essential when studying solids. It provides information on how the material responds to temperature change and more precisely on phase transitions occurring, *e.g.*, melting, crystallization, sublimation, decomposition, polymorphic and other solid-solid transformations.

DSC is a thermoanalytical technique that measures the heat flow as a function of temperature necessary to establish a nearly-zero temperature difference between the sample and the reference. When the sample undergoes a phase transition heat will flow to the sample (endothermic transition, *e.g.*, crystallization) or out of the sample (exothermic transition, *e.g.*, melting). The results of DSC measurements can be quantified in terms of energy associated with each peak (area under the curve) as well as show the sample's purity.[108]

In some cases, DSC can be applied to establish cocrystal formation by the construction of binary phase diagrams.[29,111] DSC curves measured for a series of samples containing various ratios of cocrystal formers provide the eutectic and melting point values, if no other complicated temperature events are involved (such as recrystallization, solid-solid transformations, sublimation, partial decomposition, etc.). A schematic representation of a binary phase diagram for the formation of a cocrystal with the 1 : 1 stoichiometry is given in Fig. 4.

TG analysis allows measuring mass changes as a function of temperature[112], which is especially important when studying hydrates and solvates.

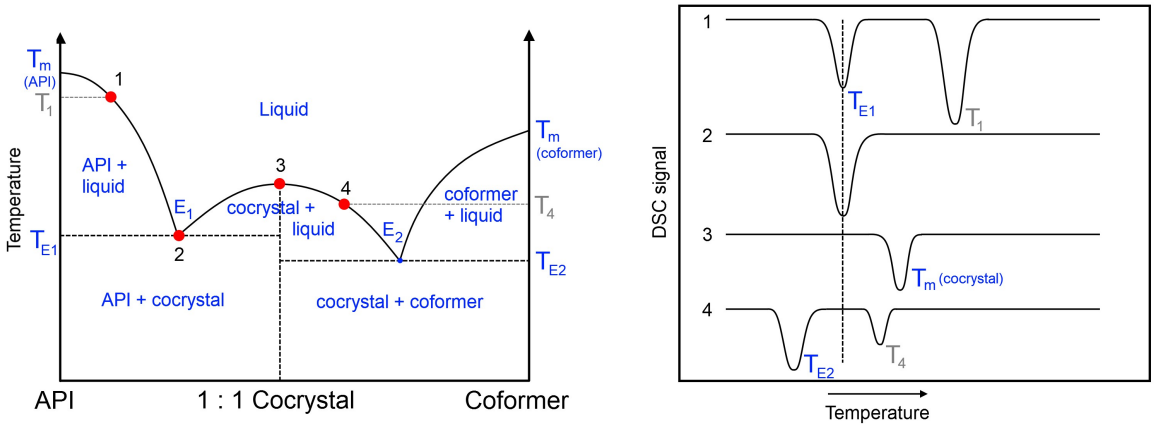


**Figure 1.4.** Schematic representation of a binary phase diagram for a 1 : 1 cocrystal (left) and (right) the corresponding DSC data for the selected four points (red); this figure only illustrates the principle of how a binary phase diagram can be constructed from the DSC data and is not based on real data.

### 1.4.4 Solid-state nuclear magnetic resonance (SS-NMR).

SS-NMR relies on the same principles as NMR in solution, but in solids, anisotropic interactions, which are averaged due to Brownian motion in liquids, affect significantly the behavior of a system of nuclear spins, causing the orientation-dependent chemical shift, chemical shift anisotropy (CSA), and intermolecular dipolar coupling which occurs when the magnetic moment of one nucleus influences the neighboring field of other nucleus; altogether, these factors produce a significant line-broadening effect in NMR spectra. Magic angle spinning (MAS) helps averaging the interactions.[113] Cross polarization (CP) can be used to increase sensitivity.[114,115]

SS-NMR spectroscopy is a powerful technique, which finds more and more application when studying materials in solid state. Pharmaceutical industry has been actively using solid-state NMR to study polymorphism, interactions between an API and an excipient in formulations, solvate/cocrystal formation, etc. SS-NMR proved to be a good complementary method to X-ray crystallography, vibrational spectroscopy, and thermal methods, traditional tools to identify various solid forms of a given compound, study their transformations and solve other solid-state structural problems. Moreover, NMR crystallography emerges in an independent field, being applied to solve structural problems in biology. [116–118]

## 1.5 Density Functional Theory: A tool to complement experimental data

Density functional theory is widely applied for diverse materials modeling problems in physics, chemistry, materials sciences, chemical engineering, geology, and other disciplines. DFT allows finding solutions to the Schrödinger equation, a fundamental equation that describes the quantum behavior of atoms and molecules. Below I will outline main concepts used in DFT, and what information it can provide when cocrystals are of concern.

The theoretical part of this chapter is mostly based on the material from the book written by D. Sholl and J. Steckel: Density Functional Theory: A practical Introduction.[119]

Before plunging into DFT, I would like to remind several key points of quantum mechanics that I find essential for further discussion.

**Quantum mechanics basics.** I will start with the *Born-Oppenheimer approximation*, according to which the nuclei and electrons in a well-defined collection of atoms (an isolated molecule or atoms in a crystal) can be treated as two separate mathematical problems. Electrons are much lighter than heavy nuclei and thus respond more rapidly to changes in their surroundings. Relying on this fact, we can describe electron motion assuming fixed positions of the atomic nuclei and find for a given set of electrons the lowest energy configuration, the *ground state*. For a given set of nuclei at positions $\mathbf{R}_1, \ldots, \mathbf{R}_M$, the ground-state energy can be expressed as a function of their positions $E(\mathbf{R}_1, \ldots, \mathbf{R}_M)$, which is known as *adiabatic potential energy surface* of the atoms.

In the simplest form, the time-independent, nonrelativistic Schrödinger equation can be represented as follows:

$$H\psi = E\psi$$

In this equation, $H$ is the Hamiltonian operator and $\psi$ is a set of solutions, or eigenstates, of the Hamiltonian. Each of these solutions, $\psi_n$, has an associated eigenvalue, $E_n$.

The form of the time-independent Schrödinger equation for a system with multiple electrons interacting with multiple nuclei is the following:

$$\left[-\frac{\hbar^2}{2m}\sum_{i=1}^{N}\nabla_i^2 + \sum_{i=1}^{N}V(\mathbf{r}_i) + \sum_{i=1}^{N}\sum_{j<i}U(\mathbf{r}_i,\mathbf{r}_j)\right]\psi = E\psi$$

where $m$ is the electron mass; the three terms in brackets define, in order, the kinetic energy of each electron, the interaction energy between each electron and the collection of atomic nuclei, and the interaction energy between different electrons; $\psi$ is the electronic wave function, which is a function of each of the spatial coordinates (spin is omitted for clarity) of each of the $N$ electrons, so $\psi = \psi(\mathbf{r}_1, \ldots, \mathbf{r}_N)$, and $E$ is the ground-state energy of the electrons.

The electron wave function can be approximated using a *Slater determinant*, in which the $N$-electron wave function is expressed as the determinant of a matrix of single-electron wave functions, thereby satisfying the antisymmetry principle.

We cannot directly observe the wave function for any particular set of coordinates, we can only measure the probability of the $N$ electrons being found at a particular set of coordinates, $\mathbf{r}_1, \ldots, \mathbf{r}_N$. This probability is $\psi^*(\mathbf{r}_1, \ldots, \mathbf{r}_N)\psi(\mathbf{r}_1, \ldots, \mathbf{r}_N)$, where asterisk indicates a complex conjugate.

The *electron density* at a particular position in space is closely related to the probability and is expressed as follows:

$$n(\mathbf{r}) = 2\sum_i \psi_i^*(\mathbf{r})\psi_i(\mathbf{r})$$

This expression represents a summation over all the occupied individual electron wave functions. The factor 2 follows from the Pauli exclusion principle, which states that each individual electron wave function can be occupied by two separate electrons provided they have different spins.

**DFT – from wave functions to electron density.** DFT computes the electron density and not the exact electron wave functions; the latter can be done using other wave-function based methods, for instance Hartree-Fock method. Albeit the advantage of being more precise, wave-function based methods require more computational resources and may not be suitable for large systems. DFT, on the other hand, may not provide the exact solution but still a solution that is satisfactory enough to draw conclusions about system's properties at a lower computational cost.

Density functional theory is based on two fundamental mathematical theorems proved by Kohn and Hohenberg and the derivation of a set of equations by Kohn and Sham.

The first theorem states that '*The ground-state energy from Schrödinger's equation is a unique functional of the electron density*.' A *functional* takes a function and defines a single number from the function, so according to the theorem, the ground-state energy $E$ can be expressed as $E[n(\mathbf{r})]$, where $n(\mathbf{r})$ is the electron density. This theorem means that we can solve the Schrödinger equation (*i.e.* find the ground-state energy) by finding the electron density, a function of only three spatial variables, rather than the wave function which is a function of $3N$ variables.

However, the first theorem does not give the exact description of the functional. The second theorem states an important property of the functional: '*The electron density that minimizes the energy of the overall functional is the true electron density corresponding to the full solution of the Schrödinger equation*.' If we knew the "true" functional than we could simply vary the electron density until the energy reaches its minimum, but since the functional is unknown, we can only use its approximate forms.

The functional in terms of the single-electron wave functions, $\psi_i(\mathbf{r})$, described by the Hohenberg-Kohn theorem can be written as follows:

$$E[\{\psi_i\}] = E_{\text{known}}[\{\psi_i\}] + E_{\text{XC}}[\{\psi_i\}]$$

When summarized, the single-electron wave functions define the electron density, $n(\mathbf{r})$. The functional above consists of two terms: the known part, $E_{\text{known}}[\{\psi_i\}]$, and everything else, $E_{\text{XC}}$.

The "known" part includes the following contributions:

$$E_{\text{known}}[\{\psi_i\}] = -\frac{\hbar^2}{m}\sum_i \int \psi_i{}^* \nabla^2 \psi_i d^3r + \int V(\mathbf{r}) n(\mathbf{r})\, d^3r + \frac{e^2}{2}\iint \frac{n(\mathbf{r})n(\mathbf{r}')}{|\mathbf{r}-\mathbf{r}'|} d^3r\, d^3r' + E_{ion}$$

The terms on the right are, in order, the electron kinetic energies, the Coulomb interactions between the electrons and the nuclei, the Coulomb interactions between pairs of electrons, and the Coulomb interactions between pairs of nuclei.

$E_{\text{XC}}[\{\psi_i\}]$ is the exchange-correlation functional which is defined to include all the quantum mechanical effects that are not included in the "known" terms.

In a set of equations suggested by Khon and Sham in order to solve the Schrödinger equation, *i.e.* to find the right electron density, each is defined for a single electron and has the following form:

$$\left[-\frac{\hbar^2}{2m}\nabla^2 + V(\mathbf{r}) + V_H(\mathbf{r}) + V_{XC}(\mathbf{r})\right]\psi_i(\mathbf{r}) = \varepsilon_i\psi_i(\mathbf{r})$$

Thus, the solutions of Khon-Sham equations are single-electron wave functions $\psi_i(\mathbf{r})$ that depend on only three spatial variables. The three potentials, $V$, $V_H$, and $V_{XC}$ define the interaction between an electron and the collection of atomic nuclei, the Hartree potential, and the exchange and correlation contributions to the single-electron equations, respectively.

The Hartree potential, defined as:

$$V_H(\mathbf{r}) = e^2\int\frac{n(\mathbf{r}')}{|\mathbf{r}-\mathbf{r}'|}d^3r$$

defines the Coulomb repulsion between the electron being considered in one of the Kohn-Sham equations and the total electron density defined by all electrons in the problem.

The exchange-correlation potential can formally be defined as a "functional derivative" of the exchange-correlation energy:

$$V_H(\mathbf{r}) = \frac{\delta E_{XC}(\mathbf{r})}{\delta n(\mathbf{r})}$$

Thus, in order to solve the Kohn-Sham equations we need to know the Hartree potential and the latter requires knowing the electron density, which in its turn is determined by the single-electron wave functions, but for finding those functions we need to solve the Kohn-Sham equations. The iterative approach helps to break this circle; the algorithm includes the following steps:

Defining an initial, trial electron density, $n(\mathbf{r})$.

Solving the Kohn-Sham equations defined from the trial electron density and finding the single-particle wave functions, $\psi_i(\mathbf{r})$.

Calculating the electron density defined by the Kohn-Sham single-particle wave functions from step 2,

$$n_{KS}(\mathbf{r}) = 2\sum_i \psi_i^*(\mathbf{r})\psi_i(\mathbf{r})$$

Comparing the calculated electron density, $n_{KS}(\mathbf{r})$, with the electron density used to solve the Kohn-Sham equations, $n(\mathbf{r})$. If the two densities are the same, then this is the ground-state electron density, and it can be used to compute the total energy. If the two densities are different, then the trial electron density must be updated in some way. Once this is done, the process begins again from step 2.

**Exchange-correlation functional.** As was already noted above, DFT calculations are not exact solutions of the full Schrödinger equation since the true functional is unknown, which results in an intrinsic uncertainty between the energy calculated by DFT and the true ground-state energies.

Hence, the energy value calculated by DFT will significantly depend on the functional used. There are several classes of functionals developed to date, *e.g.*

LDA – local density approximation derived from the uniform electron gas; in this situation, the electron density is constant at all points in space

GGA – generalized gradient approximation, which uses the local gradient in the electron density.

Two the most widely used functionals from the GGA class applied for solids are the Perdew-Wang functional (PW91) and the Perdew-Burke-Ernzerhof (PBE) functional. Choosing which functional is better in a particular case depends on the problem.

The contribution of weak vdW interactions in molecular crystals is substantial and thus in order to obtain a reliable theoretical model, these interactions have to be included into calculations. Dispersion correction methods that consider the total energy as the sum of the conventional Khon-Sham DFT energy and a correction term that accounts for vdW interactions have been recently introduced to serve the aforementioned purpose.

When applied to molecular crystals DFT calculations may be useful in the following cases: (*a*) To supplement low-quality experimental data, for instance when dealing with the structure solution from powder X-ray diffraction data; the calculations may help resolve questions about space group ambiguities or other structure-related issues. (*b*) To position hydrogen atoms. (*c*) To decide between various possible models. (*d*) To check the correctness of experimental crystal structures.

DFT calculations can be used to locate hydrogen atoms if their positions are not precise or unavailable in the initial experimental structures. However, DFT cannot resolve the question whether a crystal structure is cocrystal or salt because this would require comparing the energies of two models with different chemical bonds. DFT energies are in general less accurate when chemical bonds are concerned, partly due to intrinsic inaccuracies in heats of formation. However, comparing the relative energies of polymorphs is considered reliable since no new bonds are formed or broken and all the inaccuracies are cancelled out. The positions of hydrogen atoms calculated for the single-crystal experimental structures are considered quite reliable, but in the case of powder X-ray data, location of hydrogen atoms from DFT is limited since the initial model may not be accurate enough.[120,121]

# CHAPTER 2 | Structural insight into cocrystallization with zwitterionic co-formers: cocrystals of S-naproxen

*This chapter is based on the article published by Natalia Tumanova, Nikolay Tumanov, Koen Robeyns, Yaroslav Filinchuk, Johan Wouters and Tom Leyssens. CrystEngComm,* ***2014****, 16, 8185–8196.*


## ABSTRACT

The screening of S-naproxen, S-oxiracetam, S-diprophylline, and levetiracetam with a series of essential and nonessential amino acid co-formers has yielded cocrystals only for S-naproxen, thus showing that amino acids seem to have a preference for forming cocrystals with compounds containing a carboxyl group. Herein, we report the crystal structures of four S-naproxen cocrystals: S-naproxen/L-alanine, S-naproxen/D-alanine, S-naproxen/D-tyrosine, and S-naproxen/D-tryptophan monohydrate. All of the described cocrystals show similar structural motifs, i.e., amino acids form head-to-tail chains with strong charge-assisted hydrogen bonding, which are similar to those found in the individual amino acids, with S-naproxen molecules grafted on them. According to the systematic search of the Cambridge Structural Database for other cocrystals that involve zwitterionic co-formers, charge-assisted hydrogen bonds between amino acid molecules play an essential role, being present in the majority of structures. The results of this work provide an insight into structural aspects of cocrystallization with zwitterionic co-formers, offer new possibilities for S-naproxen pharmaceutical formulations, and can serve as guidelines when developing new cocrystals involving zwitterionic co-formers.

## 2.1 Introduction

Multicomponent crystalline systems have been known for a long time, but only recently the term cocrystal has come into wide use. Over the last decade cocrystals have gained special popularity in pharmaceutics as alternative drug formulations[19,71,122–127] as they allow one to tackle issues related to polymorphism,[128] can be formed in compounds that do not easily form salts, offer a certain degree of engineering flexibility,[12,129,130] may improve biophysical properties[63,131,132] (such as solubility or dissolution rate), stability,[133] and hygroscopicity[134,135] and make the production process more feasible[60] in comparison with pure active pharmaceutical ingredients (APIs). Despite their growing popularity scientists still argue about the exact definition of a cocrystal; however, they all agree that cocrystals can be defined as "solids that are crystalline single-phase materials composed of two or more different molecular and/or ionic compounds generally in a stoichiometric ratio which are neither solvates nor simple salts".[16]

Up to now, almost every study concerning these compounds has been oriented towards the development of alternative drug formulations.[19,71,122–127] However, cocrystals have a series of specific properties making them potent candidates for the development of solid state applications. Recently, Myerson et al. showed how cocrystallization can be used as a purification tool, separating ibuprofen–ketoprofen mixtures.[136] In 2010, Ter Horst et al. used cocrystallization as a tool to remove cinnamic acid from water at levels seven times lower than the solubility.[36] They furthermore extended this work by showing how electrochemistry can be combined with cocrystallization for the *in-situ* product removal of carboxyl acids.[35]

Although cocrystals of chiral APIs are common, chirality in cocrystals is a relatively unexplored area. Motherwell et al. showed how caffeine and theophylline behave differently with respect to DL- and D-tartaric acid.[137] In 2012, Coquerel et al. showed how cocrystallization can be used for preferential crystallization.[5] An even fewer number of studies involve cocrystals of two chiral components. Lehmann noted the formation of a diastereomeric pair of cocrystals between proline amide and mandelic acid, using this information to determine the absolute configuration.[138] The enantiospecific behavior in cocrystals was noted for the first time in 2008 by Takata et al.[139] for the Stanolone/S-tartaric acid cocrystal and again in 2011 by Thorey et al.,[140] studying the (R,R)-cyclohexanediol/R-tartaric acid cocrystal. The latter used this information to develop an enantiospecific extraction process using supercritical $CO_2$.[141]

Parallel to Thorey et al., Springuel et al. observed this particular behavior when working on levetiracetam,[4] showing an enantiospecific interaction with either S-mandelic acid or S-tartaric acid.[29] As levetiracetam is produced from a racemic mixture, with the S-enantiomer separated using chiral chromatography, they developed a novel chiral resolution technique for compounds which do not or not easily form salts based on enantiospecific cocrystallization in solution. Although the enantiospecific behavior seems to be common to cocrystals, they recently showed naproxen to form a diastereomeric pair of cocrystals with zwitterionic co-formers (D- and L-proline).[142] Ibuprofen, another member of the profen family of APIs, showed the ability to form diastereomeric salts with arginine and lysine amino acids, which found application at the industrial scale.[143]

In the context of these recent findings, we focused on cocrystals formed by S-naproxen with various amino acids. Amino acids contain both amino and carboxyl groups, which make them perfect candidates for cocrystallization. Moreover, they are natural to the body, and their use in pharmaceutical cocrystals reduces the risk of negative side effects for human health in comparison with other co-formers and may be even beneficial, improving biophysical properties of APIs. The cocrystals described in this paper can be considered potential candidates for the pharmaceutical industry. Tryptophan-based cocrystals are of special importance; they present a new formulation strategy for naproxen, and aside from the pharmaceutical activity of S-naproxen they may be a source of nonessential amino acids. Moreover, the enantiospecific behavior found in the naproxen/tyrosine system opens new horizons for developing chiral resolution techniques based on cocrystallization. From a structural point of view, amino acids are zwitterionic compounds with a strong charge-assisted hydrogen bond network, which might affect the crystallization process.[142,144] Studying their ability to form cocrystals can help to understand how the zwitterionic nature affects cocrystal formation.

## 2.2 Experimental

### Materials and methods

S-Naproxen (99%), D-proline (98%), L-valine (98%), D-alanine (98%), L-leucine (98%), D-leucine (98%), L-phenylalanine (98%), D-phenylalanine (98%), L-isoleucine (98%), D-tyrosine (98%), L-methionine (99%), and D-histidine (99%) were purchased from TCI Europe N. V.; S-oxiracetam from Angene; levetiracetam from Xiamen Top Health; S-diprophylline (99%) from HaOHUA Industry; L-asparagine (≥98%), L-cysteine (97%), L-threonine (≥98%), D-valine (98%), and DL-isoleucine (99%) from Sigma-Aldrich; L-glutamine (99%), D-serine (98%), D-threonine (98%), D-tryptophan (99+%), L-tryptophan (99%), L-proline (99%), L-alanine (99%), D-aspartic acid (99+%), and D-glutamine (98%) from Acros Organics; L-histidine (98+%), DL-serine (99%), L-tyrosine (99%), D-glutamic acid (99+%), L-aspartic acid (98+%), L-glutamic acid (99+%), and D-methionine (99%) from Alfa Aesar; L-serine (98.5–101%) from Fisher Scientific; and D-asparagine from Molekula.

For liquid-assisted grinding, we used methanol and for crystallization, ethanol and distilled water. Methanol (HPLC grade) and ethanol were purchased from VWR International.

All materials were used as received without any further purification.

### Screening

Screening was performed by liquid-assisted grinding (10 μL of methanol per ~100 mg of powder mixture with a 1 : 1 ratio) using a Retsch MM400 mixer mill for 90 min at a frequency of 30 Hz. Final powders were analyzed by X-ray powder diffraction (CuKα radiation, λ = 1.5418 Å) using a Siemens D5000 diffractometer; 2θ was scanned from 2 to 50° with a step of 0.02°. When the powder diffraction patterns of the ground materials contained new peaks, different from the peaks of the initial compounds, we assumed formation of a new phase and then tried to crystallize it from solution.

**Crystallization**

All single-crystals were grown from ethanol–water solution. S-Naproxen/L-alanine and S-naproxen/D-alanine were crystallized from an ethanol–water solution containing 97 vol% of ethanol and 3 vol% of water.[145] S-Naproxen and D- or L-alanine were taken in a ratio of 1 : 1 and put in 1.5 mL of ethanol– water at ~30 °C; solutions were stirred for 3–5 h, filtered, cooled to room temperature and seeded with the cocrystal powder obtained by liquid-assisted grinding. Square-shaped colorless S-naproxen/L-alanine or S-naproxen/D-alanine cocrystals grew from solutions along with plate-shaped S-naproxen crystals. The diffraction patterns calculated from single-crystal diffraction data of those two cocrystals matched their powder diffraction patterns from liquid-assisted grinding.

S-Naproxen/D-tryptophan monohydrate was crystallized by slow evaporation from ethanol–water solution containing 60 wt% of ethanol and 40 wt% of water. S-Naproxen and D-tryptophan were taken in the amounts relative to their solubilities (1.54 (ref. [146]) and 1.40 (ref. [147]) g/100 g, respectively) in this solution.[148] The solution was filtered and left to evaporate slowly at room temperature. Thin needle-shaped crystals of S-naproxen/D-tryptophan monohydrate were obtained. S-Naproxen and L-tryptophan treated under the same conditions cocrystallize in an unhydrated fine-powder form, similar to that obtained by grinding, as confirmed by X-ray powder diffraction and thermal analysis (see Figs. S3-S6 in Appendix A).

We were not able to grow crystals of S-naproxen/ L-tryptophan, unhydrated S-naproxen/D-tryptophan, and S-naproxen/D-tyrosine cocrystals suitable for single-crystal diffraction analysis.

**Structure determination**

The structure of S-naproxen/L-alanine was solved from single-crystal synchrotron X-ray diffraction data, which were collected using the Swiss-Norwegian Beam Lines BM01A at the European Synchrotron Radiation Facility (ESRF) (Grenoble, France), using a PILATUS 2M hybrid pixel detector at a wavelength of 0.68239 Å and a sample-to-detector distance of 144 mm; the collection mode was ω-scans. The sample was cooled to 100(1) K using an Oxford Cryostream 700 system. The data were converted and integrated using the SNBL tool-box software[149] and the CrysAlisPro software.[150]

The structures of S-naproxen/D-alanine and S-naproxen/ D-tryptophan monohydrate were solved from single-crystal X-ray diffraction data, which were collected using a MAR345 image plate detector using MoKα radiation (Rigaku UltraX 18 rotation anode, Xenocs Fox3D focusing multilayer mirror) at 150(1) K. The data were integrated using the CrysAlisPro software.

The multi-scan absorption correction procedure implemented in the CrysAlisPro software was applied in all of the single-crystal cases. The structures were solved by direct methods using the SHELXS-2013[151] program and refined by full-matrix least squares on $|F|^2$ using SHELXL-2013[151] and the shelXLe shell.[152] Non-hydrogen atoms were refined anisotropically; and hydrogen atoms were either placed on calculated positions in riding mode with temperature factors fixed at 1.2 times $U_{eq}$ of the parent atoms and 1.5 times $U_{eq}$ for methyl groups or were located from the difference Fourier map if the resolution allowed.

The structure of S-naproxen/D-tyrosine was solved from powder X-ray diffraction data, which were collected using the Swiss-Norwegian beamline BM1A at the European Synchrotron Radiation Facility (ESRF) (Grenoble, France), using a PILATUS 2M hybrid pixel detector at a wavelength of 0.823065 Å and a sample-to-detector distance of 443 mm. These parameters along with image plate tilt angles were calibrated using a standard $LaB_6$ sample. The two-dimensional diffraction images were integrated using the ESRF Fit2D[153] program. The pattern was indexed using DICVOL04.[90] The $P2_1$ space group was suggested, taking into account systematic absences and considering the chiral nature of molecules in the unit cell. Le Bail fit was done using the FOX[91] program. The structure was solved by global optimization in direct space using the FOX program and refined by the Rietveld method (for Rietveld refinement see Fig. 1) using the Fullprof suite.[96] Molecular models of S-naproxen and D-tyrosine were imported from the single-crystal structural models taken from the Cambridge Structural Database (COYRUD12[154] and FAZHET01,[155] respectively). The following groups were made rigid in order to keep a proper planar geometry: carboxylate, a carboxyl group, and benzene rings. The position, orientation and conformation of molecules were optimized. To constrain bond distances and valence angles, 56 distance restraints were applied for interatomic distances and 93 for angles. The background was described by linear interpolation between selected points.

The synchrotron X-ray diffraction patterns of unhydrated S-naproxen/D-tryptophan and S-naproxen/L-tryptophan were measured using the MS-X04SA beam line at the Swiss Light Source (SLS) (PSI, Switzerland) using a 1D microstrip detector MYTHEN II at a wavelength of 0.775045 Å, and the zero shift was −0.0079°. The wavelength and zero shift values were calibrated using a standard NIST 640d Si sample. Indexing and Le Bail fit were performed using FOX. The samples were prepared by liquid-assisted grinding in the same manner as for screening, and they showed poor crystallinity resulting in broad peaks, which rendered it difficult to find the structures from these powder data.

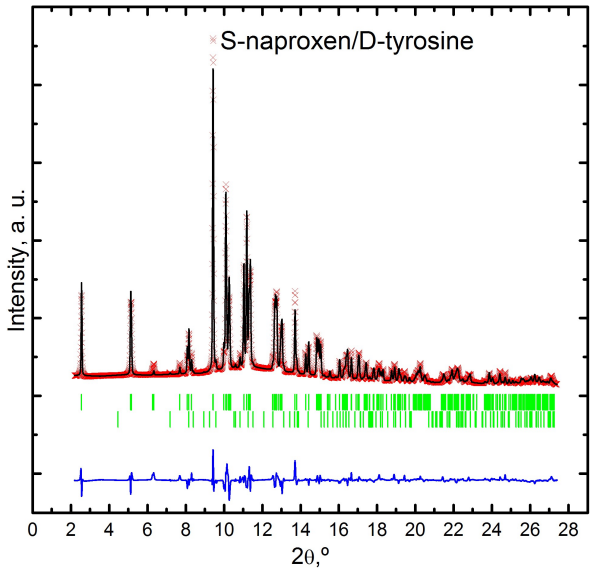


**Figure 2.1.** The Rietveld refinement plot of S-naproxen/D-tyrosine. Red crosses and the black line show experimental and calculated data, respectively; the blue line is the difference profile; and green marks indicate Bragg positions for S-naproxen/D-tyrosine cocrystal (up) and S-naproxen (bottom).

The figures were generated using Mercury;[156] the cif files were finalized using the Platon[157] and Encifer[158] programs. Table 2.1 summarizes the details of crystal data, data collection, and refinement.

**Table 2.1.** Experimental details.

| | S-naproxen/L-alanine | S-naproxen/D-alanine | S-naproxen/ D-tryptophan monohydrate | S-naproxen/ D-tyrosine |
|---|---|---|---|---|
| *Crystal data* | | | | |
| Chemical formula | $C_{14}H_{14}O_3 \cdot C_3H_7NO_2$ | $C_{14}H_{14}O_3 \cdot C_3H_7NO_2$ | $C_{14}H_{14}O_3 \cdot C_{11}H_{12}N_2O_2 \cdot H_2O$ | $C_{14}H_{14}O_3 \cdot C_9H_{11}NO_3$ |
| $M_r$ (g mol$^{-1}$) | 319.35 | 319.35 | 452.49 | 411.44 |
| Crystal system | Orthorhombic | Orthorhombic | Orthorhombic | Monoclinic |
| Space group | $P2_12_12_1$ | $P2_12_12_1$ | $P2_12_12_1$ | $P2_1$ |
| Temperature (K) | 100 | 150 | 150 | 295 |
| a (Å) | 5.05836 (11) | 5.3366 (4) | 5.88418 (16) | 9.4508 (4) |
| b (Å) | 7.1121 (3) | 6.9013 (6) | 11.3844 (3) | 5.9725 (2) |
| c (Å) | 45.2723 (17) | 44.227 (4) | 34.6863 (9) | 18.9525 (7) |
| α (°) | 90 | 90 | 90 | 90 |
| β (°) | 90 | 90 | 90 | 103.814 (2) |
| γ (°) | 90 | 90 | 90 | 90 |
| V (Å$^3$) | 1628.69 (10) | 1628.9 (2) | 2323.56 (11) | 1038.83 (7) |
| Z | 4 | 4 | 4 | 2 |
| Radiation type | Synchrotron, λ = 0.68239 Å | MoKα | MoKα | Synchrotron, λ = 0.823065 Å |
| Specimen shape, size (mm) | 0.15 × 0.13 × 0.02 | 0.10 × 0.08 × 0.03 | 0.29 × 0.09 × 0.05 | Powder |
| *Data collection* | | | | |
| Diffractometer | Pilatus 2M | MAR345 image plate | MAR345 image plate | Pilatus 2M |
| Method | Single-crystal | Single-crystal | Single-crystal | Powder |
| No. of measured, independent and observed [I>2σ(I)] reflections | 14 337, 5462, 5314 | 6347, 1712, 1424 | 15 442, 4245, 3244 | * |
| $R_{int}$ | 0.034 | 0.093 | 0.093 | |
| θ values (°) | $\theta_{max}$ = 32.358, $\theta_{min}$ = 2.595 | $\theta_{max}$ = 23.2049, $\theta_{min}$ = 2.2974 | $\theta_{max}$ = 25.2987, $\theta_{min}$ = 2.9304 | $2\theta_{min}$ = 2.2002 $2\theta_{max}$ = 27.3981 $2\theta_{step}$ = 0.005579 |
| *Refinement* | | | | |
| R factors and goodness of fit | $R[F^2 > 2\sigma(F^2)]$ = 0.050, $wR(F^2)$ = 0.135, S = 1.10 | $R[F^2 > 2\sigma(F^2)]$ = 0.083, $wR(F^2)$ = 0.225, S = 1.14 | $R[F^2 > 2\sigma(F^2)]$ = 0.046, $wR(F^2)$ = 0.099, S = 1.03 | $R_{wp}$ = 5.986, $R_{exp}$ = 0.182, $R_{Bragg}$ = 8.990 |
| No. of reflections/data points† | 5462 | 1712 | 4245 | 4519 |
| No. of parameters | 231 | 212 | 314 | 23 |
| CCDC number | 985631 | 985632 | 985633 | 985634 |

(*) In the case of powder data, estimation of the number of effective reflections is difficult due to peak overlap and highly depends on the resolution; we do not provide this number as its value is usually overestimated by crystallographic software and may lack meaning

(†) In the case of powder data: number of data points

**Search in the Cambridge Structural Database (CSD)**

We used the Cambridge Structural Database[159] (CSD 5.34, last updated May 2013) to study the statistics on amino acids and naproxen as cocrystal formers, *i.e.*, the number of entries for cocrystals that are formed between amino acids and compounds that contain hydroxyl, carboxyl or amide groups and for cocrystals formed by naproxen with various co-formers. The ConQuest 1.15[159] program was applied to search and retrieve information and the Mercury 3.3[156] software to visualize and explore structural peculiarities of found compounds.

The queries for amino acids with three types of co-formers— containing a carboxyl, hydroxyl or amide group—were built by drawing the general form of an amino acid in the zwitterionic form and a desired group for the co-former linked to any atom and setting the contact type interaction (using the ADD 3D mode) between the centroids of the carboxylate in the amino acid and of the corresponding group in the co-former.

We narrowed the search to non-halogen non-metallic compounds with the heaviest permitted atom being sulfur and with phosphorus and fluorine-containing compounds being excluded; we also omitted compounds with sulfonate and nitrate groups. The following additional filters were applied: 3D coordinates being determined, not polymeric and only organics. The hit lists were additionally checked, only cocrystals containing standard amino acids were included, and all of the irrelevant compounds (including clathrates) were crossed out. Co-formers that contained either both amide and carboxyl groups or both hydroxyl and carboxyl groups were considered carboxyl-type co-formers. The same structures obtained under different conditions were counted as one. Cocrystal solvates and hydrates were also included in the results and counted as individual compounds. The search results are summarized in Tables S2-S4 in Appendix A.

The query to the search for naproxen cocrystals was created by drawing a molecule of naproxen and applying the same filters: 3D coordinates being determined, not polymeric and only organics. Irrelevant entries were deleted from the final hit list.

## 2.3 Results and discussion

In this paper, we focus on studying S-naproxen cocrystals with both essential and nonessential amino acids and, in this context, the ability of amino acids to form cocrystals with other types of co-formers. For this reason four different reference compounds were selected (Diagram 2.1): S-naproxen, as it contains a carboxyl group and is shown to form cocrystals with amino acids;[142] levetiracetam, as this molecule is shown to be a potent cocrystal former containing two amide functionalities;[29] S-oxiracetam, another compound of the racetam family, which besides the two amide functionalities also contains a hydroxyl group and forms cocrystals as well;[134] and diprophylline, a xanthine derivative, which is structurally related to caffeine and theophylline, both of which are frequently used in cocrystallization studies.[82,160–162] Liquid-assisted grinding of these active pharmaceutical ingredients (APIs) with a series of amino acids showed that only S-naproxen was capable of forming cocrystals (see Table S1 in Appendix A). Although levetiracetam and oxiracetam have already been shown to be prone to cocrystal formation,[29,134] they do not seem to respond well to amino-acid co-formers, nor does diprophylline. Based on the structural formulas

in Diagram 2.1 and the screening results, amino acids seem to have a preference for forming cocrystals with compounds containing a carboxyl group.

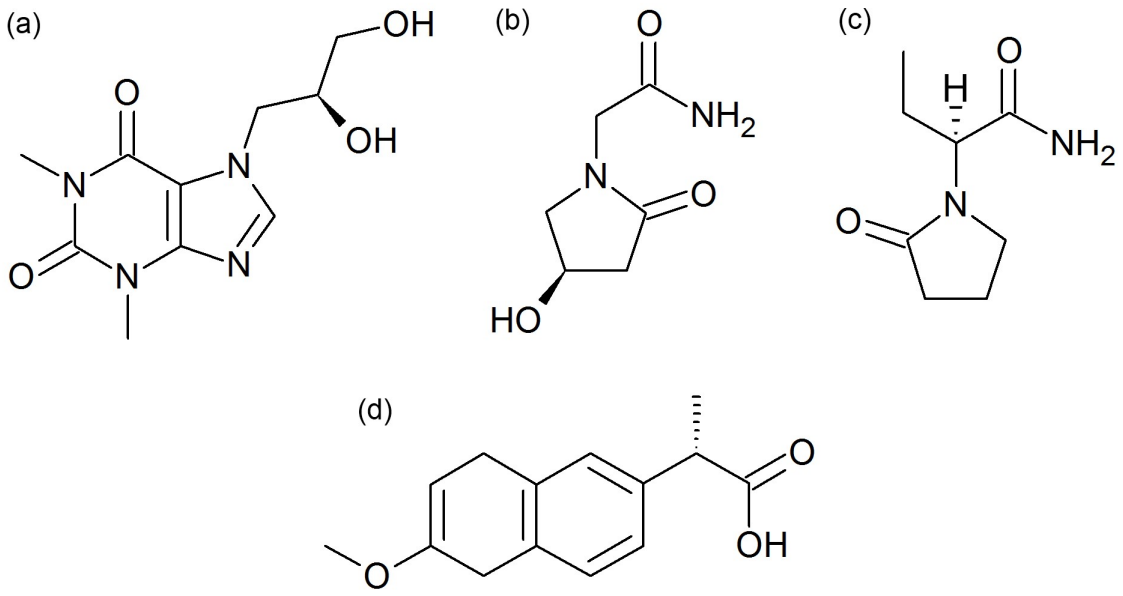


**Diagram 2.1.** Structural formulas of (a) S-diprophylline, (b) S-oxiracetam, (c) levetiracetam, and (d) S-naproxen.

Herein, we report and analyze the structures of four novel S-naproxen cocrystals: three structures that involve alanine and tyrosine, nonessential amino acids, and one structure that involves tryptophan, an essential amino acid. The structural analysis of obtained cocrystals is followed by the discussion of the results of the CSD search.

### 2.3.1 S-Naproxen/L-alanine and S-naproxen/D-alanine

The asymmetric unit of S-naproxen/L-alanine contains one molecule of S-naproxen in the neutral form and one molecule of L-alanine in the zwitterionic form, which are linked via a N1–H1···O1 hydrogen bond formed between a positively charged amino group of L-alanine and a carboxyl group of S-naproxen (Fig. 2.2g). The molecules of L-alanine form infinite head-to-tail $C^1_1$ (5) chains in the [100] direction—the structural motif, typical for crystalline amino acids,[163–165]—due to hydrogen bonding between a positively charged amino group of one amino acid (tail) and a carboxylate (head) of an adjacent molecule. Chains connect to one another via N1–H1C···O5 hydrogen bonds, forming a folded sheet parallel to the (001) plane (Fig. 2.2a, d). Each L-alanine molecule links two molecules of S-naproxen, sharing each of them with an adjacent L-alanine molecule from a neighboring head-to-tail chain: the first naproxen molecule attaches to the amino acid sheet from one side by a N1–H1A···O1 hydrogen bond, and the second naproxen molecule attaches to the sheet from the opposite side by a O2–H2···O4 hydrogen bond. Both hydrogen bonds involve the carboxyl acid group of S-naproxen and either a charged amino group or a carboxylate of L-alanine. Overall, we can describe the structure as composed of "sandwich-like" motifs; each motif consists of a folded amino acid sheet ("core") surrounded by S-naproxen molecules from both sides. Amino acids within a sheet are linked by strong N–H···O charge-assisted hydrogen bonds; no hydrogen bonding appears between S-naproxen molecules themselves. "Sandwich-like"

motifs join one another by weak interactions (therefore the structure is characterized by a 2D hydrogen bond network) (Fig. 2.2a, d).

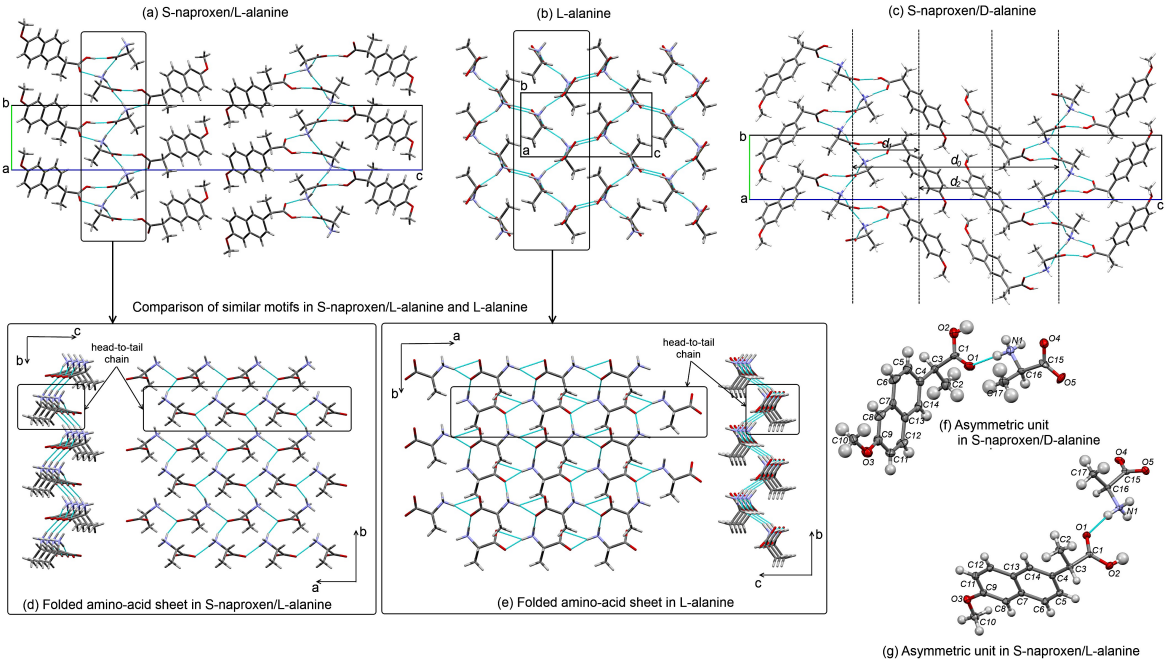


**Figure 2.2.** Crystal packing of the (a) S-naproxen/L-alanine cocrystal, (b) L-alanine (rectangular regions in (a) and (b) confine a folded amino-acid sheet), and (c) S-naproxen/D-alanine (distances $d_0$, $d_1$, and $d_2$ are explained in the text); the folded amino-acid sheet in (d) S-naproxen/L-alanine and (e) L-alanine (in bc and ab projections, naproxen molecules are omitted for clarity); and displacement ellipsoid plots showing the atom numbering scheme and 50% probability displacement ellipsoids of (f) S-naproxen/D-alanine and (g) S-naproxen/L-alanine.

In the structure of S-naproxen/D-alanine, molecules arrange in the same manner as in S-naproxen/L-alanine. D-Alanine molecules form head-to-tail chains, linked in folded sheets, each surrounded by S-naproxen molecules, thereby yielding "sandwich-like" motifs (Fig. 2.2c, f). The hydrogen bond network is similar to that observed in S-naproxen/ D-alanine with minor differences in the hydrogen bond distances (see Tables S5 and S6 in Appendix A). The distance between the planes passing through the centers of two neighboring "sandwich-like" motifs, $d_0$ (each plane was constructed by first calculating centroids for amino acid molecules from two neighboring "sandwich-like" motifs and then drawing a surface through them; all other planes were constructed in the same manner from centroids of corresponding molecules), in S-naproxen/L-alanine slightly exceeds the corresponding value observed for S-naproxen/D-alanine: 22.636 Å against 22.114 Å, respectively, and in agreement with a slightly longer c parameter in S-naproxen/L-alanine: 45.2723(17) Å against 44.227(4) Å, respectively (for distance notations see Fig. 2.2c). Within a head-to-tail chain, amino acid molecules lie closer to one another in S-naproxen/L-alanine than in S-naproxen/D-alanine [the D–A distances are 2.838(2) Å and 2.933(7) Å, respectively] and, correspondingly, the a parameter in S-naproxen/ L-alanine is shorter [5.05836(11) Å against 5.3366(4) Å]. The distance, $d_1$, between the planes passing through S-naproxen molecules and the amino acid "core" within a "sandwich-like" fragment remains similar in both structures: 7.198 Å in S-naproxen/L-alanine and 7.121 Å in S-naproxen/D-alanine; whereas the distance, $d_2$, between the layers formed by S-naproxen from two neighboring

"sandwich-like" fragments is longer in S-naproxen/L-alanine than in S-naproxen/ D-alanine: 8.240 Å against 7.198 Å, since S-naproxen molecules in S-naproxen/D-alanine pack in a more tilted manner relative to the c axis than in S-naproxen/L-alanine, allowing a closer packing. However, those packing differences hardly influence the packing indices (Kitaigorodskii type) of these two structures, which have almost the same values: 68.9% (the percent of filled space) in S-naproxen/L-alanine against 68.7% in S-naproxen/D-alanine.

The motifs that amino acid molecules form in the S-naproxen/D-alanine and S-naproxen/L-alanine cocrystals resemble those observed in the crystal structures of the individual amino acids, L-alanine and D-alanine. In L-alanine (LALNIN53[166]), we distinguish three types of N–H···O hydrogen bonds: 1) between molecules within a $C^2_1$ (6) infinite head-to-tail chain; 2) between infinite chains linked in folded sheets; and 3) between folded sheets (Fig. 2.2b, e). The L-alanine molecules in the cocrystal behave similarly, i.e., they form head-to-tail amino acid chains that form a folded sheet, like mentioned in 1) and 2). Molecules within a chain in the individual amino acids are linked through bifurcated N–H···O hydrogen bonds; whereas in S-naproxen/L-alanine and S-naproxen/ D-alanine cocrystals, the amine function forms a hydrogen bond with only one oxygen atom of the carboxylate group, while another oxygen serves as an acceptor in the O–H···O hydrogen bond with S-naproxen (Fig. 2.2d, e) This similarity in the arrangement of amino acids within a folded sheet in the cocrystals and the original amino acids highlights the important role of the strong charge-assisted amino acid hydrogen bonds.

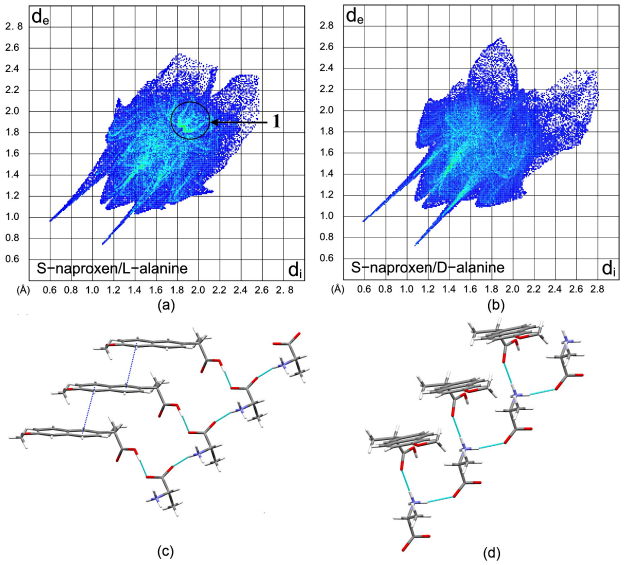


**Figure 2.3.** Two dimensional fingerprint plots of S-naproxen in (a) S-naproxen/L-alanine and (b) S-naproxen/D-alanine and structural fragments of (c) S-naproxen/L-alanine (dotted blue lines indicate π–π interactions) and (d) S-naproxen/D-alanine.

According to the fingerprint plots generated from the Hirshfeld surfaces[167] for S-naproxen in the S-naproxen/D-alanine and S-naproxen/L-alanine cocrystals, the main differences observed between these diastereomeric pairs are the presence of π–π stacking interactions (region 1 in Fig. 3a, 4.8% of all of the interactions) and a decreased percentage of C–H···π inter-actions in S-naproxen/L-alanine (19.6% against 27.4%) (Fig. 2.3). These differences agree well with the

structural peculiarities. In S-naproxen/L-alanine, S-naproxen molecules arrange so as to allow interactions between the benzene rings, whereas in S-naproxen/D-alanine, these are shifted relative to one another, increasing the percentage of C–H···π interactions but completely reducing π–π interactions (Fig. 2.3c, d).

### 2.3.2 S-Naproxen/D-tryptophan monohydrate

The asymmetric unit of S-naproxen/D-tryptophan monohydrate contains one molecule of S-naproxen in the neutral form that links one molecule of D-tryptophan in the zwitterionic form via a N1–H1A···O1 hydrogen bond and one water molecule via N1–H1B···O6 (Fig. 2.4a). The general structural motif is similar to that observed in S-naproxen/L-alanine and S-naproxen/ D-alanine cocrystals, i.e., "sandwich-like" fragments that connect to one another by weak interactions (Fig. 2.4b). D-Tryptophan molecules form $C^1_1(5)$ head-to-tail chains through N1–H1C···O5 charge-assisted hydrogen bonds between a positively charged amino group and a carboxylate in the [100] direction (Fig. 2.4b, c). In contrast to the above-described structures of S-naproxen/ L-alanine and S-naproxen/D-alanine, head-to-tail chains in S-naproxen/D-tryptophan monohydrate do not join one another directly but rather via water molecules and S-naproxen, i.e., water molecules enter the space between two neighboring head-to-tail amino acid chains, forming a N1–H1B···O6 bond with an amino acid molecule from one chain and O6–H6B···O5 with an amino acid from the neighboring chain (Fig. 2.4c). The carboxyl group of S-naproxen links three molecules of D-tryptophan: two from the same chain by N1–H1A···O1 (as an acceptor) and O2–H2···O4 (as a donor) hydrogen bonds and one from the neighboring chain via a N2–H2D···O1 bond with the cyclic N–H group. Thus, the "sandwich-like" motif in S-naproxen/D-tryptophan monohydrate consists of an amino-acid layer, parallel to the (001) plane and composed of infinite head-to-tail chains linked via water and S-naproxen molecules grafted on it from both sides (Fig. 2.4b).

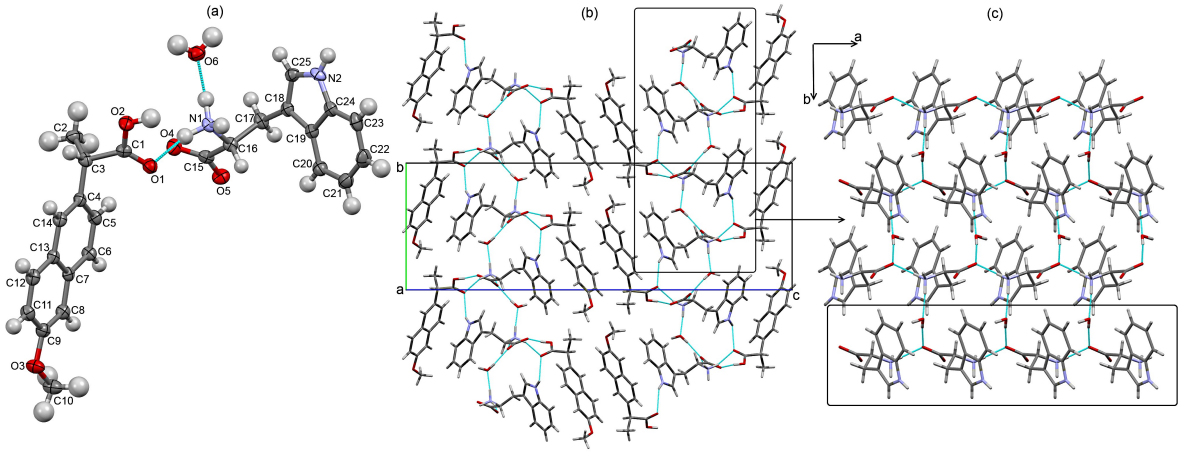


**Figure 2.4.** (a) The displacement ellipsoid plot showing the atom numbering scheme and 50% probability displacement ellipsoids of S-naproxen/ D-tryptophan monohydrate; (b) crystal packing of S-naproxen/D-tryptophan monohydrate, the rectangular region confines the structural fragment formed by amino-acid head-to-tail chains and water molecules; the same fragment is shown in (c) in the ab projection (the rectangular region in (c) contours one of the head-to-tail chains).

We failed to find a structure for D-tryptophan (the CSD reports the structure of D-tryptophan, DEZHIZ,[168] but only the unit cell parameters are available without atomic coordinates). The

reported structure of L-tryptophan[169] shows a rather complex head-to-tail N–H···O hydrogen bonding ($Z'$ = 16). Tryptophan in the cocrystal keeps its ability to form infinite head-to-tail chains.

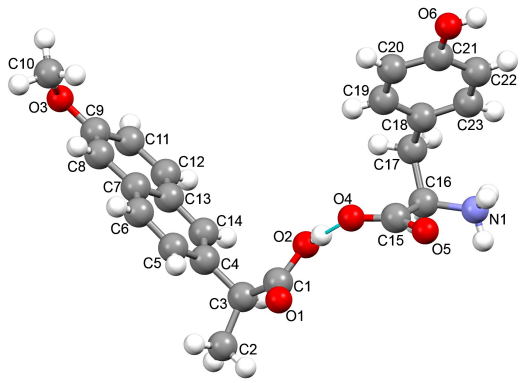


**Figure 2.5.** The asymmetric unit cell in S-naproxen/D-tyrosine (numbering scheme).

### 2.3.3 S-Naproxen/D-tyrosine

The asymmetric unit of S-naproxen/D-tyrosine contains one molecule of S-naproxen in the neutral form that links one molecule of D-tyrosine in the zwitterionic form via a O2–H2···O4 hydrogen bond (Fig. 2.5). We clearly see the essential role of charge-assisted hydrogen bonds between amino acid molecules, i.e., D-tyrosine in the cocrystal tends to form infinite $C^1_1$ (5) head-to-tail chains in the [010] direction with molecules linked via N1–H1C···O4 hydrogen bonds; these chains look exactly the same as in individual D-tyrosine (Fig. 2.6). Owing to the presence of a hydroxyl group attached to the benzene ring, two complementary head-to-tail chains link one another through O6–H6A···O5 and N1–H1B···O6 bonds, forming a "tube" in the [010] direction (Fig. 2.6c, d).

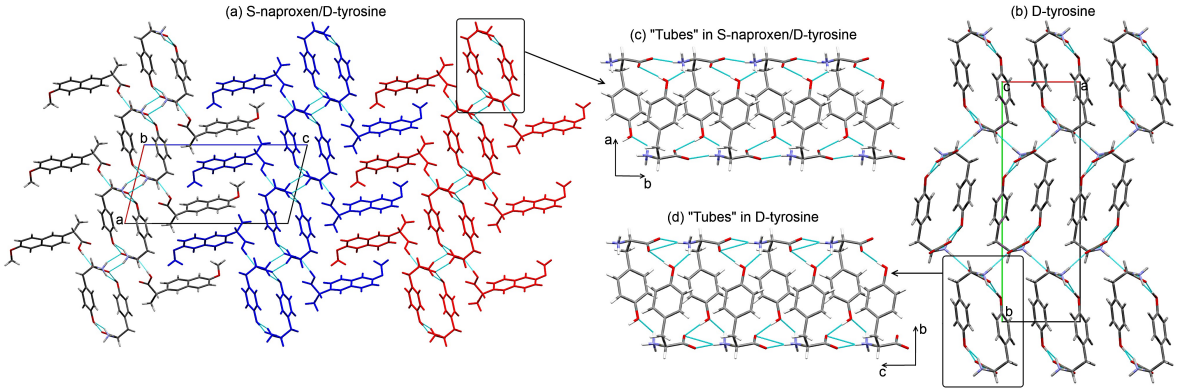


**Figure 2.6.** (a) Structural fragments of S-naproxen/D-tyrosine (red and blue color – two neighboring "sandwich-like" motifs stacked to one another in a "zip-like" manner); (b) structural fragments of D-tyrosine (rectangular regions in (a) and (b) highlight a similar motif, "tubes", formed by amino acid molecules in the cocrystal and the individual amino acid); (c) the "tube" motif in S-naproxen/D-tyrosine along the b axis; and (d) the "tube" motif in D-tyrosine along the c axis.

Each amino acid in the tube connects one S-naproxen molecule by O2–H2···O4 hydrogen bonds. The tubes stack on one another via N1–H1A···O5 hydrogen bonds along the c axis, thereby forming an amino acid "core" that attaches S-naproxen otherwise not linked by hydrogen bonds (Fig. 2.6a). Thus, the structure of S-naproxen/D-tyrosine can be still considered in terms of

"sandwich-like" motifs, which, in contrast to the above-discussed structures, connect to one another in a "zip-like" manner by weak interactions (see Fig. 2.6a, two neigh-boring "sandwich-like" fragments are colored red and blue).

### 2.3.4 Comparison with known structures from the CSD

So far we showed that amino acid co-formers have a tendency to form cocrystals with compounds that contain a carboxyl acid group, and furthermore, we showed that even within these compounds, the main hydrogen bonding patterns found in the amino acid co-former are maintained, with the neutral API grafted onto these elements.

To verify these observations with respect to the literature, a systematic Cambridge Structural Database search was performed. The CSD reports only two naproxen-amino acid compounds; in both cases, the amino acid is S-arginine which cocrystallizes with S- and R-naproxen (the refcodes are JASHOB[170] and QANPEB,[170] respectively); the compounds formed are salts: a proton moves from the carboxyl group of naproxen to the amino group of S-arginine. Thus, naproxen becomes negatively charged, whereas S-arginine becomes positively charged. Tilborg et al. described four other cocrystals: S-naproxen/D-proline, S-naproxen/L-proline, L-proline/RS-naproxen, and DL-proline/RS-naproxen (FEVZOX, FEVZUD, BEXGUI, and BEYTUW, respectively), in which no proton transfer occurs between the co-formers – S-naproxen molecules are in the neutral form, and proline is zwitterionic.[32] To our knowledge, no other cocrystals formed by naproxen and amino acids have been reported. The structural motifs observed in all of the above mentioned structures containing proline or arginine are similar to those found in our cocrystals: "sandwich-like" fragments which link one another by weak interactions and are composed of an amino-acid "core" with naproxen molecules attached from both sides.

Although S-arginine in the aforementioned salts preserves head-to-tail linking, the molecules form dimers rather than infinite head-to-tail chains found in S-arginine (TAQBIY[171]).

In S-naproxen/L-proline and S-naproxen/D-proline cocrystals, proline molecules form infinite head-to-tail chains, which connect to one another in a zig-zag manner forming a folded sheet to which naproxen molecules attach from both sides, yielding "sandwich-like" motifs, therefore showing head-to-tail linking similar to the individual L-proline crystals. The other two published cocrystals from the naproxen–proline family are hydrates and show slightly different hydrogen bonding patterns between amino acids, with water molecules playing an essential role. In L-proline/RS-naproxen monohydrate, water "glues" separate amino acid molecules not directly linked by hydrogen bonding. In DL-proline/RS-naproxen, water chains join infinite amino acid head-to-tail zig-zag chains to one another. Those kinds of interactions with water are typical for proline—in its individual crystal hydrates, water serves as a "glue" between separate head-to-tail chains.

Thus, from the above-considered crystal structures of cocrystals, amino acids seem to form a "platform" which then "guides" the arrangement of S-naproxen molecules. Although this simplified situation seems to hold for naproxen, this is no longer the case when considering other amino-acid cocrystals.

To understand how the discussed amino acids behave with respect to other compounds, we performed a systematic CSD search (excluding all halogen-containing compounds). We failed to find any cocrystals for D-tyrosine, so we considered only cocrystals formed by tryptophan, alanine, arginine, and proline. Multicomponent systems show greater structural complexity than compounds in their individual forms, since different types of molecules in one crystal lattice mutually influence one another (conformations, torsion angles, packing, etc.). This brings along difficulties in identifying similar structural motifs. Thus, when comparing several cocrystals/salts, we rather mention similar structural trends than identical structural motifs. We analyzed 51 cocrystals/salts formed by alanine, tryptophan, proline, and arginine (formed by alanine: CAPKEL,[172] AHERAG,[173] BEYVAD,[174] BOQTEG,[175] IMEGIR,[176] IROVAM,[177] NELPUP,[178] PAVYIW,[179] XUGMER,[180] and YEJYIV;[181] by tryptophan: HAGBOG,[182] LAQXIM,[183] NUQHIR,[184] TPTPCM,[185] TRYPTB, and UGITAG;[186] by proline: NASGIG,[187] NAZGOM,[187] NAZGUS,[187] NAZHAZ,[187] EXIBOC,[188] GIVROS,[189] IHUMAZ,[190] LABZUJ,[191] OLIZAL,[192] POCKHAY10,[193] QIJYIR,[173] VESCUS,[194] ZEZHIV,[195] and NISVOA01;[196] and by arginine: ADAVIK,[197] EWINAZ,[198] GOLFOC,[199] JASHOB,[170] LARASC20,[200] MUPNUG,[201] MUPPAO,[201] NOSXAU,[202] NOSXEY,[202] OFIWUW,[203] ORUXEF,[204] QAMXEI,[205] QAMXIM,[205] QANPEB,[170] RIFXAG,[206] RIFXEK,[206] TEFLUL,[207] TEFMAS,[207] TIDCAK,[208] YOWDET,[209] and YOWDIX[209]).

The comparison of structural motifs found in those structures reveals that amino acids tend to form infinite head-to-tail chains owing to N–H···O charge-assisted hydrogen bonding between their amino and carboxylate groups; this motif occurs in the majority of analyzed structures; chains do not necessarily connect to one another—they can be linked through an intermediate, i.e., co-former or solvent molecules (when we deal with cocrystal hydrates or solvates). However, in some structures, amino acid molecules form only dimers or form hydrogen bonds only with co-former molecules but not with each other. A number of structures show "sandwich-like" motifs, as we observed for the naproxen cocrystals, but the "core" formed by amino acid molecules is not necessarily composed of similar motifs as those observed in individual amino acids. It would therefore not be entirely accurate to state that the interactions between amino acids remain identical in the cocrystals, as the nature of the second cocrystal former can significantly affect the cocrystallization process.

We suggest that the first factor responsible for the formation of a cocrystal with an amino acid co-former is the strength of the hydrogen bonds formed between a co-former and an amino acid; if these bonds are competitive in strength with strong charge-assisted N–H···O bonds between zwitter-ionic molecules, one observes unlinked amino acid molecules that form hydrogen bonds only with a co-former but not with each other. In this context, the presence of functional groups in a co-former prone to hydrogen bonding has a crucial role on the final cocrystal structure. The second factor is the size of the co-former. If the co-former is bulky, it will influence the packing significantly, and hereby, affect the structural arrangement of the amino acids.

Overall, if a compound forms weak hydrogen bonds with a selected amino acid, then one can expect motifs that resemble those found in individual amino acid crystals, but if the compound molecules themselves form strong hydrogen bonds with amino acid molecules, such similar patterns might not be seen. Thus, as we saw in the case of naproxen, only one functional group

allows formation of hydrogen bonds, which is not enough to counterbalance strong charge-assisted hydrogen bonds between amino acid molecules, and these latter keep forming hydrogen bond motifs, similar to those observed in individual amino acids. However, the arrangement of naproxen molecules around those amino-acid motifs is determined by bulky naproxen which tends to pack in a stacking manner on each side of the amino acid "core".

This conclusion agrees well with the results of screening. We found cocrystals only for naproxen, which contains a carboxyl group prone to hydrogen bonding, but not for the other APIs that contain hydroxyl and/or amide groups with weaker hydrogen bonding potential. The search of the Cambridge Structural Database showed that amino acids form many cocrystals with compounds that contain a carboxyl group but only a few with compounds that contain only a hydroxyl or amide group (95, 21, and 2 entries, respectively; see Tables S2-S4 in Appendix A), which also confirms the above-mentioned key factors in cocrystal formation.

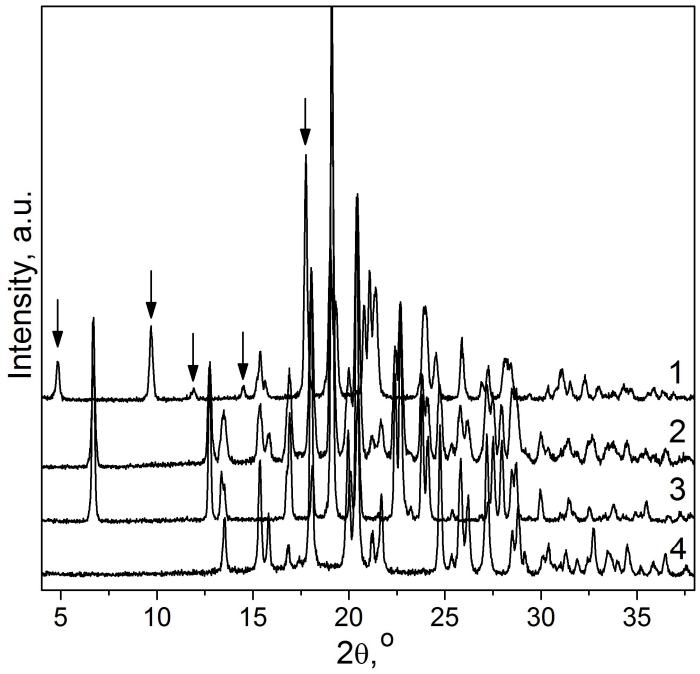


**Figure 2.7.** Diffraction patterns (CuKα radiation) of (1) S-naproxen ground with D-tyrosine (liquid-assisted grinding shows the formation of a new phase, several new peaks which are indicated with arrows), (2) S-naproxen ground with L-tyrosine, (3) S-naproxen, and (4) L- or D-tyrosine.

Among the 21 compounds formed by amino acids with hydroxyl-containing compounds (see Table S2 in Appendix A), only three types of co-formers were found: picric acid, squaric acid, and (2S,3R,4R,5S,6R)-2-(3-(4-ethylbenzyl)-phenyl)-6-hydroxymethyl-tetrahydro-2H-pyran-3,4,5-triol; in the first two cases, the compounds were salts (i.e., proton transfer occurred between an amino acid and a co-former) and for the latter, cocrystals (i.e., no proton transfer). Searching for amide-containing co-formers gave only two entries (see Table S4 in Appendix A), both contain nitrogen in the cycle. In the group of carboxyl-containing compounds (see Table S3 in Appendix A), the most studied co-formers were oxalic, maleic, tartaric, and mandelic acids (23, 14, 11, and

9 entries, respectively). All of the compounds with oxalic and maleic acids were salts, whereas among the rest of compound, both salts and cocrystals existed.

The results of the CSD search highlight the complexity of multicomponent systems, illustrating well the ability of the studied molecules to form both cocrystals and salts, which is referred to in the literature as the salt–cocrystal continuum[23,24] (see Tables S2-S4 in Appendix A).

Finally, we would like to note the importance of chirality in cocrystal formation. A selected compound of a particular chirality might form a cocrystal with one chiral co-former but not with its mirror image. We observed such an enantiospecific behavior in the S-naproxen/tyrosine system, i.e., S-naproxen cocrystallized with D- but not with L-tyrosine. Fig. 2.7 shows that, after grinding, S-naproxen and D-tyrosine yielded a new phase, whereas S-naproxen and L-tyrosine remained a physical mixture. This observation can be used to construct an effective resolution of racemic naproxen using enantiospecific cocrystallization in solution.

## 2.4 Conclusions

Zwitterionic co-formers are characterized by the presence of strong charge-assisted hydrogen bonds, which lead to great structural complexity in cocrystals, highlighting the relative importance of all hydrogen bonding interactions, and especially, between an amino acid co-former and a target compound—the latter has to be strong enough to counterbalance potentially strong charge-assisted hydrogen bonds that exist in the crystal lattices of individual amino acids. Due to this fact, amino acids are effective in the case of carboxyl acids but fail when dealing with other studied compounds. As we saw from the examples with naproxen, amino acids can pre-serve motifs similar to those observed in their individual crystals. This observation can be helpful when solving structures from powder data or performing theoretical simulations.

Although amino acids seem to form diastereomeric cocrystal pairs more often, the S-naproxen/tyrosine system behaves enantiospecifically. Thus, since amino acids play a crucial role in the body, the possibility of an enantiospecific behavior is an interesting issue to bear in mind when dealing with biological aspects. Another promising application of enantiospecific systems is enantiomeric resolution of racemic drugs in pharmaceutical industry based on cocrystal engineering principles.[30] Moreover, to our knowledge, this cocrystal is the very first reported cocrystal found for tyrosine. We successfully solved its structure from synchrotron X-ray powder diffraction data, thus providing another example of how powerful structure determination techniques from powder data are.

# CHAPTER 3 | Opening Pandora's Box: Chirality, Polymorphism, and Stoichiometric Diversity in Flurbiprofen/Proline Cocrystals

*This chapter is based on the article to be published by Natalia Tumanova, Nikolay Tumanov, Koen Robeyns, Franziska Fischer, Luca Fusaro, Fabrice Morelle, Voraksmy Ban, Geoffroy Hautier, Franziska Emmerling, Yaroslav Filinchuk, Johan Wouters, Tom Leyssens, 2017.*


## ABSTRACT

Cocrystallizing various combinations of enantiopure and racemic forms of flurbiprofen and proline, we discovered extreme complexity. Depending on the chirality and cocrystallization conditions, the system exhibits polymorphism (up to 4 polymorphs for e.g. RS-flurbiprofen/L-proline), is prone to forming cocrystal solvates (R-flurbiprofen/L-proline) and gives occurrence to stoichiometrically diverse cocrystals (besides 1 : 1 stoichiometry, 2 : 1 as well as exotic 1 : 2 and even 1 : 3 stoichiometries are observed). We focused on liquid-assisted grinding to produce cocrystals, including the discussion on the solvents' role in the process. The nature of solvent was found to significantly affect the outcome, resulting in differing reaction rates and in some cases reaction pathways. Analyzing the results of ball-milling and *in-situ* ball-milling, we established a stepwise mechanism for the formation of several 1 : 1 cocrystals through the 2 : 1 phase. PXRD data collected *in-situ* upon varying temperature revealed additional phases emerging at higher temperatures and one phase crossover. Exploring structural peculiarities of obtained cocrystals and analyzing their energies calculated by DFT-D3, we gained additional insight into the reaction pathway of cocrystal formation and whether there is a correlation between the energies and chirality.

## 3.1 Inroduction

Multicomponent crystalline systems have been extensively studied for many years,[8] however the term "cocrystal" has been introduced only recently.[9,11,16,24,28] Cocrystals are of the most interest to pharmaceutical industry as they allow varying pharmacological properties of drugs, e. g., improving bioavailability, dissolution rate, hygroscopicity, stability, etc.,[1–3] without modifying the chemical nature of the active pharmaceutical ingredient (API). In this context most of the studies to date have been dedicated to cocrystals as alternative drug formulations[19,71,122–127]. Moreover, owing to some specific properties, cocrystals can also be used in other crystallization applications, for instance, as a purification tool[35,36,39,136] or for chiral resolution[4–6,41,210].

Chirality is common among APIs: which enantiomer is used in a drug can be crucial for its therapeutic effect[26]. Since a substantial part of drugs are chiral, the question how they respond to cocrystallization with chiral or nonchiral co-formers is of great interest to the pharmaceutical industry. Friscic *et al.* showed that caffeine and theophylline behave differently when cocrystallized with DL- and D-tartaric acid.[137] They further extended this work investigating the effects of chirality on physical properties of cocrystals, including the melting point, by combining crystallographic and thermochemical studies for cocrystals with chiral and racemic co-formers.[211] Eddleston *et al.* applied cocrystallization via solid-state grinding to study the possibility of enantiomeric resolution in malic acid/tartaric acid system.[212] Takata *et al.* noted for the first time an enantiospecific behavior for stanolone/S-tartaric acid and later Thorey *et al.* for (R,R)-cyclohexanediol/R-tartaric acid cocrystal.[139,140] Springuel *et al.* showed that levetiracetam cocrystalllizes with S-mandelic or S-tartaric acid, but not with their R-forms;[22,28] they have also established enantiospecific behavior to be quite common among chiral cocrystals.[29] Zwitterionic co-formers, on the other hand, seem to have preference to form diastereomeric pairs of cocrystals: for example, S-naproxen was found to form diastereomeric cocrystals with alanine, proline, and tryptophan amino acids; and only one enantiospecific case was found for D-tyrosine.[32,142,144] Ibuprofen when cocrystallized with lysine or arginine amino acids forms diastereomeric salts which have been applied at industrial scale[143].

This work profoundly studies the flurbiprofen/proline system, through cocrystallizing various combinations of enantiopure as well as racemic forms of the initial compounds. Flurbiprofen (see Diagram 3.1) is a non-steroidal anti-inflammatory drug used to treat acute or chronic painful conditions, *i.e.* rheumatic arthritis, osteoarthritis, alkylosing spondylitis, as well as for dental pain.[27] Cocrystallization with nicotinamide has already been applied to flurbiprofen with the purpose of improving its mechanical properties, dissolution performance and hygroscopicity[135]. Amino acids are natural to the body and their use in pharmaceutical cocrystals is less dangerous in comparison with other co-formers; moreover, cocrystallization with amino acids may even be beneficial: in the crystalline form, they are zwitterionic and form strong charge-assisted hydrogen bonding networks,[163–165,213] which when combined with an API may increase the stability and the melting point of the latter, or may improve its solubility and dissolution rate.

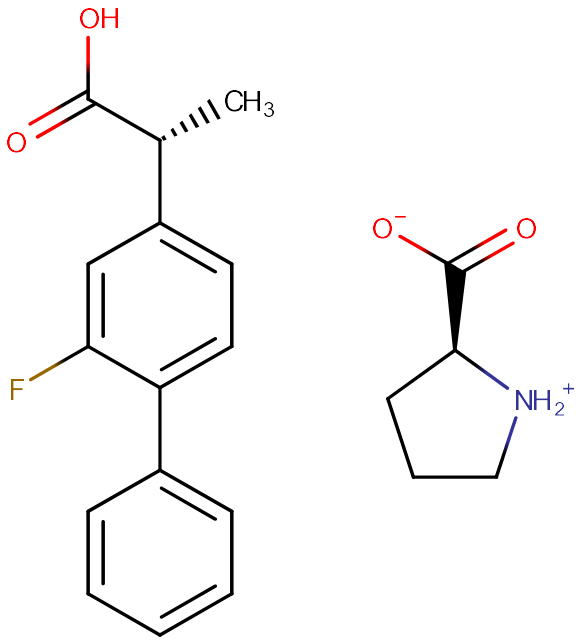


**Diagram 3.1.** Chemical structures of flurbiprofen and proline molecules.

Proline (see Diagram 3.1) is widely used in various cocrystal applications. Recently D- and L-proline have been successfully applied to alter the solubility and pharmacokinetics of a series of flavonoids[214,215]. Cocrystals of dapagliflozin, a drug used to treat type II diabetes, with proline have been patented[216] (in the patent cocrystals are referred as crystalline complexes). There are examples of proline cocrystals with naproxen, a non-steroidal anti-inflammatory drug[142] and with β-C-arylglucoside, another promising compound to treat diabetes[187]. L-proline has found application in chiral resolution through diastereomeric salt or cocrystal formation[189,196,217] (again in these refs. cocrystals are referred as crystalline complexes). It was also studied in relation to conformational polymorphism[190] and even applied to create an amino acid derived semiconductor[192]. Proline was found to easily form cocrystals or salts with carboxylic acids[188,191,193,195,218–221], for instance its tartrate may be considered as a material for nonlinear optical applications[222], as well as boronic acids[223,224]. Thus, proline is a very promising co-former and studying how it responds to cocrystallization represents an interesting topic to date.

In this contribution, we discuss the extreme complexity discovered for the flurbiprofen/proline system: depending on the enantiopure or racemic forms used and the cocrystallization conditions, the system exhibits polymorphism (up to 4 polymorphs for only one combination), is prone to forming cocrystal solvates and stoichiometrically diverse cocrystals (1 : 1, 2 : 1, 1 : 2, and even 1 : 3 flurbiprofen : proline). Analyzing the results of ball-milling, *in-situ* ball-milling, crystallization from solution, X-ray diffraction upon varying temperature, we established conditions that favor formation of the found cocrystals; the focus was on liquid-assisted grinding and the solvent's role in cocrystallization. Exploring structural peculiarities of cocrystals and analyzing their energies calculated by DFT-D3, we intended to gain additional insight into the cocrystallization aspects of this system.

## 3.2 Experimental section

All compounds used in this work were purchased from Sigma Aldrich and used without further purification. Commercial racemic flurbiprofen was identified as the *P*-1 polymorph, CCDC REF FLUBIP[225].

**Laboratory liquid-assisted grinding.** R-flurbiprofen was screened with a series of amino acids by liquid-assisted grinding; the compounds were mixed in a 1 : 1 ratio (~50 mg of powder in total, 5 μL of MeOH) in 2 mL Eppendorf tubes and put into a Retsch MM400 mixer mill for 60 or 90 min at a frequency of 30 Hz. Table S1 in supplementary materials lists all the amino acids used. Positive hits were found only for L- and D-proline.

Further liquid-assisted grinding with five different solvents, methanol, ethanol, acetonitrile, isopropanol and water (~50-100 mg of powder in total, 3-10 μL of solvent, 25-90 min, 30 Hz, 1 : 1, 2 : 1, 1 : 2 ratios, 1 : 3 ratio was additionally used for the R-flurbiprofen/L-proline combination) was performed for various combinations of enantiopure and racemic flurbiprofen with as well enantiopure and racemic proline.

Resulting powders were analyzed by powder X-ray diffraction (CuKα radiation, λ = 1.5418 Å) using a Siemens D5000 diffractometer (2θ was scanned from 2 to 50° with a step of 0.02°) or a X'pert PRO PANalytical diffractometer (2θ scanned from 4.022 to 49.990° with a step of 0.017°). Diffraction patterns of pure phases were simulated using the Mercury[156] software; the structures of L-proline (CCDC REF PROLIN[226]), L-proline monohydrate (CCDC REF RUWGEV[227]), DL-proline (CCDC REF QANRUT[228] and QANRUT01[229]), DL-proline monohydrate (CCDC REF DLPROM01[230]), and RS-flurbiprofen (CCDC REF FLUBIP[225] (*P*-1) and FLUBIP02[231] ($P2_1/n$)) were taken from the Cambridge Structural Database[159].

Diffraction data of selected powder samples were measured using synchrotron radiation source. Some of these data were used for structure determination. Tables S3-S8 in Appendix B summarize liquid-assisted grinding experiments and their outcomes as well as information on how the samples were analyzed.

**Synchrotron X-ray diffraction data collection *in-situ* under variable temperature.** Selected powders obtained by liquid-assisted grinding were packed into 0.5 mm glass capillaries and measured upon heating at a rate of 2 °C/min. All powder diffraction data, except *in-situ* experiment for 1 : 3 R-flurbiprofen/L-proline sample, were collected during heating using synchrotron radiation source: MS-X04SA beam line at the Swiss Light Source (SLS) (PSI, Switzerland) equipped with a 1D microstrip detector MYTHEN II. The measurements were performed at λ = 0.77494, 0.77663, 0.62173, 0.708 Å with a step of 0.0036°. The wavelength was calibrated using a standard NIST 640d Si sample. Selected diffraction patterns were used for structure determination from X-ray powder data (see below for further details). The 1 : 3 R-flurbiprofen/L-proline sample (sample *10* in Table S3) was measured *in-situ* upon heating (2 °C/min) at the Swiss-Norwegian beamline BM1A at the European Synchrotron Radiation Facility (ESRF) (Grenoble, France), using a PILATUS 2M hybrid pixel detector at a wavelength of 0.7458 Å. The information on samples analyzed upon heating can be found in Tables S3-S8 in Appendix B.

***In-situ* ball-milling synchrotron X-ray diffraction data collection.** *In-situ* ball-milling X-ray diffraction experiments were performed at the μSpot beamline (BESSY II, Helmholtz Centre Berlin for Materials and Energy, Germany) using a Pulverisette 23 (Fritsch, Germany) ball mill and Perspex jars; the frequency was 50 Hz. Compounds were mixed and the solvent was added right before the experiment, except one sample for RS-flurbiprofen/L-proline which, due to technical issues, was in contact with solvent for 2 h before being ground. Details for each experiment (duration of milling, amount of solvent, amounts of initial compounds) are summarized in Table S2. A beam diameter of 100 μm at a photon flux of $1 \times 10^9$ $s^{-1}$ at a ring current of 100 mA was used. The experiments were performed at a wavelength of 1.000 Å using a double crystal monochromator Si (111). The spot size on the sample was 200 μm. Scattered intensities were collected with a two-dimensional X-ray detector (MarMosaic, CCD 3072 × 3072 pixels, pixel size 73 μm)[232]. Measurements were carried out every 30 s with a delay time of 3 or 4 s between two measurements. The occasionally observed doubling of reflections is caused by diffraction of two different areas in the reaction jar, due to differences in the distance between the detector and the sample. Obtained two-dimensional diffraction images were integrated (2θ vs. intensity) using the program Fit2D[153]. Diffraction patterns were background corrected and plotted as 2D film representation using the Powder3D program[233].

**Production of single crystals.**

*R-flurbiprofen* single crystals were obtained from ethanol solution by evaporation crystallization (~20 mg were dissolved in 1 mL of solvent and the solution was slowly evaporated at room temperature).

*R-flurbiprofen/L-proline 1 : 2 (1 : 2 R/L)* single crystals grew directly in the Eppendorf tube containing the sample obtained by isopropanol-assisted grinding (1 : 3 ratio), providing the tube was kept closed and some traces of solvent still left.

*R-flurbiprofen/L-proline 2 : 1 (2 : 1 R/L)* single crystals were obtained from a methanol solution through evaporation, using powder obtained by methanol-assisted grinding of R-flurbiprofen and L-proline taken in the 2 : 1 ratio (~20 mg were dissolved in 1 mL of solvent and the solution was slowly evaporated at room temperature).

*R-flurbiprofen/L-proline/methanol solvate 1 : 1 (1 : 1 R/L/MeOH)* single crystals were grown from a methanol solution on cooling, using powder obtained by methanol-assisted grinding of R-flurbiprofen and L-proline taken in the 1 : 1 ratio (~20 mg were dissolved in 1 mL of solvent and cooled to -15 °C).

*R-flurbiprofen/L-proline/ethanol solvate 1 : 1 (1 : 1 R/L/EtOH)* single crystals were grown from an ethanol solution on cooling, using powder obtained by methanol-assisted grinding of R-flurbiprofen and L-proline taken in the 1 : 1 ratio (~20 mg were dissolved in 1 mL of solvent and cooled to -15 °C). As will be discussed below, methanol-assisted grinding results in the 1 : 1 R/L/MeOH. However, methanol can evaporate from the structure over time. The powder sample used for crystallization in this case was prepared several weeks before and therefore the amount of methanol left might have been negligible in comparison with ethanol molecules in solution. This would explain why we obtained the ethanol solvate from the initial methanol solvate sample.

*R-flurbiprofen/D-proline 1 : 1 (1 : 1 R/D)* single crystals were grown from an ethanol solution using powder obtained by methanol-assisted grinding in the 1 : 1 ratio (~20 mg were dissolved in 1 mL of solvent and cooled to -15 °C).

*R-flurbiprofen/D-proline 2 : 1 (2 : 1 R/D)* single crystals were grown from an ethanol solution by evaporation crystallization, using powder obtained by 2 : 1 isopropanol-assisted grinding (~20 mg were dissolved in 1.5 mL of solution).

*R-flurbiprofen/DL-proline 2 : 1 (2 : 1 R/DL)* single crystals were grown from a methanol solution. 65 mg of R-flurbiprofen and 15 mg of DL-proline were dissolved in 5 mL of solvent and cooled to -15 °C.

*RS-flurbiprofen/D-proline 1 : 1 pol II (1 : 1 RS/L pol II)*, which is a mirror image of RS-flurbiprofen/L-proline 1 : 1 pol II (1 : 1 RS/L pol II), single crystals grew directly in the Eppendorf tube containing the sample obtained by ethanol-assisted grinding (1 : 1 ratio), providing the tube was kept closed and some traces of solvent still left.

*RS-flurbiprofen/L-proline 1 : 1 pol IV (1 : 1 RS/L pol IV)* single crystals were grown from an ethanol solution. 65 mg of RS-flurbiprofen and 15 mg of L-proline were dissolved in 5 mL of solvent and cooled to room temperature.

*RS-flurbiprofen/L-proline 2 : 1 (2 : 1 RS/L)* single crystals were grown from a methanol solution. 35 mg of RS-flurbiprofen and 55 mg of L-proline were dissolved in 5 mL of solvent at 60 °C and cooled to -10 °C.

*RS-flurbiprofen/DL-proline 1 : 1 (1 : 1 RS/DL)* was crystallized from an ethanol solution on cooling, using powder obtained by 1 : 1 acetonitrile-assisted grinding. ~20 mg of material were dissolved in 1.5 mL of solvent at 60 °C and cooled to room temperature.

*L-proline pol I* was recrystallized from absolute ethanol solution upon cooling. ~40 mg of L-proline were dissolved in 1.5 mL of solvent at 60 °C and cooled to 0 °C.

**Single-crystal X-ray diffraction structure determination.** The structures of *R-flurbiprofen*, *1 : 1 R/D*, *1 : 1 R/L/MeOH solvate, 1 : 1 R/L/EtOH*, *2 : 1 R/L* at 150(1) K and *1 : 1 RS/DL* at room temperature were solved from single-crystal X-ray diffraction data, collected on a MAR345 image plate detector using Mo*K*α radiation (Rigaku UltraX 18 rotation anode, Xenocs Fox3D focusing multilayer mirror). The data were integrated using the CrysAlisPro[150] software. The multi-scan absorption correction procedure implemented in the CrysAlisPro software was applied. The structures were solved by direct methods using the SHELXS-97[151] or by the dual-space algorithm implemented in SHELXT[234] program and refined by full-matrix least squares on $|F|^2$ using SHELXL-2016/4 or SHELXL-2014/7[235] and the shelXLe[152] shell. Non-hydrogen atoms were refined anisotropically; and hydrogen atoms were located from the difference Fourier map but placed on calculated positions in riding mode with equivalent isotropic temperature factors fixed at 1.2 times $U_{eq}$ of the parent atoms and 1.5 times $U_{eq}$ for methyl groups.

The structures of *2 : 1 R/DL* and *L-proline pol I* at 150(1) K (L-proline was also measured at room temperature), and 1 : 2 R/L, *1 : 1 R/L/MeOH solvate, 2 : 1 RS/L*, *1 : 1 RS/L* pol II, *1 : 1 RS/L* pol IV and *2 : 1 R/D* at room temperature were solved from single-crystal X-ray diffraction

data collected using an Oxford Diffraction Gemini Ultra R diffractometer (Cu*K*α radiation). The structure solution procedure was the same as for the structures mentioned in the previous paragraph.

Disorder was observed in almost all structures: fluorine in the benzene ring of flurbiprofen was disordered over two sites due to the rotation around C-C bond between the benzene rings; some proline molecules were disordered as well due to proline's conformational flexibility. Figures illustrating disorder in proline molecules are given in supplementary materials (Figs. S65-S69 in Appendix B).

The crystal data, data collection, and refinement details are summarized in Table 1.

The figures were generated using the Mercury program[156]; cif files were finalized using the Encifer[158] program.

**Table 3.1.** Crystal data, data collection, and refinement details.

| | 1 : 1 R/L pol I | 1 : 1 R/L pol II | 2 : 1 R/L | 1 : 3 R/L |
|---|---|---|---|---|
| *Crystal data* | | | | |
| Chemical formula | $C_{15}H_{13}FO_2 \cdot C_5H_9NO_2$ | $C_{15}H_{13}FO_2 \cdot C_5H_9NO_2$ | $2(C_{15}H_{13}FO_2) \cdot C_5H_9NO_2$ | $C_{15}H_{13}FO_2 \cdot 3(C_5H_9NO_2)$ |
| $M_r$ | 359.39 | 359.39 | 603.64 | 589.65 |
| Crystal system, space group | Triclinic, $P1$ | Monoclinic, $P2_1$ | Monoclinic, $P2_1$ | Orthorhombic, $P2_12_12_1$ |
| Temperature (K) | 345 | 375 | 150 | 300 |
| $a$, $b$, $c$ (Å) | 5.81938(17), 6.3341(2), 26.6334(10) | 5.8702(8), 23.954(4), 13.253(2) | 5.7851(4), 44.639(2), 6.1901(3) | 5.6866(7), 19.677(3), 26.317(4) |
| α, β, γ (°) | 88.0448(19), 88.312(2), 73.664(2) | 90, 96.287(10), 90 | 90, 110.815(6), 90 | 90, 90, 90 |
| $V$ (Å$^3$) | 941.33(5) | 1852.3(5) | 1494.18(15) | 2944.7(7) |
| Z | 2 | 4 | 2 | 4 |
| $D_x$ (Mg m$^{-3}$) | 1.268 | 1.289 | 1.342 | 1.330 |
| Melting point (°C) | n/a | n/a | 158(1) | 157(1) |
| Radiation type | Synchrotron, λ = 0.77494 Å | Synchrotron, λ = 0.62173 Å | Mo $K\alpha$ | Synchrotron, λ = 0.7458 Å |
| Specimen shape, size (mm) | Capillary, 4 × 0.5 | Capillary, 4 × 0.5 | 0.42 × 0.34 × 0.03 | Capillary, 4 × 0.5 |
| *Data collection* | | | | |
| Diffractometer | Mythen II | Mythen II | MAR345 image plate | PILATUS@SNBL |
| Method | powder | powder | single-crystal | powder |
| No. of measured, independent and observed reflections | * | * | 8493, 8493, 6960 | * |
| $R_{int}$ | – | – | 0(‡) | – |
| θ values (°) | $2\theta_{min}$ = 1.505, $2\theta_{max}$ = 32.000, $2\theta_{step}$ = 0.004 | $2\theta_{min}$ = 1.505, $2\theta_{max}$ = 32.000, $2\theta_{step}$ = 0.004 | $\theta_{max}$ = 25.4, $\theta_{min}$ = 3.5 | $2\theta_{min}$ = 2.146, $2\theta_{max}$ = 34.998, $2\theta_{step}$ = 0.013 |
| *Refinement* | | | | |
| $R$ factors and goodness of fit | $R_p$ = 3.41, $R_{wp}$ = 4.42, $R_{exp}$ = 0.56, $R_{Bragg}$ = 6.58, $\chi^2$ = 62.094 | $R_p$ = 0.93, $R_{wp}$ = 1.31, $R_{exp}$ = 0.65, $R_{Bragg}$ = 2.35, $\chi^2$ = 4.12 | $R[F^2 > 2\sigma(F^2)]$ = 0.040, $wR(F^2)$ = 0.111, $S$ = 1.07 | $R_p$ = 7.28, $R_{wp}$ = 10.71, $R_{exp}$ = 0.09, $R_{Bragg}$ = 7.30, $\chi^2$ = 14954 |
| No. of reflections/data points† | 8472 | 8472 | 8493 | 2657 |
| No. of parameters | varied | varied | 422 | varied |
| CCDC number | 1537401 | 1537402 | 1537403 | 1537404 |

(*) In the case of powder data, estimation of the number of effective reflections is difficult due to peak overlap and highly depends on the resolution; we do not provide this number as its value is usually overestimated by crystallographic software and may lack meaning
(†) In the case of powder data: number of data points
(‡) refined as a twin against HKLF5 formatted reflections, imposing Merge 0.

**Table 3.1 (continue).** Crystal data, data collection, and refinement details.

| | 1 : 2 R/L | 1 : 1 R/L/MeOH | 1 : 1 R/L/EtOH | 1 : 1 RS/D pol I |
|---|---|---|---|---|
| *Crystal data* | | | | |
| Chemical formula | $C_{15}H_{13}FO_2 \cdot 2(C_5H_9NO_2)$ | $2(C_{15}H_{13}FO_2) \cdot 2(C_5H_9NO_2) \cdot CH_4O$ | $C_{15}H_{13}FO_2 \cdot C_5H_9NO_2 \cdot 0.5(C_2H_6O)$ | $2(C_{15}H_{13}FO_2) \cdot 2(C_5H_9NO_2)$ |
| $M_r$ | 474.52 | 750.81 | 382.43 | 718.79 |
| Crystal system, space group | Monoclinic, $P2_1$ | Monoclinic, $C2$ | Monoclinic, $C2$ | Monoclinic, $P2_1$ |
| Temperature (K) | 295 | 150 | 150 | 295 |
| $a$, $b$, $c$ (Å) | 5.99344(10), 9.49502(16), 20.9123(4) | 9.8450(7), 7.0135(5), 26.8389(19) | 9.8380(4), 7.5051(3), 25.8385(9) | 5.7912(3), 17.3320(12), 18.2738(11) |
| α, β, γ (°) | 90, 90.4325(16), 90 | 90, 90.528(7), 90 | 90, 94.510(4), 90 | 90, 96.658(3), 90 |
| $V$ (Å$^3$) | 1190.04(4) | 1853.1(2) | 1901.87(13) | 1821.84(19) |
| Z | 2 | 2 | 4 | 2 |
| $D_x$ (Mg m$^{-3}$) | 1.324 | 1.346 | 1.336 | 1.310 |
| Melting point (°C) | 140(2) | n/a | n/a | n/a |
| Radiation type | Cu $K\alpha$ | Mo $K\alpha$ | Mo $K\alpha$ | Synchrotron, $\lambda = 0.776188$ Å |
| Specimen shape, size (mm) | 0.29 × 0.08 × 0.03 | 0.40 × 0.35 × 0.20 | 0.35 × 0.28 × 0.03 | Capillary, 4 × 0.5 |
| *Data collection* | | | | |
| Diffractometer | Oxford Diffraction Gemini Ultra R | MAR345 image plate | MAR345 image plate | Mythen II |
| Method | single-crystal | single-crystal | single-crystal | powder |
| No. of measured, independent and observed reflections | 10467, 4206, 4028 | 5663, 2874, 2726 | 7645, 3335, 2901 | * |
| $R_{int}$ | 0.025 | 0.035 | 0.028 | – |
| θ values (°) | $\theta_{max} = 67.2$, $\theta_{min} = 4.2$ | $\theta_{max} = 25.4$, $\theta_{min} = 3.0$ | $\theta_{max} = 25.5$, $\theta_{min} = 3.2$ | $2\theta_{min} = 1.962$ $2\theta_{max} = 29.999$ $2\theta_{step} = 0.004$ |
| *Refinement* | | | | |
| $R$ factors and goodness of fit | $R[F^2 > 2\sigma(F^2)] = 0.030$, $wR(F^2) = 0.078$, $S = 1.05$ | $R[F^2 > 2\sigma(F^2)] = 0.038$, $wR(F^2) = 0.104$, $S = 1.10$ | $R[F^2 > 2\sigma(F^2)] = 0.054$ $wR(F^2) = 0.131$ $S = 1.13$ | $R_p = 5.84$, $R_{wp} = 6.93$, $R_{exp} = 0.33$, $R_{Bragg} = 8.74$, $\chi^2 = 445.632$ |
| No. of reflections/data points† | 4206 | 2874 | 3335 | 7901 |
| No. of parameters | 322 | 262 | 301 | varied |
| CCDC number | 1537405 | 1537407 | 1537408 | 1537413 |

(*) In the case of powder data, estimation of the number of effective reflections is difficult due to peak overlap and highly depends on the resolution; we do not provide this number as its value is usually overestimated by crystallographic software and may lack meaning
(†) In the case of powder data: number of data points

**Table 3.1 (continue).** Crystal data, data collection, and refinement details.

| | 1 : 1 RS/L pol II | 1 : 1 RS/D pol III | 1 : 1 RS/L pol IV | 2 : 1 RS/L |
|---|---|---|---|---|
| *Crystal data* | | | | |
| Chemical formula | $C_{15}H_{13}FO_2 \cdot C_5H_9NO_2$ | $2(C_{15}H_{13}FO_2) \cdot 2(C_5H_9NO_2)$ | $2(C_{15}H_{13}FO_2) \cdot 2(C_5H_9NO_2)$ | $2(C_{15}H_{13}FO_2) \cdot C_5H_9NO_2$ |
| $M_r$ | 359.38 | 718.79 | 718.77 | 603.64 |
| Crystal system, space group | Triclinic, $P1$ | Monoclinic, $P2_1$ | Triclinic, $P1$ | Triclinic, $P1$ |
| Temperature (K) | 295 | 420 | 295 | 295 |
| $a$, $b$, $c$ (Å) | 5.76337(18), 11.2468(4), 14.2595(4) | 5.91137(19), 24.1621(9), 13.0953(4) | 5.68560(16), 6.4145(3), 26.4325(9) | 5.8399(4), 6.3302(4), 22.3600(14) |
| α, β, γ (°) | 91.372(3), 100.713(3), 92.925(3) | 90, 95.667(2), 90 | 87.568(3), 89.083(3), 70.624(3) | 95.277(5), 95.033(6), 108.947(6) |
| $V$ (Å$^3$) | 906.47(5) | 1861.28(11) | 908.58(6) | 772.40(9) |
| Z | 2 | 2 | 1 | 1 |
| $D_x$ (Mg m$^{-3}$) | 1.317 | 1.283 | 1.314 | 1.298 |
| Melting point (°C) | 151(1) | 191(2) | n/a | 162(1) |
| Radiation type | Cu $K\alpha$ | Synchrotron, λ = 0.77663 Å | Cu $K\alpha$ | Cu $K\alpha$ |
| Specimen shape, size (mm) | 0.32 × 0.08 × 0.02 | Capillary, 4 × 0.5 | 0.38 × 0.06 × 0.06 | 0.28 × 0.08 × 0.03 |
| *Data collection* | | | | |
| Diffractometer | Oxford Diffraction Gemini Ultra R | Mythen II | Oxford Diffraction Gemini Ultra R | Oxford Diffraction Gemini Ultra R |
| Method | single-crystal | powder | single-crystal | single-crystal |
| No. of measured, independent and observed reflections | 11862, 11862, 8929 | * | 11711, 4613, 4348 | 10562, 3682, 3503 |
| $R_{int}$ | 0.036 for twin1 | – | 0.031 | 0.047 |
| θ values (°) | $\theta_{max}$ = 67.1, $\theta_{min}$ = 3.2 | $2\theta_{min}$ = 3.006 $2\theta_{max}$ = 24.001 $2\theta_{step}$ = 0.004 | $\theta_{max}$ = 67.1, $\theta_{min}$ = 3.4 | $\theta_{max}$ = 67.3, $\theta_{min}$ = 4.0 |
| *Refinement* | | | | |
| $R$ factors and goodness of fit | $R[F^2 > 2\sigma(F^2)]$ = 0.036, $wR(F^2)$ = 0.092, $S$ = 0.86 | $R_p$ = 0.87, $R_{wp}$ = 1.24, $R_{exp}$ = 0.47, $R_{Bragg}$ = 2.13, $\chi^2$ = 7.022 | $R[F^2 > 2\sigma(F^2)]$ = 0.035, $wR(F^2)$ = 0.089, $S$ = 1.03 | $R[F^2 > 2\sigma(F^2)]$ = 0.046, $wR(F^2)$ = 0.125, $S$ = 1.03 |
| No. of reflections/data points† | 11862 | 5833 | 4613 | 3682 |
| No. of parameters | 508 | varied | 524 | 448 |
| CCDC number | 1537414 | 1537415 | 1537416 | 1537417 |

(*) In the case of powder data, estimation of the number of effective reflections is difficult due to peak overlap and highly depends on the resolution; we do not provide this number as its value is usually overestimated by crystallographic software and may lack meaning
(†) In the case of powder data: number of data points

**Table 3.1 (continue).** Crystal data, data collection, and refinement details.

| | 1 : 1 RS/DL | 2 : 1 R/D | 1 : 1 R/D | 2 : 1 R/DL |
|---|---|---|---|---|
| *Crystal data* | | | | |
| Chemical formula | $C_{15}H_{13}FO_2 \cdot C_5H_9NO_2$ | $2(C_{15}H_{13}FO_2) \cdot C_5H_9NO_2$ | $C_{15}H_{13}FO_2 \cdot C_5H_9NO_2$ | $2(C_{15}H_{13}FO_2) \cdot C_5H_9NO_2$ |
| $M_r$ | 359.38 | 603.64 | 359.38 | 603.64 |
| Crystal system, space group | Monoclinic, $P2_1/n$ | Monoclinic, $P2_1$ | Monoclinic, I2 | Monoclinic, $P2_1$ |
| Temperature (K) | 297 | 295 | 150 | 150 |
| $a$, $b$, $c$ (Å) | 5.9312(3), 23.7365(12), 12.8615(6) | 5.9554(2), 44.661(2), 6.1553(3) | 27.054(6), 5.7902(5), 25.974(6) | 5.9251(3), 44.193(3), 6.1136(4) |
| α, β, γ (°) | 90, 95.425(4), 90 | 90, 109.156(5), 90 | 90, 116.96(3), 90 | 90, 109.455(7), 90 |
| $V$ (Å$^3$) | 1802.60(14) | 1546.50(14) | 3626.5(14) | 1509.45(18) |
| Z | 4 | 2 | 8 | 2 |
| $D_x$ (Mg m$^{-3}$) | 1.324 | 1.296 | 1.316 | 1.328 |
| Melting point (°C) | 194(1) | 153(1) | 145(1) | 149(1) |
| Radiation type | Mo $K\alpha$ | Cu $K\alpha$ | Mo $K\alpha$ | Cu $K\alpha$ |
| Specimen shape, size (mm) | 0.55 × 0.08 × 0.07 | 0.18 × 0.12 × 0.03 | 0.40 × 0.05 × 0.02 | 0.23 × 0.10 × 0.03 |
| *Data collection* | | | | |
| Diffractometer | MAR345 image plate | Oxford Diffraction Gemini Ultra R | MAR345 image plate | Oxford Diffraction Gemini Ultra R |
| Method | single-crystal | single-crystal | single-crystal | single-crystal |
| No. of measured, independent and observed reflections | 11473, 3324, 2277 | 16551, 5481, 4987 | 4951, 2957, 1992 | 8838, 4361, 4011 |
| $R_{int}$ | 0.052 | 0.034 | 0.075 | 0.026 |
| θ values (°) | $\theta_{max}$ = 25.5, $\theta_{min}$ = 3.3 | $\theta_{max}$ = 67.3, $\theta_{min}$ = 4.0 | $\theta_{max}$ = 19.6, $\theta_{min}$ = 3.0 | $\theta_{max}$ = 62.8, $\theta_{min}$ = 4.0 |
| *Refinement* | | | | |
| $R$ factors and goodness of fit | $R[F^2 > 2\theta(F^2)]$ = 0.064, $wR(F^2)$ = 0.165, $S$ = 1.06 | $R[F^2 > 2\theta(F^2)]$ = 0.038, $wR(F^2)$ = 0.102, $S$ = 1.04 | $R[F^2 > 2\theta(F^2)]$ = 0.083, $wR(F^2)$ = 0.189, $S$ = 1.05 | $R[F^2 > 2\theta(F^2)]$ = 0.045, $wR(F^2)$ = 0.105, $S$ = 1.10 |
| No. of reflections/data points | 3324 | 5481 | 2957 | 4361 |
| No. of parameters | 275 | 448 | 471 | 496 |
| CCDC number | 1537418 | 1537409 | 1537410 | 1537411 |

(*) In the case of powder data, estimation of the number of effective reflections is difficult due to peak overlap and highly depends on the resolution; we do not provide this number as its value is usually overestimated by crystallographic software and may lack meaning
(†) In the case of powder data: number of data points

**Table 3.1 (continue).** Crystal data, data collection, and refinement details.

| | 1 : 1 R/DL | L-proline pol I | L-proline pol II | R-flurbiprofen |
|---|---|---|---|---|
| *Crystal data* | | | | |
| Chemical formula | $2(C_{15}H_{13}FO_2)\cdot C_5H_9NO_2\cdot C_5H_9NO_2$ | $C_5H_9NO_2$ | $C_5H_9NO_2$ | $C_{15}H_{13}FO_2$ |
| $M_r$ | 718.79 | 115.13 | 115.13 | 244.25 |
| Crystal system, space group | Monoclinic, $P2_1$ | Orthorhombic, $P2_12_12_1$ | Triclinic, P1 | Orthorhombic, $P2_12_12_1$ |
| Temperature (K) | 295 | 100 | 413 | 150 |
| $a$, $b$, $c$ (Å) | 5.84419(9), 23.1523(3), 13.5593(2) | 5.28018(12), 8.8794(2), 11.5307(2) | 5.21242(7), 5.92921(12), 9.52184(18) | 5.6535(3), 13.2097(7), 16.0709(9) |
| α, β, γ (°) | 90, 97.4871(9), 90 | 90, 90, 90 | 87.8578(13), 89.9133(18), 87.6845(13) | 90, 90, 90 |
| $V$ (Å$^3$) | 1819.02(5) | 540.61(2) | 293.83(1) | 1200.20(11) |
| Z | 2 | 4 | 2 | 4 |
| $D_x$ (Mg m$^{-3}$) | 1.312 | 1.415 | 1.301 | 1.352 |
| Melting point (°C) | n/a | 227(2) | n/a | 109(1) |
| Radiation type | Synchrotron, λ = 0.77494 Å | Cu $K\alpha$ | Synchrotron, λ = 0.62127 Å | Mo $K\alpha$ |
| Specimen shape, size (mm) | Capillary, 4 × 0.5 | 0.16 × 0.09 × 0.03 | Capillary, 4 × 0.5 | 0.20 × 0.03 × 0.02 |
| *Data collection* | | | | |
| Diffractometer | Mythen II | Oxford Diffraction Gemini Ultra R | Mythen II | MAR345 image plate |
| Method | powder | single-crystal | powder | single-crystal |
| No. of measured, independent and observed reflections | * | 1785, 882, 831 | * | 7437, 2138, 1648 |
| $R_{int}$ | – | 0.022 | – | 0.094 |
| θ values (°) | $2\theta_{min}$ = 1.375 $2\theta_{max}$ = 32.000 $2\theta_{step}$ = 0.004 | $\theta_{max}$ = 66.9, $\theta_{min}$ = 6.3 | $2\theta_{min}$ = 2.513 $2\theta_{max}$ = 24.001 $2\theta_{step}$ = 0.004 | $\theta_{max}$ = 25.2, $\theta_{min}$ = 3.0 |
| *Refinement* | | | | |
| $R$ factors and goodness of fit | $R_p$ = 1.97, $R_{wp}$ = 2.55, $R_{exp}$ = 0.40, $R_{Bragg}$ = 2.47, $\chi^2$ = 41.216 | $R[F^2 > 2\sigma(F^2)]$ = 0.034, $wR(F^2)$ = 0.091, $S$ = 1.08 | $R_p$ = 0.78, $R_{wp}$ = 1.09, $R_{exp}$ = 0.71, $R_{Bragg}$ = 1.39, $\chi^2$ = 2.341 | $R[F^2 > 2\sigma(F^2)]$ = 0.074, $wR(F^2)$ = 0.134, $S$ = 1.12 |
| No. of reflections/data points | 8508 | 983 | 5969 | 2138 |
| No. of parameters | varied | 89 | varied | 165 |
| CCDC number | 1537412 | 1537420 | 1537421 | 1537422 |

(*) In the case of powder data, estimation of the number of effective reflections is difficult due to peak overlap and highly depends on the resolution; we do not provide this number as its value is usually overestimated by crystallographic software and may lack meaning
(†) In the case of powder data: number of data points

**Powder X-ray diffraction structure determination.** Powder X-ray diffraction data for structure determination were collected at the Swiss Light Source (SLS, PSI, Switzerland) at MS-X04SA beam line equipped with a 1D microstrip detector MYTHEN II. The structures *R-flurbiprofen/L-proline 1 : 1 pol I (1 : 1 R/L pol I), R-flurbiprofen/L-proline pol II (1 : 1 R/L pol II), R-flurbiprofen/L-proline 1 : 3 (1 : 3 R/L), RS-flurbiprofen/L-proline 1 : 1 pol I (1 : 1 RS/L pol I), and pol III (1 : 1 RS/L pol III), R-flurbiprofen/DL-proline 1 : 1 (1 : 1 R/DL), and L-proline pol II* were solved from powder X-ray diffraction data. The crystal data, data collection, and refinement details are summarized in Table 1.

Indexing and Le Bail fit were performed using the FOX program[91]. The structures were found by global optimization in direct space (Monte Carlo/parallel tempering algorithm) using again the FOX program[91] and further refined by the Rietveld method in the TOPAS V5[97] software, text based input files prepared in the jedit editor were used[236]. Profile parameters were found from Pawley refinement and then fixed in further Rietveld refinement. The background was described as a Chebyshev polynomial of the *n*-th order. The molecules were described as rigid body object; the following functional groups were kept rigid, for which only rotation was allowed: carboxylate, carboxyl group, and benzene rings. Bond distances and angles were put to fixed values, whereas certain torsion angles were refined. Position and orientation of the molecules were refined as well. The torsion angles and the orientation of each molecule in the asymmetric unit were refined separately in an iterative manner and then fixed in the final refinement cycle since they affected the stability of refinement. In certain structures, the molecular coordinates had to be fixed as well in order to avoid short interatomic distances. The equivalent isotropic temperature factors for hydrogen atoms were set at 1.2 times of those of parent atoms in a particular molecule.

Proline is highly flexible in terms of conformations, which may cause disorder as was observed in almost all structures solved from single-crystal X-ray diffraction. We tried to introduce disorder for proline in the refinement of powder X-ray diffraction data but it did not significantly improve the structural models and only made fit less stable, so we decided to omit it. Rietveld refinement plots are shown in Figs. S1-S7 in Appendix B.

Four cocrystal structures, *i.e.* 1 : 2 R/L, 1 : 1 RS/L pol II, 2 : 1 RS/L, and 2 : 1 R/D had been solved from powder X-ray diffraction data before we managed to obtain single crystals. These four examples represent our internal "blind test" to estimate the quality of the structures we found from powder data. Figures S61-S64 in Appendix B demonstrate overlaps of the single-crystal and powder structural models for the aforementioned cocrystals. We can clearly see that the positions of molecules can be determined quite reliably from powder X-ray data. The conformation and the orientation of flurbiprofen hardly differ from the single-crystal model, the only difference is observed for the rotation of the methyl group. On the contrary, the torsion angles and the orientation of proline may differ significantly from the single-crystal model (see Fig. S64 for the most significant difference, RMSD is 0.438 Å). The difficulty of finding the right geometry is most likely caused by disorder of the proline as was found in the single crystal structures. Thus, we can conclude that in our structural models found from powder X-ray diffraction data, the position, the orientation, and the conformation of flurbiprofen should be reliably determined whereas the geometry of proline may slightly differ.

Cif files were finalized using the Encifer[158] and the Platon[157] programs.

**DFT-D3 optimization.** Dispersion-corrected periodic DFT calculations were performed using the VASP package[237–240] with the Perdew–Burke–Ernzerhof (PBE) functional.[241] DFT calculations represent the structures at 0 K. The plane-wave cut-off energy was set to 520 eV. The convergence criterion for minimization was set on energy: < 0.0001 eV for the energy between the last two minimization steps. Both the unit cell and the atomic coordinates were relaxed simultaneously. Preliminary testing showed that, in our case, the two-step relaxation procedure (when during the first step, the unit cell is fixed and only the coordinates are relaxed; and during the second step, starting with the optimized structure from the first step, the coordinates and the unit cell are relaxed) that was recommended by Neumann *et al.*[120,121] gives approximately the same result as the one-step procedure (when both the coordinates and the unit cell are relaxed simultaneously). The total energy was calculated using the tetrahedron method with Blöchl corrections. Brillouin zone was sampled using Monkhorst-Pack *k*-point grids selected so that the density of *k* points in reciprocal space is comparable for different crystal structures; the preliminary tests for some compounds showed only slight change in energy depending on the k-grid (<0.05 % if a doubled k-grid is tested). Dispersion correction was introduced by applying the D3 correction method of Grimme[242] with Becke-Jonson damping[243]. POSCAR and KPOINTS files were generated from original CIF files using the MaterialsProject website[244]; KPOINTS files were later adapted to keep comparable *k*-point density per volume for different structures (Table S9 lists *k*-point grids taken for each structure). Since it is difficult to account for the structural disorder, in the case of disordered structures, we chose the sites with higher occupancy and set their occupancy to 1. The 1 : 1 R/L solvates and 1 : 1 R/DL were omitted as their structures represent complicated cases of disorder that is difficult to reliably account for by DFT. CONTCAR files were converted into CIF format using the Bilbao Crystallographic Server.[245] Tags in INCAR file representing the applied parameters of minimization are given on page 166 (Appendix B).

**Differential scanning calorimetry (DSC) and thermogravimetric analysis (TG).** DSC curves were measured using a DSC 821 Mettler Toledo instrument. Prior to measurements, the instrument was calibrated using indium. Standard 40 μL aluminum crucibles were used. The heating rate was 2 °C/min over the range from 25 to 200-250 °C. TG analysis was performed using a TGA/SDTA 851 Mettler Toledo instrument. Samples were put into open aluminum oxide crucibles annealed at 1100 °C. The heating rate was again 2 °C/min over a range from 25 °C to 350 °C. All experiments were carried out under nitrogen atmosphere (a flow rate of 50 ml/min). DSC and TG curves are presented in Figures S8-S29 in Appendix B.

**Solid-state NMR.** $^{15}$N NMR spectra were recorded at room temperature on a Bruker Avance-500 spectrometer operating at 11.7 T (50.6 MHz for $^{15}$N) using a 4 mm CP-MAS Bruker probe. The sample was packed in a 4 mm zirconia rotor and measured with a spinning frequency of 15 kHz. $^{15}$N CP-MAS spectra were recorded using the following acquisition parameters: 5 s relaxation delay, 2.6 μs (90°) excitation pulse, 2 ms contact time, 50 ms acquisition time. The processing comprised exponential multiplication of the FID with a line broadening factor of 1 Hz, zero-filling, Fourier transform, phase and baseline corrections. The chemical shift scale was calibrated at room temperature with respect to a sample of solid $NH_4Cl$ (39.3 ppm).[246] SS-NMR was used to confirm the ratio of the components in the 1 : 3 R/L cocrystal. The spectra are presented in Fig. S83 in Appendix B.

**Scanning electron microscopy (SEM).** SEM images were obtained using a scanning electron microscope ZEISS SUPRA 40 equipped with a thermal field emission cathode (Schottky-emitter, ZrO/W-cathode). The acceleration voltage was set to 10 kV, and the working distance was between 5.9 mm and 6.3 mm. The images were adapted with an In-lens secondary electron detector, a SE2 secondary electron detector, and a QBSD backscatter detector. In addition, the scanning electron microscope is equipped with the energy dispersive X-ray spectrometers Thermo NSS (SiLi 5665) and Bruker X-Flash 5010 3403, Quantax 400.

## 3.3 Results and discussion

In studying the five chiral combinations: R-flurbiprofen/L-proline (R/L=S/D), R-flurbiprofen/D-proline (R/D=S/L), R-flurbiprofen/DL-proline (R/DL=S/DL), RS-flurbiprofen/L-proline (RS/L=RS/D), and RS-flurbiprofen/DL-proline (RS/DL), we primarily focused on liquid-assisted grinding experiments, resorting to solution cocrystallization only for producing single crystals (see Experimental for single crystals growing conditions) and not for exhaustive solution polymorphic screen. The reasons were the following: first, liquid-assisted grinding allows rapidly obtaining relatively pure materials; second, the choice of solvents for LAG is not limited to those in which the initial compounds are well soluble (for solution cocrystallization we were obliged to use only ethanol, methanol, or their mixture with water due to a low solubility of proline in other less hydrophilic solvents, like isopropanol or acetonitrile); finally, in contrast to solution crystallization where thermodynamics play a substantial role, the products of mechanochemical reactions depend to a higher extent on kinetic factors, which may result in a wider variety of different forms that are not accessible from solution.

Despite a wide use of liquid-assisted grinding for cocrystal screening, the role of the liquid still remains poorly understood. Several approaches that describe mechanochemical cocrystal formation, including those that take into account solubilities, are suggested[44,75,247,248], but they remain system-dependent and in some cases it is difficult to determine which of the scenarios realizes. However, it is agreed that the presence of liquid facilitates reaction leading to a better crystallinity and purer product in comparison with neat grinding[44,71]. Various examples show that the use of different solvents may result in the formation of different reaction products[106,249]. As will be shown below flurbiprofen/proline cocrystals represent another example of how the nature of the solvent can be crucial for the final product outcome: it not only affects the reaction rate, but also leads to different reaction pathways.

Our work consisted of several steps. (1) The first step included screening for cocrystal forms done by liquid-assisted grinding followed by X-ray powder diffraction analysis. Cases, in which new diffraction peaks were observed, were considered as potential cocrystals. (2) The second step was to identify and determine the structures of new forms, and included crystallization from solution as well as X-ray powder diffraction analysis using synchrotron data. (3) The third step was measuring DSC and TGA profiles for selected samples with the purpose of determining melting points for identified cocrystals and the mass loss upon heating. For some compounds, the DSC curves showed complicated shapes with endothermic and exothermic peaks, which was an indication for probable phase transformations. This is why we decided (4) to study those samples

under variable temperature: powders obtained by liquid-assisted grinding and packed in capillaries were measured using synchrotron radiation upon heating. As conditions may differ when performing an experiment in a sealed capillary and in a DSC capsule (with a small hole), the diffraction data obtained upon heating may not match exactly the DSC curve (taking into account a wide variety of forms for this system, due to the difference in experimental conditions, some of them may appear in DSC and not in PXRD and vice versa). Thus, in detail, we will be discussing only the behavior of samples in capillary and not their DSC curves, as the former is more representative and easier to interpret. As several identified cocrystals revealed the existence of various stoichiometric forms: 1 : 2, 1 : 1, and 2 : 1, and even 1 : 3 (flurbprofen : proline) at the fifth step, (5) we performed *in-situ* ball-milling experiments monitored by synchrotron radiation to establish the reaction pathway for selected systems. A stepwise mechanism of cocrystal formation has been already reported for the glycine/oxalic acid system[250]; another example reported by Coquerel *et al.* presents a step-wise polymorphic transformation of racemic modafinil[251]. *In-situ* monitoring of ball-milling reactions by X-ray diffraction and/or Raman spectroscopy allows a non-invasive analysis of reaction products and phase changes; it is a key technique when studying mechanisms of mechanochemical transformations[78,80,81,104–106]. (6) The final step was calculating by DFT-D3 and analyzing the crystal energies of the obtained cocrystals.

We will, first, present and discuss the experimental results obtained for each system; second, we will move on to the structural peculiarities of found cocrystals; and, finally, we will look into the results of DFT-D3 calculations and how they correlate with our experimental work.

### 3.3.1 R-flurbiprofen/L-proline

R-flurbiprofen/L-proline (R/L) is the system with which we started opening our Pandora's Box when we identified by PXRD the presence of a new phase in the initial methanol-assisted grinding screening. When we tried to index the obtained sample using synchrotron powder diffraction data we could not obtain a reliable result, this is why we started suspecting the presence of other phases. We repeated liquid-assisted grinding in the presence of ethanol, isopropanol, and acetonitrile, varying the ratios of the initial compounds: 1 : 1, 2 : 1, and 1 : 2. Again, the results were inconsistent. Differential scanning calorimetry and synchrotron powder diffraction upon variable temperature helped us to trace existing phases. The results are summarized in Scheme 1.

From Scheme 1 we see that the R/L system can form seven different forms: two 1 : 1 co-crystal solvates with methanol and ethanol, one 1 : 2, 2 : 1, and 1 : 3 form, two 1 : 1 polymorphs (see Structural analysis section for further description). We also observed one unknown form (unknown phase I) which was detected in the sample obtained by ethanol-assisted grinding in the 1 : 2 ratio. Unfortunately, the amount of that phase was not enough to perform reliable indexing and structure solution. We will further discuss in more detail the results of liquid-assisted grinding in the presence of various solvents as well as powder X-ray diffraction data obtained *in-situ* upon heating. The section will be concluded by the analysis of *in-situ* ball-milling data. All the experiments performed for the R/L system can be found in Table S3 in Appendix B.

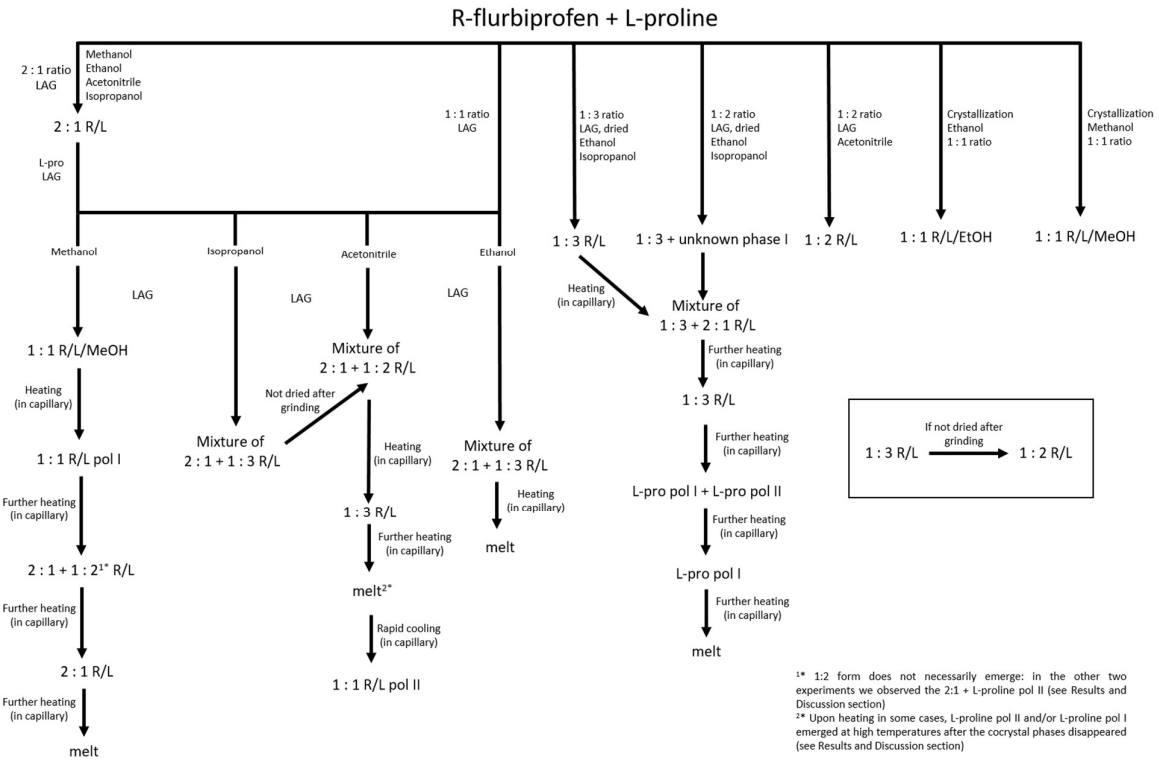


**Scheme 3.1.** Existing phases for the R-flurbiprofen/L-proline system and conditions under which they can be obtained.

***Methanol-assisted grinding.*** In 1 : 1 methanol-assisted grinding we obtained a solvated form of the 1 : 1 cocrystal (see samples *1-4* in Table S3). The same solvate crystallizes from methanol solution (see Experimental Section). Owing to its small size, methanol can enter the space between the proline molecules (see Structural Analysis). Upon heating, methanol is removed from the crystal structure resulting in the 1 : 1 cocrystal form (1 : 1 R/L pol I). However, the non-solvated 1 : 1 cocrystals cannot be obtained using other solvents (ethanol, isopropanol or acetonitrile); liquid-assisted grinding with those solvents led to (1 : 2 + 2 : 1) or (2 : 1 + 1 : 3) mixtures. From solution crystallization, we also obtained a solvated form with ethanol (1 : 1 R/L/EtOH), which has a very similar structure to the methanol solvate but was never observed in ethanol grinding experiments. This can likely be explained by the larger size of ethanol molecules.

Formation of the 1 : 1 R/L/MeOH cocrystal solvate in methanol-assisted grinding experiments was confirmed by comparing the experimental diffraction pattern with that simulated from the single-crystal structure of the 1 : 1 R/L/MeOH solvate crystallized from solution as well as by differential scanning calorimetry and thermogravimetric analysis. Thermogravimetric curve had a characteristic step starting at 70 °C corresponding to the removal of 0.5 equivalent of methanol from the sample (Fig. S18); the corresponding DSC analysis shows a complicated behavior of the sample upon heating, (Figs. S17 and S19 in Appendix B), which is why we decided to measure variable temperature X-ray diffraction data for this sample in a capillary.

Figure 1 shows the diffraction patterns collected upon heating (sample *1* in Table 3S, Appendix B). We see that methanol starts being removed already around 42 °C, with the solvate being transformed into the non-solvated 1 : 1 R/L pol I cocrystal – a full conversion is reached around

85 °C; upon further heating this phase starts disappearing with a mixture of (1 : 2 + 2 : 1) R/L cocrystals emerging at the same time; at 115 °C all the peaks of the 1 : 1 phase have disappeared; then the 1 : 2 phase melts (around 128 °C) followed by the melting of the 2 : 1 form at 147 °C. In some other analyzed samples, we did not see the 1 : 2 phase, but a mixture of 2 : 1 phase + a previously unknown polymorph of L-proline, which we called polymorph II (see sample *2* in Table S3, Appendix B), the structure of the latter was solved from PXRD, but it is out of the scope of this article and will not be discussed in detail; in that case it was first the 2 : 1 form that melted and then L-proline pol II.

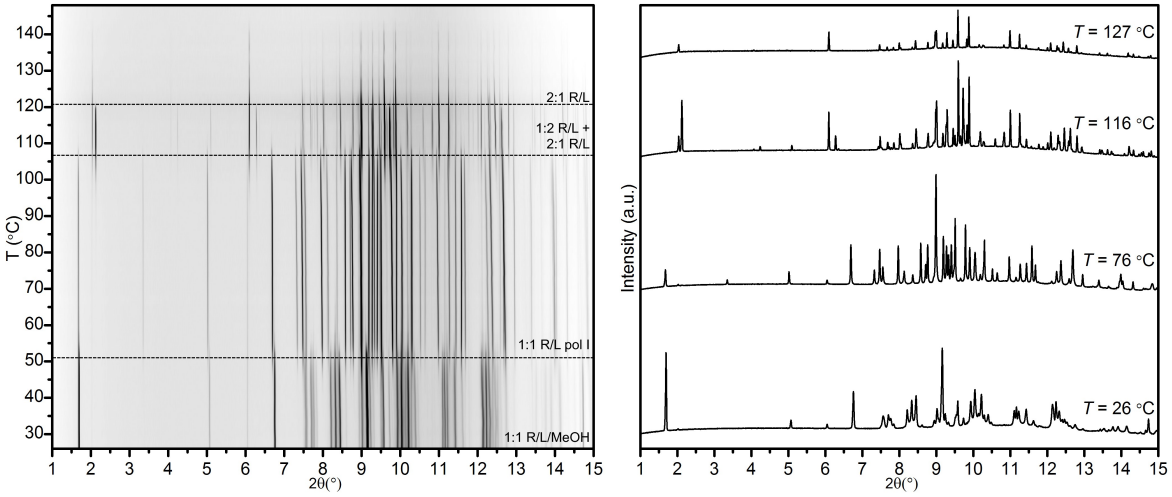


**Figure 3.1**. Powder X-ray diffraction patterns measured *in-situ* upon heating (from 26 °C to 150 °C) at a heat rate of 2 °C/min for the R/L sample prepared by methanol-assisted grinding in 1 : 1 ratio (sample *1* in Table S3), λ = 0.77494 Å: (left) film representation; (right) diffraction patterns at selected temperatures. *T* = 26 °C – 1 : 1 R/L/MeOH; *T* = 76 °C – 1 : 1 R/L pol I; *T* = 116 °C – a mixture of 2 : 1 R/L and 1 : 2 R/L; and *T* = 127 °C – 2 : 1 R/L.

***Acetonitrile-assisted grinding*** resulted in a mixture of the 2 : 1 and 1 : 2 cocrystals if the initial compounds were taken in 1 : 1 ratio; and in almost pure 1 : 2 cocrystal if the initial ratio was 1 : 2 (see samples *13* and *14* in Table S3, Appendix B).

***Ethanol- and isopropanol-assisted grinding.*** Preliminary PXRD analysis of ethanol- and isopropanol-assisted grinding samples revealed the presence of new phases. To identify those new phases we measured *in-situ* X-ray diffraction upon variable temperature and solid state NMR for the selected samples. We found that the sample prepared by ethanol-assisted grinding in the 1 : 1 ratio contained a mixture of the 2 : 1 R/L and a new phase. Upon heating both phases melted at the same time with the end set being 140 °C (sample *6* in Table S3, see Fig. S55 for X-ray diffraction data), which means that either we were in the eutectic point or the phases had close melting points. Indexing of the peaks belonging to this new phase revealed a structure with an orthorhombic unit cell and a volume of around 3000 Å, which corresponded to the 1 : 3 stoichiometry. The 1 : 3 stoichiometry was confirmed by solid-state NMR which was measured for a different sample obtained by 1 : 3 ethanol-assisted grinding (sample *10* in Table S3, see Fig. S83 for the 15N NMR spectrum, Appendix B) whose diffraction pattern contained the same peaks as the aforementioned sample. The structure of 1 : 3 R/L was determined from powder X-

ray diffraction data. The melting point of the 1 : 3 R/L phase indeed turned out to be very close to that of the 2 : 1 R/L cocrystal, 157 against 158 °C, respectively.

Further experiments showed that 1 : 3 R/L phase when left in a closed Eppendorf tube after grinding may transform into the 1 : 2 R/L phase (see samples *9*, *18*, *19* in Table S3, Appendix B); thus, the single crystals of the latter grow directly in the Eppendorf tube if some traces of solvents are still present (samples after grinding look slightly wet).

The emergence of the 1 : 3 R/L was also detected when the sample prepared by 1 : 2 isopropanol-assisted grinding was heated in capillary (see Fig. S57a in Appendix B). Its diffraction pattern (synchrotron PXRD) showed a mixture of the 1 : 2 and 2 : 1 forms, however, this sample initially did contain 1 : 3 R/L directly after grinding that, afterward, due to the presence of solvent, later recrystallized into 1 : 2 R/L (sample 19 in Table S3). Moreover, after everything melted, this sample was rapidly cooled to room temperature, resulting in another unknown form, the indexing of which revealed another polymorph of the 1 : 1 stoichiometry, 1 : 1 R/L pol II (see Fig. S57b in Appendix B).

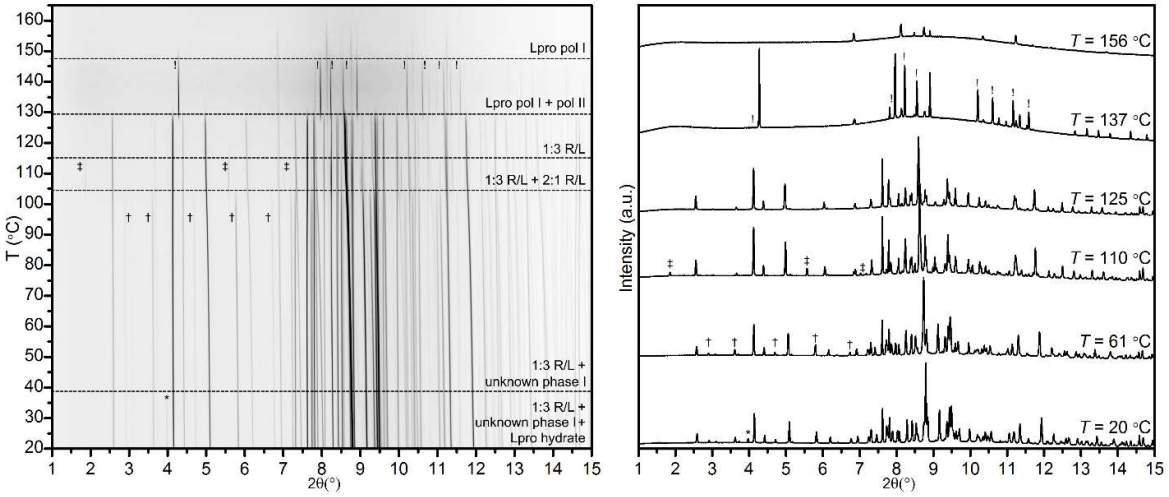


**Figure 3.2**. Powder X-ray diffraction patterns measured *in-situ* upon heating (from 20 °C to 165 °C) at a heat rate of 2 °C/min for the R/L sample prepared by ethanol-assisted grinding in 1 : 1 ratio and dried (sample *11* in Table S3), λ = 0.708 Å: (left) film representation; (right) diffraction patterns at selected temperatures. *T* = 20 °C – a mixture of 1 : 3 R/L, unknown phase I, and L-proline hydrate (marked as '*'); *T* = 31 °C – a mixture of 1 : 3 R/L and unknown phase I (marked as '†'); *T* = 110 °C – a mixture of 1 : 3 R/L and 2 : 1 R/L (marked as '‡'); *T* = 125 °C – 1 : 3 R/L; *T* = 137 °C – a mixture of L-proline pol I and L-proline pol II (marked as '!'); and *T* = 156 °C – L-proline pol I

Since 1 : 3 R/L turned out to be unstable if small amounts of solvent are present, we prepared the other 1 : 3 and 1 : 2 samples by ethanol-assisted grinding and dried them by slightly heating the ground material at ~60 °C (see samples *10* and *11* in Table S3, respectively, Appendix B). Both samples were measured *in-situ* upon heating. The resultant diffraction patterns for the 1 : 2 and 1 : 3 samples are presented in Fig. 3.2 and in Fig. S60 (Appendix B), respectively. Interestingly, in the 1 : 2 sample, besides the 1 : 3 R/L, we detected another new phase which we called the unknown phase I; whereas the 1 : 3 sample was cleaner and contained only traces of some impurities that we were unable to identify due to their small amount. Figure 2 shows that the 1 : 2 sample exhibits complex behavior upon heating: all the impurities disappear with increasing temperature followed by the emergence of the 2 : 1 R/L phase which is present within a 10 °C

temperature range; when 2 : 1 R/L disappears, we finally observe the pure major phase, 1 : 3 R/L. Melting of 1 : 3 R/L is followed by simultaneous emergence of two polymorphs of proline, with polymorph II disappearing first with increasing temperature.

Moreover, from the results obtained for the R/L system, it seemed that in 1 : 1 grinding the 2 : 1 R/L form emerged first and then if the amount of L-proline allowed and depending on the solvent used, 1 : 2 or 1 : 3 forms appeared as well. To verify this hypothesis we performed a step-by-step grinding experiment: we first ground the initial compounds in the 2 : 1 (flurbiprofen/proline) ratio in the presence of four different solvents and then added the equimolar amount of L-proline to the obtained samples and ground again. Grinding of the initial components taken in the 2 : 1 ratio always resulted in the 2 : 1 R/L cocrystal (see samples *5*, *8*, *15*, *17* in Table S3, Appendix B), no matter which solvent was used. The results of grinding after L-proline was added were indeed the same as from the 1 : 1 grinding (see Figs. S30-S34 for comparison of diffraction patterns, Appendix B). We went further and performed *in-situ* ball-milling experiments discussed below to monitor the appearance of phases directly.

***In-situ* ball-milling.** Seeing all the complexity of the R/L system, we decided to do *in-situ* ball-milling experiments, first, to confirm that indeed the 2 : 1 phase emerges first during grinding and, second, to see what is going on with the samples containing cocrystal mixtures. For this purpose we did ball-milling for 25 min (as from our experience, this time was enough for conversion) in the presence of methanol, ethanol, acetonitrile, and isopropanol for R-flurbiprofen and L-proline taken in the 1 : 1 ratio. Figure 3 shows 2D film representations of X-ray diffraction data collected *in-situ* during grinding.

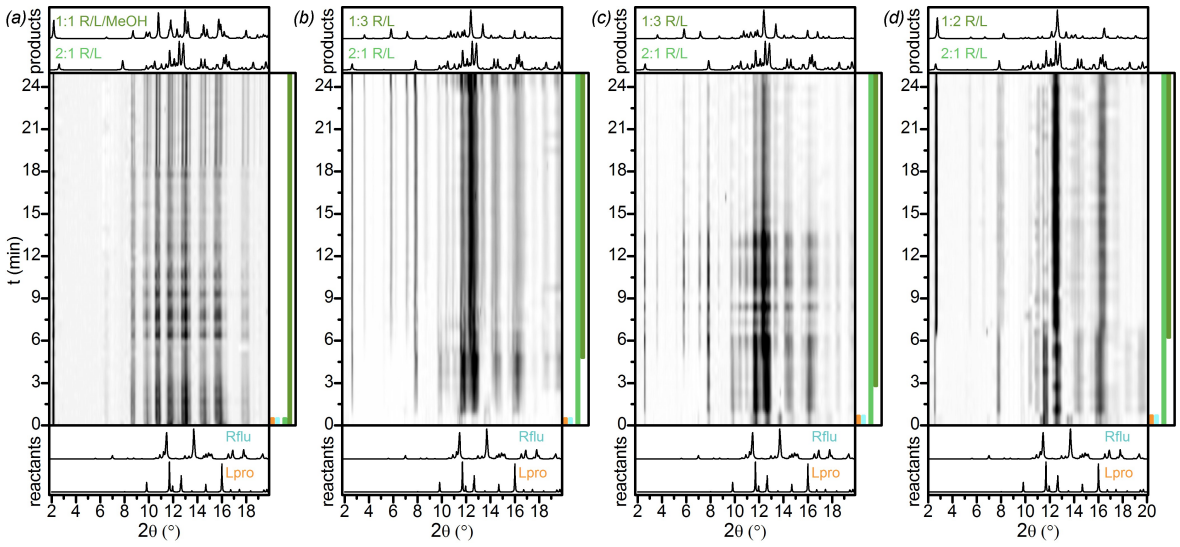


**Figure 3.3.** *In-situ* ball-milling X-ray diffraction patterns for the R/L system, λ = 1 Å: (a) methanol-, (b) ethanol-, (c) isopropanol-, and (d) acetonitrile-assisted grinding. Colored bands on the right side of each image represent the presence of phases and are shown only for illustrative purpose.

Methanol-assisted grinding (Fig. 3.3a) shows a tiny amount of the 2 : 1 phase emerging at the same time as 1 : 1 R/L/MeOH solvate. Reaction happens within seconds, we almost do not see any of the initial components. Since the reaction is fast, most likely it proceeds within the time of the first

frame being measured, thereby not allowing us to resolve whether the 2 : 1 phase appears first or both phases appear in parallel. However, from the step-by-step grinding we showed that 2 : 1 R/L cocrystal converts into 1 : 1 R/L/MeOH if ground with L-proline in the presence of methanol (see Fig. S30 in Appendix B). The latter may be an indication that the 2 : 1 R/L is an intermediate phase in methanol-assisted grinding.

Acetonitrile-assisted grinding (Fig. 3.3d) clearly shows that the 2 : 1 phase appears first followed by the emergence of the 1 : 2 cocrystal; the final powder contains both 2 : 1 R/L and 1 : 2 R/L.

Isopropanol- and ethanol-assisted grinding (Figs. 3.3b and 3.3c) both result in a mixture of the 2 : 1 R/L and 1 : 3 R/L phases. In these three experiments (with acetonitrile, ethanol, and isopropanol), a substantial amount of 2 : 1 R/L preserves in the resultant powders. The results of the step-by-step grinding (see Figs. S31-S33 in Appendix B) are in agreement with the *in-situ* ball-milling data and lead to the same result as the one-step 1 : 1 grinding: it is clear that the formation of the 2 : 1 phase precedes the formation of other phases, but this information is not sufficient to establish whether or not the 2 : 1 phase plays the role of an intermediate.

Concluding this section, the R/L system is capable of forming cocrystals with four different stoichiometries: 1 : 1 (R/L pol I and R/L pol II), 1 : 2, 1 : 3, and 2 : 1, as well as two co-crystal solvates. Methanol grinding experiments lead to the 1:1 co-crystal solvate, which upon desolvatation results in the 1 : 1 R/L pol I not observed by grinding with any other solvents; acetonitrile-, ethanol-, and isopropanol-assisted grinding experiments with the 1 : 1 ratio of the initial components results in mixtures of cocrystals with different stoichiometries, (2 : 1 R/L + 1 : 2 R/L) or (2 : 1 R/L + 1 : 3 R/L). *In-situ* PXRD upon variable temperature reveals complicated phase transformations upon heating. And *in-situ* ball-milling demonstrates that the 2 : 1 R/L phase is likely forming first during grinding experiments.

### 3.3.2 R-flurbiprofen/D-proline

R-flurbiprofen/D-proline (R/D) is much less complex than the R/L system, highlighting the importance of chirality in co-crystal systems. The results obtained by liquid-assisted grinding in the presence of various solvents are summarized in Scheme 3.2.

For the R/D system we have found only two forms with stoichiometries of 1 : 1 and 2 : 1. The experiments performed for this system are summarized in Table S4 (Appendix B). Step-by-step grinding was performed as well to establish the order of emerging compounds: liquid-assisted grinding of the initial compounds taken in the 2 : 1 ratio (R-flurbiprofen/D-proline) results in the 2 : 1 R/D form; these 2 : 1 samples reground with additional amount of D-proline lead to the 1 : 1 form; the latter can be obtained directly by 1 : 1 ratio grinding (see Fig. S35 in Appendix B).

***In-situ* ball-milling** in the presence of methanol or isopropanol shows similar results (see Figs. 3.4a and 3.4b). However, in the case of methanol the separate 2 : 1 stage is seen only for a short period of time after which the 1 : 1 and 2 : 1 products coexist, whereas in the case of isopropanol the 2 : 1 stage is more pronounced with the 1 : 1 cocrystal starting to appear much later. These results indicate that the reaction proceeds much faster in the presence of methanol than isopropanol, and indicate the 2 : 1 phase to be kinetically favored.

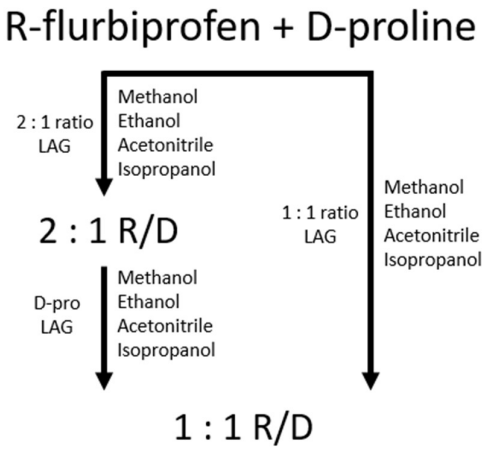


**Scheme 3.2.** Existing phases for the R-flurbiprofen/D-proline system and conditions under which they can be obtained.

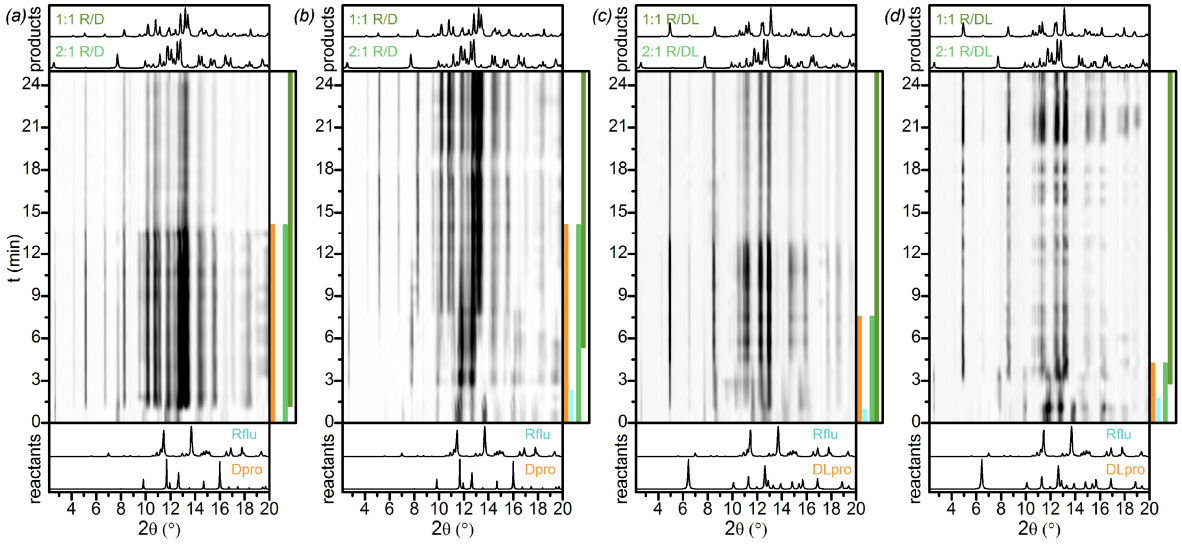


**Figure 3.4.** *In-situ* ball-milling X-ray diffraction patterns for the R/D system, λ = 1 Å: (a) methanol- and (b) isopropanol-assisted grinding, and for the R/DL system, (c) methanol- and (d) isopropanol-assisted grinding (1 : 1 ratio). Colored bands on the right side of each image represent the presence of phases and are shown only for illustrative purpose.

### 3.3.3 R-flurbiprofen/DL-proline

The R-flurbiprofen/DL-proline (R/DL) system behaves similarly to the R/D system. We again found only two forms: 1 : 1 and 2 : 1 (see Scheme 3.3). All the performed experiments for this system are summarized in Table 5S in Appendix B.

Albeit the apparent simplicity of the system, the DSC curve for the 1 : 1 R/DL cocrystal looked suspicious: the peak which presumably should have corresponded to melting was broad and appeared over a rather wide temperature range (Fig. S29 in Appendix B). We therefore decided to measure this sample *in-situ* upon heating. The results are represented in Fig. 3.5.

*In-situ* synchrotron powder X-ray diffraction data revealed the occurrence of a phase crossover. In such transformations, the structure changes gradually upon changing temperature with the symmetry being preserved rather than abruptly as in some other types of phase transitions.

The plots given in Fig. 3.5 show how the unit cell parameters behave upon heating. The parameters exhibit a continuous change with increasing temperature, typical of phase crossover transformations. Over the entire heating range, the parameters *a* and *b* elongate by 1.9 and 3.6 %, respectively, whereas the parameter *c* shortens by 4.7 %. The volume grows by 1.8 % and then drops by approximately 1 % during phase crossover, which indicates that the structure settles to a more efficient packing in comparison to the structure just before the phase crossover starts. Calculation of the first derivatives (dotted lines in the graphs in Fig. 3.5) allowed us to estimate the critical point, which was around 138 °C.

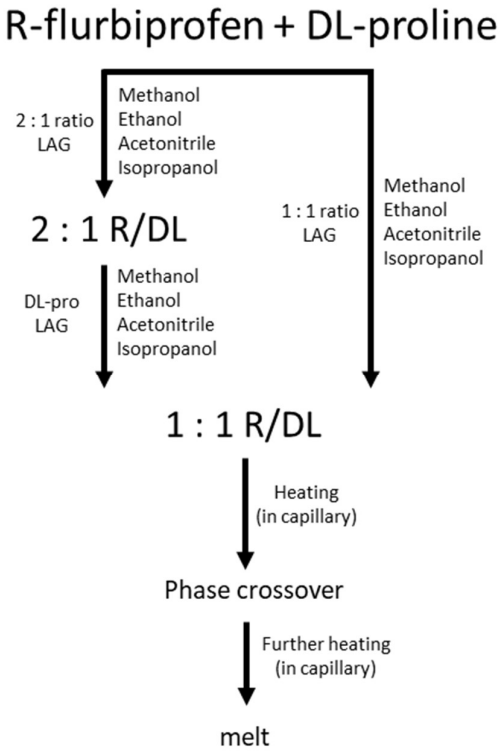


**Scheme 3.3.** Existing phases for the R-flurbiprofen/DL-proline system and conditions under which they can be obtained

If we look at the evolution of diffraction patterns upon heating, the half-width of the peaks associated with the *c* parameter changes the most noticeably, for instance the 002 reflection. The 002 reflection, initially overlapping with reflection 031, shifts right, which is associated with the shortening of the *c* parameter (Fig. 3.5, the inset to the film representation). Moreover, the half-width of this peak significantly broadens during phase crossover in comparison to other peaks and then narrows again when the phase crossover is finished (Fig. 3.5, the inset to the selected diffraction patterns).

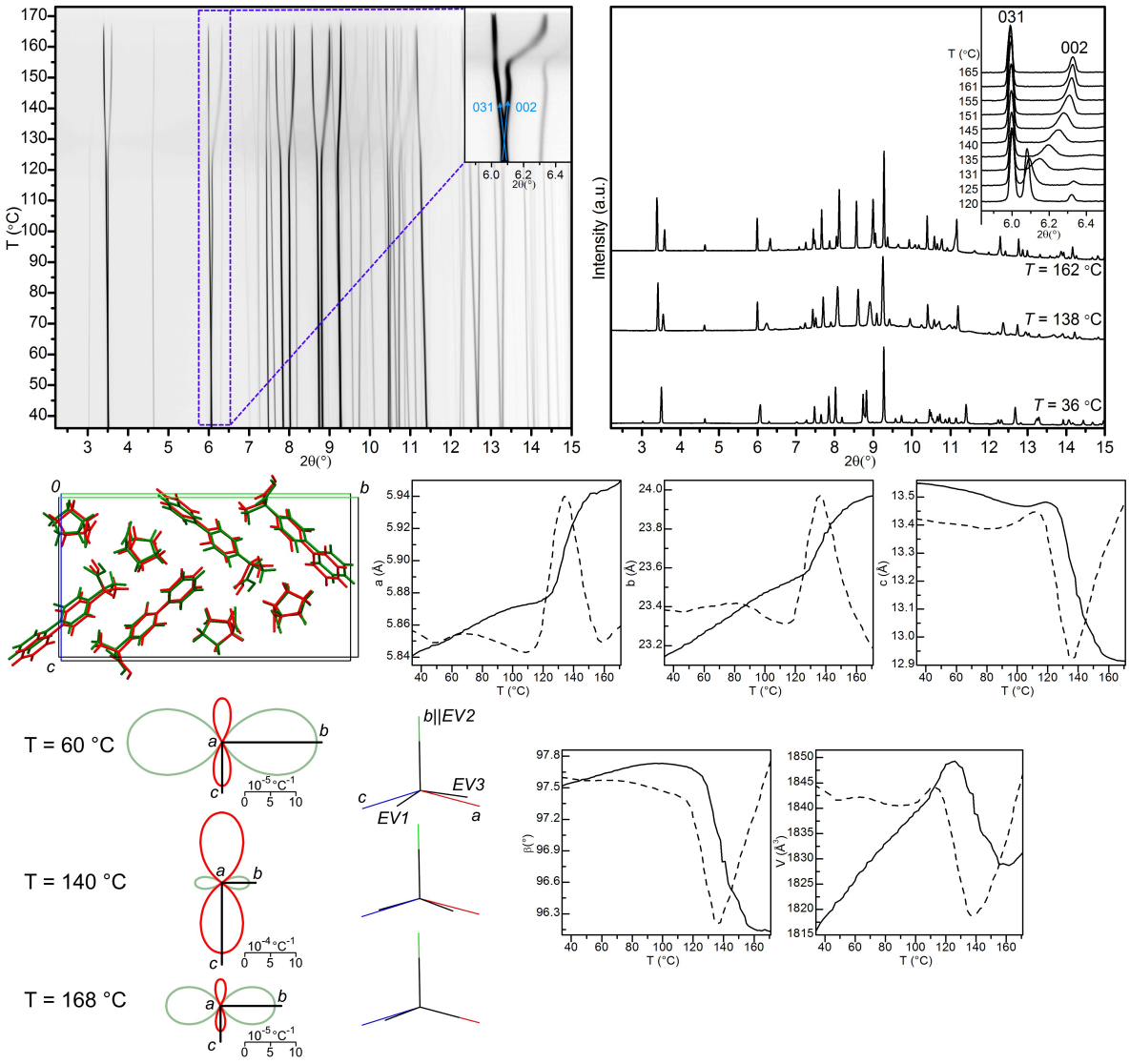


**Figure 3.5.** Phase crossover in 1 : 1 R/DL cocrystal. Upper part: powder X-ray diffraction patterns measured *in-situ* upon heating (from 36 to 173 °C) at a rate of 2 °C/min for R/DL sample prepared by ethanol-assisted grinding in 1 : 1 ratio, λ = 0.708 Å (sample *7* in Table S5); (left) film representation; (right) diffraction patterns at selected temperatures - $T$ = 36 °C (initial structure), $T$ = 138 °C (critical temperature), and $T$ = 162 °C (after phase crossover). Insets represent the change in the positions of the peaks with *hkl* 031 and 002. Bottom part, left: overlap of the initial structure at room temperature (red) and the structure after phase crossover (green) and below, the tensor representation of thermal expansion; tensors were calculated at 60 °C, 140 °C, and 168 °C; *EV1*, *EV2*, and *EV3* are the tensor eigenvectors; green represents positive thermal expansion and red is negative thermal expansion. Bottom part, right: change in the unit cell parameters with temperature (*a*, *b*, *c*, β, and volume); dotted lines represent the first derivative from these data.

Thermal expansion is an anisotropic property and can be represented by a symmetrical second rank tensor. Using the TEV program[252], we calculated the thermal expansion tensor in three temperature points that represent three segments (the first two segments were approximated with the second-order polynomial and the third with the first-order polynomial): (1) thermal expansion before the phase crossover (34-91 °C); (2) within the phase crossover region (129-154 °C); (3) after the phase crossover (164-171 °C). The direction of tensor eigenvector *EV1* is associated with

the *c* axis; *EV2* is parallel to the axis *b*; and *EV3* vector is associated with the axis *a* (see representation of axes in Fig. 3.5).

According to the calculated tensors (see Fig. 3.5, representation of tensors in three temperature points), the system behaves similarly in segments (1) and (3), expanding along the *a* and *b* axes and slightly shrinking along the *c* axis; the magnitude of thermal expansion along *b* is almost twice as high at 60 °C than at 168 °C, whereas it is almost the same along the *a* axis at both temperatures. In segment (2), system completely changes its behavior, drastically shrinking along the *c* axis and only slightly expanding along the *a* and *b* axes; the magnitude of thermal expansion at 140 °C is by a factor of 10 higher than that at 60 or 168 °C. Table S11 in Appendix B lists the absolute tensor eigenvalues.

The initial structure does not undergo significant changes due to phase crossover (see overlap in Fig. 3.5), which is expected as order-disorder transformations are mostly associated with disorder occurring at certain sites and not radical structural changes. The structures of all obtained cocrystals will be discussed in more detail in the Structural analysis section of this article. However, for clarity we repeat certain important points here for 1 : 1 R/DL. The structure of 1 : 1 R/DL cocrystal is composed of proline chains connecting flurbiprofen. Proline chains in their turn are made of proline molecules interconnected in the head-to-tail manner via strong charge-assisted N-H…O hydrogen bonds. The chains are parallel to the *a* axis and exactly in this direction we see the least thermal expansion, which explains why the *a* parameter becomes the least affected (increase by 1.9 %). The result is not surprising as strong interactions between proline molecules render the structure in this direction quite robust and less sensitive to temperature changes. On the contrary, the structure's response on heating is more pronounced in the *b* and *c* directions, where weak van der Waals interactions prevail.

Thus, we saw how seemingly simple case of the R/DL system turns out to be a rather complex one. A phase crossover was detected only for this combination of enantiopure flurbiprofen and racemic proline.

***In-situ* ball-milling.** Reaction in methanol-assisted grinding is fast and gives the impression that both phases appear at the same time, whereas isopropanol-assisted grinding shows well that the 2 : 1 phase appears first (see Figs. 3.4c and 3.4d). We believe that reaction in isopropanol is slower, this is why we can clearly distinguish both steps, whereas in the presence of methanol we miss the 2 : 1 step due to its fast conversion into the 1 : 1 cocrystal, and only see the region where both the 2 : 1 and 1 : 1 phases coexist. This result is in agreement with step-by-step grinding experiment: 2 : 1 R/DL converts into 1 : 1 R/DL if reground with an equimolar amount of DL-proline (see Fig. S37 in Appendix B).

### 3.3.4 RS-flurbiprofen/L-proline (RS-flurbiprofen/D-proline)

RS-flurbiprofen/L-proline (RS/L) exhibits a wide variety of different forms, five in total: four polymorphs of the 1 : 1 phase and one 2 : 1 form. Conditions under which these forms can be obtained are summarized in Scheme 3.4. The experiments performed are summarized in Tables S7 and S8 in Appendix B.

In terms of stoichiometry, RS/L system behaves similarly to those described above. Reaction starts with the formation of the 2 : 1 phase which then transforms into 1 : 1 phase. However, the 2 : 1 impurity in the final samples was quite significant in some cases, for instance in acetonitrile-assisted grinding in most of the experiments, the reaction stopped at the 2 : 1 phase without going any further no matter the grinding duration (see samples *6-10* in Table S7 and *6-9* in Table S8, Appendix B); isopropanol-assisted grinding sometimes resulted only in the 2 : 1 phase as well (see samples *16-20* in Table S7 and *15-18* in Table S8, Appendix B).

The initial compounds seemed to react best in methanol- and ethanol-assisted experiments. If the duration of grinding was sufficient, methanol- and ethanol-assisted grindings resulted in either one or another form of a 1 : 1 stoichiometry cocrystal (see, for instance, samples *1*, *3-5*, *12*, *13*, *15* in Table S7, Appendix B); we called these two forms polymorph I and polymorph II. Isopropanol-assisted grinding always resulted in polymorph II exclusively (if the reaction did not stop at the 2 : 1 stage) (see sample *15* in Table S8, Appendix B).

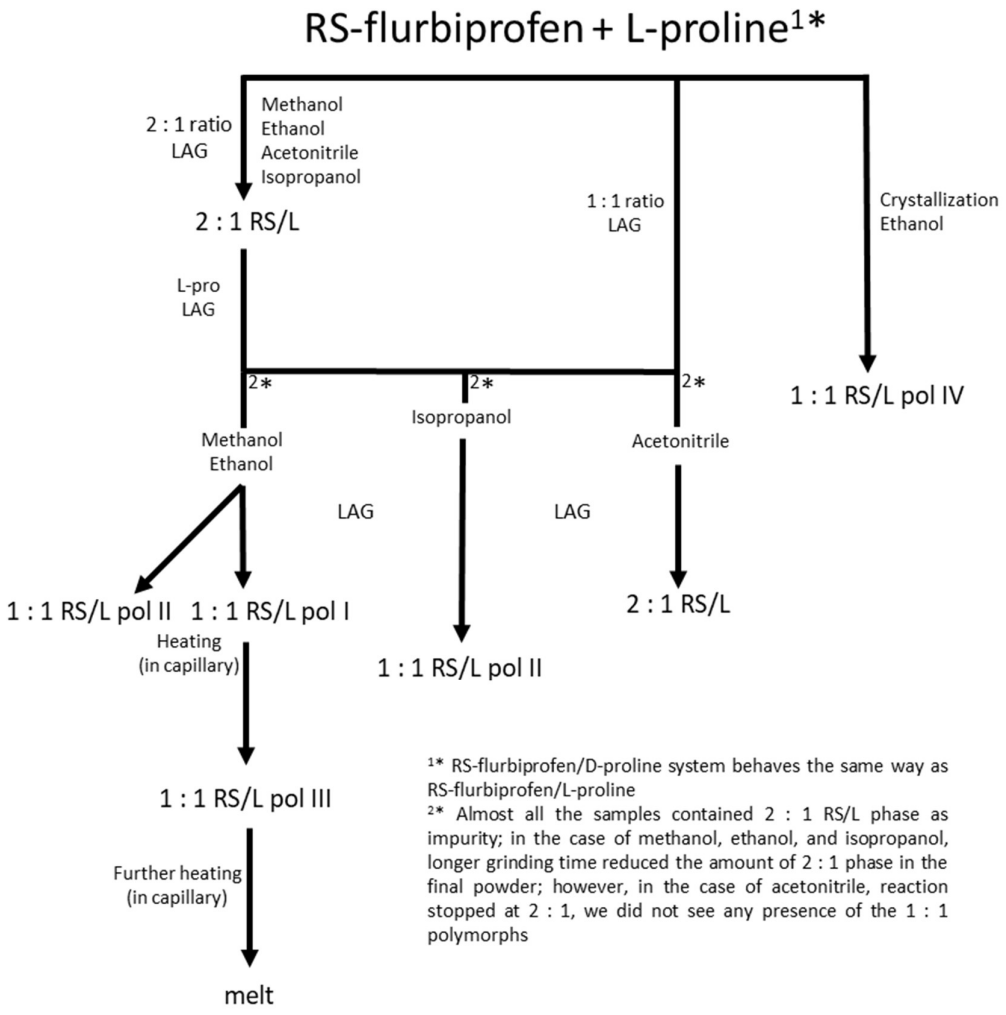


**Scheme 3.4.** Existing phases for the RS-flurbiprofen/L-proline system and conditions under which they can be obtained

DSC curves measured for the samples containing polymorphs I and II had a complex shape (see Figs. S23, S24, and S28 in Appendix B). Therefore, we decided to collect synchrotron diffraction data for these samples upon heating. The first sample prepared by methanol-assisted grinding (sample *1* in Table S8, Appendix B) initially contained 1 : 1 RS/D pol I and traces of the 2 : 1 phase. During heating, we first observed melting of the first phase – polymorph I (the end set is 137 °C) – then at the same time with the disappearance of the 2 : 1 impurity (which ended at 144 °C), another phase emerged, which turned out to be another 1 : 1 cocrystal which we called polymorph III; the latter completely melted at 189 °C (Fig. 3.6a). When heating the second sample that was prepared by isopropanol-assisted grinding (sample *15* in Table S8 in Appendix B) and contained 1 : 1 RS/D pol II, we also observed polymorph III emerging around 134 °C (Fig. 3.6b).

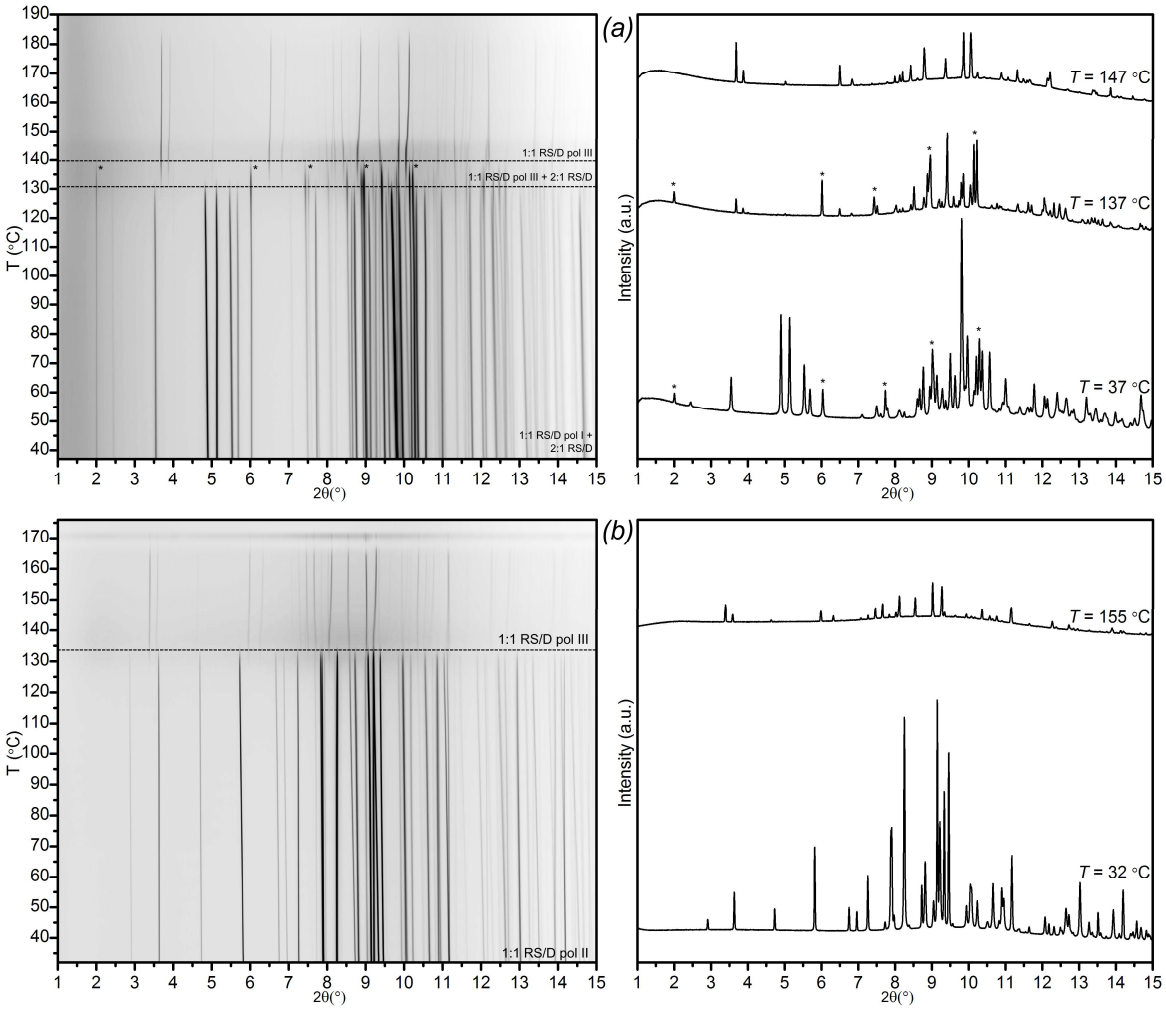


**Figure 3.6.** Powder X-ray diffraction patterns measured *in-situ* upon heating at a rate of 2 °C/min for (a) the RS/D sample prepared by methanol-assisted grinding in 1 : 1 ratio and heated from 37 to 190 °C, λ = 0.776188 Å (sample *1* in Table S8) and (b) the RS/D sample prepared by isopropanol-assisted grinding and heated from 32 to 176 °C, λ = 0.708 Å (sample *15* in Table S8): (left) film representation; (right) diffraction patterns at selected temperatures. (a) *T* = 37 °C – a mixture of 2 : 1 RS/D (marked as '*') and 1 : 1 RS/D pol I; *T* = 137 °C - a mixture of 2 : 1 RS/D (marked as '*') and 1 : 1 RS/D pol III; and *T* = 147 °C – 1 : 1 RS/D pol III. (b) *T* = 32 °C – 1 : 1 RS/D pol II and *T* = 155 °C – 1 : 1 RS/D pol III.

When crystallizing single-crystals for this system from solution, we did not succeed in obtaining any of these three polymorphs, but from ethanol solution we managed to crystallize a fourth unknown polymorph of the 1 : 1 stoichiometry, which we called polymorph IV.

***In-situ* ball-milling** in the presence of different solvents clearly shows that the 2 : 1 RS/L phase emerges first. During the *in-situ* experiments we did not observe formation of the 1 : 1 RS/L polymorph I, no matter which solvent was used or the duration of grinding. Figure S51 in Appendix B compares methanol-grinding for 25 min and 1 h – in both cases the resultant phase was 1 : 1 RS/L pol II. The reaction is the fastest in the presence of methanol. The kinetically favored 2 : 1 phase is not consumed completely and is present as impurity in the final powder (Fig. 3.7a).

Reaction in the presence of ethanol is slower, but on the other hand, the transformation from the 2 : 1 into 1 : 1 is more abrupt and happens within seconds, moreover, the final powder seems to be much more pure than in the case of methanol (Fig. 3.7b).

Reaction in the presence of acetonitrile and isopropanol is much slower and not always ends with the 1 : 1 phase (Figs. 3.7c and 3.7d). Thus, we can observe a substantial amount of the 2 : 1 as impurity in the final powder. Samples ground in the presence of acetonitrile become sticky which probably prevents good mixing of the compounds and thereby hinders transformation of the 2 : 1 phase into 1 : 1. One sample ground for 30 min showed some presence of the 1 : 1 phase in the end (Fig. S52 in Appendix B), but the second sample ground for 25 min resulted only in the 2 : 1 phase (Fig. 3.7c). In the case of isopropanol, the reaction was repeated three times and the 1 : 1 phase was detected only for the sample which was in contact with solution for 2h before being ground (Fig. S53 in Appendix B). The results of *in-situ* ball-milling are in agreement with the step-by-step experiments performed on the laboratory shaker mill, in which we did not always ended up with the 1 : 1 phase neither: the reaction outcome significantly depended on the solvent used and the milling time; methanol-and ethanol-assisted grinding reactions showed the highest chance of conversion into the 1 : 1 phase (Fig. S39-S45 in Appendix B).

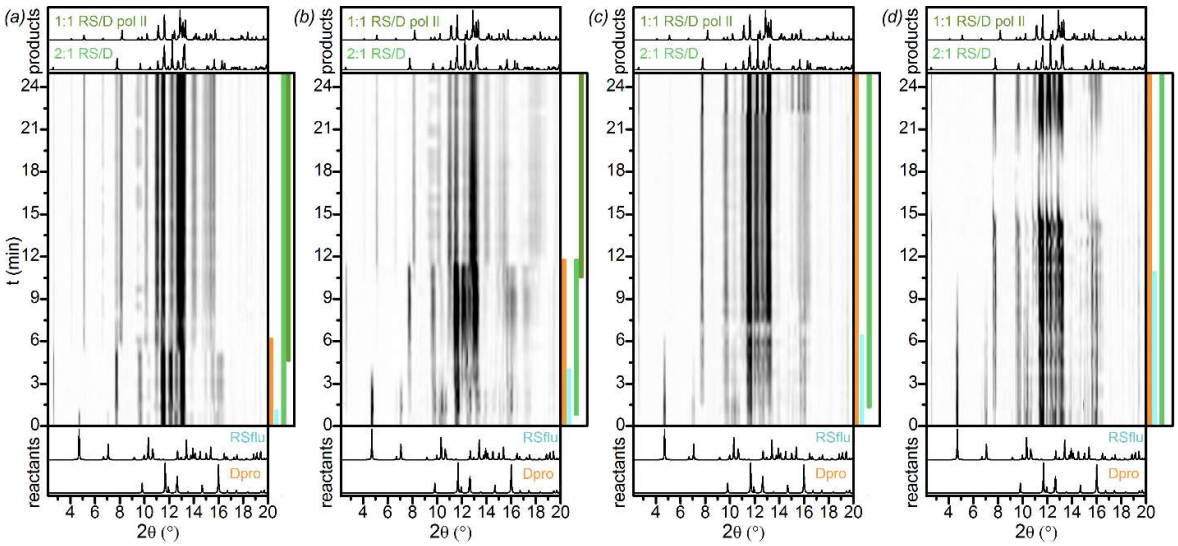


**Figure 3.7.** *In-situ* ball-milling X-ray diffraction patterns for the RS/D system, λ = 1 Å: (a) methanol-, (b) ethanol-, (c) isopropanol-, and (d) acetonitrile-assisted grinding. Colored bands on the right side of each image represent the presence of phases and are only for illustrative purpose.

In conclusion, the RS/L combination can lead to five forms: one with the 2 : 1 stoichiometry, and four 1 : 1 polymorphs. Laboratory ethanol- or methanol-assisted ball-milling led to polymorphs I or II. Isopropanol-assisted grinding always resulted in the polymorph II (or reaction stopped at 2 : 1 phase). Acetonitrile-assisted grinding in most cases stopped at the formation of the 2 : 1 phase. *In-situ* ball-milling showed that the reaction proceeds through the 2 : 1 phase.

### 3.3.5 RS-flurbiprofen/DL-proline

RS-flurbiprofen/DL-proline (RS/DL) is the simplest system in which we observed only one 1 : 1 cocrystal (see Scheme 3.5). The experiments performed are summarized in Table S6 in Appendix B. At the same time, despite being the simplest with only one cocrystal form, this system behaved peculiarly when ground in the 2 : 1 ratio with ethanol, isopropanol or acetonitrile: in those cases, a conglomerate, which is a mixture of the 2 : 1 RS/L and 2 : 1 RS/D cocrystals, emerged (see samples *5*, *8*, and *11* in Table S6, Appendix B). Adding one equivalent of DL-proline to the products of the 2 : 1 grinding resulted in the formation of the 1 : 1 RS/DL cocrystal (see Figs. S47-S49 in Appendix B). Surprisingly, 2 : 1 methanol-assisted grinding did not lead to the conglomerate, but to the 1 : 1 RS/DL and RS-flurbiprofen remaining(see sample *2* in Table S6, Appendix B).

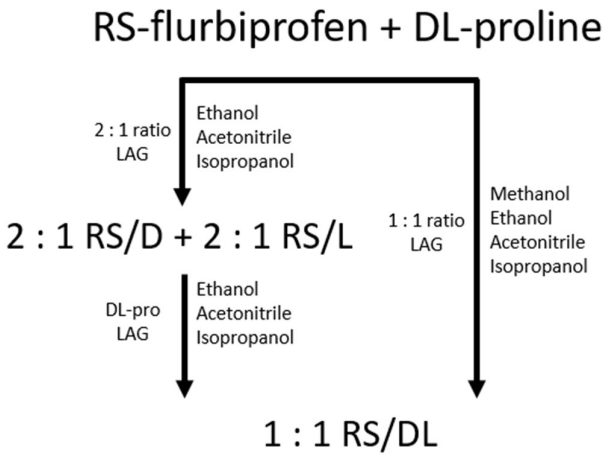


**Scheme 3.5.** Existing phases for the RS-flurbiprofen/L-proline system and conditions under which they can be obtained.

In order to understand the reaction pathway and to clarify whether the conglomerate emerges only in the case of 2 : 1 grinding or whether it is an intermediate product in 1 : 1 grinding as well, we performed *in-situ* ball-milling experiments.

The formation of the 2 : 1 RS/L-RS/D conglomerate was detected for liquid-assisted grinding in the presence of all the solvents. In the case of 1 : 1 methanol-assisted grinding, a tiny amount was observed only at the very beginning, whereas isopropanol-assisted grinding showed that this product is present for several minutes and only then disappears (Figs. 3.9a and 3.9b in Appendix B). Such a difference between methanol- and isopropanol-assisted grindings most likely results from different reaction rates: as was already noticed for other systems, reaction in the presence of methanol is the fastest, and is slower in the presence of isopropanol. Grindings in the 2 : 1 ratio in

the presence of the same solvents showed that both the conglomerate and the 1 : 1 RS/DL phase are present among the final products (Figs. 3.9c and 3.9d in Appendix B).

From the *in-situ* ball-milling data it seems that the conglomerate and the 1 : 1 RS/DL emerge in parallel and probably on competitive terms during synthesis, since both phases coexist. However, the conglomerate can react with an additional amount of DL-proline, resulting in the formation of

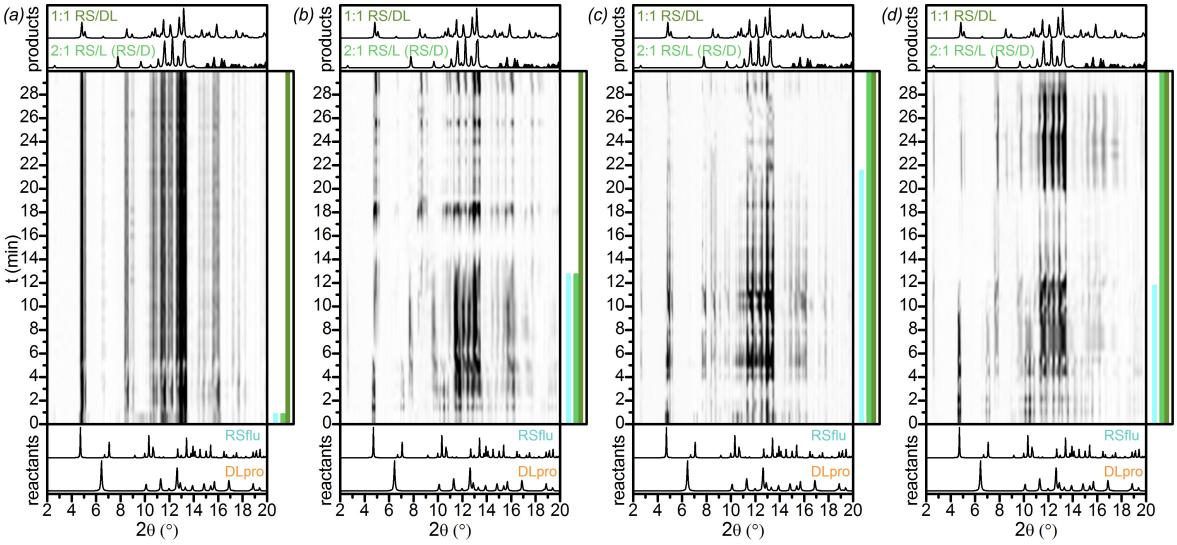


1 : 1 RS/DL, which was seen from the step-by-step grinding experiment, where the resultant powders of a 2 : 1 grinding were ground with an additional amount of DL-proline, which led to the formation of 1 : 1 RS/DL (see Figs. S47-S49 in Appendix B).

**Figure 3.9.** *In-situ* ball-milling X-ray diffraction patterns for the RS/DL system, λ = 1 Å: (a) 1 : 1 methanol-, (b) 1 : 1 isopropanol-, (c) 2 : 1 methanol-, and (d) 2 : 1 isopropanol-assisted grinding. Colored bands on the right side of each image represent the presence of phases and are only for illustrative purpose

Thus, we can conclude that no matter if the formation of the conglomerate precedes to the formation of 1 : 1 RS/DL or whether the conglomerate and 1 : 1 RS/DL phase appear as competitive products during reaction, the conglomerate tends to transform into 1 : 1 RS/DL upon grinding if proline is present in a sufficient amount. The nature of solvent is important as well. For instance, in the presence of methanol, the conglomerate may transform faster into 1 : 1 RS/DL. The conglomerate was not observed in the case of 2 : 1 methanol-assisted grinding, or was only present in small amounts undetectable in the preliminary diffraction experiments on our laboratory diffractometer, due to the fast conversion rates.

The *In-situ* X-ray diffraction data measured upon heating for the 2 : 1 isopropanol-assisted grinding clearly demonstrated the presence of the conglomerate (Fig. 3.8). The initial sample contained mostly a mixture of the 2 : 1 RS/L-RS/D conglomerate and RS-flurbiprofen; the 1 : 1 RS/DL cocrystal was present in negligible amounts. Upon heating, the RS-flurbiprofen impurity melts first, leaving pure conglomerate phase, which upon further heating disappears followed by the emergence of the 1 : 1 RS/DL cocrystal.

Hence, the RS/DL system is an interesting example, which demonstrates the possibility of conglomerate formation with the 2 : 1 stoichiometry and its further conversion into the 1 : 1 RS/DL cocrystal.

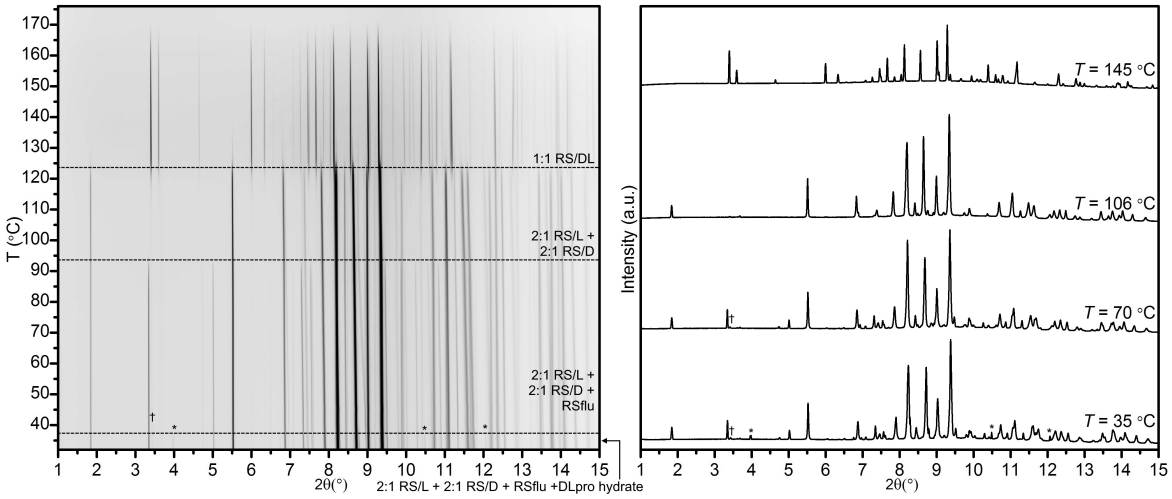


**Figure 3.8.** Powder X-ray diffraction patterns measured *in-situ* upon heating (from 35 to 177 °C) at a of 2 °C/min for the RS/DL sample prepared by isopropanol-assisted grinding in 2 : 1 ratio, λ = 0.708 Å: (left) film representation; (right) diffraction patterns at selected temperatures (sample *8* in Table S6). (a) *T* = 35 °C – a mixture of RS-flurbiprofen, 2 : 1 RS/L (2 : 1 RS/D), DL-proline hydrate (marked as '*') and a negligible amount of 1 : 1 RS/DL (marked as '†'); *T* = 70 °C – a mixture of RS-flurbiprofen, 2 : 1 RS/L (2 : 1 RS/D), and a negligible amount of 1 : 1 RS/DL (marked as '†'); *T* = 106 °C – a mixture of 2 : 1 RS/L (2 : 1 RS/D) and a negligible amount of 1 : 1 RS/DL (marked as '†'); *T* = 145 °C – 1 : 1 RS/DL.

Several words should be said about water assisted-grinding for all the aforementioned systems. Water-assisted grinding always stopped at the 2 : 1 forms in all systems, except for RS/DL (see samples *20-22* in Table S3, 13-15 in Table S4, *13-15* in Table S5, *21-26* in Table S7, and *19-21* in Table S8, Appendix B). Such a behavior may be caused by the ability of proline to form hydrates. Proline hydrates were observed among the products of the water-assisted grinding reactions. Hydration may complicate the reaction mechanism, as we do not know how hydrated water is involved into the reaction: whether it acts as "solvent" or is sort of "trapped" in the crystalline state and not easily available to participate in the reaction[73,248]. Probably, when formed, proline hydrates are very stable and do not break easily, thereby preventing the formation of the 1 : 1 phases due to a lack of available proline. We left beyond the scope of this work the investigation of the probable mechanisms of water-assisted grinding, which is too complex and may be a subject for a separate article.

Concluding the section on liquid-assisted grinding results, we note that the composition of the resultant powder of liquid-assisted grinding reactions significantly depend on the solvent used. This is most likely related to solution behavior of both compounds. Flurbiprofen and proline reach the best solubility in methanol and ethanol, thus reactions in these solvents proceed faster with a higher chance of obtaining pure products. Even though flurbiprofen is relatively soluble in acetonitrile and isopropanol, proline is almost insoluble in those solvents, which may be the reason why reactions proceed slower. According to one of the mechanisms suggested in literature[74,75] that can be applied to our systems, added liquid facilitates diffusion of molecules from the reactant to

the product phase via an intermediate solution phase, and the rate of diffusion increases during grinding as it is inversely proportional to the particle size.

The nature of solvent may affect reaction in other ways as well, for example, preventing good mixing by rendering the powder sticky or somehow modifying other surface properties that are crucial for interactions[253]. There might be some other factors in play, for instance, the energy of the ball-miller or the jar material, as they both directly determine the intensity of mechanochemical treatment. For example, we never saw any traces of the 1 : 1 RS/L pol I cocrystal in *in-situ* ball-milling experiments probably due to a different device or a different jar used in comparison with laboratory ball-milling. The total amount of powder and the amount of liquid may as well be of great importance. As when working with large amounts, it becomes trickier to establish the right amount of liquid, which, on the one hand, would be enough for complete conversion, and, on the other hand, would not dissolve a substantial part of the material making the process look rather like slurrying than grinding. The crystallite size of initial materials may affect the reaction rate as well, since smaller crystallites mean a larger reactive surface area. Thus, we conclude that solubility may not be the only issue in grinding reactions and other factors should not be underestimated.

Concerning the *in-situ* experiments upon heating, as we mentioned above, phase transformations upon heating may not be the same in capillary or in DSC capsule due to the different experimental setups. Thus, experimental DSC curves and PXRD data collected upon variable temperature should be compared with a great care especially when dealing with multicomponent systems. In this work, we did not examine DSC data in detail, but rather used it as a sign for probable complexity and existence of various phases in a sample. We focused mostly on the PXRD synchrotron data collected upon heating to explore phase transformations occurring in the samples whose DSC curves had a complicated shape. However, these data should also be considered with caution. Since we deal with samples that were obtained by grinding and since several cocrystals are possible, such samples may contain a very small amount of various phases (seeds) that may not be detectable by PXRD; upon heating, less stable forms melt allowing more stable forms to crystallize from those previously undetectable seeds. Thus, depending on which phases were initially present in the sample, the result of the *in-situ* PXRD upon heating may differ from sample to sample. This could explain, for example why in the case of 1 : 1 R/L/MeOH sample in one case we see 1 : 2 R/L appearing and in another case we see L-proline pol II instead (Figs. 1 and S54 in Appendix B). Another example is the RS/DL system: the initial compounds were ground in a 2 : 1 ratio in the presence of isopropanol; the initial sample, which contained an almost negligible amount of 1 : 1 RS/DL, transformed completely into 1 : 1 RS/DL upon heating. In this case, we cannot really say, whether such a transformation into 1 : 1 RS/DL would take place if the initial sample did not contain any 1 : 1 RS/DL; moreover, it would not be possible to prove the complete absence of 1 : 1 RS/DL in the sample– small seeds may still be present, but undetectable. Heating rate may also be of great importance in such experiments since, if the heating is too fast, phase changes may occur very quickly and can thus be missed. Despite the aforementioned uncertainties, *in-situ* PXRD experiments upon variable temperature is a great tool to discover new phases difficult to obtain at ambient conditions and to trace phase transformations[254–256]; such experiments nicely complement thermogravimetric data, which sometimes may be tricky to interpret.

In the last section of this article we will discuss in detail the crystal energies of the obtained cocrystals calculated by DFT-D3, which will give us an additional insight into the results discussed above, including possible reaction mechanisms, cocrystal stability and correlations with chirality.

## 3.4 Structural Analysis

Among all found structures, we can distinguish 5 types of packing. Depending on the chirality, a particular system can adopt one or several packing types (see Scheme 3.6). Each of the types will be discussed below in detail; the selected structures are given in Fig. 3.9.

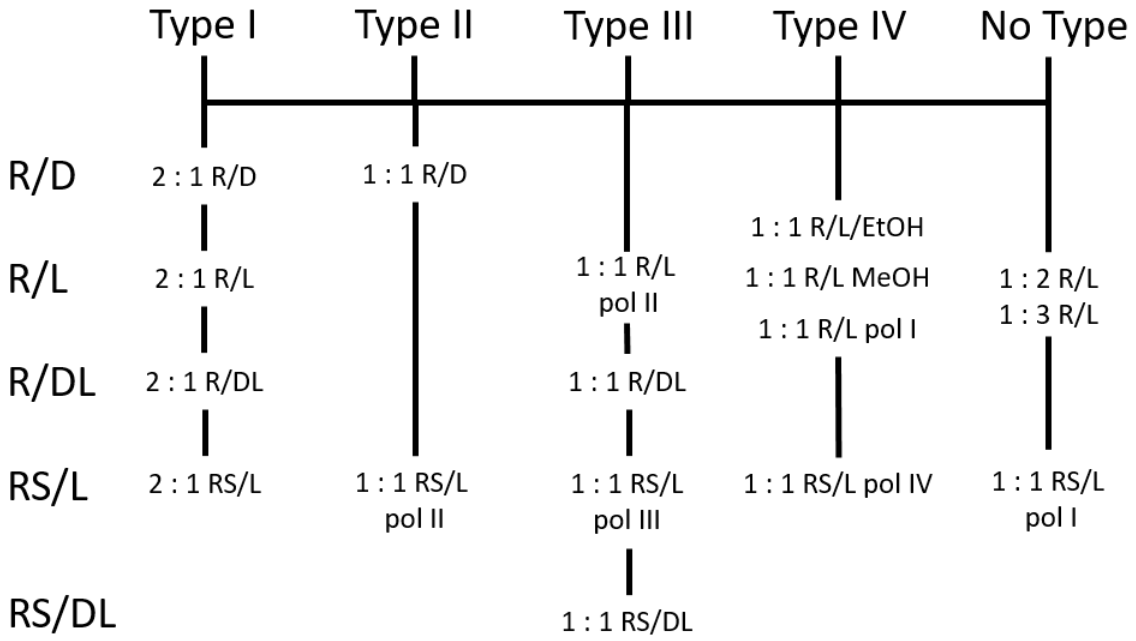


**Scheme 3.6.** Structural types distinguished for flurbiprofen/proline cocrystals.

**Type I packing** corresponds to the 2 : 1 stoichiometry and is observed in all systems (R/L, R/D, RS/L, and R/DL), except RS/DL. In the structures of this type, proline molecules form single infinite head-to-tail chains along the *a* axis, connecting one another by N-H…O hydrogen bonds; the carboxyl group of each proline molecule connects two flurbiprofen molecules by O-H…O hydrogen bonds, thereby forming a layered "sandwich-like" structure: the core of each "sandwich", made of proline, attaches flurbiprofen from both sides. The structure of 2 : 1 R/DL is almost identical to the 2 : 1 R/D, except that in the former D- and L-proline share one position (see Fig. S70 in Appendix B). The R/D fragment of the 2 : 1 R/DL cocrystal is almost identical to 2 : 1 R/D (Fig. S71 in Appendix B), whereas the orientation and position of R-flurbiprofen differ significantly from that found in 2 : 1 R/L (Fig. S72 in Appendix B).

Due to similarity, diffraction patterns of the cocrystals with the type I packing have peaks extremely close to one another making it difficult to distinguish between them without either good quality powder X-ray or single-crystal diffraction data (see Fig. S73 in Appendix B).

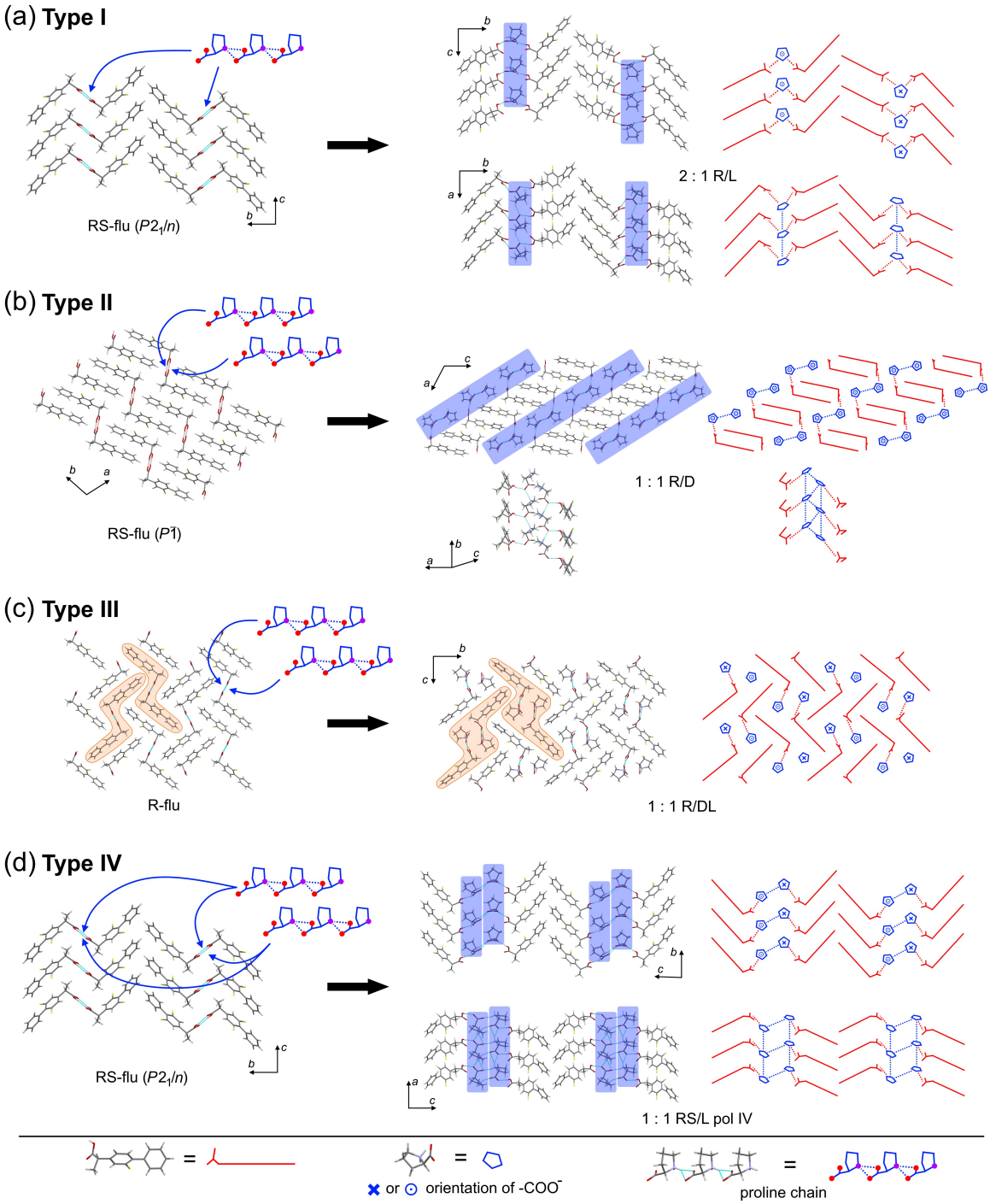


**Figure 3.9.** Crystal packing in selected cocrystals representing four structural types distinguished for flurbiprofen/proline system. In (d) the disorder of proline is omitted for clarity.

**Type II packing** corresponds to the 1 : 1 stoichiometry and is observed in 2 systems: R/D and RS/L pol II. Proline molecules form double infinite head-to-tail chains along the *b* axis, which are connected via N-H…O hydrogen bonding; each proline connects one flurbiprofen by O-H…O hydrogen bonds. Double proline chains situated on top of one another form layers; stacked molecules of flurbiprofen form layers as well.

**Type III packing** corresponds to the 1 : 1 stoichiometry and is observed in 4 systems: R/L ( pol II), RS/DL, RS/L ( pol I and III), and R/DL. Proline head-to-tail chains arrange in pairs along the *a* axis with each proline connecting one flurbiprofen. The structure is made of blocks formed by two proline chains, each attaching flurbiprofen. Symmetry-independent flurbiprofen molecules are situated almost orthogonally with respect to one another.

**Type IV packing** corresponds to 1 : 1 stoichiometry and is observed in 2 systems: R/L (including its methanol and ethanol solvates) and RS/L pol IV. This type of packing represents another "sandwich-like" structure: in the case of RS/L pol IV, proline molecules form double head-to-tail chains with flurbiprofen molecules attached from both sides; and in the case of R/L, solvent molecules enter the space between proline chains, forming solvates.

**"No type" packing.** The structures with 1 : 2 and 1 : 3 stoichiometry found for the R/L system and the 1 : 1 RS/L pol I structure were not assigned to any of the aforementioned types as they are unique.

In the 1 : 2 R/L cocrystal (Fig. 3.10a), there are two types of head-to-tail proline chains which are situated perpendicular to one another: the chains of the first type that are along the *b* axis connect flurbiprofen from both sides and the chains of the second type which are along the *a* axis are connected only to proline molecules of the first type and not to flurbiprofen. Flurbiprofen molecules are arranged in a stacked manner.

In the 1 : 3 R/L cocrystal (Fig. 3.10b), there are three symmetry-independent interconnected proline chains, all in the same direction along the *a* axis, and flurbiprofen again is connected to only one of them. Overall, the structure can be described in terms of proline and flurbiprofen blocks situated in a staggered order.

In the 1 : 1 RS/L pol I cocrystal (Fig. 3.11c), we again see proline chains situated in pairs which run along the *a* axis. Each proline connects one flurbiprofen. Overall, the structure can be described as "brickwork", in which each "brick" consists of two prolines and two flurbiprofens; the "bricks" are infinite in the *a* direction as proline chains are infinite.

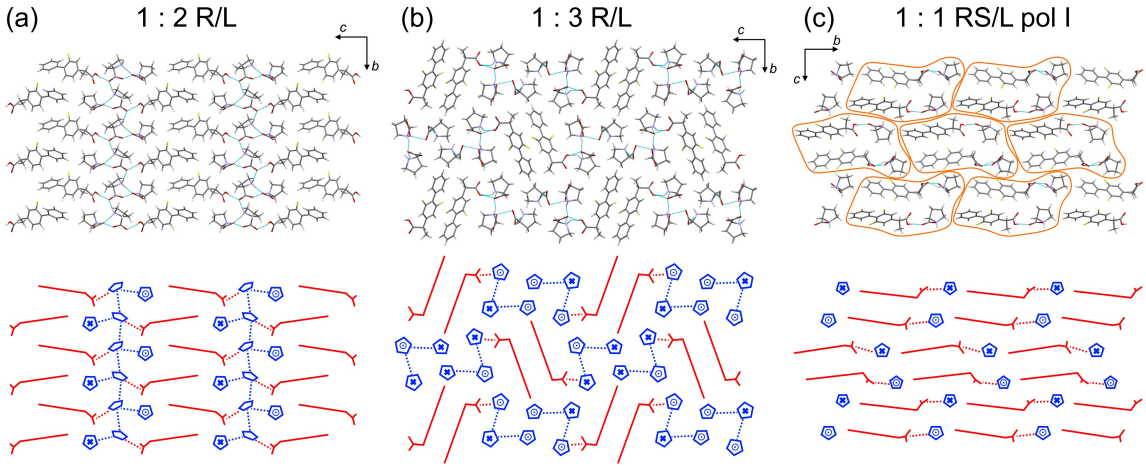


**Figure 3.10.** Crystal packing in the cocrystals from "No type" category.

Hence, these structural data show that, in its cocrystals with flurbiprofen, proline molecules form infinite head-to-tail chains: single chains (type I), single chains situated by pairs (types III and IV), double interconnected chains (types II and IV). Proline molecules attach flurbiprofen via O-H…O hydrogen bonds between their carboxyl group and the carboxyl group of flurbiprofen; finally, altogether these flurbiprofen/proline units, in most cases, pack into layered structures (types I, II, IV, 1 : 2 R/L) or constitute "block-like" structures (type III, 1 : 3 R/L, 1 : 1 RS/L pol I).

If we compare the packing of flurbiprofen molecules in pure flurbiprofen and its cocrystals, we see that, in the latter, flurbiprofen tends to pack in a similar manner with proline chains wedged in between. For example, in the cocrystals of packing types I and IV flurbiprofen is arranged similarly to RS-flurbiprofen ($P2_1/n$); the cocrystals with type II packing resemble RS-flurbiprofen ($P$-1); and the cocrystals of type III have flurbiprofen packed as in R-flurbiprofen (Fig. 3.9). This observation is not surprising as interactions between flurbiprofen molecules contribute significantly to the overall structure and, thus, flurbiprofen molecules arrange in the most favorable way.

In the cocrystals, proline in its turn keeps forming strong charge-assisted hydrogen bonding typical of amino acids (for packing in L-pro pol I and II see Fig. S74 in Appendix B); this leads to higher melting points of cocrystals (see Table 1 for the values of the melting points) as the percentage of strong interactions in the latter increases significantly in comparison with pure enantiopure ($T_m$ = 109 °C) or racemic flurbiprofen ($T_m$ = 115 °C), thereby establishing a good example of structure-property relationship.

SEM images of selected samples obtained by grinding (sample *1* in Table S7, containing a mixture of 1 : 1 RS/L pol II and 2 : 1 RS/L; sample *5* in Table S3, containing 2 : 1 R/L and a small amount of R-flurbiprofen impurity; and sample *6* in Table S8, containing a mixture of 2 : 1 RS/D and D-proline, Appendix B) are presented in Fig. 3.11. All of them show crystalline materials with mostly needle-shaped crystallites; this fact is in agreement with solution crystallization, by which we also obtained needle-shaped single crystals. This result is not surprising, as crystals tend to grow faster in the direction of the strongest bonds; and in our case, this is the direction coinciding with proline head-to-tail chains with strong charge-assisted hydrogen bonding.

Analysis of other cocrystals with proline found in the Cambridge Structural Database (CSD) shows that proline is quite flexible in terms of packing and cocrystallizes even with very bulky compounds (see for example, CCDC REF CIPVUU, CIPZIM,[216] DUCJUP[257], NAZGUS, NAZHAZ[187]). Proline molecules within a particular structure always form hydrogen bonds with one another producing head-to-tail chains. For example, known cocrystals of proline and naproxen[142] (CCDC REF FEVZOX, FEVZUD) adopt type IV packing according to our classification. The cocrystal of 1,1-Dicyano-2-(4-hydroxyphenyl)ethene and L-proline[190] is an example of type II packing (CCDC REF IHUMAZ). Type III and Type IV packings can be found among flavonoid cocrystals with proline (CCDC REF EJEQAN, EJEQOB for type III and EJEPUG, EJEQIV for type IV)[214]. Depending on the number of functional groups prone to hydrogen bonding in the co-former, proline may also produce stoichiometrically diverse cocrystals, for instance 1 : 2 stoichiometry (co-former : proline) can be observed in cocrystals with fumaric acid (CCDC REF GIHSOH and GIHSUN)[221], with aminobenzoic acid (CCDC REF CIDBOH)[220] or with the drug dapagliflozin (CCDC REF CIPVUU[216]). Hydrates and solvates of

proline cocrystals are often encountered as well (see CCDC REF BEXGUI, BEXTUW[142], NAZGOM[187]). As for flurbiprofen, only two cocrystals were found in the database: a 2 : 1 cocrystal with 4,4'-bipyridine (CCDC REF HUPPEN[129]) and a 1 : 1 cocrystal with nicotinamide (CCDC REF QOBGAR[258]); and none of them are chiral. The cocrystal with 4,4'-bipyridine adopts type I packing, except that 4,4'-bipyridine does not form chains as proline. The cocrystal with nicotinamide can be described by a type IV packing ("sandwich-like" motifs) according to our classification.

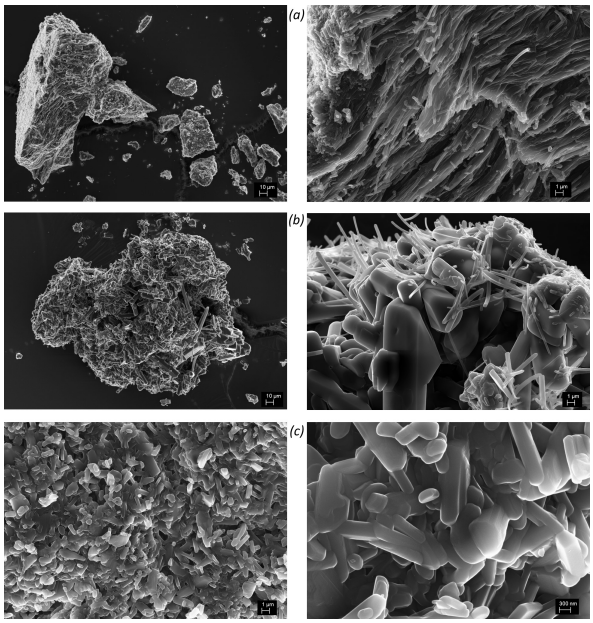


**Figure 3.11.** SEM images in different magnitudes of (a) RS-flu/L-pro sample containing a mixture of 1 : 1 RS/L pol II and 2 : 1 RS/L (left 10 μm and right 1 μm), (b) R-flu/L-pro sample containing 2 : 1 R/L and a small amount of R-flurbiprofen as impurity (left 10 μm and right 1 μm), and (c) RS-flu/D-pro sample containing mixture of 2 : 1 RS/D and D-proline (left 1 μm and right 300 nm). All samples were prepared by liquid-assisted grinding.

Hence, flurbiprofen/proline cocrystals adopt 4 types of crystal packing, which resemble different types of packing found for pure flurbiprofen. Exotic cocrystals with 1 : 2 and 1 : 3 flurbiprofen/proline stoichiometry, in which flurbiprofen is connected to only one of the proline molecules, were found for the R/L system. Existence of the aforementoioned stoichiometries highlights the importance of strong charge-assisted hydrogen bonds between proline molecules and their ability to unite proline chains without their connection to the main co-former (flurbiprofen). From the analysis of our structures and other structures from the CSD, we conclude that proline molecules in cocrystals tend to form chains by connecting one another in the head-to-tail manner – a behavior similar to pure proline; between flurbiprofen molecules weak van der Waals interactions prevail.

## 3.5 DFT: Analysis of Calculated Energies

Density functional theory is widely used for various materials modeling problems. DFT methods are based on computing the electron density, not the electron wave function. In contrast to the wave-function based methods that can converge to the exact solution of the Schrödinger equation, DFT methods give only the approximate solution, which is highly dependent on the functional

used. Since the exact functional of the Hohenberg-Kohn theorem is not known, there is an intrinsic uncertainty between the energies calculated by DFT and the true ground-state energies of the Schrödinger equation. Another weakness of DFT is its inaccurate estimation of van der Waals (vdW) interactions, whose contribution is substantial in molecular crystals. Dispersion correction methods that consider the total energy as the sum of the conventional Khon-Sham DFT energy and a correction term that accounts for vdW interactions help to overcome the abovementioned problem and obtain reasonable results. Hence, the energies obtained by DFT calculations highly depend on the initial choice of parameters, including the functional, *k* point grids, energy cut-off, convergence criterion, etc.[119]

This being said, we emphasize that the energies calculated for our cocrystals must not be considered as absolute values but rather compared relatively to one another. In this contribution, we primarily used DFT-D3 to validate the structures solved from powder X-ray diffraction data. Secondary, we analyzed whether the calculated energies of cocrystals correlate with the structural peculiarities.

**Validation of the structures solved from powder.** DFT calculations are widely used to check the correctness of the structures found from powder X-ray diffraction data.[120] We followed the procedure and calculated RMSD values (using the Mercury[156] program) for the initial structures solved from PXRD and DFT optimized structures (only the molecules in the asymmetric part were compared, hydrogen atoms were not included). The best match between the experimental and calculated structures was obtained for L-proline pol II: RMSD was only 0.246 Å; taking into account that the structure was solved at 116 °C and is prone to disorder of the ring, we find this result more than satisfactory. RMSD values obtained for the cocrystals were higher: 0.824 Å for 1 : 1 R/DL; 0.631 Å for 1 : 1 RS/D pol I; 0.631 Å for RS/D pol III; 1.33 Å for 1 : 1 R/L pol I; 1.28 Å for 1 : 1 R/L pol II; and 0.671 Å for 1 : 3 R/L. However, overlapping of the experimental and DFT-optimized structures (see Fig. S76-S82 in Appendix B) reveals that high RMSD values result mostly from a significant shrinkage in one or several directions. One of the probable reasons why the structures significantly shrink can be the fact that the DFT calculations in our case represent the structures at 0 K and not at the original experimental temperature. Probable disorder of proline molecules can be another cause of high RMSD values. Disorder of the proline ring was observed in almost all the structures solved from single-crystal X-ray diffraction data (see Figs. S65-S69 in Appendix B); thus, we do not see any reason why it should not be the case for the structures solved from the powder X-ray diffraction data. Since DFT optimization kept the structural integrity and taking into account the aforementioned factors, we conclude that the solved structures should be considered correct.

**Energy, chirality, and structural peculiarities.** All the structures after DFT optimization kept their structural integrity; the change in the volume of the unit cell was less than 5 % for the majority of the structures (see Table S10 in Appendix B). The structures with the Type I packing (2 : 1 stoichimetry cocrystals) and 1 : 1 RS/L pol IV and 1 : 1 R/L pol I belonging to the Type IV packing underwent a substantial shrinkage of the one of the unit cell parameters (up to 8-9 Å for some of the structures, see Table S10 in Appendix B), which can be associated with the fact that DFT calculations represent the structures at 0 K and not the original experimental temperature. All compounds that exhibit type I packing, including pure RS-flurbiprofen ($P2_1/n$), respond similarly

to the DFT optimization procedure, differing only by the extent of shrinkage. The maximum reduction in the length of the corresponding unit cell parameter was around 8-9 Å and was observed for 2 : 1 R/L, 2 : 1 R/D, and pure RS-flurbiprofen $P2_1/n$ (see Table S10 in Appendix B). On the contrary, the shrinkage in the 2 : 1 RS/L, 1 : 1 R/L pol I, and 1 : 1 RS/L pol IV was only around 3-4 Å. Figures S75 in Appendix B depicts the aforementioned observation.

The total energies calculated for the optimized structures are listed in Table 3.2. Comparing the energies calculated for the flurbiprofen/proline cocrystals, we suggest that the structures with lower energy may have a more efficient bonding than the structures with higher energy.

It is important to note that, first, DFT calculations in our case do not account for the temperature effects and, second, the energy difference between certain cocrystals is quite small and may result from a computational error. This is why ordering by the energy should not be considered as absolute true evidence of the efficiency of interactions in the crystal, but it should rather serve as approximate guidance.

**Table 3.2.** Total energies calculated for cocrystals by DFT-D3.

| Structure | $E$, eV | $E_{\text{per unit}}$*, eV |
|---|---|---|
| 2 : 1 R/L | -1016.3814 | -508.1907 |
| 2 : 1 R/D | -1016.5369 | -508.2685 |
| 2 : 1 RS/L | -508.6012 | -508.6012 |
| 1 : 2 R/L | -815.4795 | -407.7398 |
| 1 : 3 R/L† | -2033.6389 | -508.4097 |
| 1 : 1 R/L pol I† | -609.0941 | -304.5470 |
| 1 : 1 R/L pol II† | -1219.1133 | -304.7783 |
| 1 : 1 R/D | -1221.6640 | -305.4160 |
| 1 : 1 R/DL† | -1221.4001 | -305.3500 |
| 1 : 1 RS/D pol I† | -1218.8140 | -304.7035 |
| 1 : 1 RS/L pol II | -610.8884 | -305.4442 |
| 1 : 1 RS/D pol III† | -1220.0258 | -305.0065 |
| 1 : 1 RS/L pol IV | -610.5163 | -305.2582 |
| 1 : 1 RS/DL | -1221.8909 | -305.4727 |
| L-proline pol I | -408.7061 | -102.1765 |
| R-flurbiprofen | -813.4549 | -203.3637 |

(*) ”unit” means a ‘cocrystal unit’, for instance for 2 : 1 R/L the unit consists of 2 molecules of R-flurbiprofen and 1 molecule of L-proline, for 1 : 1 R/L the unit consists of 1 molecule of R-flurbiprofen and 1 molecule of L-proline, etc.
(†) structures were solved from powder X-ray diffraction data

When studying chiral cocrystals, common sense tells us that the possibility of cocrystal formation between a pair of chiral co-formers highly depends on how their three-dimensional structures

"suit" each other. A parallel can be made with chiral drugs: since the human body is amazingly enantioselective, a particular drug enantiomer would only act on the biological sites whose three-dimensional structure allows interaction. Thus, in cocrystals we can expect that some of the chiral combinations of co-formers will be more favorable than the others. Recent studies in the field of chiral cocrystallization have indeed shown that enantiomers may respond differently to cocrystallization when probed with chiral co-formers; some examples are briefly outlines in the Introduction section to this chapter.

The melting points, as they directly depend on the interactions may serve as an indication of packing efficiency and the strength of interactions, which in their turn can be related to the chirality, *i.e.* how the three-dimensional structures of co-formers "suit" one another.

First, we compared the energies of the 2 : 1 cocrystals. The lowest energy was observed for the RS-L pair, which may indicate that this pair of co-formers "suit" each other better than the R-L or R-D pairs whose energies are slightly higher. The melting point for the 2 : 1 RS/L (162 °C) cocrystal was also slightly higher than that of 2 : 1 R/L (158 °C) or 2 : 1 R/D (153 °C), which may mean more efficient interactions in the structure and thus is in agreement with the statement above.

Second, we ranged the 1 : 1 cocrystals in the following order of increasing total energy:

1 : 1 RS/DL ($T_m$ = 194 °C) → 1 : 1 RS/L pol II ($T_m$ = 151 °C) → 1 : 1 R/D ($T_m$ = 145 °C) → 1 : 1 R/DL → 1 : 1 RS/L pol IV → 1 : 1 RS/L pol III → 1 : 1 R/L pol II → 1 : 1 RS/L pol I → 1 : 1 R/L pol I

Unfortunately, we do not have the melting points for all the compounds, but the melting points found for the first three cocrystals with the lowest energies indicate that this sequence does not lack sense. The 1 : 1 RS/DL cocrystal has the lowest energy and the highest melting point, which is a reasonable result as having more enantiomers available means that the system has more possibilities at its disposal to choose the most efficient packing interactions. The last cocrystal in this sequence was obtained only from the corresponding methanol solvate, when the solvent evaporated upon heating, and was not observed under any other synthetic conditions. Thus, this cocrystal is definitely not the system's first choice when making interactions and may probably be the last if the system has other options at hand.

Calculated Kitaigorodsky packing indexes varied from 65 to 70 (percent of filled space) and did not show any correlation with the energies, thereby indicating that overall packing efficiency hardly differ from structure to structure. Although, the overall packing efficiency may not differ much, the strength and amount of certain interactions might vary to a higher extent. However, it is difficult to quantify the exact contributions of various interactions in molecular crystals as the latter are held together by weak interactions, such as hydrogen bonds or vdW interactions. Hence, correlating the energies and certain interactions cannot be easily done.

The energies calculated for the R/L cocrystals may also help to clarify the state of affairs in this system. It appears that the 1 : 3 R/L cocrystal, which was highly unstable and converted into 1 : 2 R/L cocrystal if not dried properly after grinding, has much higher formation energy (143.14 kJ/mol) than any of the other forms in the R/L system. In contrast, the 1 : 2 phase has the lowest negative formation energy (-2.22 kJ/mol), which can be the reason why the 1 : 3 cocrystal converts

so easily into 1 : 2 in the presence of trace amounts of solvent. (The formation energies in this case were calculated the from the $E_{\text{per unit}}$ values given in Table 3.2 as follows:

$\Delta E = E_{\text{cocrystal}} - (aE_{\text{co-former-1}} + bE_{\text{co-former-2}})$,

where $a$ and $b$ coefficients represent the stoichiometric ratio.)

Thus, DFT-D3 calculations can be used not only for the validation of the structures solved from powder X-ray diffraction data, but may also bring some insights into structure-related issues.

## 3.6 Conclusions

Flurbiprofen/proline cocrystals represent an example of great complexity that can be reached when working with two chiral co-formers. Various combinations of enantiopure and racemic flurbiprofen and proline produced in total 17 cocrystals, including polymorphs and stoichiometrically diverse forms. Depending on the structure packing pattern, found cocrystals were divided into 5 groups; the last group contained cocrystals with unique structures, including exotic 1 : 2 and 1 : 3 R/L cocrystals in which flurbiprofen was connected to only one of the proline molecules in the asymmetric unit. Combining different techniques, with powder X-ray diffraction and liquid-assisted grinding being the major tools, helped us to establish conditions of cocrystal formation and gain insight into reaction pathways. *In-situ* ball-milling confirmed that the 2 : 1 cocrystals are the most kinetically favorable and emerge first during grinding. A stepwise mechanism was suggested for the formation of certain 1 : 1 cocrystals, with the 2 : 1 phase being converted into the 1 : 1 as reaction proceeds. The solvents' role in liquid-assisted grinding proved to be extremely important as it affected the reaction rate and in some cases the reaction outcome. *In-situ* PXRD collected upon varying temperature revealed additional cocrystals that emerge at higher temperatures and one phase crossover. Analyzing the structural data found in the CSD and our own results, we conclude that proline is highly prone to cocrystallization and can serve as a promising co-former for various applications. However, as we saw by the example of flurbiprofen/proline system, extreme complexity of proline-based cocrystals, like multiple polymorphs, stoichiometric diversity, incorporation of solvent, may be the other side of the coin and should not be underestimated.

# CONCLUSIONS AND PERSPECTIVES

This work focused on studying amino acids as potential co-formers for pharmaceutical cocrystals. In the first part, by the example of naproxen/amino acid cocrystals, we established several general trends typical of zwitterionic compounds. In the second part, by the example of flurbiprofen/proline cocrystals, and with the help of a unique combination of cutting-edge characterization techniques, we demonstrated how a relatively easy system may result in a large variety of cocrystal forms.

In the Preface chapter I outlined several important questions raised in this work and now I would like to provide answers that we learned.

The **first questions** are related to **amino acids as cocrystal formers**:

- *What sort of APIs do amino acids tend to cocrystallize with?*
- *How do amino acids behave when cocrystallized with APIs, taking into account the zwitterionic nature of the former?*
- *What properties of APIs can be changed through cocrystallization with amino acids?*
- *What are the challenges when producing cocrystals with amino acids?*
- *Under which conditions can various cocrystals be obtained, including polymorphs, stoichiometrically diverse forms or solvates/hydrates and can the outcome be controlled?*

Since all these questions are interconnected, and the answer to one question may be a key point in another question as well, I provide the answers altogether below in order to avoid repetitiveness.

From the initial cocrystal screening performed for a series of APIs and a series of amino acids, we found that amino acids seem to cocrystallize only with compounds that possessed a carboxyl group: only naproxen and flurbiprofen yielded cocrystals, whereas other compounds (levetiracetam, oxiracetam, and dyprophilline) failed. A search in the CSD revealed plenty of cocrystals with carboxylic acids (including those in which proton transfer occurred resulting in salts) and only few cocrystals with other compounds.Such behavior of amino acids may result from their zwitterionic nature: strong charge-assisted hydrogen bonds existing in amino acids render their crystal lattice highly robust and thus not easily breakable. In order for a cocrystal to be formed, the target compound should be able to provide a competitive hydrogen bonding network. The tendency of amino acids to form head-to-tail chains via charged-assisted N-H…O hydrogen bonds preserves in cocrystals.

Introducing charge-assisted hydrogen bonds into the structure of APIs helps to significantly increase the melting point, thereby providing a way to work with compounds that melt at low temperatures. Since most of the amino acids are readily soluble in water, they may potentially improve the dissolution rate and bioavailability if cocrystallized with APIs. However, the latter does not lack a challenging aspect.

When working with amino acids in solution, the main challenge lies in the solubility. A large difference in the solubility of the API and the amino acid will lead to a highly incongruent system, in which obtaining their cocrystal becomes almost impossible as the cocrystallization zone in the phase diagram becomes too narrow. The same obstacle may prevent producing cocrystals with better dissolution rate or bioavailability as recrystallization into one of the initial cocrystal formers may occur almost immediately after the cocrystal is placed into solution. Incongruent behavior can

be overcome by using mixed solvents, for example, alcohol/water; tuning the solvent composition may allow approaching congruent behavior with a larger cocrystallization zone and thus, higher cocrystal yield. However, the tendency of many amino acids to form hydrates or solvates can make the crystallization process more complicated.

Cocrystals of amino acids can be prepared by different ways, including liquid-assisted grinding and solution approaches. However, the choice of the solvent is crucial for the process, even in liquid-assisted grinding where its amount is extremely small relative to the solid phase. For the flurbiprofen/proline system, we found that the solvent significantly affects the reaction outcome, affecting its rate or even leading to different products.

Even though the carboxyl group and the amino group in amino acids are both prone to hydrogen bonding, we managed to obtain only a few cocrystals: out of around 20 amino acids screened naproxen formed cocrystals only with 4 of them, alanine, tryptophan, tyrosine, and proline; whereas, flurbiprofen cocrystallized only with proline. Such behavior can be again related to the strong-charged assisted hydrogen bonding and robustness of pure amino acid structures. However, this behavior should not be considered as a negative side of amino acids, which are the main building units of proteins in the human body, and if they readily cocrystallized with almost any substance, the body integrity could be compromised.

**The second important question concerned chirality** issues. By the example of naproxen cocrystals, we showed that both the formation of diastereomeric pairs (naproxen/alanine and naproxen/tryptophan) and the enantiospecific behavior (naproxen/tyrosine) are possible.

The flurbiprofen/proline system turned out to be extremely complicated. Various combinations of enantiopure and racemic flurbiprofen and proline yielded in total 17 cocrystals, including polymorphs, stoichiometrically diverse forms, and cocrystal solvates. A two-step mechanism of formation of 1 : 1 cocrystals via an intermediate 2 : 1 form was established. The R-flurbiprofen/L-proline combination resulted in the richest variety of forms, including exotic 1 : 2 and 1 : 3 (flurbiprofen : proline) cocrystals, in which flurbiprofen is connected to only one proline molecule. Meanwhile, the R-flurbipfrofen/D-proline combination turned out to be the simplest, yielding only two forms: 1 : 1 and 2 : 1 cocrystals. When studying chiral cocrystals, common sense tells us that the possibility of cocrystal formation between a pair of chiral co-formers highly depends on how their three-dimensional structures “suit” each other. Thus, in cocrystals we can expect that some of the chiral combinations of co-formers will be more favorable than the others; it may even result in the enatiospecific behavior when only one the enantiomers is capable of forming a cocrystal. Introducing racemic compounds to the system may result in a more efficient packing as with more chiral centers at hand, the system has more possibilities to find a better molecular arrangement in comparison with the pairs of pure enantiomers.

**The final question concerned characterization methods**: *what are the best and how they can be combined*. In order to untangle the complicated flurbiprofen/proline system, we had to combine various cutting-edge characterization techniques. Simple laboratory PXRD allowed detection of new potential cocrystal phases. DSC and TGA helped identifying systems with complex behavior upon temperature. Single-crystal X-ray analysis was essential for finding the crystal structures. Synchrotron X-ray diffraction analysis upon varied temperature nicely complemented DSC and TGA data providing direct monitoring of phase changes upon temperature increase. Synchrotron X-ray diffraction data were indispensable for structure solution from powder when no single

crystals were available. Solid-state NMR was used as a complementary technique to find the ratio of the cocrystal components needed for structure solution from PXRD. *In-situ* ball-milling results provided insight into the liquid-assisted grinding reactions and the solvents' role in the process. DFT calculations complemented our experimental data by giving the energy characteristics of our systems and also as a validation method for the structures found from the powder X-ray diffraction data. Thus, we conclude that, although X-ray diffraction methods are the most powerful in the context of this research, application of other complementary techniques is crucial when dealing with complicated systems. The knowledge about cutting-edge characterization techniques and how they can be combined when working with complex cases may be applied not only to the cocrystallization field but also to other problems involving solid-state substances.

Hence, the work presented in this thesis intends to help understanding various aspects of cocrystallization involving zwitterionic co-formers and active pharmaceutical ingredients, also accounting for the chirality issues. Amino acids can be considered promising co-formers for various cocrystallization applications as they are natural to the body and thus less toxic than other potential co-formers. We believe the results of this work to be interesting not only from the fundamental but also the application point of view as the information learnt through studying profen/amino acid systems, can be of great value when developing cocrystals for industrial applications.

In the context of perspectives, as I mentioned in the Introduction sections to the Chapters 2 and 3, amino acids are already widely applied at industrial scales, for example Ibuprofen/arginine and Ibuprofen/lysine salts[143] or cocrystals with L-proline[189,196,217]. However, our work shows that amino acids may bring many hidden surprises that should not be underestimated. We highlight that the detailed examination of solid-state characteristics of any potentially applied amino acid cocrystals, including extensive polymorphic studies in different solutions, are absolutely necessary for the development of robust and predictable crystalization processes. Working with amino acids is challenging and finding the right conditions to control the cocrystallization outcome may take a considerable amount time. However, we would still recommend the use of amino acids if they present an opportunity of improving the therapeutic performance of a drug. The application of amino acids for chiral resolution techniques, on the other hand, may be limited to simple systems, in which the number of potential cocrystal forms does not exceed a reasonable number.

# REFERENCES


(1) Jones, W.; Motherwell, W. D. S.; Trask, A. V. *MRS Bull.* **2011**, *31* (11), 875–879.

(2) Brittain, H. G. *J. Pharm. Sci.* **2013**, *102* (2), 311–317.

(3) Schultheiss, N.; Newman, A. *Cryst. Growth Des.* **2009**, *9* (6), 2950–2967.

(4) Springuel, G.; Leyssens, T. *Cryst. Growth Des.* **2012**, *12* (7), 3374–3378.

(5) Mahieux, J.; Gonella, S.; Sanselme, M.; Coquerel, G. *CrystEngComm* **2012**, *14* (1), 103–111.

(6) Iwama, S.; Kuyama, K.; Mori, Y.; Manoj, K.; Gonnade, R. G.; Suzuki, K.; Hughes, C. E.; Williams, P. A.; Harris, K. D. M.; Veesler, S.; Takahashi, H.; Tsue, H.; Tamura, R. *Chemistry* **2014**, *20* (33), 10343–10350.

(7) http://reference.iucr.org/dictionary/Crystal http://reference.iucr.org/dictionary/Crystal.

(8) Kitaigorodsky, A. I. *Molecular Crystals and Molecules*; Academic Press, 1973.

(9) Zukerman-Schpector, J.; Tiekink, E. R. T. *Zeitschrift für Krist.* **2008**, *223* (3/2008), 233–234.

(10) Schmidt, J.; Snipes, W. *Int. J. Radiat. Biol. Relat. Stud. Physics, Chem. Med.* **1968**, *13* (2), 101–109.

(11) Desiraju, G. R. *CrystEngComm* **2003**, *5* (82), 466–467.

(12) Aakeröy, C. B.; Salmon, D. J. *CrystEngComm* **2005**, *7* (72), 439–448.

(13) Bond, A. D. *CrystEngComm* **2007**, *9* (9), 833–834.

(14) Parkin, A.; Gilmore, C. J.; Wilson, C. C. *Zeitschrift für Krist.* **2008**, *223* (6/2008), 430.

(15) Dunitz, J. D. *CrystEngComm* **2003**, *5* (91), 506.

(16) Aitipamula, S.; Banerjee, R.; Bansal, A. K.; Biradha, K.; Cheney, M. L.; Choudhury, A. R.; Desiraju, G. R.; Dikundwar, A. G.; Dubey, R.; Duggirala, N.; Ghogale, P. P.; Ghosh, S.; Goswami, P. K.; Goud, N. R.; Jetti, R. R. K. R.; Karpinski, P.; Kaushik, P.; Kumar, D.; Kumar, V.; Moulton, B.; Mukherjee, A.; Mukherjee, G.; Myerson, A. S.; Puri, V.; Ramanan, A.; Rajamannar, T.; Reddy, C. M.; Rodriguez-Hornedo, N.; Rogers, R. D.; Row, T. N. G.; Sanphui, P.; Shan, N.; Shete, G.; Singh, A.; Sun, C. C.; Swift, J. a.; Thaimattam, R.; Thakur, T. S.; Kumar Thaper, R.; Thomas, S. P.; Tothadi, S.; Vangala, V. R.; Variankaval, N.; Vishweshwar, P.; Weyna, D. R.; Zaworotko, M. J. *Cryst. Growth Des.* **2012**, *12* (5), 2147–2152.

(17) https://www.fda.gov/food/ingredientspackaginglabeling/gras/.

(18) Bernstein, J. *Polymorphism in molecular crystals*; Oxford University Press, 2002.

(19) *Pharmaceutical Salts and Co-crystals*; Wouters, J., Quéré, L., Eds.; RSC Drug Discovery; Royal Society of Chemistry: Cambridge, 2011.

(20) In *IUPAC Compendium of Chemical Terminology*; IUPAC: Research Triagle Park, NC.

(21) McKie, D.; McKie, C. *Crystalline solids*; Nelson, 1974.

(22) Arunan, E.; Desiraju, G. R.; Klein, R. A.; Sadlej, J.; Scheiner, S.; Alkorta, I.; Clary, D. C.;

Crabtree, R. H.; Dannenberg, J. J.; Hobza, P.; Kjaergaard, H. G.; Legon, A. C.; Mennucci, B.; Nesbitt, D. J. *Pure Appl. Chem* **2011**, *83* (8), 1637–1641.

(23) Childs, S. L.; Stahly, G. P.; Park, A. *Mol. Pharm.* **2007**, *4* (3), 323–338.

(24) Aakeröy, C. B.; Fasulo, M. E.; Desper, J. *Mol. Pharm.* **2007**, *4* (3), 317–322.

(25) Bruice, P. Y. *Organic chemistry*; Pearson/Prentice Hall, 2004.

(26) Nguyen, L. A.; He, H.; Pham-Huy, C. *Int. J. Biomed. Sci.* **2006**, *2* (2), 85–100.

(27) https://www.drugbank.ca/drugs/DB00712 https://www.drugbank.ca/drugs/DB00712.

(28) Desiraju, G. R. *J. Am. Chem. Soc.* **2013**, *135* (27), 9952–9967.

(29) Springuel, G.; Norberg, B.; Robeyns, K.; Wouters, J.; Leyssens, T. *Cryst. Growth Des.* **2012**, *12* (1), 475–484.

(30) Li, Z. J.; Abramov, Y.; Bordner, J.; Leonard, J.; Medek, A.; Trask, A. V. *J. Am. Chem. Soc.* **2006**, *128* (25), 8199–8210.

(31) Friščić, T. *Chem. Soc. Rev.* **2012**, *41* (9), 3493–3510.

(32) Tumanova, N.; Tumanov, N.; Robeyns, K.; Filinchuk, Y.; Wouters, J.; Leyssens, T. *CrystEngComm* **2014**, *16* (35), 8185–8196.

(33) Li, Z.; Yang, B.-S.; Jiang, M.; Eriksson, M.; Spinelli, E.; Yee, N.; Senanayake, C. *Org. Process Res. Dev.* **2009**, *13* (6), 1307–1314.

(34) Aakeröy, C. B.; Wijethunga, T. K.; Desper, J. *J. Mol. Struct.* **2014**, *1072*, 20–27.

(35) Urbanus, J.; Roelands, C. P. M.; Mazurek, J.; Verdoes, D.; ter Horst, J. H. *CrystEngComm* **2011**, *13* (8), 2817–2819.

(36) Urbanus, J.; Roelands, C. P. M.; Verdoes, D.; Jansens, P. J.; ter Horst, J. H. *Cryst. Growth Des.* **2010**, *10* (3), 1171–1179.

(37) Springuel, G.; Robeyns, K.; Norberg, B.; Wouters, J.; Leyssens, T. *Cryst. Growth Des.* **2014**, *14* (8), 3996–4004.

(38) George, F.; Tumanov, N.; Norberg, B.; Robeyns, K.; Filinchuk, Y.; Wouters, J.; Leyssens, T. *Cryst. Growth Des.* **2014**, *14* (6), 2880–2892.

(39) Billot, P.; Hosek, P.; Perrin, M.-A. *Org. Process Res. Dev.* **2013**, *17* (3), 505–511.

(40) Childs, S. L.; Rodríguez-Hornedo, N.; Reddy, L. S.; Jayasankar, A.; Maheshwari, C.; McCausland, L.; Shipplett, R.; Stahly, B. C. *CrystEngComm* **2008**, *10* (7), 856–864.

(41) Springuel, G.; Collard, L.; Leyssens, T. *CrystEngComm* **2013**, *15* (39), 7951–7958.

(42) Nehm, S. J.; Rodríguez-Spong, B.; Rodríguez-Hornedo, N. *Cryst. Growth Des.* **2005**, *6* (2), 592–600.

(43) Bethune, S. J.; Huang, N.; Jayasankar, A.; Rodríguez-Hornedo, N. *Cryst. Growth Des.* **2009**, *9* (9), 3976–3988.

(44) Friščić, T.; Jones, W.; Fris, T. *Cryst. Growth Des.* **2009**, *9* (3), 1621–1637.

(45) Leyssens, T.; Tumanova, N.; Robeyns, K.; Candoni, N.; Veesler, S. *CrystEngComm* **2014**, *16* (41), 9603–9611.

(46) Aitipamula, S.; Chow, P. S.; Tan, R. B. H. *CrystEngComm* **2014**, *16* (17), 3451–3465.

(47) Sokolov, A. N.; Friscić, T.; MacGillivray, L. R. *Journal of the American Chemical Society*. March 8, 2006, pp 2806–2807.

(48) Etter, M. C.; Frankenbach, G. M.; Adsmond, D. A. *Mol. Cryst. Liq. Cryst. Inc. Nonlinear Opt.* **1990**, *187* (1), 25–39.

(49) Morimoto, M.; Kobatake, S.; Irie, M. *Chem. Commun.* **2008**, *121* (3), 335–337.

(50) Stahl, P. H.; Wermuth, C. G.; International Union of Pure and Applied Chemistry. *Handbook of pharmaceutical salts : properties, selection, and use*; VHCA, 2011.

(51) Jain, N.; Yalkowsky, S. H. *J. Pharm. Sci.* **2001**, *90* (2), 234–252.

(52) Newman, A. W.; Reutzel□Edens, S. M.; Zografi, G. *J. Pharm. Sci.* **2008**, *97* (3), 1047–1059.

(53) Trask, A. V.; Motherwell, W. D. S.; Jones, W. *Cryst. Growth Des.* **2005**, *5* (3), 1013–1021.

(54) Friščić, T.; Fábián, L.; Burley, J. C.; Reid, D. G.; Duer, M. J.; Jones, W. *Chem. Commun.* **2008**, No. 14, 1644–1646.

(55) Karki, S.; Friscić, T.; Jones, W.; Motherwell, W. D. S. *Mol. Pharm.* **2007**, *4* (3), 347–354.

(56) Sovizi, M. R. *J. Therm. Anal. Calorim.* **2010**, *102* (1), 285–289.

(57) Lu, E.; Rodríguez-Hornedo, N.; Suryanarayanan, R. *CrystEngComm* **2008**, *10* (6), 665.

(58) Bak, A.; Gore, A.; Yanez, E.; Stanton, M.; Tufekcic, S.; Syed, R.; Akrami, A.; Rose, M.; Surapaneni, S.; Bostick, T.; King, A.; Neervannan, S.; Ostovic, D.; Koparkar, A. *J. Pharm. Sci.* **2008**, *97* (9), 3942–3956.

(59) Basavoju, S.; Boström, D.; Velaga, S. P. *Pharm. Res.* **2008**, *25* (3), 530–541.

(60) Remenar, J. F.; Peterson, M. L.; Stephens, P. W.; Zhang, Z.; Zimenkov, Y.; Hickey, M. B. *Mol. Pharm.* **2007**, *4* (3), 386–400.

(61) Remenar, J. F.; Morissette, S. L.; Peterson, M. L.; Moulton, B.; MacPhee, J. M.; Guzmán, H. R.; Almarsson, Ö. *J. Am. Chem. Soc.* **2003**, *125* (28), 8456–8457.

(62) Griffin, J. P. (John P.; Wiley InterScience (Online service). *The textbook of pharmaceutical medicine*; Wiley-Blackwell, 2009.

(63) McNamara, D. P.; Childs, S. L.; Giordano, J.; Iarriccio, A.; Cassidy, J.; Shet, M. S.; Mannion, R.; O'Donnell, E.; Park, A. *Pharm. Res.* **2006**, *23* (8), 1888–1897.

(64) Katdare, A.; Chaubal, M. V. *Excipient development for pharmaceutical, biotechnology, and drug delivery systems*; Informa Healthcare, 2006.

(65) https://www.fda.gov/downloads/Drugs/Guidances/UCM281764.pdf.

(66) Puschner, B.; Poppenga, R. H.; Lowenstine, L. J.; Filigenzi, M. S.; Pesavento, P. A. *J. Vet. Diagnostic Investig.* **2007**, *19* (6), 616–624.

(67) Horst, J. H. ter; Cains, P. W. *Cryst. Growth Des.* **2008**, *8* (7), 2537–2542.

(68) ter Horst, J. H.; Deij, M. a.; Cains, P. W. *Cryst. Growth Des.* **2009**, *9* (3), 1531–1537.

(69) Fucke, K.; Myz, S. A.; Shakhtshneider, T. P.; Boldyreva, E. V.; Griesser, U. J. *New J. Chem.*

**2012**, *36* (10), 1969–1977.

(70) Padrela, L.; Rodrigues, M. A.; Velaga, S. P.; Fernandes, A. C.; Matos, H. A.; de Azevedo, E. G. *J. Supercrit. Fluids* **2010**, *53* (1–3), 156–164.

(71) Friščić, T.; Jones, W. *J. Pharm. Pharmacol.* **2010**, *62* (11), 1547–1559.

(72) Delori, A.; Friscic, T.; Jones, W.; Friščić, T.; Jones, W. *CrystEngComm* **2012**, *14* (7), 2350–2362.

(73) James, S. L.; Adams, C. J.; Bolm, C.; Braga, D.; Collier, P.; Friščić, T.; Grepioni, F.; Harris, K. D. M.; Hyett, G.; Jones, W.; Krebs, A.; Mack, J.; Maini, L.; Orpen, G.; Parkin, I. P.; Shearouse, W. C.; Steed, J. W.; Waddell, D. C. *Chem. Soc. Rev.* **2012**, *41* (1), 413–447.

(74) Bowmaker, G. a; Hanna, J. V; Hart, R. D.; Skelton, B. W.; White, A. H. *Dalton Trans.* **2008**, *2636* (39), 5290–5292.

(75) Bowmaker, G. A. *Chem. Commun.* **2013**, *49* (4), 334–348.

(76) Boldyrev, V. V; Tkacova, K. *J. Mater. Synth. Process.* **2000**, *8*, 121–132.

(77) *Reactivity of Molecular Solids*, Volume 3 e.; Boldyrev, V. V., Boldyreva, E. V., Eds.; John Wiley & Sons LTD, 1999.

(78) Halasz, I.; Puškarić, A.; Kimber, S. a J.; Beldon, P. J.; Belenguer, A. M.; Adams, F.; Honkimäki, V.; Dinnebier, R. E.; Patel, B.; Jones, W.; Strukil, V.; Friščić, T. *Angew. Chem. Int. Ed. Engl.* **2013**, *52* (44), 11538–11541.

(79) Klimakow, M.; Leiterer, J.; Kneipp, J.; Rössler, E.; Panne, U.; Rademann, K.; Emmerling, F. *Langmuir* **2010**, *26* (13), 11233–11237.

(80) Fischer, F.; Lubjuhn, D.; Greiser, S.; Rademann, K.; Emmerling, F. *Cryst. Growth Des.* **2016**, *16* (10), 5843–5851.

(81) Batzdorf, L.; Fischer, F.; Wilke, M.; Wenzel, K.-J.; Emmerling, F. *Angew. Chemie Int. Ed.* **2015**, *54* (6), 1799–1802.

(82) Leyssens, T.; Springuel, G.; Montis, R.; Candoni, N.; Veesler, S. *Cryst. Growth Des.* **2012**, *12* (3), 1520–1530.

(83) Ainouz, A.; Authelin, J.-R.; Billot, P.; Lieberman, H. *Int. J. Pharm.* **2009**, *374* (1–2), 82–89.

(84) Ooi, L. *Principles of x-ray crystallography*; Oxford University Press, 2010.

(85) Müller, P.; Herbst-Irmer, R.; Spek, A. L.; Schneider, T. R.; Sawaya, M. R. *Crystal Structure Refinement*; Oxford University Press, 2006.

(86) Blake, A. J.; Clegg, W. *Crystal structure analysis : principles and practice*; Oxford University Press, 2009.

(87) *Structure Determination from Powder Diffraction Data*; David, W. I. F., Shankland, K., McCusker, L. B., Bärlocher, C., Eds.; Oxford University Press, 2006.

(88) Visser, J. W. *J. Appl. Crystallogr.* **1969**, *2* (3), 89–95.

(89) Werner, P. E.; Eriksson, L.; Westdahl, M. *J. Appl. Crystallogr.* **1985**, *18* (5), 367–370.

(90) Boultif, A.; Louër, D. *J. Appl. Crystallogr.* **2004**, *37* (5), 724–731.

(91) Favre-Nicolin, V.; Černý, R. *J. Appl. Crystallogr.* **2002**, *35* (6), 734–743.

(92) Altomare, A.; Caliandro, R.; Camalli, M.; Cuocci, C.; Da Silva, I.; Giacovazzo, C.; Giuseppina Moliterni, A. G.; Spagna, R. *J. Appl. Crystallogr.* **2004**, *37* (6), 957–966.

(93) Markvardsen, A. J.; David, W. I. F.; Johnson, J. C.; Shankland, K. *Acta Crystallogr. Sect. A Found. Crystallogr.* **2001**, *57* (1), 47–54.

(94) Pawley, G. . *J. Appl. Cryst* **1981**, *14*, 357–361.

(95) Le Bail, A. *Powder Diffr.* **2005**, *20* (4), 316–326.

(96) Rodríguez-Carvajal, J. *Phys. B Condens. Matter* **1993**, *192* (1–2), 55–69.

(97) Coelho, A. A. Coelho Software, Brisbane 2012.

(98) Harris, K. D. M.; Tremayne, M.; Lightfoot, P.; Bruce, P. G. *J. Am. Chem. Soc.* **1994**, *116* (8), 3543–3547.

(99) Andreev, Y. G.; MacGlashan, G. S.; Bruce, P. G. *Phys. Rev. B* **1997**, *55* (18), 12011–12017.

(100) Earl, D. J.; Deem, M. W. *Phys. Chem. Chem. Phys.* **2005**, *7* (23), 3910–3916.

(101) McGreevy, R. L.; Pusztai, L. *Mol. Simul.* **1988**, *1* (6), 359–367.

(102) Dollase, W. A. *J. Appl. Crystallogr.* **1986**, *19* (4), 267–272.

(103) Young, R. A. (Robert A. *The Rietveld method*; International Union of Crystallograhy, 1993.

(104) Gracin, D.; Strukil, V.; Friščić, T.; Halasz, I.; Užarević, K. *Angew. Chem. Int. Ed. Engl.* **2014**, *53* (24), 6193–6197.

(105) Užarević, K.; Halasz, I.; Friščić, T. *J. Phys. Chem. Lett.* **2015**, *6* (20), 4129–4140.

(106) Fischer, F.; Heidrich, A.; Greiser, S.; Benemann, S.; Rademann, K.; Emmerling, F. *Cryst. Growth Des.* **2016**, *16* (3), 1701–1707.

(107) Tumanov, N.; Ban, V.; Poulain, A.; Filinchuk, Y. *J. Appl. Crystallogr.* **2017**, *50* (4), 7535–7570.

(108) Skoog, D. A.; Holler, F. J.; Nieman, T. A. *Principles of instrumental analysis*; Brooks/Cole, 1998.

(109) *Practical Raman Spectroscopy*; Gardiner, D. J., Graves, P. R., Eds.; Springer Berlin Heidelberg: Berlin, Heidelberg, 1989.

(110) Harwood, L. M.; Moody, C. J. *Experimental organic chemistry : principles and practice*; Blackwell Scientific Publications, 1990.

(111) Cooke, C. L.; Davey, R. J.; Black, S.; Muryn, C.; Pritchard, R. G. *Cryst. Growth Des.* **2010**, *10* (12), 5270–5278.

(112) Coats, A. W.; Redfern, J. P. *Analyst* **1963**, *88* (1053), 906–924.

(113) Schaefer, J.; Stejskal, E. O. *J. Am. Chem. Soc.* **1976**, *98* (4), 1031–1032.

(114) Schaefer, J. In *Encyclopedia of Magnetic Resonance*; John Wiley & Sons, Ltd: Chichester, UK, 2007.

(115) Laws, D. D.; Bitter, H.-M. L.; Jerschow, A. *Angew. Chemie Int. Ed.* **2002**, *41* (17), 3096–

3129.

(116) Harris, R. K. *J. Pharm. Pharmacol.* **2007**, *59* (2), 225–239.

(117) Berendt, R. T.; Sperger, D. M.; Munson, E. J.; Isbester, P. K. *TrAC Trends Anal. Chem.* **2006**, *25* (10), 977–984.

(118) Rossi, P.; Macedi, E.; Paoli, P.; Bernazzani, L.; Carignani, E.; Borsacchi, S.; Geppi, M. *Cryst. Growth Des.* **2014**, *14* (5), 2441–2452.

(119) Sholl, D. S.; Steckel, J. A. *Density functional theory : a practical introduction*; Wiley, 2009.

(120) Van de Streek, J.; Neumann, M. a. *Acta Crystallogr. Sect. B Struct. Sci. Cryst. Eng. Mater.* **2014**, *70* (6), 1020–1032.

(121) Van De Streek, J.; Neumann, M. a. *Acta Crystallogr. B.* **2010**, *66* (Pt 5), 544–558.

(122) Trask, A. V. *Mol. Pharm.* **2007**, *4* (3), 301–309.

(123) Qiao, N.; Li, M.; Schlindwein, W.; Malek, N.; Davies, A.; Trappitt, G. *Int. J. Pharm.* **2011**, *419* (1–2), 1–11.

(124) Vishweshwar, P.; McMahon, J. A.; Bis, J. A.; Zaworotko, M. J. *J. Pharm. Sci.* **2006**, *95* (3), 499–516.

(125) Shan, N.; Zaworotko, M. J. *Drug Discov. Today* **2008**, *13* (9–10), 440–446.

(126) Miroshnyk, I.; Mirza, S.; Sandler, N. *Expert Opin. Drug Deliv.* **2009**, *6* (4), 333–341.

(127) Brittain, H. G. In *Profiles of drug substances, excipients, and related methodology*; Elsevier Inc., 2011; Vol. 36, pp 361–381.

(128) Vishweshwar, P.; McMahon, J. A.; Peterson, M. L.; Hickey, M. B.; Shattock, T. R.; Zaworotko, M. J. *Chem. Commun. (Camb).* **2005**, *36* (36), 4601–4603.

(129) Walsh, R. D. B.; Bradner, M. W.; Fleischman, S.; Morales, L. A.; Moulton, B.; Rodríguez-Hornedo, N.; Zaworotko, M. J. *Chem. Commun.* **2003**, No. 2, 186–187.

(130) Cincić, D.; Friscić, T.; Jones, W. *Chemistry* **2008**, *14* (2), 747–753.

(131) Blagden, N.; de Matas, M.; Gavan, P. T.; York, P. *Adv. Drug Deliv. Rev.* **2007**, *59* (7), 617–630.

(132) Aakeröy, C. B.; Forbes, S.; Desper, J. *J. Am. Chem. Soc.* **2009**, *131* (47), 17048–17049.

(133) Rahman, Z.; Agarabi, C.; Zidan, A. S.; Khan, S. R.; Khan, M. A. *AAPS PharmSciTech* **2011**, *12* (2), 693–704.

(134) Wang, Z.-Z.; Chen, J.-M.; Lu, T.-B. *Cryst. Growth Des.* **2012**, *12* (9), 4562–4566.

(135) Chow, S. F.; Chen, M.; Shi, L.; Chow, A. H. L.; Sun, C. C. *Pharm. Res.* **2012**, *29* (7), 1854–1865.

(136) Hsi, K. H.-Y.; Chadwick, K.; Fried, A.; Kenny, M.; Myerson, A. S. *CrystEngComm* **2012**, *14* (7), 2386–2388.

(137) Friščić, T.; Fábián, L.; Burley, J. C.; Jones, W.; Motherwell, W. D. S. *Chem. Commun.* **2006**, No. 48, 5009–5011.

(138) Bock, D. A.; Lehmann, C. W. *CrystEngComm* **2012**, *14* (5), 1534–1537.

(139) Takata, N.; Shiraki, K.; Takano, R.; Hayashi, Y.; Terada, K. *Cryst. Growth Des.* **2008**, *8* (8), 3032–3037.

(140) Thorey, P.; Bombicz, P.; Szilágyi, I. M.; Molnár, P.; Bánsághi, G.; Székely, E.; Simándi, B.; Párkányi, L.; Pokol, G.; Madarász, J. *Thermochim. Acta* **2010**, *497* (1–2), 129–136.

(141) Székely, E.; Bánsághi, G.; Thorey, P.; Molnár, P.; Madarász, J.; Vida, L.; Simándi, B. *Ind. Eng. Chem. Res.* **2010**, *49* (19), 9349–9354.

(142) Tilborg, A.; Springuel, G.; Norberg, B.; Wouters, J.; Leyssens, T. *CrystEngComm* **2013**, *15* (17), 3341–3350.

(143) Kwan, K. C. Patent EP0424028 A2, 1991.

(144) Tilborg, A.; Norberg, B.; Wouters, J. *Eur. J. Med. Chem.* **2014**.

(145) Scott D. Reynolds, Hsien-Hsin Tung, S. W. Patent US4994604 A, 1991.

(146) Pacheco, D. P.; Martínez, F. *Phys. Chem. Liq.* **2007**, *45* (5), 581–595.

(147) Nozaki, Y.; Tanford, C. *J. Biol. Chem.* **1971**, *246* (7), 2211–2217.

(148) Rager, T.; Hilfiker, R. *Zeitschrift für Phys. Chemie* **2009**, *223* (7), 793–813.

(149) Dyadkin, V. SNBL Tool box, Swiss Norwegian Beamline at ESRF: Grenoble, France 2013.

(150) Agilent Technologies. Agilent Technologies UK Ltd.: Oxford, UK 2013.

(151) Sheldrick, G. M. *Acta Crystallogr. A.* **2008**, *64* (Pt 1), 112–122.

(152) Hübschle, C. B.; Sheldrick, G. M.; Dittrich, B. *J. Appl. Crystallogr.* **2011**, *44* (Pt 6), 1281–1284.

(153) Hammersley, A. P.; Svensson, S. O.; Hanfland, M.; Fitch, A. N.; Hausermann, D. *High Press. Res.* **1996**, *14* (4), 235–248.

(154) King, M. D.; Buchanan, W. D.; Korter, T. M. *Phys. Chem. Chem. Phys.* **2011**, *13* (10), 4250–4259.

(155) A.Leahey and M.M.Olmstead. *Priv. Commun.* **2001**.

(156) Macrae, C. F.; Bruno, I. J.; Chisholm, J. A.; Edgington, P. R.; McCabe, P.; Pidcock, E.; Rodriguez-Monge, L.; Taylor, R.; van de Streek, J.; Wood, P. A. *J. Appl. Crystallogr.* **2008**, *41* (2), 466–470.

(157) Spek, A. L. *Acta Crystallogr. D. Biol. Crystallogr.* **2009**, *65* (2), 148–155.

(158) Allen, F. H.; Johnson, O.; Shields, G. P.; Smith, B. R.; Towler, M. *J. Appl. Crystallogr.* **2004**, *37* (2), 335–338.

(159) Allen, F. H. *Acta Crystallogr. B.* **2002**, *58*, 380–388.

(160) Bucar, D.-K.; Henry, R. F.; Lou, X.; Duerst, R. W.; Borchardt, T. B.; MacGillivray, L. R.; Zhang, G. G. Z. *Mol. Pharm.* **2007**, *4* (3), 339–346.

(161) Bučar, D.-K.; Henry, R. F.; Lou, X.; Duerst, R. W.; MacGillivray, L. R.; Zhang, G. G. Z. *Cryst. Growth Des.* **2009**, *9* (4), 1932–1943.

(162) Alhalaweh, A.; Kaialy, W.; Buckton, G.; Gill, H.; Nokhodchi, A.; Velaga, S. P. *AAPS PharmSciTech* **2013**, *14* (1), 265–276.

(163) Vinogradov, S. N. *Int. J. Pept. Protein Res.* **1979**, *14* (4), 281–289.

(164) Suresh, C. G.; Vijayan, M. *Int. J. Pept. Protein Res.* **2009**, *22* (2), 129–143.

(165) Boldyreva, E. Boeyens J.F. and Ogilvie J.C.A., Ed.; Springer, 2008; pp 167–192.

(166) Minkov, V. S.; Chesalov, Y. A.; Boldyreva, E. V. *J. Struct. Chem.* **2011**, *51* (6), 1052–1063.

(167) McKinnon, J. J.; Spackman, M. a; Mitchell, A. S. *Acta Crystallogr. Sect. B Struct. Sci.* **2004**, *60* (6), 627–668.

(168) B. Khawas. *Indian J. Phys., A* **1985**, *59*, 219.

(169) Görbitz, C. H.; Törnroos, K. W.; Day, G. M. *Acta Crystallogr. B.* **2012**, *68* (Pt 5), 549–557.

(170) Vayá, I.; Jiménez, M. C.; Miranda, M. A. *Tetrahedron: Asymmetry* **2005**, *16* (12), 2167–2171.

(171) Courvoisier, E.; Williams, P. A.; Lim, G. K.; Hughes, C. E.; Harris, K. D. M. *Chem. Commun. (Camb).* **2012**, *48* (22), 2761–2763.

(172) Ghazaryan, V. V.; Fleck, M.; Petrosyan, A. M. *J. Mol. Struct.* **2012**, *1015*, 51–55.

(173) Rajagopal, K.; Subha Nandhini, M.; Krishnakumar, R. V; Natarajan, S. *Acta Crystallogr. Sect. E Struct. Reports Online* **2002**, *58* (11), o1306–o1308.

(174) Takahashi, Y.; Fujii, I. *Anal. Sci. X-ray Struct. Anal. Online* **2004**, *20*, x77–x78.

(175) Alagar, M.; Krishnakumar, R. V; Nandhini, M. S.; Natarajan, S. *Acta Crystallogr. Sect. E Struct. Reports Online* **2001**, *57* (9), o855–o857.

(176) Zakharov, B. A.; Boldyreva, E. V. *Acta Crystallogr. Sect. C Cryst. Struct. Commun.* **2011**, *67* (2), o47–o51.

(177) Hu, Z.-Q.; Xu, D.-J.; Xu, Y.-Z. *Acta Crystallogr. Sect. E Struct. Reports Online* **2004**, *60* (2), o269–o271.

(178) Subha Nandhini, M.; Krishnakumar, R. V; Natarajan, S. *Acta Crystallogr. Sect. E Struct. Reports Online* **2001**, *57* (8), o666–o668.

(179) Amimoto, K.; Nishioka, Y. *Acta Crystallogr. Sect. E Struct. Reports Online* **2012**, *68* (6), o1720–o1720.

(180) Hu, Z.-Q.; Xu, D.-J.; Xu, Y.-Z.; Wu, J.-Y.; Chiang, M. Y. *Acta Crystallogr. Sect. C Cryst. Struct. Commun.* **2002**, *58* (10), o612–o614.

(181) Subha Nandhini, M.; Krishnakumar, R. V.; Natarajan, S. *Acta Crystallogr. Sect. E Struct. Reports Online* **2001**, *57* (7), o633–o635.

(182) Ishida, T.; Nagata, H.; In, Y.; Doi, M.; Inoue, M.; Extine, M. W.; Wakahara, A. *Chem. Pharm. Bull. (Tokyo).* **1993**, *41* (3), 433–438.

(183) Rodrigues, V. H.; Costa, M. M. R. R.; Belsley, M.; Matos Gomes, E. de. *Acta Crystallogr. Sect. E Struct. Reports Online* **2012**, *68* (3), o920–o920.

(184) Di, K. *Acta Crystallogr. Sect. E Struct. Reports Online* **2010**, *66* (5), o1125–o1126.

(185) Gartland, G. L.; Freeman, G. R.; Bugg, C. E. *Acta Crystallogr. Sect. B Struct. Crystallogr. Cryst. Chem.* **1974**, *30* (7), 1841–1849.

(186) Fujii, I. *X-ray Struct. Anal. Online* **2009**, *25*, 35–36.

(187) Deshpande, P. P.; Singh, J.; Pullockaran, A.; Kissick, T.; Ellsworth, B. A.; Gougoutas, J. Z.; Dimarco, J.; Fakes, M.; Reyes, M.; Lai, C.; Lobinger, H.; Denzel, T.; Ermann, P.; Crispino, G.; Randazzo, M.; Gao, Z.; Randazzo, R.; Lindrud, M.; Rosso, V.; Buono, F.; Doubleday, W. W.; Leung, S.; Richberg, P.; Hughes, D.; Washburn, W. N.; Meng, W.; Volk, K. J.; Mueller, R. H. *Org. Process Res. Dev.* **2012**, *16* (4), 577–585.

(188) Jin, Z. M.; Pan, Y. J.; Hu, M. L.; Shen, L.; Li, M. C.; Min Jin, Z.; Jiang Pan, Y.; Lin Hu, M.; Shen, L.; Chao Li, M. *Cryst. Res. Technol.* **2003**, *38* (11), 1009–1012.

(189) Ramanathan, C. R.; Periasamy, M. *Tetrahedron: Asymmetry* **1998**, *9* (15), 2651–2656.

(190) Timofeeva, T. V.; Kuhn, G. H.; Nesterov, V. V.; Nesterov, V. N.; Frazier, D. O.; Penn, B. G.; Antipin, M. Y. *Cryst. Growth Des.* **2003**, *3* (3), 383–391.

(191) Prasad, G. S.; Vijayan, M. *Acta Crystallogr. Sect. B Struct. Sci.* **1993**, *49* (2), 348–356.

(192) Qu, X.; Lu, J.; Zhao, C.; Boas, J. F.; Moubaraki, B.; Murray, K. S.; Siriwardana, A.; Bond, A. M.; Martin, L. L. *Angew. Chem. Int. Ed. Engl.* **2011**, *50* (7), 1589–1592.

(193) Fu, T. Y.; Scheffer, J. R.; Trotter, J. *Acta Crystallogr. Sect. C Cryst. Struct. Commun.* **1997**, *53* (9), 1259–1262.

(194) A.P.Marchand and W.H.Watson. *Priv. Commun.* **2006**.

(195) Aakeröy, C. B.; Bahra, G. S.; Brown, C. R.; Hitchcock, P. B.; Patell, Y.; Seddon, K. R.; Bao-Sheng, L. *Acta Chem. Scand.* **1995**, *49*, 762–767.

(196) Hu, X.; Shan, Z.; Chang, Q. *Tetrahedron: Asymmetry* **2012**, *23* (18–19), 1327–1331.

(197) Saraswathi, N. T.; Vijayan, M. *Acta Crystallogr. B.* **2001**, *57* (Pt 6), 842–849.

(198) Kinsel, G. R.; Zhao, Q.; Narayanasamy, J.; Yassin, F.; Rasika Dias, H. V.; Niesner, B.; Prater, K.; St. Marie, C.; Ly, L.; Marynick, D. S. *J. Phys. Chem. A* **2004**, *108* (15), 3153–3161.

(199) M Ramos-Silva, J. P. *Zeitschrift für Krist. New Cryst. Struct.* **1999**, *214*, 326–328.

(200) Sudhakar, V.; Vijayan, M. *Acta Crystallogr. Sect. B Struct. Crystallogr. Cryst. Chem.* **1980**, *36* (1), 120–125.

(201) Saraswathi, N. T.; Vijayan, M. *Acta Crystallogr. Sect. B Struct. Sci.* **2002**, *58* (6), 1051–1056.

(202) Chandra, N. R.; Prabu, M. M.; Venkatraman, J.; Suresh, S.; Vijayan, M. *Acta Crystallogr. Sect. B Struct. Sci.* **1998**, *54* (3), 257–263.

(203) Srinivasan, P.; Vidyalakshmi, Y.; Gopalakrishnan, R. *Cryst. Growth Des.* **2008**, *8* (7), 2329–2334.

(204) Cherukuvada, S.; Babu, N. J.; Nangia, A. *J. Pharm. Sci.* **2011**, *100* (8), 3233–3244.

(205) Roy, S.; Singh, D. D.; Vijayan, M. *Acta Crystallogr. Sect. B Struct. Sci.* **2005**, *61* (1), 89–95.

(206) Selvaraj, M.; Thamotharan, S.; Roy, S.; Vijayan, M. *Acta Crystallogr. B.* **2007**, *63* (Pt 3), 459–468.

(207) Nagata, H.; In, Y.; Tomoo, K.; Doi, M.; Ishida, T.; Wakahara, A. *Chem. Pharm. Bull. (Tokyo).* **1995**, *43* (11), 1836–1843.

(208) Angelova, O.; Velikova, V.; Kolev, T.; Radomirska, V. *Acta Crystallogr. Sect. C Cryst. Struct. Commun.* **1996**, *52* (12), 3252–3256.

(209) Prasad, G. S.; Vijayan, M. *Int. J. Pept. Protein Res.* **1990**, *35* (4), 357–364.

(210) Sánchez-Guadarrama, O.; Mendoza-Navarro, F.; Cedillo-Cruz, A.; Jung-Cook, H.; Arenas-García, J. I.; Delgado-Díaz, A.; Herrera-Ruiz, D.; Morales-Rojas, H.; Höpfl, H. *Cryst. Growth Des.* **2016**, *16* (1), 307–314.

(211) Friščić, T.; Jones, W. *Faraday Discuss.* **2007**, *136*, 167–178.

(212) Eddleston, M. D.; Arhangelskis, M.; Friščić, T.; Jones, W. *Chem Commun* **2012**, *48* (92), 11340–11342.

(213) de Maere d'Aertrycke, J. B.; Robeyns, K.; Willocq, J.; Leyssens, T. *J. Cryst. Growth* **2017**.

(214) He, H.; Huang, Y.; Zhang, Q.; Wang, J. R.; Mei, X. *Cryst. Growth Des.* **2016**, *16* (4), 2348–2356.

(215) Liu, M.; Hong, C.; Yao, Y.; Shen, H.; Ji, G.; Li, G.; Xie, Y. *Eur. J. Pharm. Biopharm.* **2016**, *107*, 151–159.

(216) Bien, J. T.; Deshpande, P. P.; Dimarco, J. D.; Gougoutas, J. Z.; Grosso, J. A.; Lai, C.; Lobinger, H.; Nirschl, A. A.; Ramakrishnan, S.; Riebel, P.; Singh, J.; Chenchi, W. Patent WO 2008/002824 A1, 2008.

(217) Shyam Sundar, M.; Talele, H. R.; Mande, H. M.; Bedekar, A. V.; Tovar, R. C.; Muller, G. *Tetrahedron Lett.* **2014**, *55* (10), 1760–1764.

(218) Subha Nandhini, M.; Krishnakumar, R. V.; Natarajan, S.; Nandhini, M. S.; Krishnakumar, R. V. *Acta Crystallogr. Sect. C Cryst. Struct. Commun.* **2001**, *57* (4), 423–424.

(219) Anitha, K.; Athimoolam, S.; Natarajan, S. *Acta Crystallogr. Sect. C Cryst. Struct. Commun.* **2006**, *62* (9), o567–o570.

(220) Athimoolam, S.; Natarajan, S. *Acta Crystallogr. Sect. C Cryst. Struct. Commun.* **2007**, *63* (5), o283–o286.

(221) Tilborg, A.; Leyssens, T.; Norberg, B.; Wouters, J. *Cryst. Growth Des.* **2013**, *13* (6), 2373–2389.

(222) Thukral, K.; Vijayan, N.; Singh, B.; Bdikin, I.; Haranath, D.; Maurya, K. K.; Philip, J.; Soumya, H.; Sreekanth, P.; Bhagavannarayana, G. *CrystEngComm* **2014**, *16* (39), 9245–9254.

(223) Hernández-Paredes, J.; Olvera-Tapia, A. L.; Arenas-García, J. I.; Höpfl, H.; Morales-Rojas, H.; Herrera-Ruiz, D.; Gonzaga-Morales, A. I.; Rodríguez-Fragoso, L. *CrystEngComm* **2015**, *17* (28), 5166–5186.

(224) Rogowska, P.; Cyrański, M. K.; Sporzyński, A.; Ciesielski, A. *Tetrahedron Lett.* **2006**, *47* (9), 1389–1393.

(225) Flippen, J. L.; Gilardi, R. D.; IUCr. *Acta Crystallogr. Sect. B Struct. Crystallogr. Cryst. Chem.* **1975**, *31* (3), 926–928.

(226) Kayushina, R.L., Vainshtein, B. K. *Krist. (Crystallogr. Rep.)* **1965**, *10*, 833.

(227) Janczak, J.; Luger, P. *Acta Crystallogr. Sect. C Cryst. Struct. Commun.* **1997**, *53* (12), 1954–1956.

(228) Myung, S.; Pink, M.; Baik, M. H.; Clemmer, D. E. *Acta Crystallogr. Sect. C Cryst. Struct. Commun.* **2005**, *61* (8), 506–508.

(229) Hayashi, Y.; Matsuzawa, M.; Yamaguchi, J.; Yonehara, S.; Matsumoto, Y.; Shoji, M.; Hashizume, D.; Koshino, H. *Angew. Chemie - Int. Ed.* **2006**, *45* (28), 4593–4597.

(230) Padmanabhan, S.; Suresh, S.; Vijayan, M. *Acta Crystallogr. Sect. C Cryst. Struct. Commun.* **1995**, *51* (10), 2098–2100.

(231) Grzesiak, A. L.; Matzger, A. J. *J. Pharm. Sci.* **2007**, *96* (11), 2978–2986.

(232) Paris, O.; Li, C.; Siegel, S.; Weseloh, G.; Emmerling, F.; Riesemeier, H.; Erko, A.; Fratzl, P. *J. Appl. Cryst* **2007**, *40*, 466–470.

(233) Hinrichsen, B.; Dinnebier, R. E.; Jansen, M. In *Commission on Powder Diffraction. Hrsg.: Int. Union of Crystallography Newsletter.*; 2005; pp 12–22.

(234) Sheldrick, G. M. *Acta Crystallogr. Sect. A Found. Adv.* **2015**, *71* (1), 3–8.

(235) Sheldrick, G. M. *Acta Crystallogr. Sect. C Struct. Chem.* **2015**, *71* (1), 3–8.

(236) Evans, J. S. O. *Mater. Sci. Forum* **2010**, *651*, 1–9.

(237) Kresse, G.; Hafner, J. *Phys. Rev. B* **1993**, *47* (1), 558–561.

(238) Kresse, G.; Hafner, J. *Phys. Rev. B* **1994**, *49* (20), 14251–14269.

(239) Kresse, G.; Furthmüller, J. *Comput. Mater. Sci.* **1996**, *6* (1), 15–50.

(240) Kresse, G.; Furthmüller, J. *Phys. Rev. B* **1996**, *54* (16), 11169–11186.

(241) Perdew, J. P.; Burke, K.; Ernzerhof, M. *Phys. Rev. Lett.* **1996**, *77* (18), 3865–3868.

(242) Grimme, S.; Antony, J.; Ehrlich, S.; Krieg, H. *J. Chem. Phys.* **2010**, *132* (15), 154104.

(243) Grimme, S.; Ehrlich, S.; Goerigk, L. *J. Comput. Chem.* **2011**, *32* (7), 1456–1465.

(244) https://materialsproject.org/ https://materialsproject.org/.

(245) http://www.cryst.ehu.es/cgi-bin/cryst/programs/mcif2vesta/index.php.

(246) Bertani, P.; Raya, J.; Bechinger, B. *Solid State Nucl. Magn. Reson.* **2014**, *61–62*, 15–18.

(247) Friščić, T.; Childs, S. L.; Rizvi, S. A. A.; Jones, W. *CrystEngComm* **2009**, *11* (3), 418.

(248) Boldyreva, E. *Chem. Soc. Rev.* **2013**, *42* (18), 7719–7738.

(249) Braga, D.; Giaffreda, S. L.; Grepioni, F.; Chierotti, M. R.; Gobetto, R.; Palladino, G.; Polito, M. *CrystEngComm* **2007**, *9* (10), 879–881.

(250) Tumanov, I. A.; Achkasov, A. F.; Boldyreva, E. V.; Boldyrev, V. V. *CrystEngComm* **2011**, *13* (7), 2213–2216.

(251) Linol, J.; Morelli, T.; Petit, M.-N.; Coquerel, G. *Cryst. Growth Des.* **2007**, *7* (9), 1608–1611.

(252) Langreiter, T.; Kahlenberg, V. *Crystals* **2015**, *5* (1), 143–153.

(253) Boldyreva, E. *Frontiers in Mechanochemistry and Mechanical Alloying*; Kumar, R., Srikanth, S., Mehrotra, S. P., Eds.; CSIR-National Metallurgical Laboratory: Jamshedpur, 2011.

(254) Ravnsbaek, D.; Filinchuk, Y.; Cerenius, Y.; Jakobsen, H. J.; Besenbacher, F.; Skibsted, J.; Jensen, T. R. *Angew. Chemie Int. Ed.* **2009**, *48* (36), 6659–6663.

(255) Ravnsbæk, D. B.; Filinchuk, Y.; Cerný, R.; Jensen, T. R. *Zeitschrift für Krist.* **2010**, *225* (12), 557–569.

(256) Černý, R.; Filinchuk, Y. *Zeitschrift für Krist.* **2011**, *226* (12), 882–891.

(257) Muramulla, S.; Arman, H. D.; Zhao, C.-G.; Tiekink, E. R. T. *Acta Crystallogr. Sect. E Struct. Reports Online* **2009**, *65* (12), o3070–o3070.

(258) Blagden, N.; Coles, S. J.; Berry, D. J. *CrystEngComm* **2014**, *16* (26), 5753–5761.

# APPENDIX A | Supporting information for Chapter 2

Table S1. Screening of APIs with amino acids (liquid-assisted grinding, ~100 mg of mixture, 10 µL of methanol, 90 min at 30 Hz)

| Amino acid | S-Naproxen 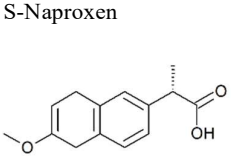 | S-oxiracetam 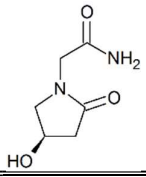 | Levetiracetam 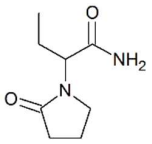 | Diprophylline 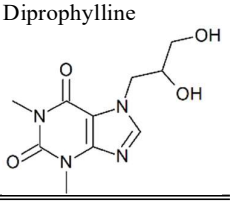 |
|---|---|---|---|---|
| L-asparagine | — | — | — | — |
| D-asparagine | — | — | — | — |
| L-cysteine | — | — | — | — |
| L-glutamine | — | — | — | — |
| D-glutamine | — | — | — | — |
| L-histidine | — | — | — | — |
| D-histidine | — | — | — | — |
| DL-serine | — | — | — | — |
| L-serine | — | — | — | — |
| D-serine | — | — | — | — |
| D-threonine | — | — | — | — |
| L-threonine | — | — | — | — |
| D-tryptophan | +† | — | — | — |
| L-tryptophan | + | — | — | — |
| L-tyrosine | — | — | — | — |
| D-tyrosine | +* | — | — | — |
| L-proline | known | — | — | — |
| D-proline | known | — | — | — |
| L-valine | — | — | — | — |
| D-valine | — | — | — | — |
| L-alanine | +* | — | — | — |
| D-alanine | +* | — | — | — |
| L-leucine | — | — | — | — |
| D-leucine | — | — | — | — |
| L-phenyalanine | — | — | — | — |
| D-phenylalanine | — | — | — | — |
| L-isoleucine | — | — | — | — |
| DL-isoleucine | — | — | — | — |
| L-methionine | — | — | — | — |
| D-methionine | — | — | — | — |
| L-aspartic acid | — | — | — | — |
| D-aspartic acid | — | — | — | — |
| L-glutamic acid | — | — | — | — |
| D-glutamic acid | — | — | — | — |

(—) no new phases detected; (+) new phases detected; (+*) structures solved; (+†) cocrystal hydrate identified

Table S2. Cocrystals/salts with amino acid co-formers found in the Cambridge Structural Database (CSD) for compounds with a hydroxyl group ("salt/cocrystal" means that the compound contain both ionized and non-ionized molecules)

| *No.* | *refcode* | *name* | *nature* |
|---|---|---|---|
| 1 | CAPKEL | L-alaninium L-alanine picrate monohydrate | salt |
| 2 | ABEHOF | L-Valinium picrate | salt |
| 3 | FOGYEG | L-Leucine L-leucinium picrate | salt |
| 4 | HAGBOG | L-Tryptophan picric acid | cocrystal |
| 5 | ATONAZ | L-Threonine picrate | salt |
| 6 | PAHCIL | DL-valine DL-valinium picrate | salt/cocrystal |
| 7 | QQQBTG02 | glycinium glycine picrate | salt/cocrystal |
| 8 | TPTPCM | DL-Tryptophan picrate methanol solvate | salt |
| 9 | WAMPOQ | L-Asparaginium picrate | salt |
| 10 | XAZNAO | DL-methionine DL-methioninium picrate | salt/cocrystal |
| 11 | YAMVIS | DL-Phenylalanine DL-phenylalaninium picrate | salt/cocrystal |
| 12 | CONVAD | L-lysinium monohydrogen squarate monohydrate | salt |
| 13 | CONVEH | bis(L-lysinium) bis(monohydrogen squarate) squarate dihydrogen squarate dihydrate | salt |
| 14 | NUYFUI | (L)-(-)-Asparaginium hydrogen squarate hemihydrate | salt |
| 15 | PAZCUO | L-(+)-Serinium hydrogensquarate | salt |
| 16 | NAZGAY | (2S,3R,4R,5S,6R)-2-(3-(4-Ethylbenzyl)-phenyl)-6-hydroxymethyltetrahydro-2H-pyran-3,4,5-triol bis(L-phenylalanine) monohydrate | cocrystal |
| 17 | NAZGEC | (2S,3R,4R,5S,6R)-2-(3-(4-Ethylbenzyl)-phenyl)-6-hydroxymethyltetrahydro-2H-pyran-3,4,5-triol L-phenylalanine monohydrate | cocrystal |
| 18 | NAZGIG | (2S,3R,4R,5S,6R)-2-(3-(4-Ethylbenzyl)-phenyl)-6-hydroxymethyltetrahydro-2H-pyran-3,4,5-triol bis(L-proline) tetrahydrate | cocrystal |
| 19 | NAZGOM | (2S,3R,4R,5S,6R)-2-(3-(4-Ethylbenzyl)-phenyl)-6-hydroxymethyltetrahydro-2H-pyran-3,4,5-triol bis(L-proline) ethanol solvate monohydrate | cocrystal |
| 20 | NAZGUS | (2S,3R,4R,5S,6R)-2-(3-(4-Ethylbenzyl)-phenyl)-6-hydroxymethyltetrahydro-2H-pyran-3,4,5-triol L-proline | cocrystal |
| 21 | NAZHAZ | (2S,3R,4R,5S,6R)-2-(3-(4-Ethylbenzyl)-phenyl)-6-hydroxymethyltetrahydro-2H-pyran-3,4,5-triol bis(L-proline) | cocrystal |

Table S3. Cocrystals/salts with amino acid co-formers found in the Cambridge Structural Database (CSD) for compounds with a carboxyl group ("salt/cocrystal" means that the compound contain both ionized and non-ionized molecules)

| *No.* | *refcode* | *name* | *nature* |
|---|---|---|---|
| 1 | ADAVOQ | L-Histidinium hydrogen glutarate monohydrate | salt |
| 2 | ADAVUV | L-Histidinium L-histidine hydrogen glutarate | salt/cocrystal |
| 3 | AHERAG | L-Alaninium tartrate | salt |
| 4 | AWIHIY | Glycinium hydrogen malonate | salt |
| 5 | AWIHOE | Glycine glutaric acid | cocrystal |
| 6 | BEYVAD | (R)-2-(Phenoxy)propionic acid (S)-alanine | cocrystal |
| 7 | BOQTEG | L-Alaninium maleate | salt |
| 8 | BOWKOO | DL-Cysteinium semioxalate | salt |
| 9 | CAMWOD | DL-Histidine malonic acid | cocrystal |
| 10 | CAMWUJ | L-Histidine malonic acid | cocrystal |
| 11 | CAVCUY | L-Lysinium L-tartrate | salt |
| 12 | EDAXIQ | L-Phenylalaninium maleate | salt |
| 13 | ETEYOR | DL-Threoninium hydrogen maleate | salt |
| 14 | EWOZIZ | bis(DL-Valine) succinic acid | cocrystal |
| 15 | FONJAU | (R)-Methioninium(R)-mandelate (R)-mandelate (R)-mandelic acid | salt/cocrystal |
| 16 | GALPIT | (R)-2-Phenoxypropionic acid (S)-valine | cocrystal |
| 17 | GINGEK | L-Argininium maleate dihydrate | salt |
| 18 | GOLZIR | Glycinium hydrogen fumarate glycine solvate monohydrate | salt/cocrystal |
| 19 | GOMDAO | (S)-2-Amino-3-(1H-indol-3-yl)propanoic acid acetic acid monohydrate | cocrystal |
| 20 | HAGYEU | bis(DL-Valine) fumaric acid | cocrystal |
| 21 | HAGZUL | L-Leucinium oxalate | salt |
| 22 | HIDGOQ | L-Cysteine L-tartrate monohydrate | cocrystal |
| 23 | IMEGIR | DL-Alaninium semioxalate monohydrate | salt |
| 24 | IREKAR | (R)-Phenylalanine (R)-mandelic acid | cocrystal |
| 25 | IROVAM | (S)-Alanine (S)-mandelic acid | cocrystal |
| 26 | IXAVEI | DL-Histidinium DL-tartrate | salt |
| 27 | IZAJUO | D-Histidinium (2S,3S)-tartrate | salt |
| 28 | JAXZIS | L-Phenylalanine benzoic acid solvate | cocrystal |
| 29 | JOTKIM | L-Phenylalanine L-phenylalaninium formate | salt/cocrystal |
| 30 | KOHPOM | DL-Lysine hemisuccinate hemisuccinic acid | salt/cocrystal |
| 31 | KOHPUS | L-Lysine hemisuccinate | salt |
| 32 | LAWKIE | L-(R)-cysteine L-(S)-mandelic acid | cocrystal |
| 33 | LERXUD | Glycine D-tartaric acid | cocrystal |
| 34 | LGPYRG | L-Glutamic acid L-pyroglutamic acid monohydrate | cocrystal |
| 35 | LHISTM | L-Histidinium dihydrogen-trimesate acetone solvate | salt |
| 36 | LOCJET | DL-Cysteinium hemikis(oxalate) | salt |
| 37 | LOCLOF | L-Cysteinium hydrogen oxalate | salt |
| 38 | LYSASP | L-Lysine L-aspartate | salt |
| 39 | MIFQUN | bis(DL-Serinium)oxalate dihydrate | salt |
| 40 | MOCXUX | DL-Methioninium maleate | salt |
| 41 | MOHDIX | L-lysine bis(hydrogen oxalate) monohydrate | salt |
| 42 | MUGKAA | L-Tryptophan formic acid solvate | cocrystal |
| 43 | MUPNUG | DL-arginine semimalonate monohydrate | salt |
| 44 | MUPPAO | L-arginine semimalonate | salt |
| 45 | MUVXAC | bis(DL-Aspartic acid) oxalate | salt |
| 46 | NELPUP | DL-Alaninium oxalate | salt |
| 47 | NEPXIR | Glycine phthalic acid | cocrystal |
| 48 | NOBYAE | L-Histidine 4,5-imidazoledicarboxylic acid | cocrystal |
| 49 | NOBYEI | L-Lysine 4,5-imidazoledicarboxylic acid | cocrystal |
| 50 | NONZOF | (S)-Phenylalanine (S)-mandelic acid | cocrystal |
| 51 | NONZUL | (R)-Phenylalanine (S)-mandelic acid | cocrystal |
| 52 | NOSXAU | DL-Arginine hydrogen oxalate | salt |
| 53 | NOSXEY | L-Arginine hydrogen oxalate | salt |
| 54 | NUQHIR | L-Tryptophan pyridine-2,4-dicarboxylic acid ethanol solvate | cocrystal |
| 55 | OJEPEY | L-Phenylalanine fumaric acid | cocrystal |
| 56 | PAVYIW | (S)-Alanine (S)-2-phenoxypropionic acid | cocrystal |
| 57 | QOYJUJ | DL-Lysinium semi-glutarate | salt |
| 58 | QOYKAQ | L-Lysinium semi-glutarate | salt |
| 59 | QURSUR | DL-Valinium hydrogen maleate | salt |
| 60 | RALRUS | L-phenylalanine L-phenylalaninium malonate | salt |
| 61 | RARXOX01 | L-Histidine oxalate | salt |
| 62 | RAZPUE | L-(R)-cysteine D-(R)-mandelic acid | cocrystal |

| | | | |
|---|---|---|---|
| 63 | REHTII | L-Arginine dioxalate | salt |
| 64 | REJZUC | L-Histidinium hydrogen L-malate | salt |
| 65 | RENBAN | Glycinium hydrogen maleate | salt |
| 66 | REPFEX | DL-Threoninium oxalate | salt |
| 67 | RIFXAG | bis(DL-Arginine) hydrogen bis(DL-tartaric acid) | cocrystal |
| 68 | RIHMEB | L-Lysine hydrogen D-tartrate | salt |
| 69 | SITCUU | Pyridine-2,4-dicarboxylic acid serine | cocrystal |
| 70 | SUYWEP | L-Asparaginium L-tartrate | salt |
| 71 | TENVUF | L-histidinium maleate monohydrate | salt |
| 72 | TENZOV | L-histidinium bis(hydrogen maleate) | salt |
| 73 | TRYPTB | D-Tryptophan hydrogen oxalate | salt |
| 74 | TUWBOD | diglycinium oxalate methanol solvate | salt |
| 75 | UCEMEV | Glycine 3,5-dihydroxybenzoic acid monohydrate | cocrystal |
| 76 | UGITAG | L-(S)-Tryptophane D-(R)-mandelate sesquihydrate | salt |
| 77 | UKORUH | L-Histidinium L-tartrate hemihydrate | salt |
| 78 | VAGVIJ | DL-Phenylalaninium hydrogen maleate | salt |
| 79 | VAZJUD | L-Histidinium maleate sesquihydrate | salt |
| 80 | VIKLOR | DL-Phenylalanine fumaric acid | cocrystal |
| 81 | VIKLUX | bis(L-Valine) fumaric acid | cocrystal |
| 82 | WEHZAL | bis(Glycinium) oxalate | salt |
| 83 | WOVYOV | Glycinium oxalate | salt |
| 84 | XADTIF | L-Histidine semi-maleate | salt |
| 85 | XADTOL | L-lysine semi-maleate | salt |
| 86 | XENXOF | L-serinium hydrogen oxalate | salt |
| 87 | XENXUL | bis(L-serinium) oxalate dihydrate | salt |
| 88 | XOXGUM | DL-Lysinium hydrogen oxalate dihydrate | salt |
| 89 | XOXHAT | bis(L-Lysinium) oxalate bis(hydrogen oxalate) | salt |
| 90 | XUGMER | (S)-Alanine (R)-mandelic acid hemihydrate | cocrystal |
| 91 | YAGKAT | (R)-Histidinium (2R,3R)-tartrate | salt |
| 92 | YEFXOX | L-lysine hydrogen adipate | salt |
| 93 | YEJYIV | L-Alaninium oxalate | salt |
| 94 | YIFLOP | Glycinium 3-nitrophthalate | salt |
| 95 | YOWDET | L-Arginine hemisuccinate hemisuccinic acid monohydrate | salt/cocrystal |

Table S4. Cocrystals/salts with amino acid co-formers found in the Cambridge Structural Database (CSD) for compounds with an amide group

| *No.* | *refcode* | *name* | *nature* |
|---|---|---|---|
| 1 | MUYTEG | 5-Hydroxy-L-tryptophan barbituric acid | cocrystal |
| 2 | MUYVAE | 5-Hydroxy-L-tryptophan 1,3-dimethylbarbituric acid monohydrate | cocrystal |

Table S5. Selected hydrogen-bond parameters in the S-naproxen/L-alanine cocrystal

| *D*—H···*A* | *D*—H (Å) | H···*A* (Å) | *D*···*A* (Å) | *D*—H···*A* (°) |
|---|---|---|---|---|
| N1—H1A···O1 | 0.85 (3) | 2.00 (3) | 2.834 (2) | 168 (3) |
| N1—H1B···O5$^{i}$ | 0.95 (3) | 1.90 (3) | 2.838 (2) | 167 (3) |
| N1—H1C···O4$^{ii}$ | 0.88 (3) | 2.44 (3) | 2.8211 (19) | 107 (2) |
| N1—H1C···O5$^{iii}$ | 0.88 (3) | 1.95 (3) | 2.794 (2) | 161 (3) |
| O2—H2···O4$^{ii}$ | 0.97 (4) | 1.57 (4) | 2.5277 (19) | 172 (4) |

Symmetry code(s): (i) *x*+1, *y*, *z*; (ii) -*x*+1, *y*+1/2, -*z*+1/2; (iii) -*x*, *y*+1/2, -*z*+1/2.

Table S6. Selected hydrogen-bond parameters in the S-naproxen/D-alanine cocrystal

| *D*—H···*A* | *D*—H (Å) | H···*A* (Å) | *D*···*A* (Å) | *D*—H···*A* (°) |
|---|---|---|---|---|
| N1—H1A···O1 | 0.91 | 1.90 | 2.810 (7) | 177 |
| N1—H1B···O5$^{i}$ | 0.91 | 1.89 | 2.790 (7) | 168 |
| N1—H1C···O5$^{ii}$ | 0.91 | 2.05 | 2.933 (7) | 164 |
| O2—H2···O4$^{iii}$ | 0.84 | 1.68 | 2.513 (7) | 171 |

Symmetry code(s): (i) -*x*, *y*+1/2, -*z*+1/2; (ii) *x*+1, *y*, *z*; (iii) -*x*+1, *y*+1/2, -*z*+1/2.

Table S7. Selected hydrogen-bond parameters in S-naproxen/D-tryptophan monohydrate

| *D*—H···*A* | *D*—H (Å) | H···*A* (Å) | *D*···*A* (Å) | *D*—H···*A* (°) |
|---|---|---|---|---|
| N2—H2D···O1$^{i}$ | 0.89 (4) | 2.29 (3) | 2.956 (4) | 132 (3) |
| N1—H1A···O1 | 0.99 | 2.00 | 2.906 (4) | 149.8 |
| N1—H1B···O6 | 0.99 | 1.79 | 2.779 (4) | 174.5 |
| N1—H1C···O5$^{ii}$ | 0.99 | 1.77 | 2.742 (4) | 164.9 |
| O2—H2···O4$^{ii}$ | 0.94 (4) | 1.67 (4) | 2.562 (4) | 156 (4) |
| O6—H6B···O5$^{iii}$ | 0.85 (4) | 1.86 (4) | 2.703 (4) | 172 (5) |

Symmetry code(s): (i) -*x*, *y*-1/2, -*z*+3/2; (ii) *x*-1, *y*, *z*; (iii) -*x*+1, *y*-1/2, -*z*+3/2.

Table S8. Selected hydrogen-bond parameters in S-naproxen/D-tyrosine

| *D*—H···*A* | *D*—H (Å) | H···*A* (Å) | *D*···*A* (Å) | *D*—H···*A* (°) |
|---|---|---|---|---|
| N1—H1A···O5$^{i}$ | 0.916 (3) | 2.081 (3) | 2.940 (3) | 155.6 (3) |
| N1—H1B···O6$^{ii}$ | 0.915 (3) | 2.082 (3) | 2.709 (3) | 124.7 (2) |
| N1—H1C···O4$^{iii}$ | 0.908 (3) | 1.935 (3) | 2.825 (3) | 165.9 (3) |
| O2—H2···O4 | 0.853 (3) | 1.761 (3) | 2.613 (3) | 177.0 (2) |
| O6—H6A···O5$^{ii}$ | 0.815 (3) | 2.045 (3) | 2.859 (3) | 176.4 (3) |

Symmetry code(s): (i) -*x*+1, *y*-1/2, -*z*+2; (ii) -*x*+2, *y*-1/2, -*z*+2; (iii) *x*, *y*-1, *z*.

Figure S1. Experimental diffraction patter for S-naproxen ground with D-alanine (*1*) (10 μL of methanol, 90 min at 30 Hz); simulated diffraction pattern of the S-naproxen/D-alanine cocrystal (*2*); reference diffraction patterns for S-naproxen (*3*) and D-alanine (*4*). Cu*K*α radiation. Simulated diffraction pattern for S-naproxen/D-alanine (*2*) coincides with the diffraction pattern of ground material (*1*).

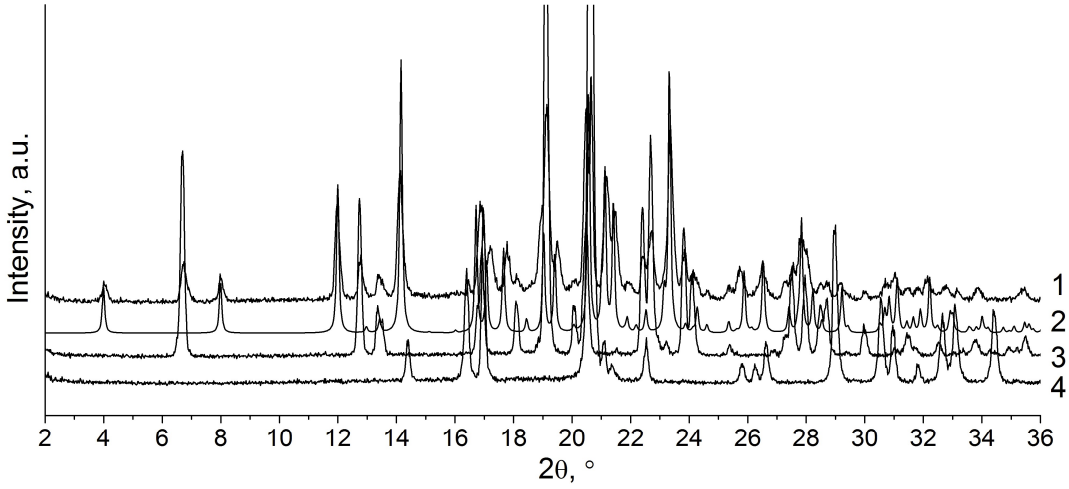


Figure S2. Experimental diffraction patter for S-naproxen ground with L-alanine (*1*) (10 μL of methanol, 90 min at 30 Hz); simulated diffraction pattern of the S-naproxen/L-alanine cocrystal (*2*); reference diffraction patterns for S-naproxen (*3*) and L-alanine (*4*). Cu*K*α radiation. Simulated diffraction pattern for S-naproxen/L-alanine (*2*) coincides with the diffraction pattern of ground material (*1*).

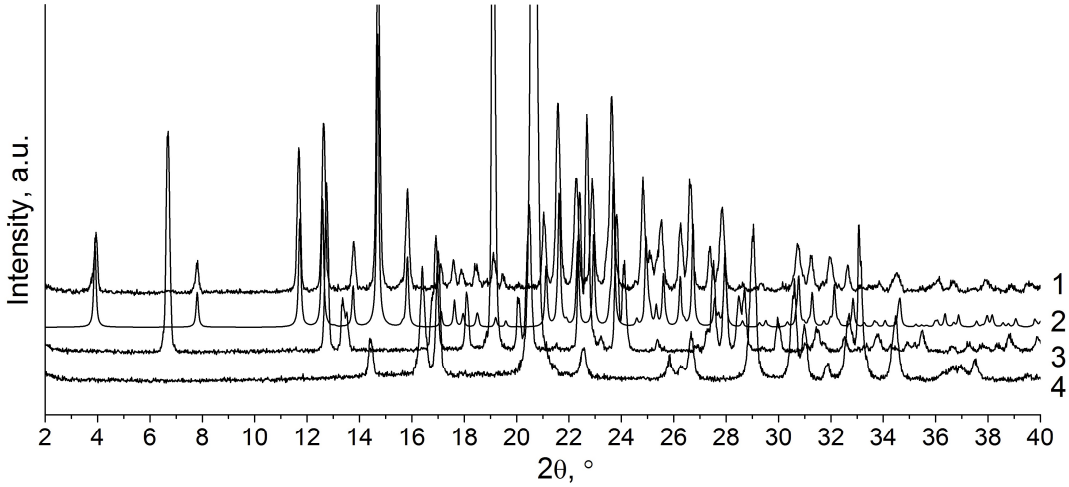

Figure S3. Comparison of the diffraction patterns (Cu*K*α radiation) of ground S-naproxen/L-tryptophan powder (*1*) (10 μL of methanol, 90 min at 30 Hz) and powder obtained from solution (60/40 % ethanol/water solution, slow evaporation, room temperature) (*2*). Both patterns show the presence of the same phase. Along with this new phase, the powder from solution (*2*) contains some amount of S-naproxen (*3*).

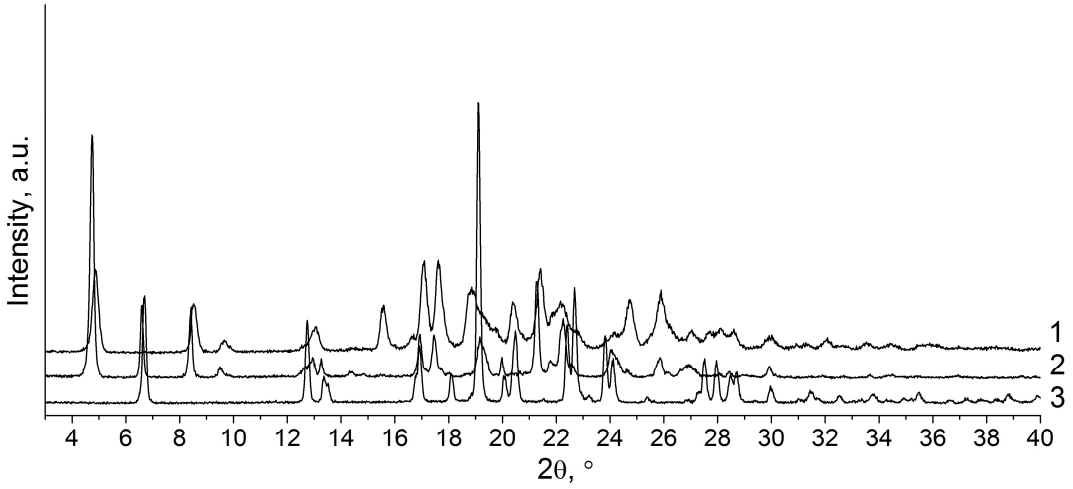


Figure S4. Experimental diffraction pattern (Cu*K*α radiation) of ground S-naproxen/D-tryptophan powder (*1*) (10 μL of methanol, 90 min at 30 Hz); simulated diffraction pattern for S-naproxen/D-tryptophan monohydrate (*2*); reference diffraction patterns for S-naproxen (*3*) and D-tryptophan (*4*). Cu*K*α radiation. Grinding of S-naproxen with D-tryptophan (*1*) yields a new phase, however different from S-naproxen/D-tryptophan monohydrate obtained from solution (arrows indicate some of the new peaks)

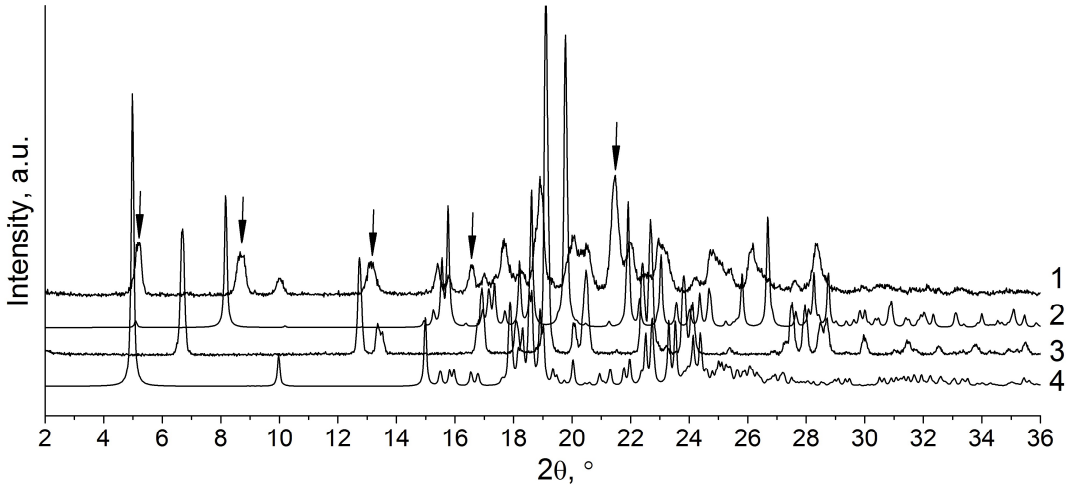

Figure S5. DSC data for S-naproxen/D-tryptophan monohydrate crystals and S-naproxen/L-tryptophan powder obtained from 60/40 % ethanol/water solution by slow evaporation. S/naproxen/L-tryptophan is in an unhydrated form

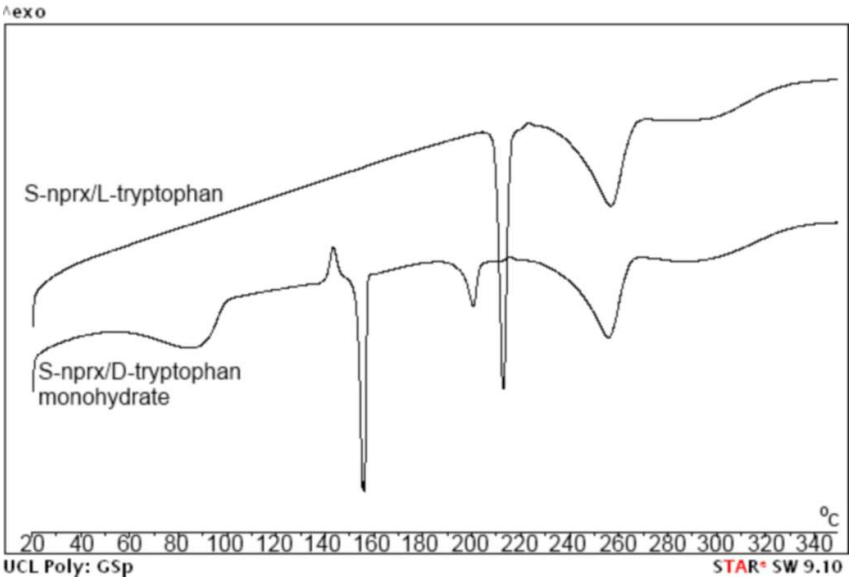


Figure S6. TGA data for S-naproxen/D-tryptophan monohydrate crystals and S-naproxen/L-tryptophan powder obtained from 60/40 % ethanol/water solution by slow evaporation S/naproxen/L-tryptophan is in an unhydrated form

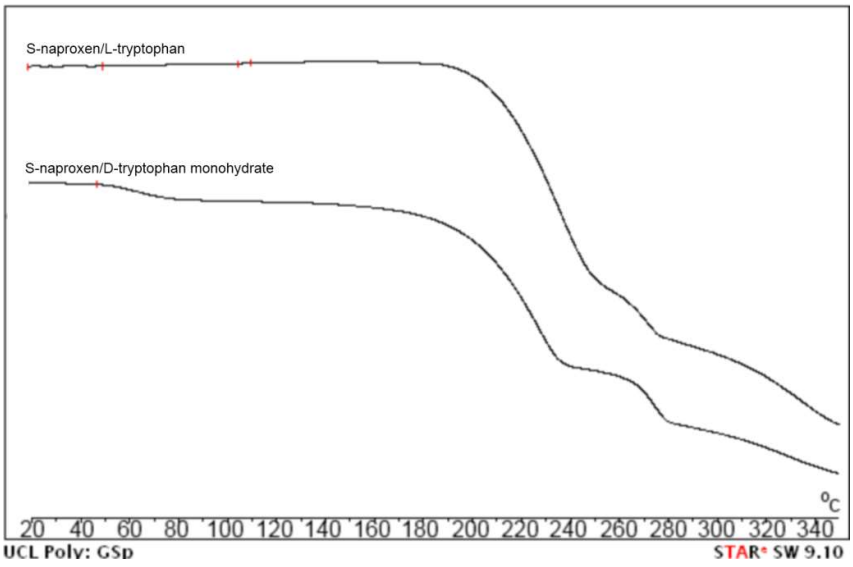

# APPENDIX B | Supporting information for Chapter 3

## Contents:


1. Initial Screening – Table S1 . . . . . 110
2. *In-situ* ball-milling experimental details – Table S2 . . . . . 111
3. Rietveld refinement plots for the structures solved from XRPD – Figures S1-S7. . . . . 112-115
4. Liquid-assisted grinding experiments for R-flurbiprofen/L-proline system – Table S3 . . . . . 116-119
5. Liquid-assisted grinding experiments for R-flurbiprofen/D-proline system – Table S4 . . . . . .120
6. Liquid-assisted grinding experiments for R-flurbiprofen/DL-proline system – Table S5 . . . . . 121-122
7. Liquid-assisted grinding experiments for RS-flurbiprofen/DL-proline system – Table S6. . . . . 123-124
8. Liquid-assisted grinding experiments for RS-flurbiprofen/L-proline system – Table S7 . . . . . .125-126
9. Liquid-assisted grinding experiments for RS-flurbiprofen/D-proline system – Table S8 . . . . . 127-128
10. Thermal analysis (DSC and TGA) for selected samples – Figures S8-S29 . . . . . 129-140
11. Step-by-step grinding experiments for R-flurbiprofen/L-proline system – Figures S30-S34 . . .141-143
12. Step-by-step grinding experiments for R-flurbiprofen/D-proline system – Figures S35-S36 . . . . . .144
13. Step-by-step grinding experiments for R-flurbiprofen/DL-proline system – Figures S37-S38 . . . . .145
14. Step-by-step grinding experiments for RS-flurbiprofen/L-proline system – Figures S39-S43 . . . . . 146-148
15. Step-by-step grinding experiments for RS-flurbiprofen/D-proline system – Figures S44-S45 . . . . .149
16. Step-by-step grinding experiments for RS-flurbiprofen/DL-proline system – Figures S46-S50 . . . . . 150-152
17. *In-situ* ball-milling x-ray diffraction experiments – Figures S51-S53 . . . . . 153-154
18. *In-situ* powder x-ray diffraction under variable temperature – Figures S54-S60. . . . . 155-159
19. Comparison of the same structures found from powder and single-crystal X-ray diffraction data – Figures S61-S64 . . . . . 160-161
20. Illustration of disorder in proline molecules – Figures S65-S69. . . . . .162-163
21. Structural peculiarities in 2 : 1 R/DL cocrystal – Figures S70-S72. . . . . 164
22. Comparison of diffraction patterns for 2 : 1 cocrystals – Figures S73 . . . . . 165
23. Packing in L-proline pol I and L-proline pol II – Figures S74 . . . . . 165
24. INCAR file . . . . . 166
25. K-point grids – Table S9 . . . . . .167
26. Initial and DFT optimized unit cell parameters – Table S10 . . . . . .168
27. Shrinkage of the structures in DFT calculations – Figures S75 . . . . . .169
28. Validation of structures from powder, overlap with experimental structure – Figures S76-S82 . . . . . .170-173
29. 15N NMR – Figures S83 . . . . . 174
30. Eigenvalues for the tensor of thermal expansion – Table S11 . . . . . 174

**Table S1.** Initial screening of R-flurbiprofen with amino acids (1 : 1 ratio, ~50-100 mg of powder in total, 5 μL of MeOH, grinding in a Retsch MM400 mixer mill for 60 min at a frequency of 30 Hz)

| Amino acid (AA) | m(AA), mg | m(R-flurbiprofen), mg ($M_r$=244,26 g/mol) | Result |
|---|---|---|---|
| L-Asparagine | 19.05 | 33.97 | no |
| L-Cysteine | 17.38 | 34.77 | no |
| L-Glutamine | 23.97 | 38.38 | no |
| L-Histidine | 22.54 | 35.40 | no |
| DL-Serine | 16.93 | 36.00 | no |
| L-Serine | 15.8 | 36.84 | no |
| D-Serine | 15.87 | 35.48 | no |
| D-Threonine | 23.37 | 41.06 | no |
| L-Threonine | 17.31 | 34.9 | no |
| D-Tryptophane | 29.22 | 30.41 | no |
| L-Tryptophane | 26.38 | 31.19 | no |
| L-Proline | 21.62 | 38.78 | yes |
| D-Proline | 26.25 | 55.19 | yes |
| L-Valine | 16.10 | 29.26 | no |
| D-Alanine | 14.20 | 38.6 | no |
| L-Leucine | 19.50 | 36.1 | no |
| D-Leucine | 18.10 | 34.0 | no |
| L-Phenylalanine | 22.20 | 32.5 | no |
| D-Phenylalanine | 20.70 | 30.5 | no |
| L-Isoleucine | 18.10 | 33.6 | No |
| L-Methionine | 20.30 | 33.4 | No |
| Trans-4-hydroxy-L-proline | 16.20 | 30.2 | No |
| L-Histidine hydrochloride monohydrate | 24.30 | 31.2 | No |
| D-Histidine | 20.40 | 32.0 | No |
| L-Histidine dihydrochloride | 24.20 | 25.6 | No |
| D-Valine | 18.00 | 37.5 | No |
| DL-Isoleucine | 17.40 | 32.5 | No |
| D-Asparagine | 19.00 | 33.6 | No |
| L-Alanine | 13.00 | 35.4 | No |
| D-Methionine | 20.40 | 33.4 | No |
| D-Aspartic acid | 20.30 | 36.5 | No |
| D-Glutamic acid | 20.90 | 33.8 | No |
| D-Glutamine | 21.00 | 34.8 | No |
| L-Aspartic acid | 18.30 | 33.0 | No |
| L-Glutamic acid | 21.00 | 34.5 | No |
| Glutamic acid hydrochloride | 21.80 | 29.2 | No |
| L-phenylglycine | 19.90 | 32.2 | No |
| D-phenylglycine | 18.50 | 30.2 | No |
| L-tyrosine | 78.26 | 38.6 | No |
| D-tyrosine | 76.38 | 36.1 | No |

**Table S2.** Experimental details of *in-situ* ball-milling experiments

| # | Sample | m(Flu), mg | m(Pro), mg | Molar ratio Flu/Pro | Solvent | Amount of solvent | Grinding duration |
|---|---|---|---|---|---|---|---|
| 1 | R-flurbiprofen + L-proline | 552.43 | 260.44 | 1 : 1 | Methanol | 200 µL | 25 min |
| 2 | R-flurbiprofen + L-proline | 555.48 | 261.82 | 1 : 1 | Isopropanol | 200 µL | 25 min |
| 3 | R-flurbiprofen + L-proline | 551.51 | 260.18 | 1 : 1 | Acetonitrile | 200 µL | 25 min |
| 4 | R-flurbiprofen + L-proline | 558.54 | 263.36 | 1 : 1 | Ethanol | 200 µL | 25 min |
| 5 | R-flurbiprofen + D-proline | 557.07 | 262.62 | 1 : 1 | Isopropanol | 200 µL | 25 min |
| 6 | R-flurbiprofen + D-proline | 556.96 | 262.93 | 1 : 1 | Methanol | 200 µL | 25 min |
| 7 | R-flurbiprofen + DL-proline | 558.52 | 263.90 | 1 : 1 | Isopropanol | 200 µL | 25 min |
| 8 | R-flurbiprofen + DL-proline | 564.46 | 266.33 | 1 : 1 | Methanol | 200 µL | 25 min |
| 9 | RS-flurbiprofen + L-proline | 557.00 | 262.78 | 1 : 1 | Methanol | 200 µL | 60 min |
| 10 | RS-flurbiprofen + D-proline | 556.17 | 262.22 | 1 : 1 | Ethanol | 200 µL | 60 min |
| 11 | RS-flurbiprofen + D-proline | 736.7 | 347.0 | 1 : 1 | Methanol | 200 µL | 25 min |
| 12 | RS-flurbiprofen + D-proline | 697.1 | 330.3 | 1 : 1 | Acetonitrile | 250 µL | 25 min |
| 13 | RS-flurbiprofen + L-proline | 691.5 | 326.3 | 1 : 1 | Methanol | 250 µL | 25 min |
| 14 | RS-flurbiprofen + L-proline | 680.7 | 323.6 | 1 : 1 | Acetonitrile | 200 µL | 30 min |
| 15 | RS-flurbiprofen + L-proline | 535.9 | 256.1 | 1 : 1 | Methanol | 200 µL | 30 min |
| 16 | RS-flurbiprofen + L-proline* | 518.0 | 247.1 | 1 : 1 | Isopropanol | 200 µL | 25 min |
| 17 | RS-flurbiprofen + D-proline | 536.5 | 255.2 | 1 : 1 | Isopropanol | 200 µL | 25 min |
| 18 | RS-flurbiprofen + L-proline | 555.0 | 264.5 | 1 : 1 | Isopropanol | 200 µL | 25 min |
| 19 | RS-flurbiprofen + DL-proline | 648.21 | 306.55 | 1 : 1 | Methanol | 200 µL | 30 min |
| 20 | RS-flurbiprofen + DL-proline | 527.65 | 251.05 | 1 : 1 | Isopropanol | 200 µL | 30 min |
| 21 | RS-flurbiprofen + DL-proline | 740.91 | 174.91 | 2 : 1 | Methanol | 200 µL | 30 min |
| 22 | RS-flurbiprofen + DL-proline | 693.99 | 164.60 | 2 : 1 | Isopropanol | 200 µL | 30 min |

*Sample was in contact with solution for 2h before being ground

## RIETVELD REFINEMENT PLOTS FOR THE STRUCTURES SOLVED FROM XRPD

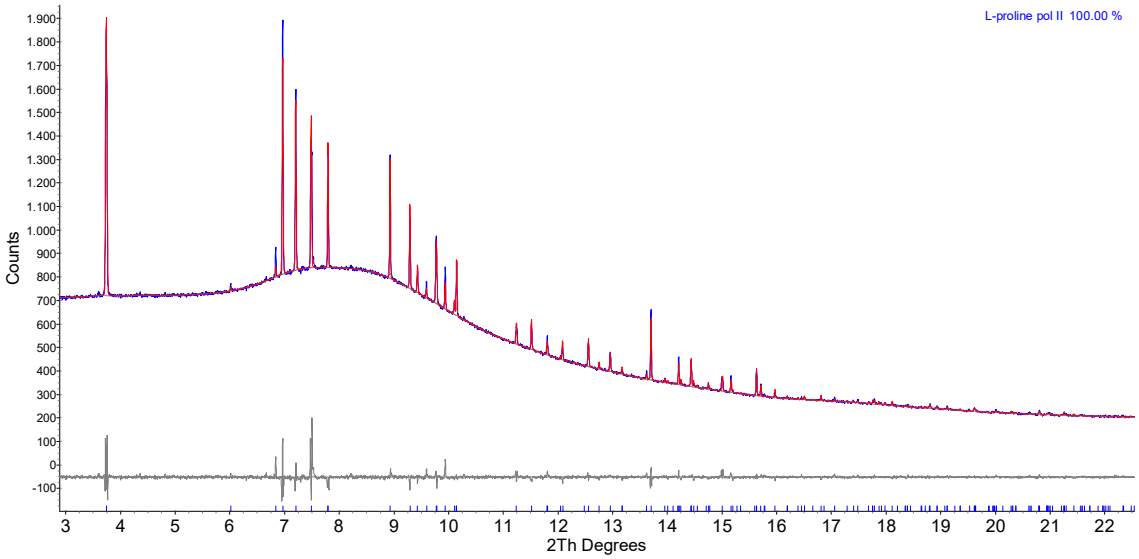


**Figure S1.** Rietveld refinement plot for L-proline polymorph II, determined from synchrotron X-ray powder data collected upon heating for the R-flurbiprofen/L-proline sample obtained by 1 : 2 ethanol-assisted grinding: λ = 0.62127 Å, *T* = 413 K, sample *9* in Table S3, see Figure S56 for the complete X-ray powder data set. Red and blue patterns represent calculated and experimental data, respectively; grey line corresponds to the difference profile; blue marks below the difference profile represent Bragg positions.

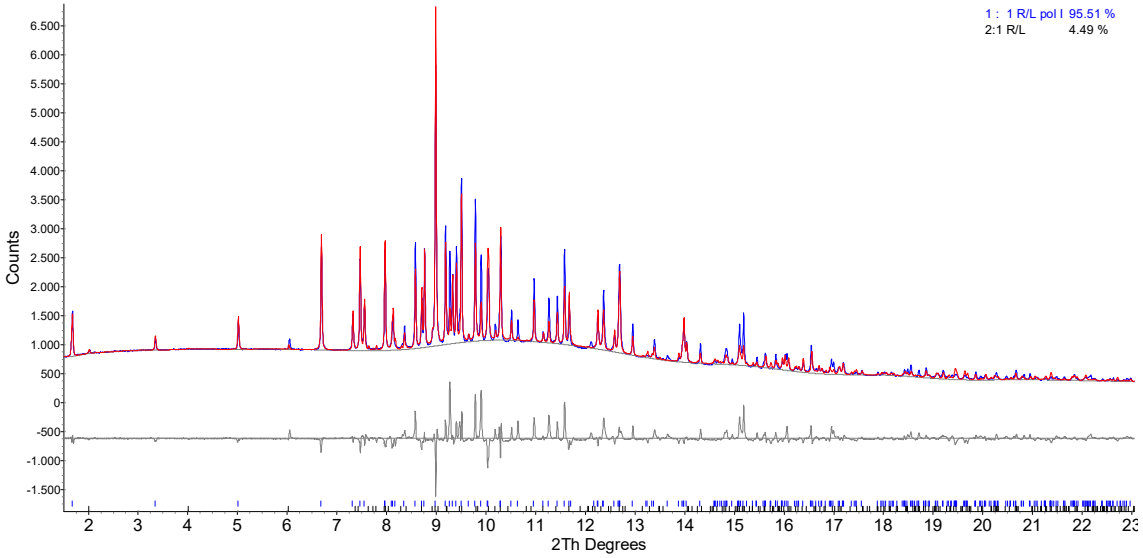


**Figure S2.** Rietveld refinement plot for the 1 : 1 R/L cocrystal polymorph I, determined from synchrotron X-ray powder data collected upon heating for the R-flurbiprofen/L-proline sample obtained by 1 : 1 methanol-assisted grinding: λ = 0.77494 Å, *T* = 344 K, sample *1* in Table S3, see Figure 1 for the complete X-ray powder data set. Red and blue patterns represent calculated and experimental data, respectively; grey line corresponds to the difference profile; blue and black marks below the difference profile represent Bragg positions for the 1 : 1 R/L pol I and 2 : 1 R/L phases, respectively.

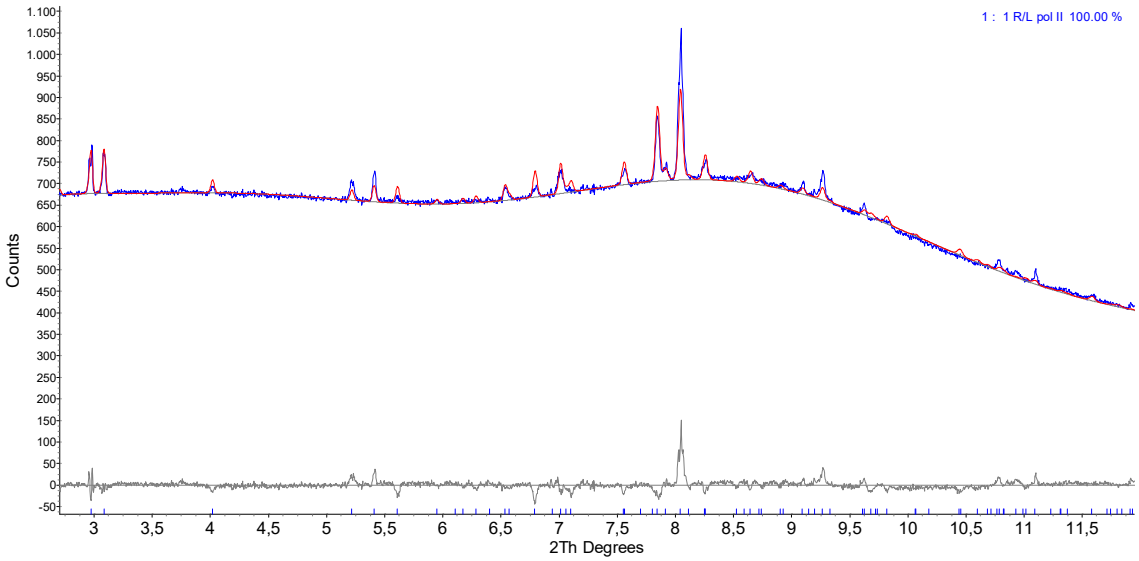


**Figure S3.** Rietveld refinement plot for 1 : 1 R/L cocrystal polymorph II, determined from synchrotron X-ray powder data collected upon cooling for the R-flurbiprofen/L-proline sample obtained by 1 : 1 isopropanol-assisted grinding: λ = 0.62127 Å, *T* = 376 K, sample *19* in Table S3, see Figure S57 for the complete data set. Red and blue patterns represent calculated and experimental data, respectively; grey line corresponds to the difference profile; blue marks below the difference profile represent Bragg positions.

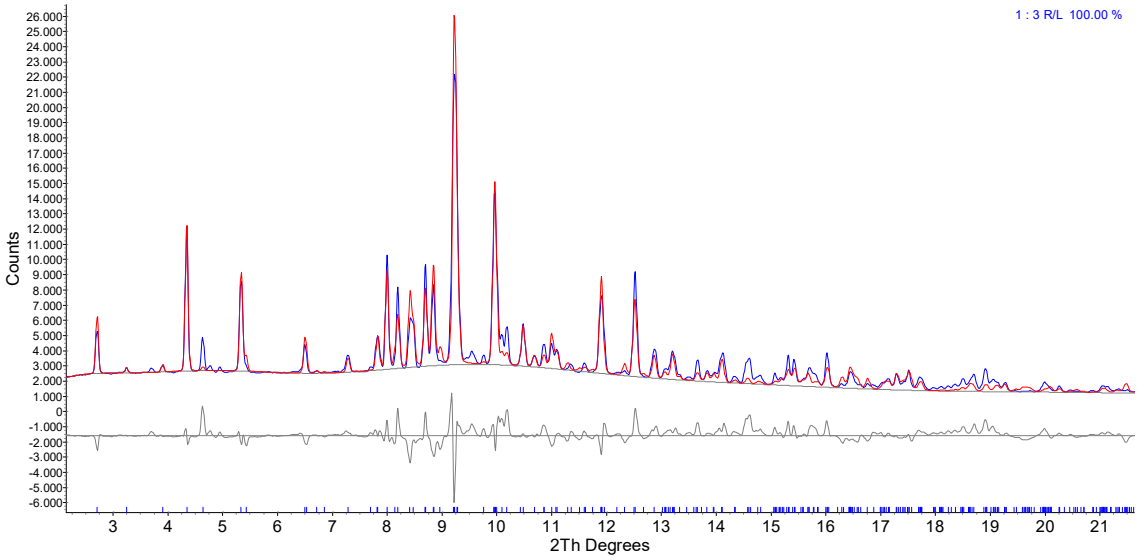


**Figure S4.** Rietveld refinement plot for 1 : 3 R/L cocrystal, determined from synchrotron X-ray powder data collected upon heating for the R-flurbiprofen/L-proline sample obtained by 1 : 3 ethanol-assisted grinding followed by drying: λ = 0.7458 Å, *T* = 300 K, sample *10* in Table S3, see Figure S60 for the complete data set. Red and blue patterns represent calculated and experimental data, respectively; grey line corresponds to the difference profile; blue marks below the difference profile represent Bragg positions.

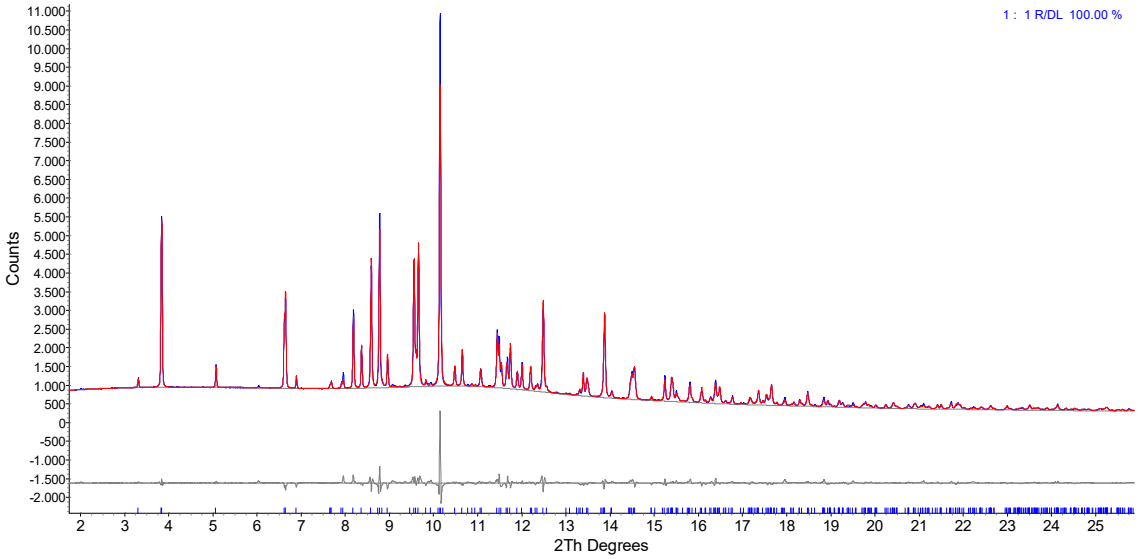


**Figure S5.** Rietveld refinement plot for 1 : 1 R/DL cocrystal, determined from synchrotron X-ray powder data collected at room temperature for the R-flurbiprofen/DL-proline sample obtained by 1 : 1 acetonitrile-assisted grinding: $\lambda = 0.77494$ Å, $T = 295$ K, sample *4* in Table S5. Red and blue patterns represent calculated and experimental data, respectively; grey line corresponds to the difference profile; blue marks below the difference profile represent Bragg positions.

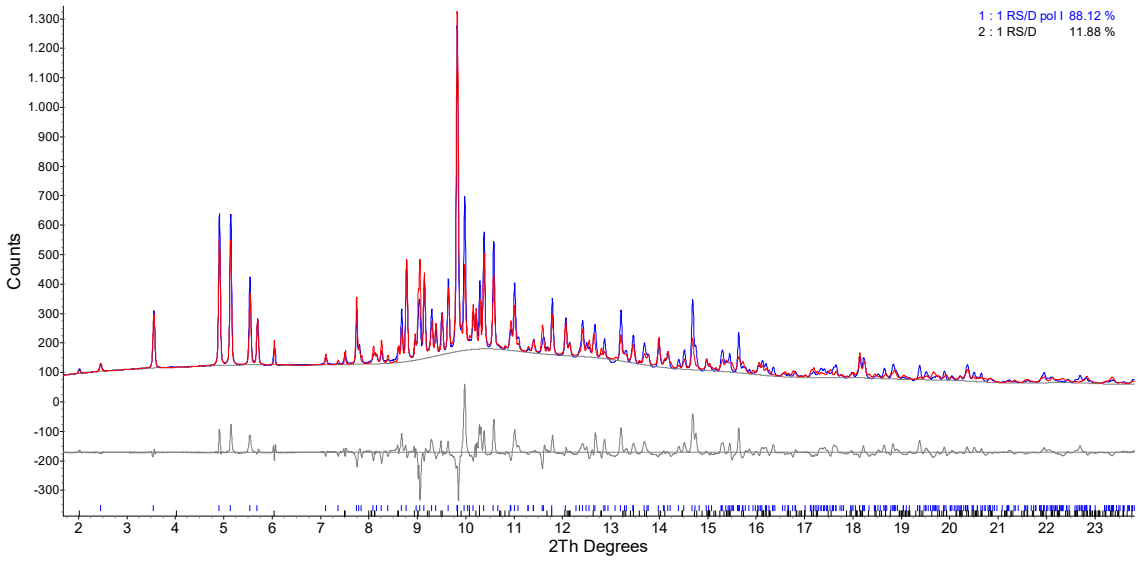


**Figure S6.** Rietveld refinement plot for 1 : 1 RS/D cocrystal polymorph I, determined from synchrotron X-ray powder data collected at room temperature for the RS-flurbiprofen/D-proline sample obtained by 1 : 1 methanol-assisted grinding: $\lambda = 0.776188$ Å, $T = 295$ K, sample *1* in Table S8. Red and blue patterns represent calculated and experimental data, respectively; grey line corresponds to the difference profile; blue marks below the difference profile represent Bragg positions for the 1 : 1 RS/D pol I and 2 : 1 RS/D phases, respectively.

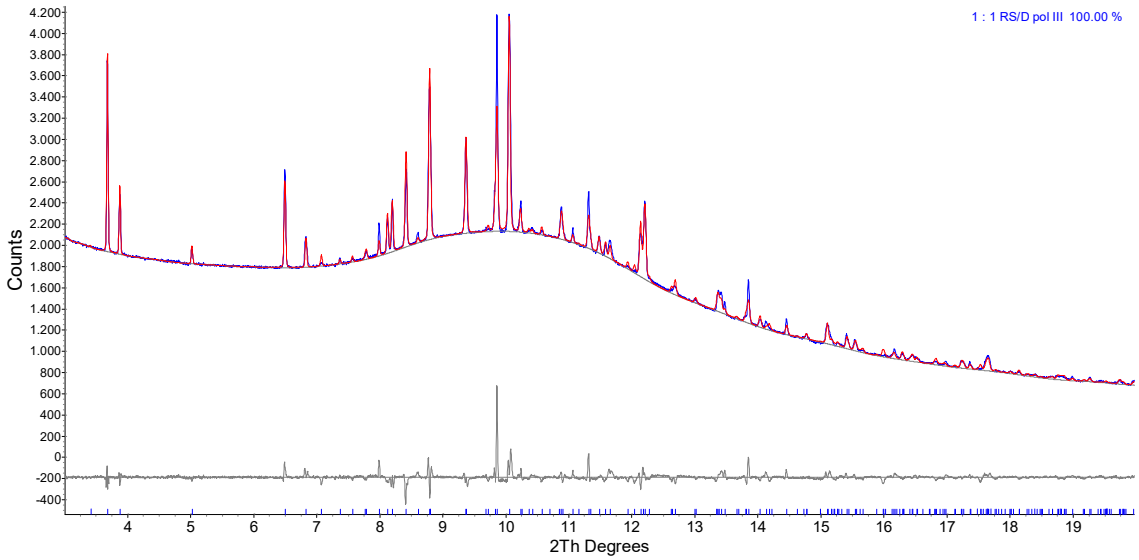


**Figure S7.** Rietveld refinement plot for 1 : 1 RS/D cocrystal polymorph III, determined from synchrotron X-ray powder data collected upon heating for the RS-flurbiprofen/D-proline sample obtained by 1 : 1 methanol-assisted grinding: $\lambda = 0.77663$ Å, $T = 420$ K, sample *1* in Table S8, see Figure 6a for the complete data set. Red and blue patterns represent calculated and experimental data, respectively; grey line corresponds to the difference profile; blue marks below the difference profile represent Bragg positions.

**Table S3.** Experimental details for laboratory liquid-assisted grinding and further analysis of obtained R-flurbiprofen/L-proline cocrystals; lab XRD was performed at Cu*K*α radiation

| # | m(R-Flu), mg | m(L-Pro), mg | Molar ratio R-Flu/L-Pro | Grinding conditions | PXRD analysis | Result | Structures determined from powder | Other analysis |
|---|---|---|---|---|---|---|---|---|
| 1 | 73.56 | 34.91 | 1 : 1 | 60 min, 30 Hz, 2 μL MeOH | Synchrotron (λ = 0.77494 Å) under variable temperature | At room temperature: 1 : 1 R/L/MeOH + 2 : 1 as impurity (small amount),<br>upon heating methanol evaporates resulting in 1 : 1 R/L pol I,<br>further heating leads to simultaneous emergence of 1 : 2 and 2 : 1 R/L phases<br>then 1 : 2 melts the first and 2 : 1 melts the last<br>(for the complete data set see **Figure 3.1)** | 1 : 1 R/L pol I, (for the Rietveld refinement plot see **Fig. S2**) | DSC (see **Fig. S17**) |
| 2 | 61.77 | 29.14 | 1 : 1 | 60 min, 30 Hz, 10 μL MeOH | Synchrotron (λ = 0.77663 Å) under variable temperature | At room temperature: 1 : 1 R/L/MeOH + 2 : 1 as impurity (small amount),<br>upon heating methanol evaporates resulting in 1 : 1 R/L,<br>further heating leads to simultaneous emergence of 2 : 1 + L-proline pol II<br>then L-proline pol II melts the first and finally 2 : 1 melts<br>(for the complete data set see **Figure S54)** | | DSC, TG (see **Figs. S18-S19**) |
| 3 | 65.1 | 31.1 | 1 : 1 | 15 min, 30 Hz, 10 μL MeOH | Synchrotron (λ = 0.77663 Å) under variable temperature | Same as sample *2* | | |
| 4 | 56.89 | 53.68 | 1 : 2 | 25 min, 30 Hz, 10 μL MeOH | Lab XRD | 1 : 1 R/L/MeOH + L-proline pol I | | |
| 5 | 69.63 | 16.39 | 2 : 1 | 60 min, 30 Hz, 2 μL MeOH | Synchrotron (λ = 1.0007 Å) | 2 : 1 R/L + R-flurbiprofen as impurity (5.43 wt%*) | | SEM (see **Fig. 3.11b**) |
| 6 | 67.19 | 31.77 | 1 : 1 | 60 min, 30 Hz, 10 μL EtOH | Synchrotron (λ = 0.77663 Å) under variable temperature | 2 : 1 R/L + 1 : 3 R/L, both phases melt simultaneously<br>(for the complete data set see **Figure S55)** | | DSC (see **Fig. S20)** |

| | | | | | | | | |
|---|---|---|---|---|---|---|---|---|
| 8 | 78.80 | 18.59 | 2 : 1 | 25 min, 30 Hz, 10 µL EtOH | Lab XRD | 2 : 1 R/L | | DSC (see **Fig. S13)** |
| 9 | 48.32 | 45.56 | 1 : 2 | 60 min, 30 Hz, 10 µL EtOH | Synchrotron (λ = 0.62173 Å) under variable temperature | Since the sample was not dried after grinding, the resultant 1 : 3 phase transformed into 1 : 2 R/L due to the presence of trace amounts of solvent and thus instead of a mixture of 1 : 3 and 1 : 2 the final sample measured at synchrotron contained only mainly 1 : 2 R/L<br>Heating resulted in the melting of the 1 : 2 R/L phase followed by the emergence of L-proline pol II and the melting of the latter<br>(for the complete data set see **Figure S56)** | L-proline pol II (for the Rietveld refinement plot see **Fig. S1**) | DSC (see **Fig. S21**) |
| 10 | 45.00 | 63.70 | 1 : 3 | 60 min, 30 Hz, 10 µL EtOH, dried | Synchrotron (λ = 0.7458 Å) under variable temperature | The initial sample mainly contains 1 : 3 R/L and trace amounts of impurities<br>Upon heating impurities melt and a small amount of 2 : 1 R/L emerges for a short time and then melts, 1 : 3 R/L phase preserves<br>Then 1 : 3 R/L melts followed by the emergence of a mixture of L-proline pol I and L-pro pol II<br>L-proline pol II starts melting first<br>(for the complete data set see **Figure S60)** | 1 : 3 R/L (for the Rietveld refinement plot see **Fig. S4**) | DSC, (see **Fig. S27**) 15N NMR (**Fig. S83**) |

| | | | | | | | | |
|---|---|---|---|---|---|---|---|---|
| 11 | 54.25 | 51.30 | 1 : 2 | 60 min, 30 Hz, 10 µL EtOH, dried | Synchrotron (λ = 0.708 Å) under variable temperature | The initial sample contains a mixture of 1 : 1 R/L, a small amount of L-proline monohydrate and a new unknown phase (presumable another cocrystal), referred as unknown phase I<br>Upon heating, first, L-proline monohydrate disappears, leaving a mixture of the 1 : 3 R/L and unknown phase I,<br>then unknown phase I disappears followed by the appearance of the small amount of 2 : 1 R/L; 1 : 3 R/L preserves;<br>then 2 : 1 R/L disappears, leaving pure 1 : 3 R/L<br>which then melts followed by the emergence of L-proline pol I and L-proline pol II<br>L-proline pol II melts the first and L-proline pol I melts the last<br>(for the complete data set see **Figure 3.2**) | | |
| 12 | 40.50 | 56.60 | 1 : 3 | 60 min, 30 Hz, 10 µL EtOH | Lab XRD | 1 : 3 R/L (plus small amounts of impurities) which after sometime transforms into 1 : 2 due to the presence of trace amount of solvent | | |
| 13 | 63.77 | 30.03 | 1 : 1 | 60 min, 30 Hz, 2 µL ACN | Synchrotron (λ = 0.776188 Å) | 2 : 1 R/L (53.37 wt %*) + 1 : 2 R/L (46.63 wt %*) – | | |
| 14 | 47.58 | 44.90 | 1 : 2 | 60 min, 30 Hz, 10 µL ACN | Synchrotron (λ = 0.62173 Å) | 1 : 2 R/L | | DSC (see **Fig. S14)** |
| 15 | 85.72 | 20.27 | 2 : 1 | 60 min, 30 Hz, 2 µL ACN | Lab XRD | 2 : 1 R/L (may contain L-proline impurity) | | |
| 16 | 54.35 | 51.30 | 1 : 2 | 60 min, 30 Hz, 10 µL ISPR | Lab XRD | Mainly 1 : 2 R/L and 2 : 1 R/L (diffraction pattern was measured sometime later than the sample was prepared), some other impurities in small amounts are present | | |
| 17 | 77.42 | 18.26 | 2 : 1 | 25 min, 30 Hz, 10 µL ISPR | Lab XRD | 2 : 1 R/L (may contain L-proline impurity) | | |

| | | | | | | | | |
|---|---|---|---|---|---|---|---|---|
| 18 | 45.50 | 64.40 | 1 : 3 | 60 min, 30 Hz, 10 µL ISPR | Lab XRD<br><br>Synchrotron ($\lambda$ = 0.708 Å) under variable temperature | 1 : 3 R/L (plus small amounts of impurities) which after sometime transforms into 1 : 2 due to the presence of trace amount of solvent – **Figure S16**<br>The initial sample contained 1 : 2 R/L, L-proline pol I and L-proline hydrate;<br>upon heating, first, L-proline hydrate disappears<br>then 1 : 2 R/L disappears followed by emergence of a tiny amount of some impurity, which then disappears, leaving pure L-proline pol I<br>(for the complete data set see **Figure S58)** | | |
| 19 | 72.61 | 34.50 | 1 : 1 | 25 min, 30 Hz, 10 µL ISPN | Synchrotron ($\lambda$ = 0.62173 Å) under variable temperature | Since the sample was not dried after grinding, the resultant phase transformed into 1 : 2 R/L due to the presence of trace amounts of solvent (see **Figure S17** for the comparison of the diffraction patterns measured right after grinding and measured using the synchrotron source later); 2 : 1 R/L preserves as impurity<br>Upon heating 1 : 2 and 2 : 1 R/L phases disappear simultaneously followed by the emergence of a small amount of 1 : 3 R/L<br>Upon cooling 1 : 1 R/L pol II crystallizes out; small amount of some impurity is also present<br>(for the complete data set see **Figure S57)** | 1 : 1 R/L pol II (for the Rietveld refinement plot see **Fig. S3**) | DSC (see **Fig. S22**) |
| 20 | 70.35 | 33.5 | 1 : 1 | 60 min, 30 Hz, 10 µL $H_2O$ | Synchrotron ($\lambda$ = 0.77663 Å) | 2 : 1 R/L (74.14 wt %*) + L-proline monohydrate (19.40 wt %*) + R-flurbiprofen (6.46 wt %) | | |
| 21 | 52.75 | 49.89 | 1 : 2 | 25 min, 30 Hz, 10 µL $H_2O$ | Lab XRD | 2 : 1 R/L + L-proline monohydrate | | |
| 22 | 74.48 | 17.62 | 2 : 1 | 25 min, 30 Hz, 10 µL $H_2O$ | Lab XRD | 2 : 1 R/L + L-proline monohydrate + R-flurbiprofen | | |

*For these samples, quick Rietveld refinement was performed to estimate roughly the weight fractions of the phases

**Table S4.** Experimental details for laboratory liquid-assisted grinding and further analysis of obtained R-flurbiprofen/D-proline cocrystals; lab XRD was performed at Cu*K*α radiation

| # | m(R-Flu), mg | m(D-Pro), mg | Molar ratio R-Flu/D-Pro | Grinding conditions | PXRD analysis | Result | Other analysis |
|---|---|---|---|---|---|---|---|
| 1 | 55.19 | 26.25 | 1 : 1 | 60 min, 30 Hz, 2 μL MeOH | Synchrotron (λ = 0.775045 Å) | 1 : 1 R/D (96.34 wt %)+ 2 : 1 R/D (3.66%) | |
| 2 | 73.71 | 17.46 | 2 : 1 | 60 min, 30 Hz, 2 μL MeOH | Synchrotron (λ = 1.0007 Å) | 2 : 1 R/D | |
| 3 | 36.14 | 34.16 | 1 : 2 | 60 min, 30 Hz, 10 μL MeOH | Lab XRD | 1 : 1 R/D + D-proline | |
| 4 | 65.1 | 30.9 | 1 : 1 | 60 min, 30 Hz, 7 μL ACN | Lab XRD | 1 : 1 R/D | |
| 5 | 75.50 | 17.78 | 2 : 1 | 60 min, 30 Hz, 10 μL ACN | Lab XRD | 2 : 1 R/D + R-flurbiprofen (small amounts) + D-proline | |
| 6 | 38.18 | 35.97 | 1 : 2 | 60 min, 30 Hz, 10 μL ACN | Lab XRD | 1 : 1 R/D + D-proline | |
| 7 | 50.49 | 23.90 | 1 : 1 | 60 min, 30 Hz, 10 μL EtOH | Lab XRD | 1 : 1 R/D | DSC (see **Fig. S10)** |
| 8 | 72.47 | 17.06 | 2 : 1 | 60 min, 30 Hz, 10 μL EtOH | Lab XRD | 2 : 1 R/D | DSC (see **Fig. S11)** |
| 9 | 40.29 | 37.98 | 1 : 2 | 60 min, 30 Hz, 10 μL EtOH | Lab XRD | 1 : 1 R/D + D-proline | |
| 10 | 77.91 | 36.46 | 1 : 1 | 60 min, 30 Hz, 2 μL ISPN | Lab XRD | 1 : 1 R/D | |
| 11 | 77.57 | 18.31 | 2 : 1 | 60 min, 30 Hz, 10 μL ISPN | Lab XRD | 2 : 1 R/D | |
| 12 | 39.72 | 37.62 | 1 : 2 | 60 min, 30 Hz, 10 μL ISPN | Lab XRD | 1 : 1 R/D + D-proline | |
| 13 | 77.91 | 36.73 | 1 : 1 | 60 min, 30 Hz, 10 μL $H_2O$ | Lab XRD | 2 : 1 R/D + R-flurbiprofen (small amounts) | |
| 14 | 71.10 | 16.75 | 2 : 1 | 60 min, 30 Hz, 10 μL $H_2O$ | Lab XRD | 2 : 1 R/D + R-flurbiprofen (small amounts) | |
| 15 | 39.42 | 37.16 | 1 : 2 | 60 min, 30 Hz,10 μL $H_2O$ | Lab XRD | 2 : 1 R/D + D-proline monohydrate | |

**Table S5.** Experimental details for laboratory liquid-assisted grinding and further analysis of obtained R-flurbiprofen/DL-proline cocrystals; lab XRD was performed at Cu*K*α radiation

| # | m(R-Flu), mg | m(DL-Pro), mg | Molar ratio R-Flu/DL-Pro | Grinding conditions | PXRD analysis | Result | Structures determined from powder | Other analysis |
|---|---|---|---|---|---|---|---|---|
| 1 | 87.60 | 41.73 | 1 : 1 | 60 min, 30 Hz, 5 μL MeOH | Synchrotron (λ = 0.77494 Å) | 1 : 1 R/DL (88.89 wt %) + 2 : 1R/DL (11.11 wt%) | | |
| 2 | 69.90 | 16.74 | 2 : 1 | 60 min, 30 Hz, 10 μL MeOH | Synchrotron (λ = 0.77663 Å) | 2 : 1 R/DL (93.47 wt %) + R-flurbiprofen (6.53 wt %) | | |
| 3 | 37.60 | 35.45 | 1 : 2 | 60 min, 30 Hz, 10 μL MeOH | Lab XRD | 1 : 1 + impurities (most likely DL-proline and DL-proline monohydrate, probably something else) | | |
| 4 | 93.61 | 44.22 | 1 : 1 | 60 min, 30 Hz, 5 μL ACN | Synchrotron (λ = 0.77494 Å) | 1 : 1 R/DL | 1 : 1 R/DL (for the Rietveld refinement plot see **Fig. S5**) | |
| 5 | 70.34 | 16.51 | 2 : 1 | 60 min, 30 Hz, 10 μL ACN | Lab XRD | 2 : 1 R/DL | | |
| 6 | 37.37 | 35.38 | 1 : 2 | 60 min, 30 Hz, 10 μL ACN | Lab XRD | 1 : 1 + impurities (most likely DL-proline and DL-proline monohydrate) | | |
| 7 | 63.86 | 30.09 | 1 : 1 | 60 min, 30 Hz, 10 μL EtOH | Synchrotron (λ = 0.708 Å) under variable temperature | 1 : 1 R/DL<br><br>Upon heating the cocrystal undergoes a phase crossover, see Discussion for more detail<br>(for the complete data set see **Figure 3.5)** | | DSC (see **Fig. S29)** |
| 8 | 73.28 | 17.27 | 2 : 1 | 60 min, 30 Hz, 10 μL EtOH | Synchrotron (λ = 0.62127 Å)<br>Synchrotron (λ = 0.708 Å) under variable temperature | 2 : 1 R/DL (94.19 wt %) + R-flurbiprofen (5.31 wt %)<br>Upon heating the cocrystal simply melts<br>(for the complete data set see **Figure S59)** | | DSC (see **Fig. S16)** |

| | | | | | | | | |
|---|---|---|---|---|---|---|---|---|
| 9 | 36.75 | 34.63 | 1 : 2 | 60 min, 30 Hz, 10 µL EtOH | Lab XRD | 1 : 1 + impurities (most likely DL-proline and DL-proline monohydrate) | | |
| 10 | 74.55 | 35.04 | 1 : 1 | 60 min, 30 Hz, 5 µL ISPN | Synchrotron ($\lambda$ = 0.77494 Å) | 1 : 1 R/DL (96.13 wt %) + 2 : 1R/DL (3.87 wt%) | | |
| 11 | 73.63 | 17.40 | 2 : 1 | 60 min, 30 Hz, 10 µL ISPN | Lab XRD | 2 : 1 R/DL | | |
| 12 | 42.25 | 39.86 | 1 : 2 | 60 min, 30 Hz, 10 µL ISPN | Lab XRD | 1 : 1 + impurities (most likely DL-proline and DL-proline monohydrate) | | |
| 13 | 59.03 | 28.49 | 1 : 1 | 60 min, 30 Hz, 10 µL $H_2O$ | Lab XRD | 2 : 1 R/DL + R-flurbiprofen + DL-proline monohydrate (+probably DL-proline) | | |
| 14 | 73.36 | 17.39 | 2 : 1 | 60 min, 30 Hz, 10 µL $H_2O$ | Lab XRD | 2 : 1 R/DL + R-flurbiprofen (+probably DL-proline and DL-proline monohydrate) | | |
| 15 | 35.08 | 33.10 | 1 : 2 | 60 min, 30 Hz, 10 µL $H_2O$ | Lab XRD | 2 : 1 R/DL + DL-proline monohydrate | | |

**Table S6.** Experimental details for laboratory liquid-assisted grinding and further analysis of obtained RS-flurbiprofen/DL-proline cocrystals; lab XRD was performed at CuKα radiation

| # | m(RS-Flu), mg | m(DL-Pro), mg | Molar ratio RS-Flu/DL-Pro | Grinding conditions | PXRD analysis | Result | Structures determined from powder | Other analysis |
|---|---|---|---|---|---|---|---|---|
| 1 | 105.88 | 50.02 | 1 : 1 | 60 min, 30 Hz, 2 μL MeOH | Synchrotron (λ = 0.776188 Å) | 1 : 1 RS/DL | | DSC (see **Fig. S15)** |
| 2 | 80.49 | 19.00 | 2 : 1 | 90 min, 30 Hz, 10 μL MeOH | Lab XRD | 1 : 1 RS/DL + RS-flurbiprofen (*P*-1) impurity | | |
| 3 | 77.55 | 73.64 | 1 : 2 | 60 min, 30 Hz, 10 μL MeOH | Lab XRD | 1 : 1 RS/DL + RS-flurbiprofen (*P*-1) + DL-proline + probably DL-proline monohydrate | | |
| 4 | 73.51 | 35.45 | 1 : 1 | 60 min, 30 Hz, 2 μL ACN | Lab XRD | 1 : 1 RS/DL | | |
| 5 | 80.88 | 19.11 | 2 : 1 | 90 min, 30 Hz, 10 μL ACN | Lab XRD | 2 : 1 RS/L + 2 : 1 RS/D + RS-flurbiprofen (*P*-1) impurity | | |
| 6 | 51.56 | 49.07 | 1 : 2 | 60 min, 30 Hz, 10 μL ACN | Lab XRD | 1 : 1 RS/DL + RS-flurbiprofen (*P*-1) + DL-proline + probably DL-proline monohydrate | | |
| 7 | 94.73 | 45.12 | 1 : 1 | 60 min, 30 Hz, 2 μL ISPN | Lab XRD | 1 : 1 RS/DL + RS-flurbiprofen (*P*-1) impurity | | |
| 8 | 80.76 | 19.18 | 2 : 1 | 90 min, 30 Hz, 10 μL ISPN | Synchrotron (λ = 0.708 Å) under variable temperature | 2 : 1 RS/L + 2 : 1 RS/D + RS-flurbiprofen (*P*-1) impurity<br><br>Upon heating RS-flurbiprofen impurity disappears first, leaving almost pure conglomerate 2 : 1 RS/L – 2 : 1 RS/D<br><br>Further heating leads to the emergence of 1 : 1 RS/DL followed by its melting<br>(for the complete data set see **Figure 3.8)** | | |
| 9 | 60.49 | 57.17 | 1 : 2 | 60 min, 30 Hz, 10 μL ISPN | Lab XRD | 1 : 1 RS/DL + RS-flurbiprofen (*P*-1) + DL-proline + probably DL-proline monohydrate | | |
| 10 | 80.17 | 37.99 | 1 : 1 | 90 min, 30 Hz, 10 μL EtOH | Lab XRD | 1 : 1 RS/DL | | |

| | | | | | | | | |
|---|---|---|---|---|---|---|---|---|
| 11 | 84.40 | 20.01 | 2 : 1 | 90 min, 30 Hz, 10 µL EtOH | Lab XRD | 2 : 1 RS/L + 2 : 1 RS/D + RS-flurbiprofen (*P*-1) impurity | | |
| 12 | 53.80 | 50.80 | 1 : 2 | 60 min, 30 Hz, 10 µL EtOH | Lab XRD | 1 : 1 RS/DL + RS-flurbiprofen (*P*-1) + DL-proline + probably DL-proline monohydrate | | |
| 13 | 71.21 | 33.71 | 1 : 1 | 60 min, 30 Hz, 2 µL $H_2O$ | Lab XRD | 1 : 1 RS/DL + RS-flurbiprofen (*P*-1) | | |
| 14 | 85.96 | 20.39 | 2 : 1 | 60 min, 30 Hz, 10 µL $H_2O$ | Lab XRD | 2 : 1 RS/L + 2 : 1 RS/D + RS-flurbiprofen (*P*-1) impurity | | |
| 15 | 67.10 | 63.55 | 1 : 2 | 60 min, 30 Hz, 10 µL $H_2O$ | Lab XRD | 1 : 1 RS/DL + RS-flurbiprofen (*P*-1) + DL-proline monohydrate | | |

**Table S7.** Experimental details for laboratory liquid-assisted grinding and further analysis of obtained RS-flurbiprofen/L-proline cocrystals; lab XRD was performed at CuKα radiation

| # | m(RS-Flu), mg | m(L-Pro), mg | Molar ratio RS-Flu/L-Pro | Grinding conditions | PXRD analysis | Result | Structures determined from powder | Other analysis |
|---|---|---|---|---|---|---|---|---|
| 1 | 68.82 | 33.20 | 1 : 1 | 60 min, 30 Hz, 2 μL MeOH | Synchrotron (λ = 0.776188 Å) | 1 : 1 RS/L pol II (81.35wt %)+ 2 : 1 RS/L (18.65 wt %) | | DSC (see **Fig. S24)** SEM **(Fig. 3.11a)** |
| 2 | 86.68 | 20.53 | 2 : 1 | 60 min, 30 Hz, 10 μL MeOH | Lab XRD | 2 : 1 RS/L | | DSC (see **Fig. S12)** |
| 3 | 56.82 | 53.71 | 1 : 2 | 60 min, 30 Hz, 10 μL MeOH | Lab XRD | 1 : 1 RS/L pol I + L-proline | | |
| 4 | 65.1 | 31.1 | 1 : 1 | 15 min, 30 Hz, 7 μL MeOH | Lab XRD | 2 : 1 RS/L + 1 : 1 RS/L pol II | | |
| 5 | 77.19 | 36.52 | 1 : 1 | 90 min, 30 Hz, 10 μL MeOH | Lab XRD | 1 : 1 RS/L pol I + probably small amount of 2 : 1 RS/L | | |
| 6 | 73.80 | 34.76 | 1 : 1 | 60 min, 30 Hz, 2 μL ACN | Synchrotron (λ = 0.776188 Å) | 2 : 1 RS/L (84.03 wt %) + L-proline (15.97 wt %) | | |
| 7 | 94.56 | 22.41 | 2 : 1 | 60 min, 30 Hz, 2 μL ACN | Lab XRD | 2 : 1 RS/L | | |
| 8 | 61.13 | 57.65 | 1 : 2 | 60 min, 30 Hz, 10 μL ACN | Lab XRD | 2 : 1 RS/L + L-proline | | |
| 9 | 65.0 | 30.8 | 1 : 1 | 15 min, 30 Hz, 7 μL ACN | Synchrotron (λ = 0.77663 Å) | 2 : 1 RS/L (84.03 wt %) + L-proline (15.97 wt %) | | |
| 10 | 73.21 | 34.51 | 1 : 1 | 90 min, 30 Hz, 10 μL ACN | Lab XRD | 2 : 1 RS/L + L-proline | | |
| 11 | 75.00 | 35.38 | 1 : 1 | 25 min, 30 Hz, 10 μL EtOH | Lab XRD | 2 : 1 RS/L + RS-flurbiprofen (*P*-1) + L-proline | | |
| 12 | 72.87 | 34.40 | 1 : 1 | 60 min, 30 Hz, 10 μL EtOH | Lab XRD | 1 : 1 RS/L pol I + 2 : 1 RS/L + probably small amount of L-proline | | |
| 13 | 71.40 | 33.67 | 1 : 1 | 90 min, 30 Hz, | Lab XRD | 1 : 1 RS/L pol I + probably small amount of L-proline | | |

| | | | | | | | | |
|---|---|---|---|---|---|---|---|---|
| | | | | 10 µL EtOH | | | | |
| 14 | 81.62 | 19.26 | 2 : 1 | 60 min, 30 Hz, 10 µL EtOH | Lab XRD | 2 : 1 RS/L | | |
| 15 | 54.01 | 51.03 | 1 : 2 | 60 min, 30 Hz, 10 µL EtOH | Lab XRD | 1 : 1 RS/L pol I + L-proline | | |
| 16 | 65.1 | 31.2 | 1 : 1 | 15 min, 30 Hz, 7 µL ISPN | Lab XRD | 2 : 1 RS/L + L-proline | | |
| 17 | 72.98 | 34.51 | 1 : 1 | 90 min, 30 Hz, 10 µL ISPN | Lab XRD | 2 : 1 RS/L + L-proline | | |
| 18 | 70.18 | 33.80 | 1 : 1 | 60 min, 30 Hz, 10 µL ISPN | Lab XRD | 2 : 1 RS/L + L-proline | | |
| 19 | 88.26 | 20.92 | 2 : 1 | 60 min, 30 Hz, 10 µL ISPN | Lab XRD | 2 : 1 RS/L | | |
| 20 | 50.82 | 47.92 | 1 : 2 | 60 min, 30 Hz, 10 µL ISPN | Lab XRD | 2 : 1 RS/L + L-proline | | |
| 21 | 72.41 | 34.24 | 1 : 1 | 60 min, 30 Hz, 2 µL $H_2O$ | Synchrotron ($\lambda$ = 0.77663 Å) | 2 : 1 RS/L (79.44 wt %) + L-proline monohydrate (18.02 wt %) + RS-flurbiprofen *P*-1 (2.53 wt %) | | |
| 22 | 74.36 | 35.06 | 1 : 1 | 90 min, 30 Hz, 10 µL $H_2O$ | Lab XRD | 2 : 1 RS/L + L-proline monohydrate + RS-flurbiprofen (*P*-1) | | |
| 23 | 65.0 | 31.2 | 1 : 1 | 60 min, 30 Hz, 7 µL $H_2O$ | Synchrotron ($\lambda$ = 0.77663 Å) | 2 : 1 RS/L (89.63 wt %) + L-proline monohydrate (8.37 wt %) + RS-flurbiprofen *P*-1 (2.00 wt %) | | |
| 24 | 65.1 | 31.0 | 1 : 1 | 15 min, 30 Hz, 7 µL $H_2O$ | Lab XRD | 2 : 1 RS/L + L-proline monohydrate | | |
| 25 | 86.83 | 20.54 | 2 : 1 | 60 min, 30 Hz, 10 µL $H_2O$ | Lab XRD | 2 : 1 RS/L | | |
| 26 | 56.43 | 53.46 | 1 : 2 | 60 min, 30 Hz, 10 µL $H_2O$ | Lab XRD | 2 : 1 RS/L + L-proline monohydrate + RS-flurbiprofen (*P*-1) | | |

**Table S8.** Experimental details for laboratory liquid-assisted grinding and further analysis of obtained RS-flurbiprofen/D-proline cocrystals; lab XRD was performed at CuKα radiation

| # | m(RS-Flu), mg | m(D-Pro), mg | Molar ratio RS-Flu/D-Pro | Grinding conditions | PXRD analysis | Result | Structures determined from powder | Other analysis |
|---|---|---|---|---|---|---|---|---|
| 1 | 71.22 | 33.60 | 1 : 1 | 60 min, 30 Hz, 2 μL MeOH | Synchrotron (λ = 0.776188 Å) under variable temperature | 1 : 1 RS/D pol I (88.18 wt%) + 2 : 1 RS/D (11.88 wt%)<br><br>Upon heating 1 : 1 RS/D pol I disappears, whereas 2 : 1 RS/D preserves<br><br>then disappearance of 2 : 1 RS/D is followed by the emergence of 1 : 1 RS/D pol III<br><br>(for the complete data set see **Figure 3.6a)** | 1 : 1 RS/D pol I<br>1 : 1 RS/D pol III<br>(for the Rietveld refinement plot see **Figs. S6 and S7**) | DSC (see **Fig. S23)** |
| 2 | 65.0 | 31.1 | 1 : 1 | 15 min, 30 Hz, 7 μL MeOH | Lab XRD | 2 : 1 RS/D + D-proline | | |
| 3 | 76.28 | 35.96 | 1 : 1 | 90 min, 30 Hz, 10 μL MeOH | Lab XRD | 1 : 1 RS/D pol I | | |
| 4 | 84.80 | 20.09 | 2 : 1 | 60 min, 30 Hz, 10 μL MeOH | Lab XRD | 2 : 1 RS/D | | |
| 5 | 61.68 | 58.25 | 1 : 2 | 60 min, 30 Hz, 10 μL MeOH | Lab XRD | 1 : 1 RS/D pol I + D-proline | | |
| 6 | 63.38 | 32.05 | 1 : 1 | 60 min, 30 Hz, 2 μL ACN | Synchrotron (λ = 0.776188 Å) | 2 : 1 RS/D (87.38 wt%) + D-proline (12.62 wt%) | | SEM (**Fig. 3.11c**) |
| 7 | 73.72 | 34.74 | 1 : 1 | 90 min, 30 Hz, 10 μL ACN | Lab XRD | 2 : 1 RS/D + D-proline | | |
| 8 | 87.79 | 20.67 | 2 : 1 | 60 min, 30 Hz, 10 μL ACN | Lab XRD | 2 : 1 RS/D + RS-flurbiprofen (*P*-1) + D-proline | | |
| 9 | 51.95 | 48.97 | 1 : 2 | 60 min, 30 Hz, 10 μL ACN | Lab XRD | 2 : 1 RS/D + D-proline | | |
| 10 | 72.09 | 33.98 | 1 : 1 | 90 min, 30 Hz, 10 μL EtOH | Lab XRD | 1 : 1 RS/D pol II | | |

| | | | | | | | | |
|---|---|---|---|---|---|---|---|---|
| 11 | 73.58 | 34.78 | 1 : 1 | 60 min, 30 Hz, 10 µL EtOH | Lab XRD | 1 : 1 RS/D pol II + 2 : 1 RS/D | | |
| 12 | 76.88 | 36.26 | 1 : 1 | 25 min, 30 Hz, 10 µL EtOH | Lab XRD | 2 : 1 RS/D + D-proline | | |
| 13 | 81.46 | 19.24 | 2 : 1 | 60 min, 30 Hz, 10 µL EtOH | Lab XRD | 2 : 1 RS/D + RS-flurbiprofen (*P*-1) + D-proline**8** | | |
| 14 | 57.00 | 53.77 | 1 : 2 | 60 min, 30 Hz, 10 µL EtOH | Lab XRD | 1 : 1 RS/D pol I + D-proline | | |
| 15 | 76.97 | 36.28 | 1 : 1 | 90 min, 30 Hz, 10 µL ISPN | Lab XRD<br><br>Synchrotron ($\lambda$ = 0.708 Å) under variable temperature | 1 : 1 RS/D pol II<br><br>Upon heating disappearance of 1 : 1 RS/D pol II is followed by the emergence of 1 : 1 RS/D pol III<br><br>(for the complete data set see **Figure 3.6b)** | | DSC<br>(see **Fig. S28)** |
| 16 | 76.36 | 37.24 | 1 : 1 | 60 min, 30 Hz, 2 µL ISPN | Lab XRD | 2 : 1 RS/D + D-proline | | |
| 17 | 81.86 | 19.28 | 2 : 1 | 60 min, 30 Hz, 10 µL ISPN | Lab XRD | 2 : 1 RS/D + RS-flurbiprofen (*P*-1) + D-proline | | |
| 18 | 53.25 | 50.22 | 1 : 2 | 60 min, 30 Hz, 10 µL ISPN | Lab XRD | 2 : 1 RS/D + D-proline | | |
| 19 | 73.82 | 34.88 | 1 : 1 | 90 min, 30 Hz, 10 µL $H_2O$ | Lab XRD | 2 : 1 RS/D + D-proline monohydrate + RS-flurbiprofen (*P*-1) | | |
| 20 | 81.30 | 19.18 | 2 : 1 | 60 min, 30 Hz, 10 µL $H_2O$ | Lab XRD | 2 : 1 RS/D + D-proline monohydrate + RS-flurbiprofen (*P*-1) | | |
| 21 | 50.58 | 47.76 | 1 : 2 | 60 min, 30 Hz, 10 µL $H_2O$ | Lab XRD | 2 : 1 RS/D + D-proline monohydrate + RS-flurbiprofen (*P*-1) | | |

**THERMAL ANALYSIS**

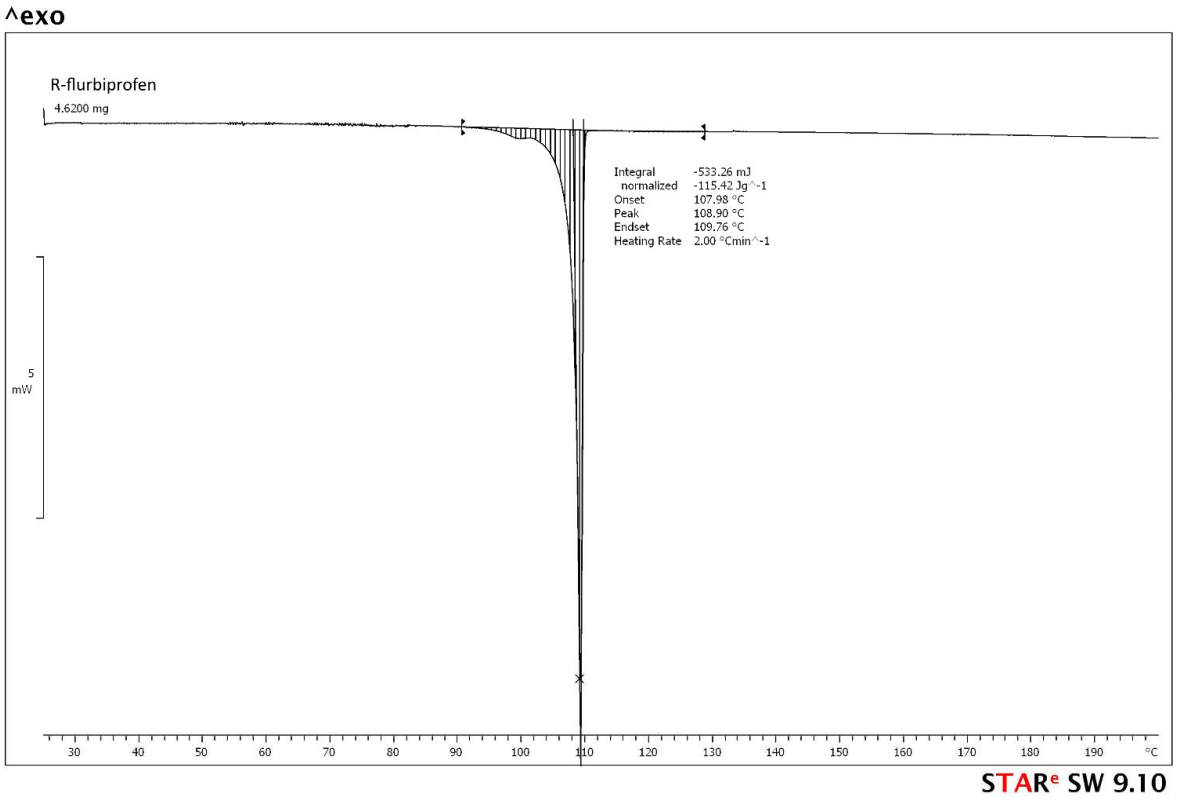


**Figure S8**. DSC curve for pure R-flurbiprofen

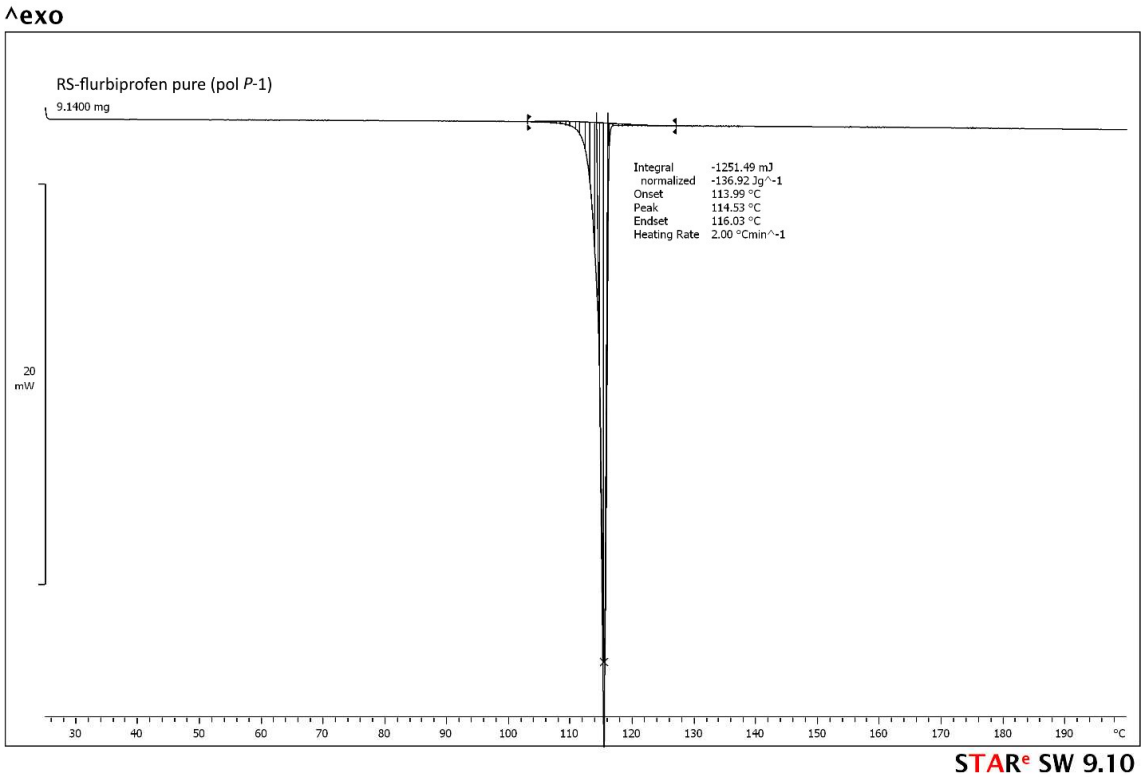


**Figure S9**. DSC curve for pure RS-flurbiprofen

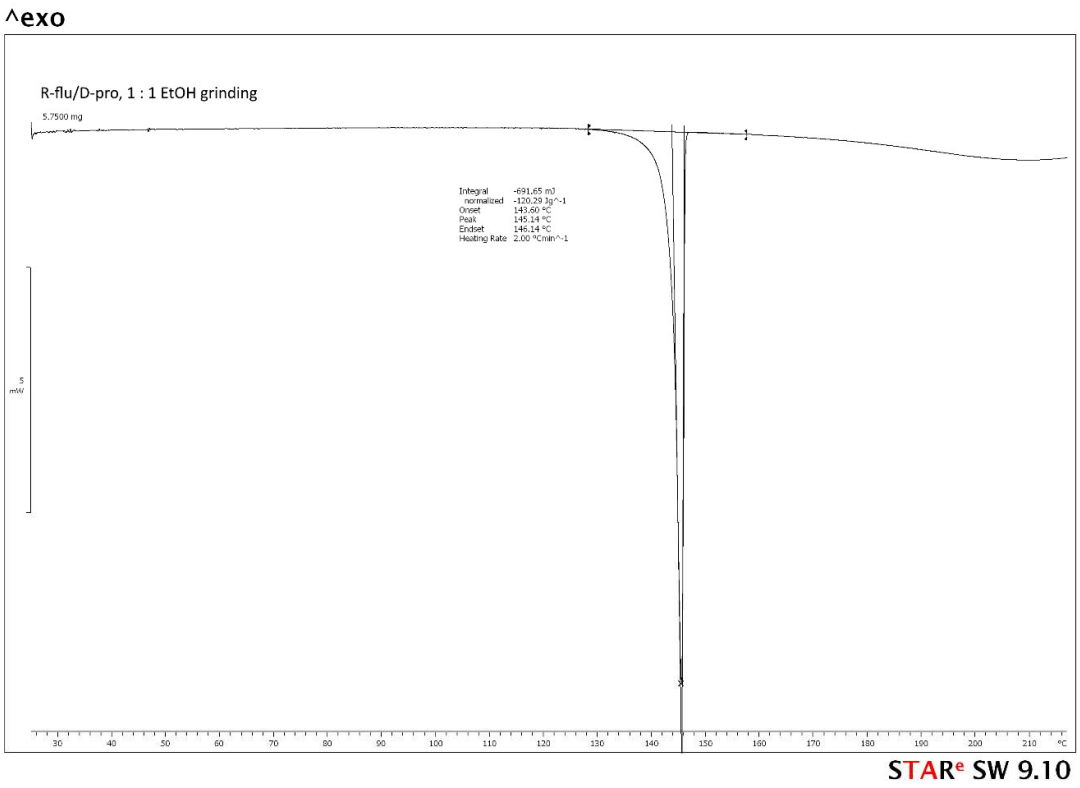


**Figure S10**. DSC curve for the R-flurbiprofen/D-proline sample prepared by ethanol-assisted grinding in 1 : 1 ratio (sample 7 in Table S4). The sample corresponds to the 1 : 1 R/D cocrystal.

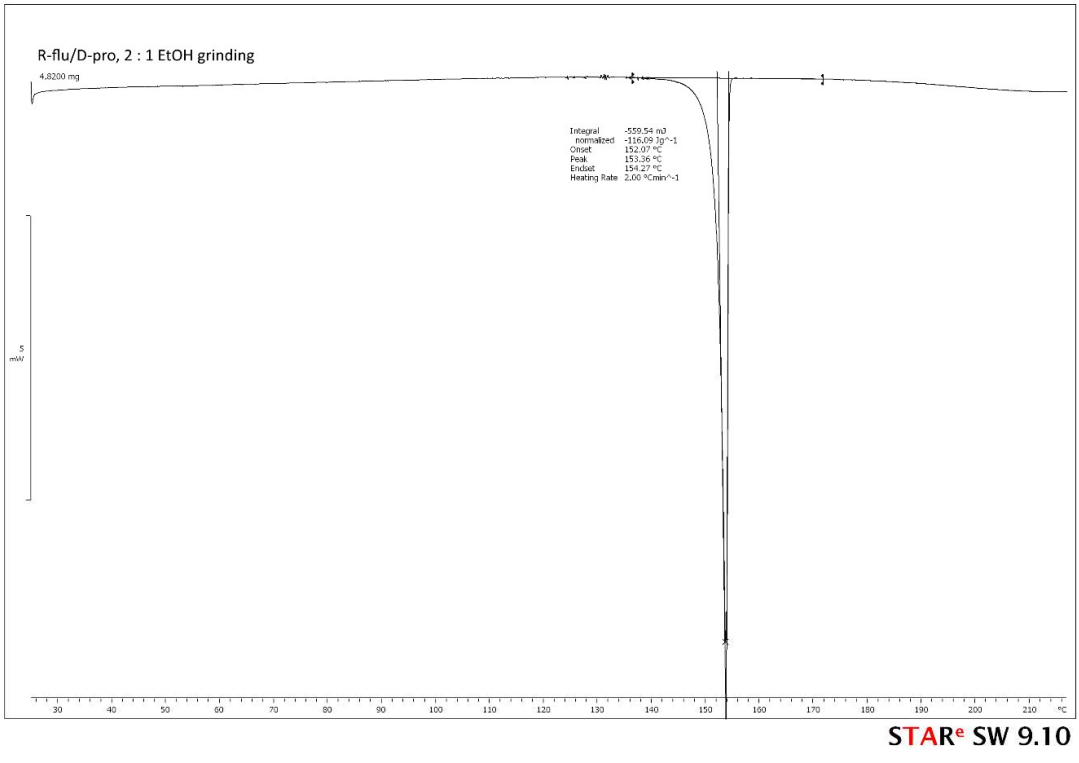


**Figure S11**. DSC curve for the R-flurbiprofen/D-proline sample prepared by ethanol-assisted grinding in 2 : 1 ratio (sample *8* in Table S4). The sample corresponds to the 2 : 1 R/D cocrystal.

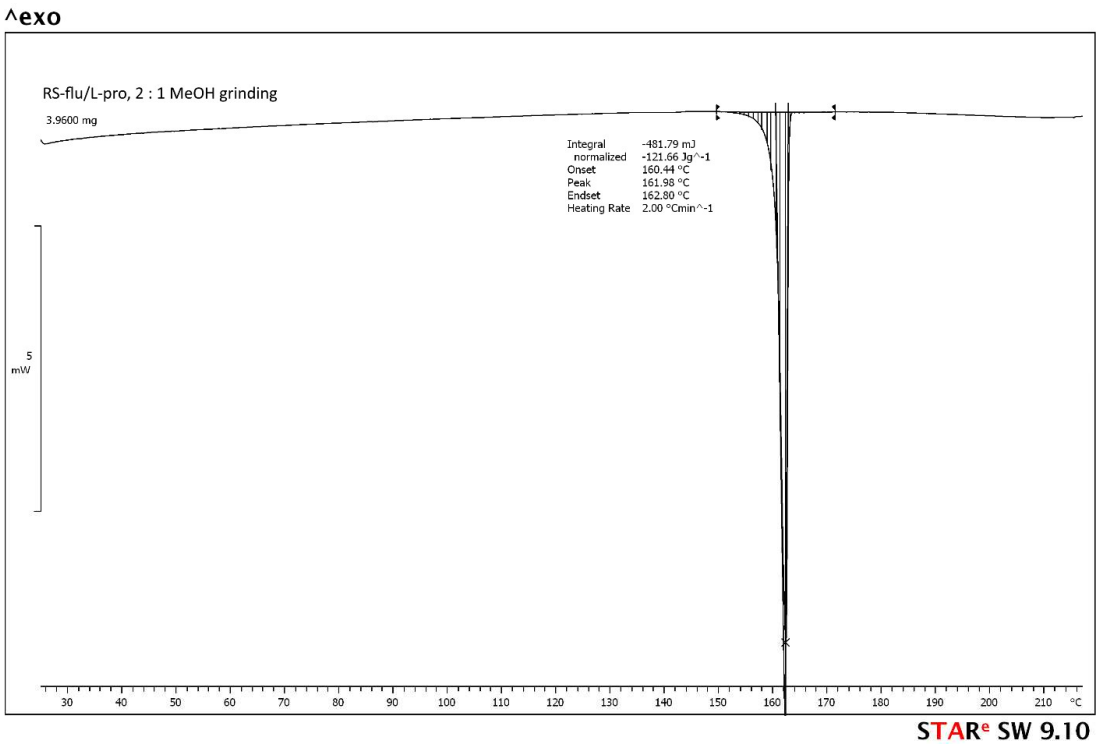


**Figure S12**. DSC curve for the RS-flurbiprofen/L-proline sample prepared by methanol-assisted grinding in 2 : 1 ratio (sample 2 in Table S7). The sample corresponds to the 2 : 1 RS/L cocrystal.

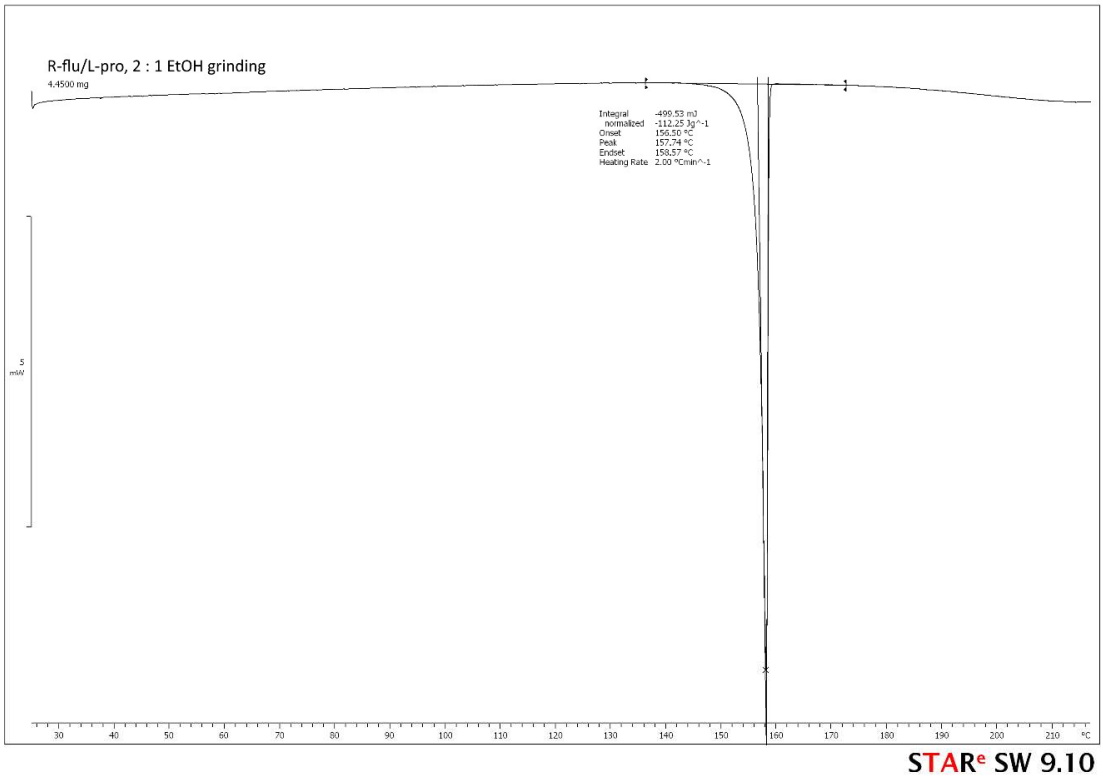


**Figure S13**. DSC curve for the R-flurbiprofen/L-proline sample prepared by ethanol-assisted grinding in 2 : 1 ratio (sample *8* in Table S3). The sample corresponds to the 2 : 1 R/L cocrystal.

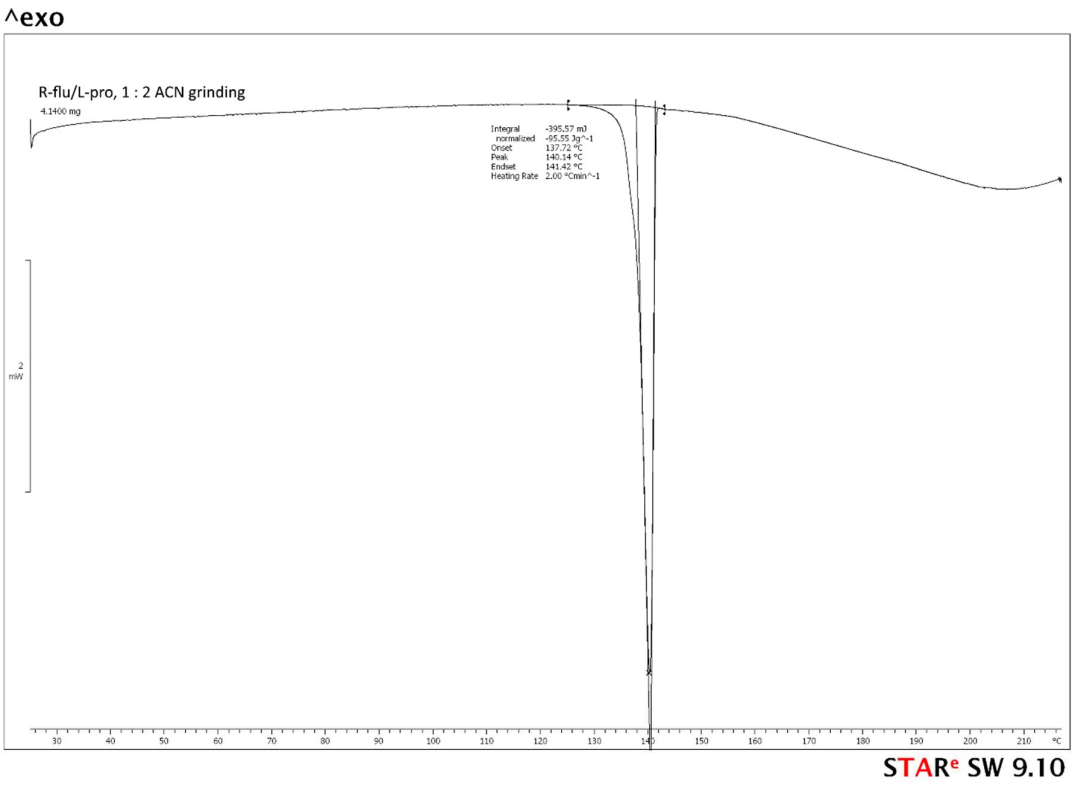


**Figure S14**. DSC curve for the R-flurbiprofen/L-proline sample prepared by acetonitrile-assisted grinding in 1 : 2 ratio (sample *14* in Table S3). The sample corresponds to the 1 : 2 R/L cocrystal.

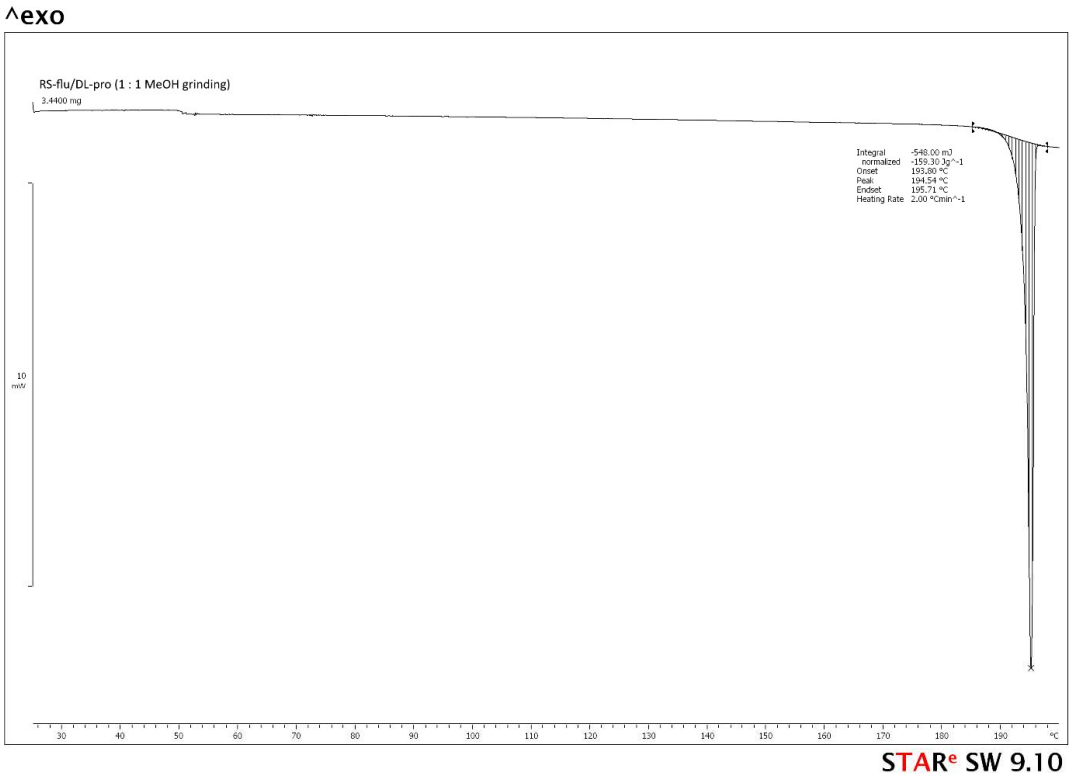


**Figure S15**. DSC curve for the RS-flurbiprofen/DL-proline sample prepared by methanol-assisted grinding in 1 : 1 ratio (sample *1* in Table S6). The sample corresponds to the 1 : 1 RS/DL cocrystal.

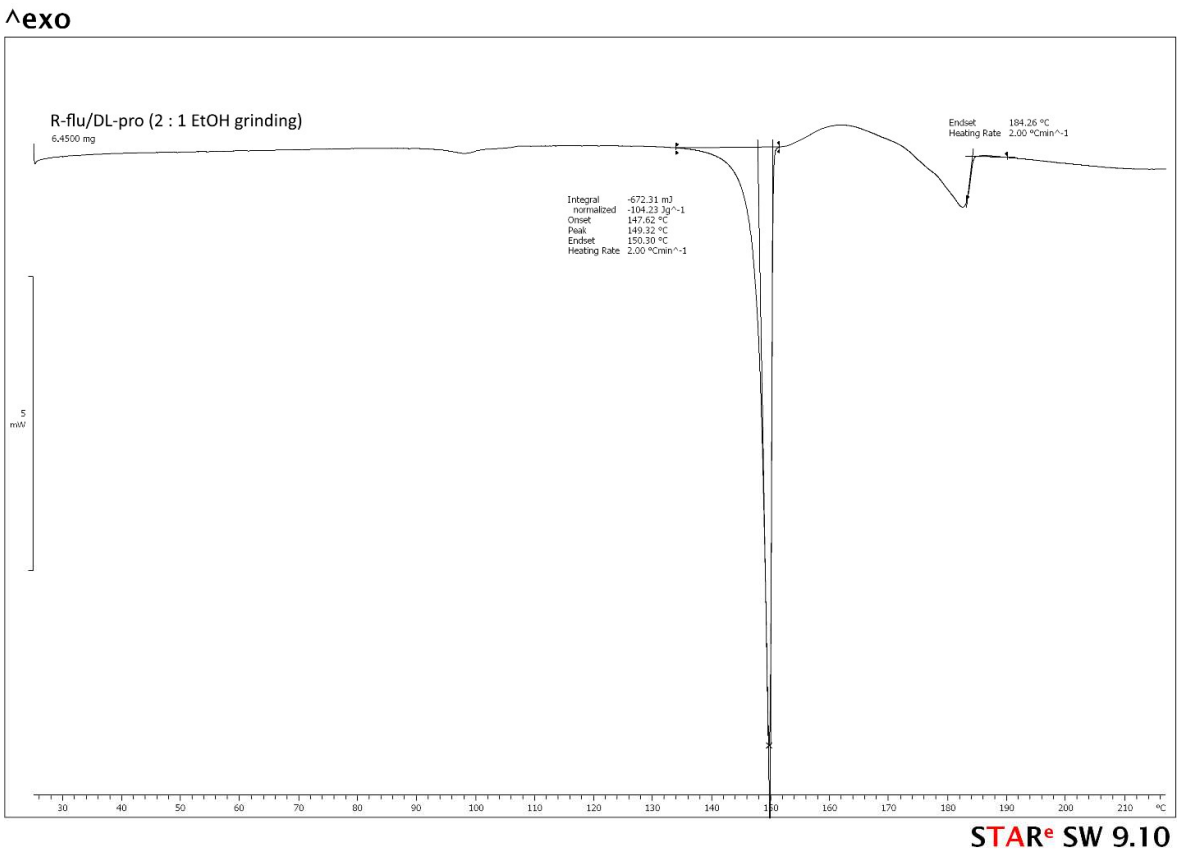


**Figure S16**. DSC curve for the R-flurbiprofen/DL-proline sample prepared by ethanol-assisted grinding in 2 : 1 ratio (sample *8* in Table S5). The sample corresponds to the 2 : 1 R/DL cocrystal. The sample contained a small amount of R-flurbiprofen, whose melting produces a small wide peak around 100°C. The peak around 180°C may correspond to the crystallization of DL-proline or another unknown event as we did not see any new phase formation during X-ray diffraction *in-situ* experiment upon heating.

**Figure S17**. DSC curve for the R-flurbiprofen/L-proline sample prepared by methanol-assisted grinding in 1 : 1 ratio (sample *1* in Table S3). When we did synchrotron measurements upon heating in a capillary we did not observe any phases after 160°C – powder melted completely. As mentioned in the main text of the article, events happening in a capillary may differ from those in a DSC capsule; this is probably why we did not observe any phases emerging after 160°C. However, the last peak may correspond to the crystallization of L-proline, as the latter has a high melting point and may emerge upon heating as we saw from X-ray *in-situ* data. A wide peak around 90°C corresponds to the evaporation of methanol.

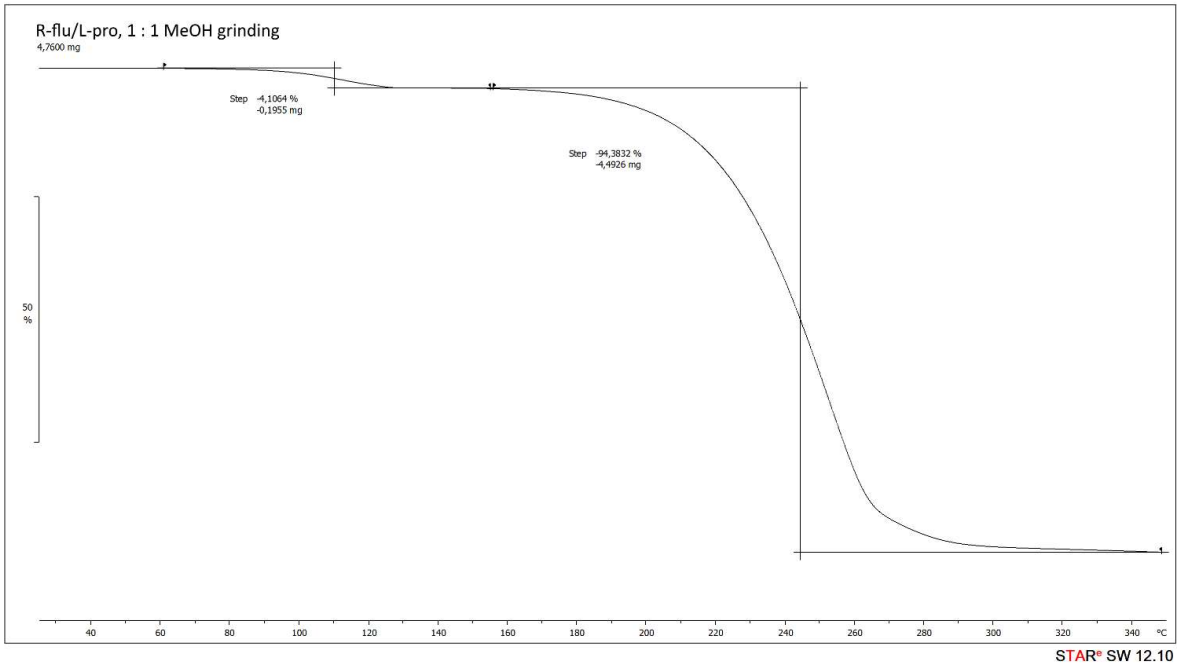


**Figure S18**. TG curve for the R-flurbiprofen/L-proline sample prepared by methanol-assisted grinding in 1 : 1 ratio (sample *1* in Table S3). A mass loss of 4% corresponds to the evaporation of methanol from the structure.

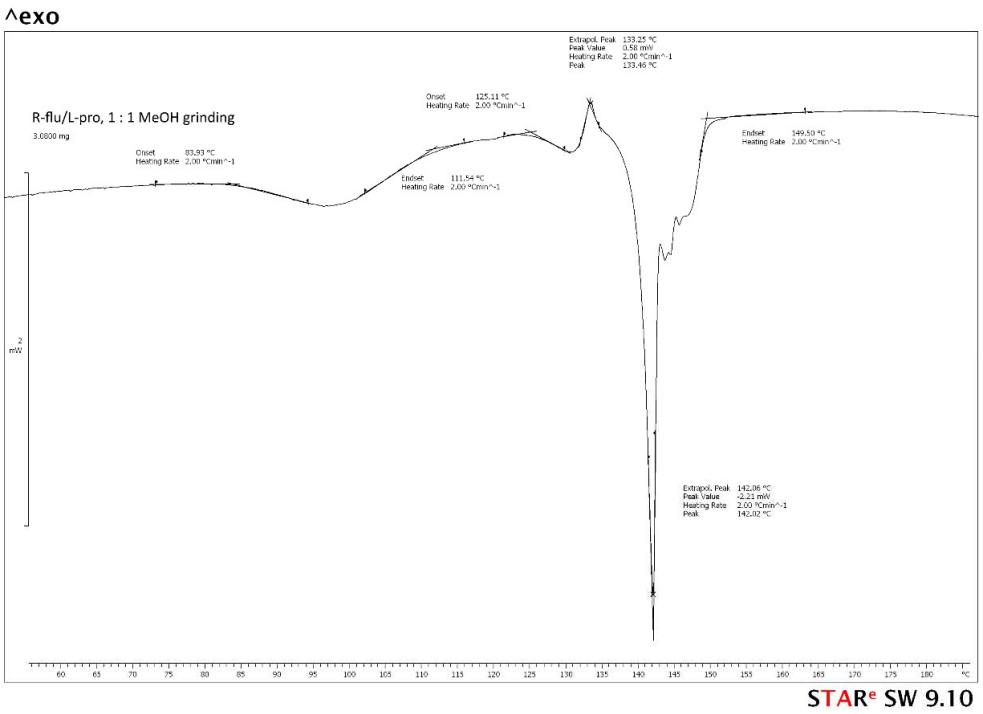


**Figure S19**. DSC curve for the R-flurbiprofen/L-proline sample prepared by methanol-assisted grinding in 1 : 1 ratio (sample *2* in Table S3). A wide peak around 90°C corresponds to the evaporation of methanol.

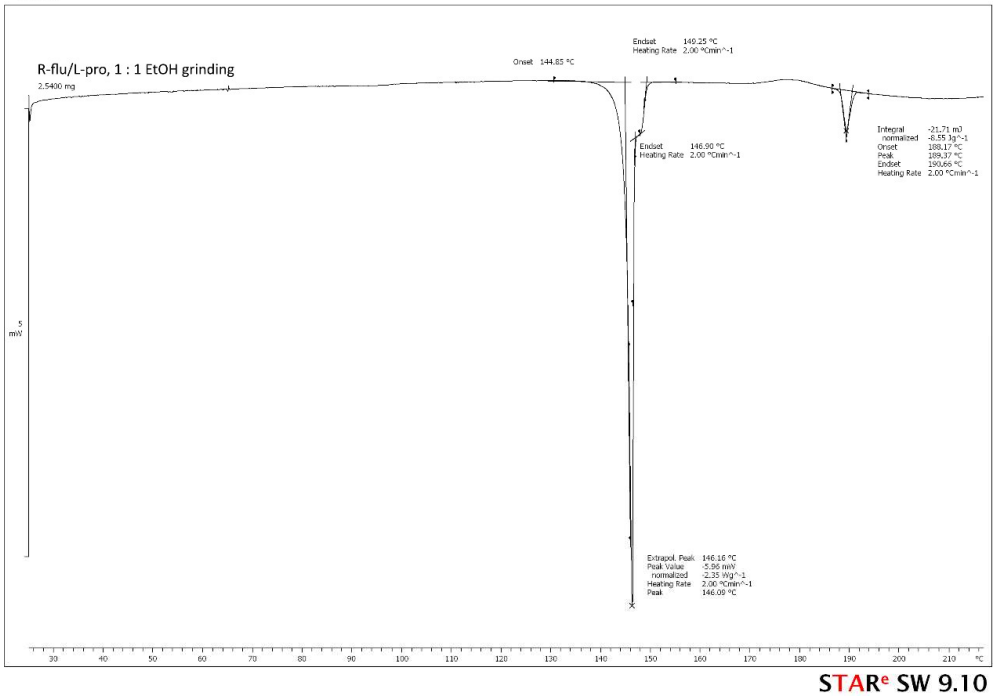


**Figure S20**. DSC curve for the R-flurbiprofen/L-proline sample prepared by ethanol-assisted grinding in 1 : 1 ratio (sample *6* in Table S3). When we did synchrotron measurements upon heating in a capillary we did not observe any phases after 160°C – powder melted completely. As mentioned in the main text of the article, events happening in a capillary may differ from those in a DSC capsule; this is probably why we did not observe any phases emerging after 160°C. However, the last peak may correspond to the crystallization of L-proline, as the latter has a high melting point and may emerge upon heating as we saw from X-ray *in-situ* data.

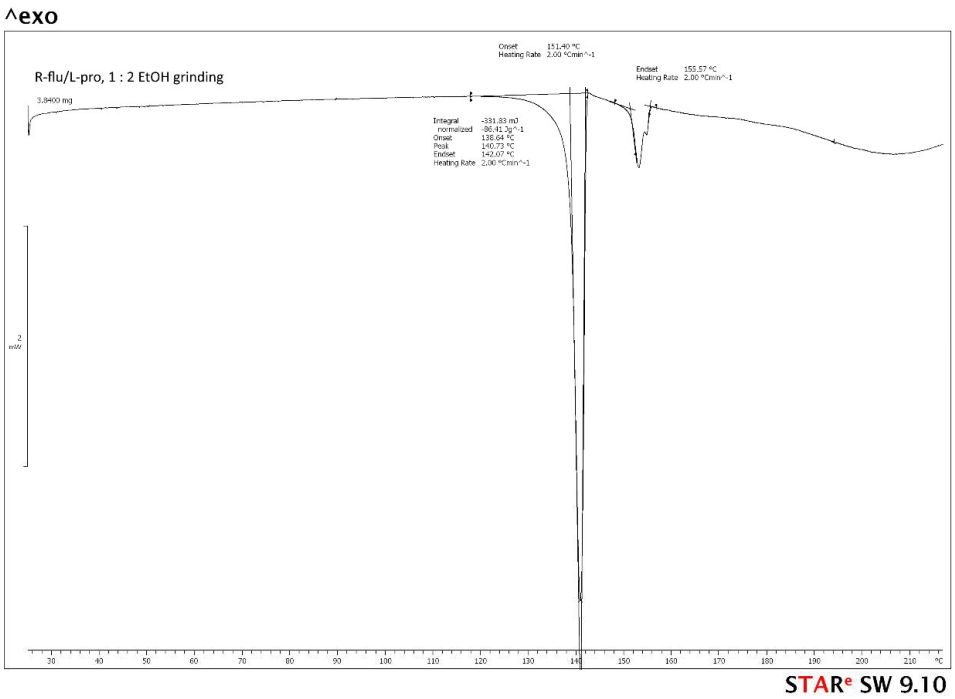


**Figure S21**. DSC curve for the R-flurbiprofen/L-proline sample prepared by ethanol-assisted grinding in 1 : 2 ratio (sample 9 in Table S3). The first peak corresponds to the melting of the 1 : 2 R/L and the second peak probably to the melting of L-proline pol II.

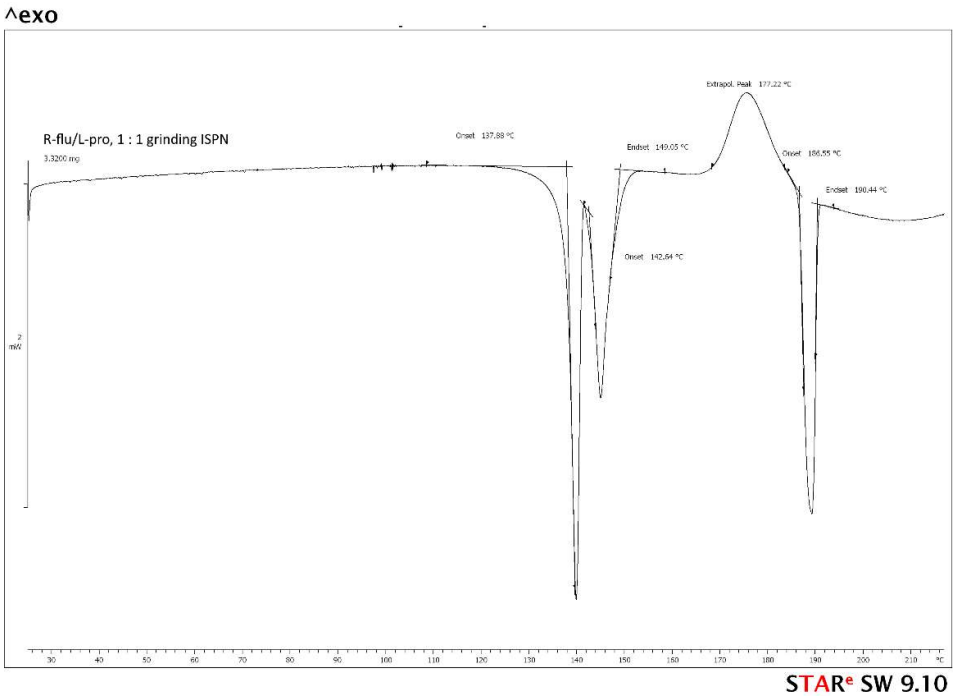


**Figure S22**. DSC curve for the R-flurbiprofen/L-proline sample prepared by isopropanol-assisted grinding in 1 : 1 ratio (sample *19* in Table S3). When we did synchrotron measurements upon heating in a capillary we did not observe any phases after 160°C – powder melted completely. As mentioned in the main text of the article, events happening in a capillary may differ from those in a DSC capsule; this is probably why we did not observe any phases emerging after 160°C. The first peak most likely corresponds to 1 : 2 R/L melting, the second one is probably the melting of 2 : 1 R/L. The last peak may correspond to the emergence and melting of L-proline.

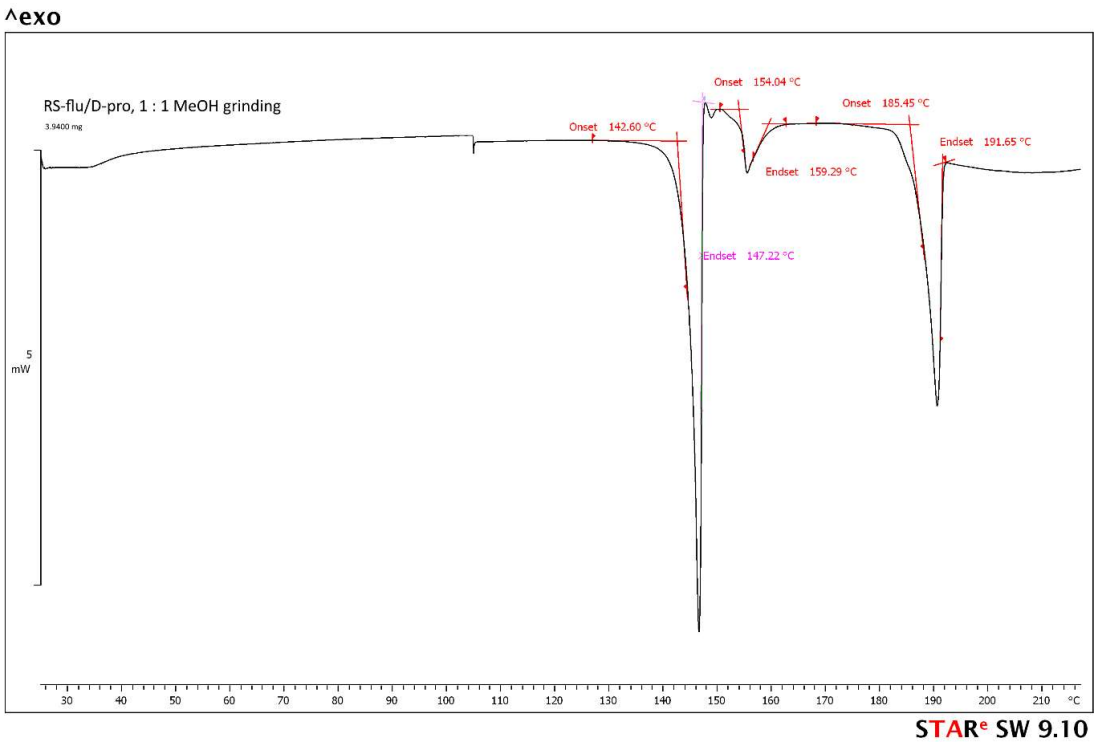


**Figure S23**. DSC curve for the RS-flurbiprofen/D-proline sample prepared by methanol-assisted grinding in 1 : 1 ratio (sample *1* in Table S8). Presumably the first peak corresponds to the melting of the 1 : 1 RS/D pol I, the second peak is the melting of the 2 : 1 impurity, and the last peak corresponds to the melting of the 1 : 1 RS/D pol III.

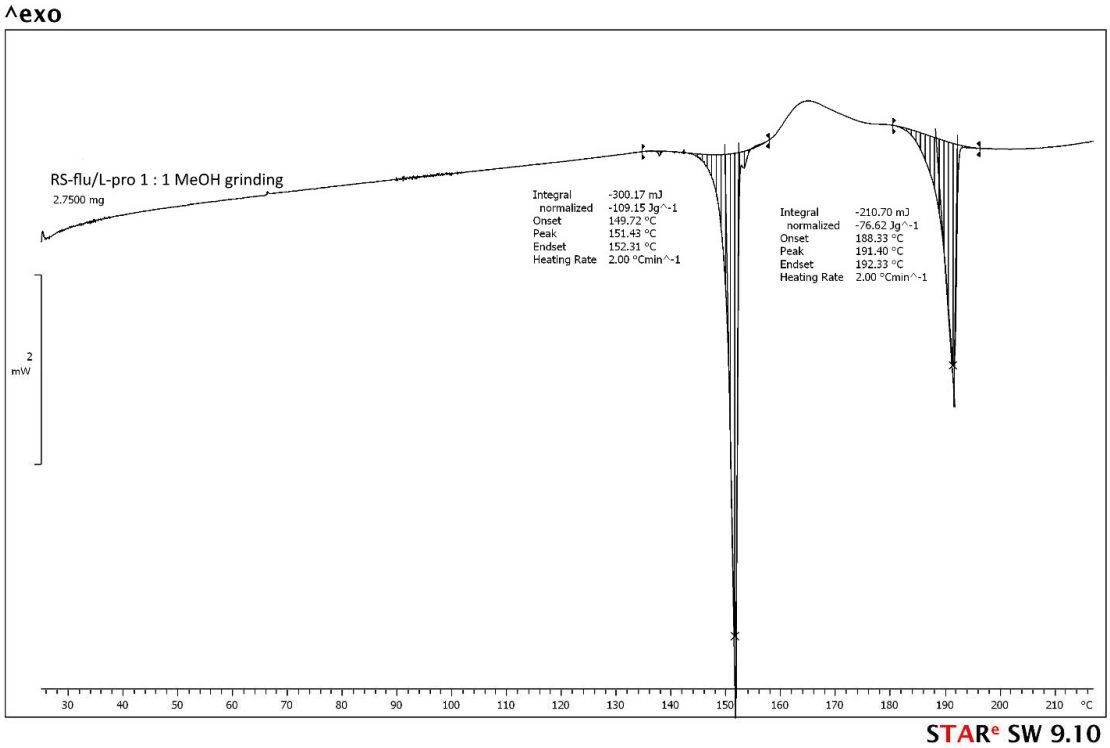


**Figure S24**. DSC curve for the RS-flurbiprofen/L-proline sample prepared by methanol-assisted grinding in 1 : 1 ratio (sample *1* in Table S7). Presumably the first peak corresponds to the melting of the 1 : 1 RS/L pol II and the 2 : 1 RS/L, and the second peak is probably the melting of the 1 : 1 RS/L pol III.

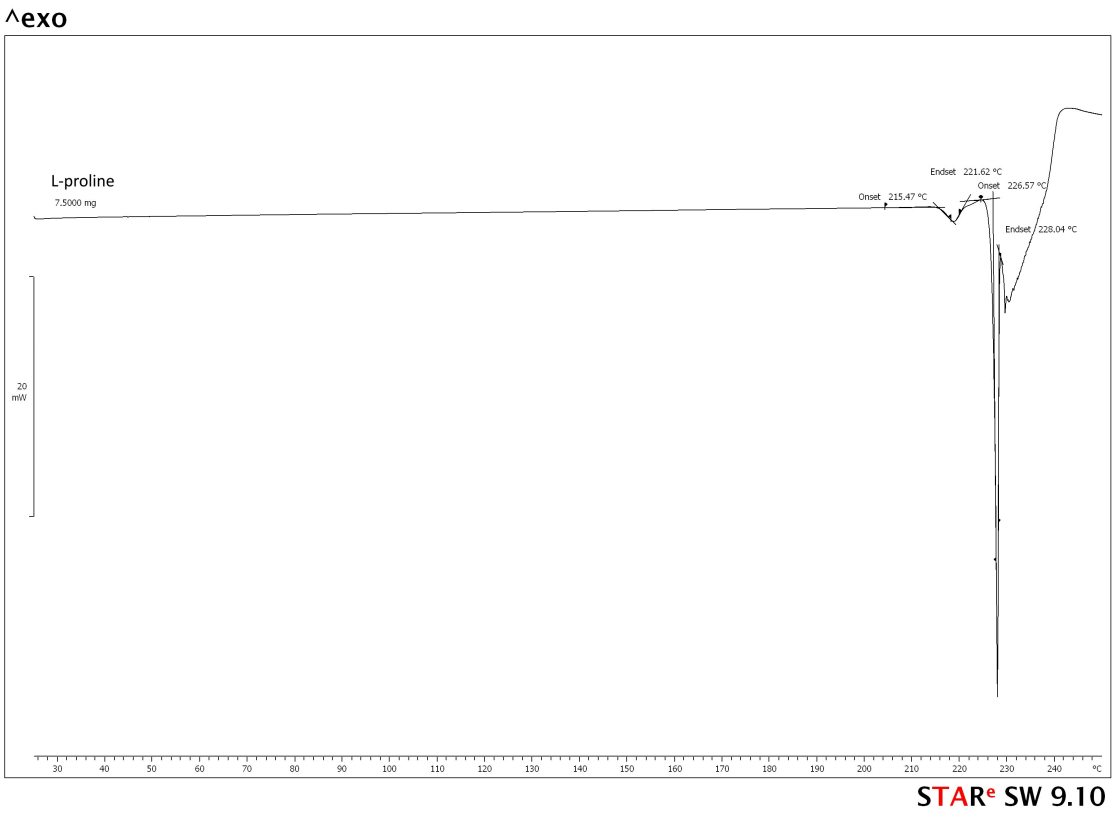


**Figure S25.** DSC curve for pure L-proline; melting is followed by degradation

**Figure S26.** DSC curve for pure DL-proline; melting is followed by degradation.

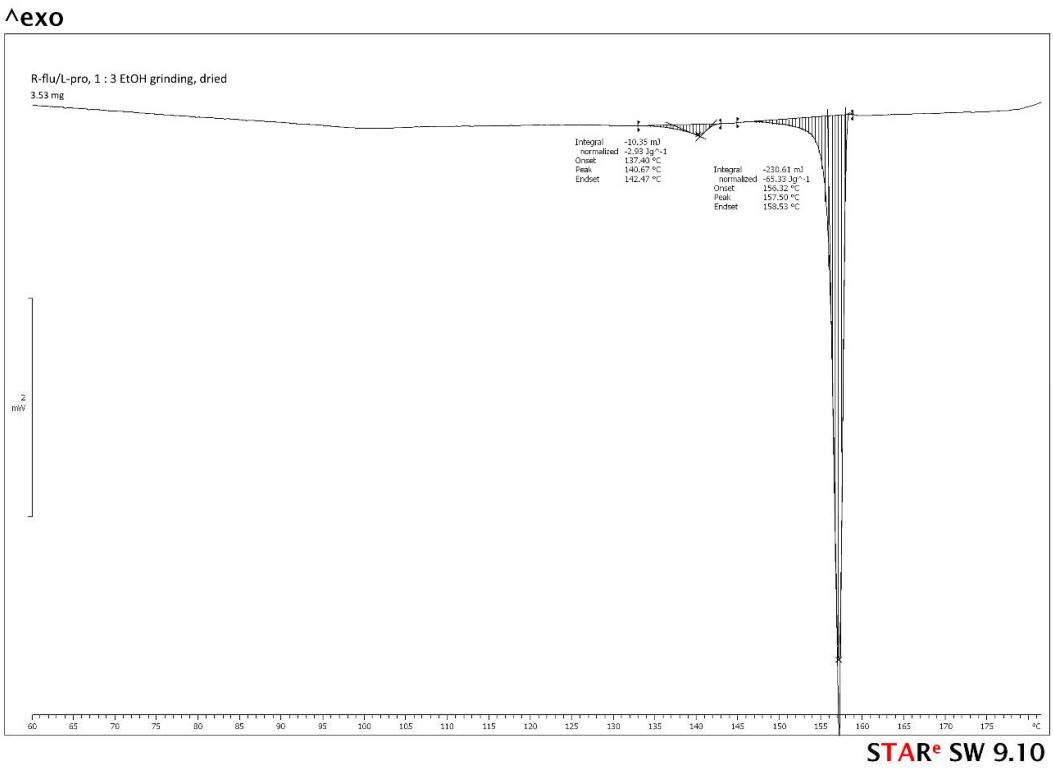


**Figure S27.** DSC curve for the R-flurbiprofen/L-proline sample prepared by ethanol-assisted grinding in 1 : 3 ratio and dried (sample *10* in Table S3). The major phase in the sample is 1 : 3 R/L cocrystal.

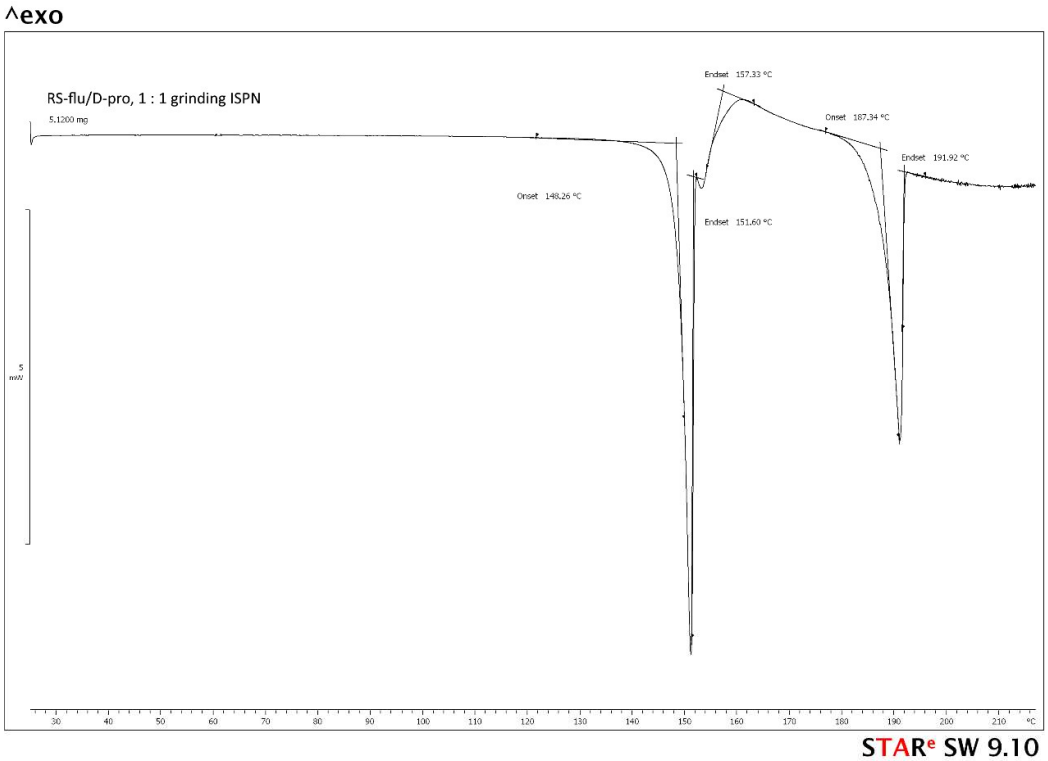


**Figure S28.** DSC curve for the RS-flurbiprofen/D-proline sample prepared by isopropanol-assisted grinding in 1 : 1 ratio (sample *10* in Table S3). The major phase in the sample is 1 : 1 RS/D pol II cocrystal, which disappears upon heating followed by crystallization of 1 : 1 RS/D pol III (whose melting correspond to the second peak).

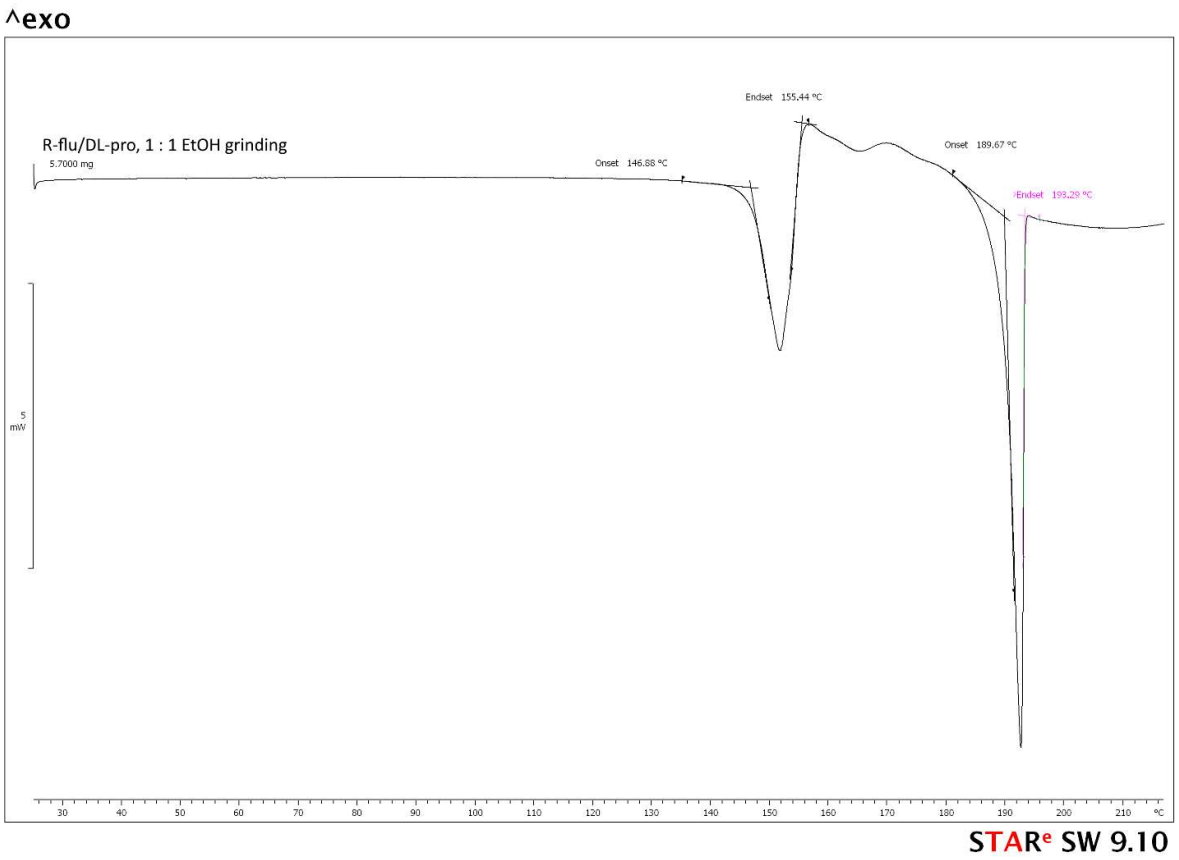


**Figure S29.** DSC curve for the R-flurbiprofen/DL-proline sample prepared by ethanol-assisted grinding in 1 : 1 ratio (sample *7* in Table S5). The sample corresponds to the 1 : 1 R/DL cocrystal. 1 : 1 R/DL cocrystal undergoes a phase crossover, which explains why the first peak is wide, see Discussion section for more details. The second peak may correspond to crystallization and melting of DL-proline, but we did not see it in *in-situ* X-ray diffraction experiment.

**STEP-BY-STEP GRINDING**

We discovered a stoichiometric diversity for flurbiprofen/proline system, and, as a preliminary step to *in-situ* ball-milling experiments, we performed step-by-step liquid-assisted grinding: first, we did grinding in the 2 : 1 ratio and, second, we added proline to the obtained samples. All the systems resulted in the same products as 1 : 1 grinding.

R-flurbiprofen/L-proline

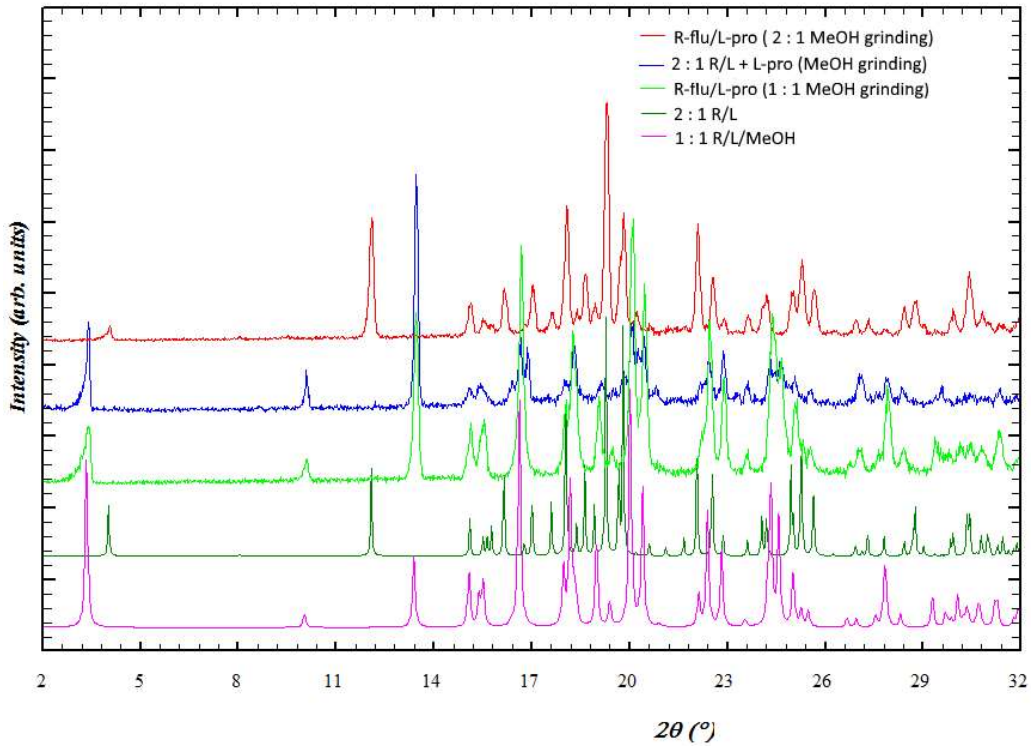


**Figure S30.** Methanol-assisted grinding:

At the first step, methanol-assisted grinding (for 25 min) results in the 2 : 1 R/L cocrystal; the second step (also for 25 min) (adding L-proline, 1 eq. of cocrystal + 1 eq. of L-proline) leads to the 1 : 1 R/L/MeOH cocrystal, which is the same product as from the grinding in the 1 : 1 ratio.

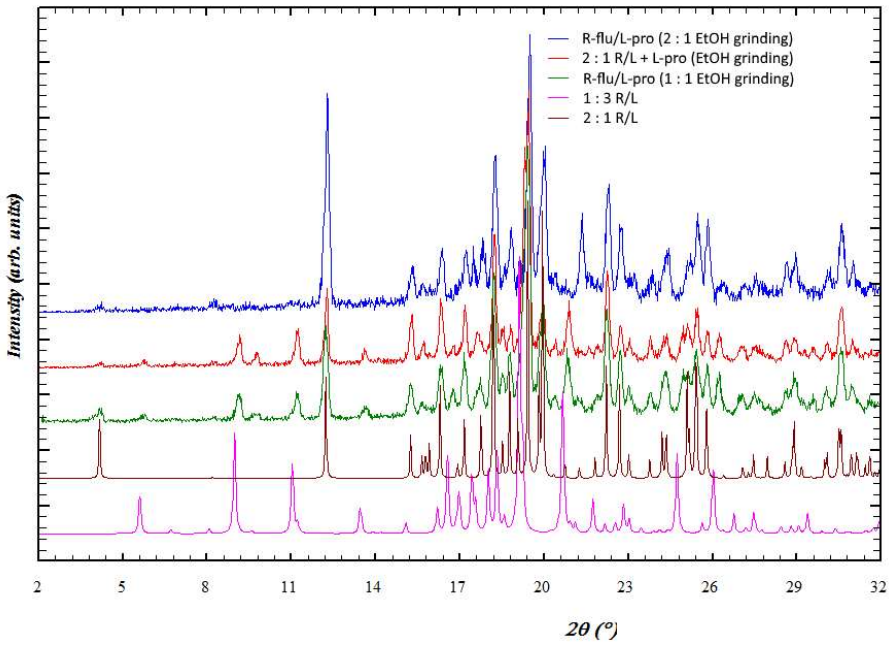


**Figure S31.** Ethanol-assisted grinding:

At the first step, ethanol-assisted grinding (for 25 min) results in the 2 : 1 R/L cocrystal; the second step (for 25 min) (adding L-proline, 1 eq. of cocrystal + 1 eq. of L-proline) leads to a mixture of 2 : 1 R/L and 1 : 3 R/L cocrystals, which is the same result as from the grinding in the 1 : 1 ratio.

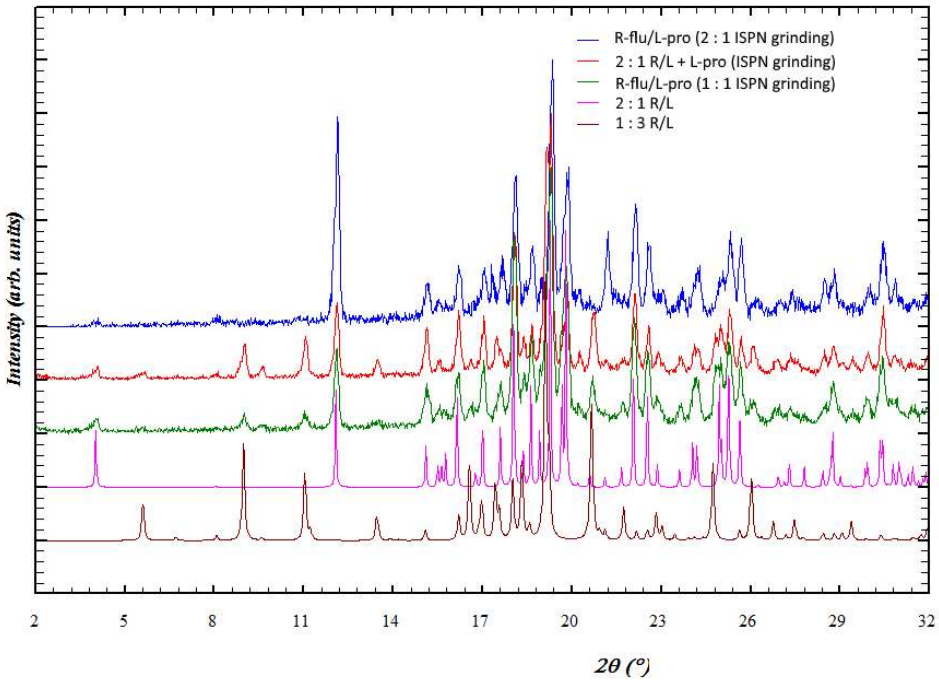


**Figure S32.** Isopropanol-assisted grinding:

At the first step, isopropanol-assisted grinding (for 25 min) results in the 2 : 1 R/L cocrystal; the second step (for 25 min) (adding L-proline, 1 eq. of cocrystal + 1 eq. of L-proline) leads to a mixture of 2 : 1 R/L and 1 : 3 R/L cocrystals, which is the same result as from the grinding in the 1 : 1 ratio.

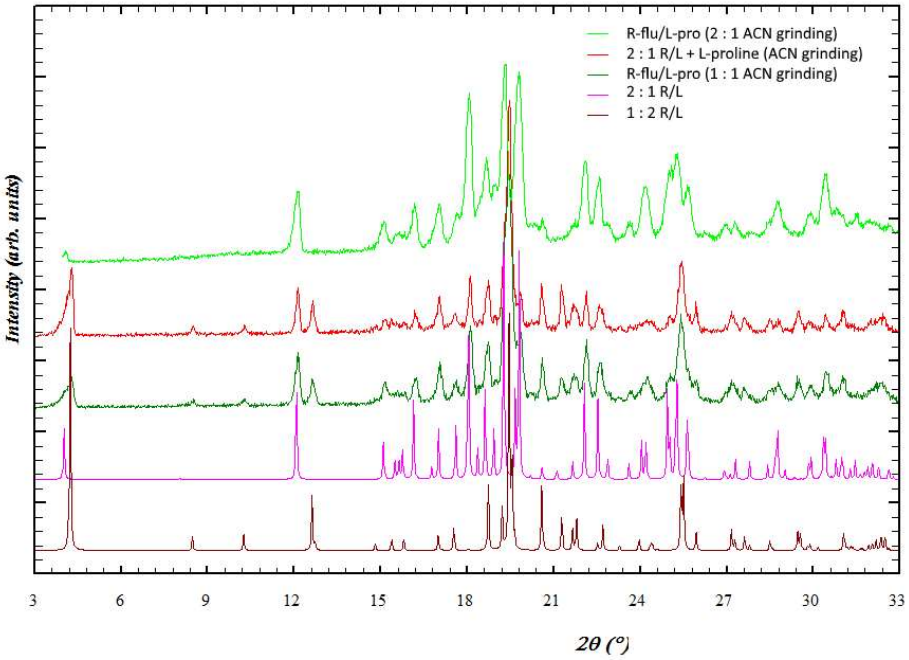


**Figure S33.** Acetonitrile-assisted grinding:

At the first step, acetonitrile-assisted grinding (for 60 min) results in the 2 : 1 R/L cocrystal; the second step (for 25 min) (adding L-proline, 1 eq. of cocrystal + 1 eq. of L-proline) leads to a mixture of 2 : 1 R/L and 1 : 2 R/L cocrystals, which is the same result as from the grinding in the 1 : 1 ratio.

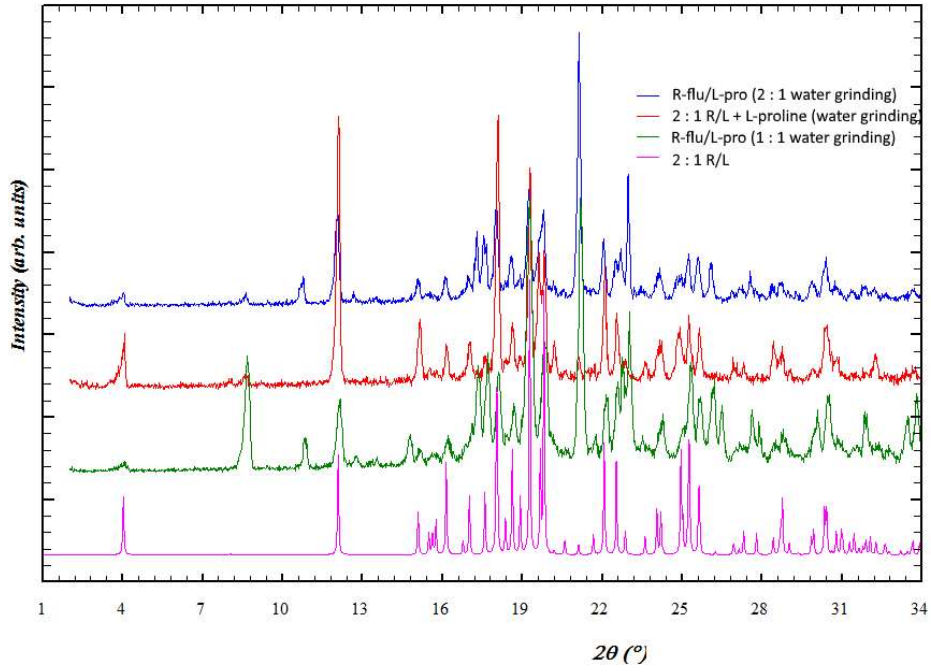


**Figure S34.** Water-assisted grinding:

At the first step, water-assisted grinding (for 25 min) results in the 2 : 1 R/L cocrystal + some non-reacted material as impurities; the second step (for 25 min) (adding L-proline, 1 eq. of cocrystal + 1 eq. of L-proline) does not lead to the formation of any other cocrystal phases: reaction stops at the 2 : 1 R/L, which is in agreement with the 1 : 1 grinding reaction.

R-flurbiprofen/D-proline

At the first step, methanol-assisted grinding (for 60 min) results in the 2 : 1 R/D cocrystal; the second step (for 60 min) (adding D-proline, 1 eq. of cocrystal + 1 eq. of D-proline) leads to the 1 : 1 R/D cocrystal, which is the same product as from the grinding in the 1 : 1 ratio. The same behavior is observed for other solvents except water, when the reaction stops at the 2 : 1 R/D phase. Diffraction patterns for the water- and methanol-assisted grinding are presented below.

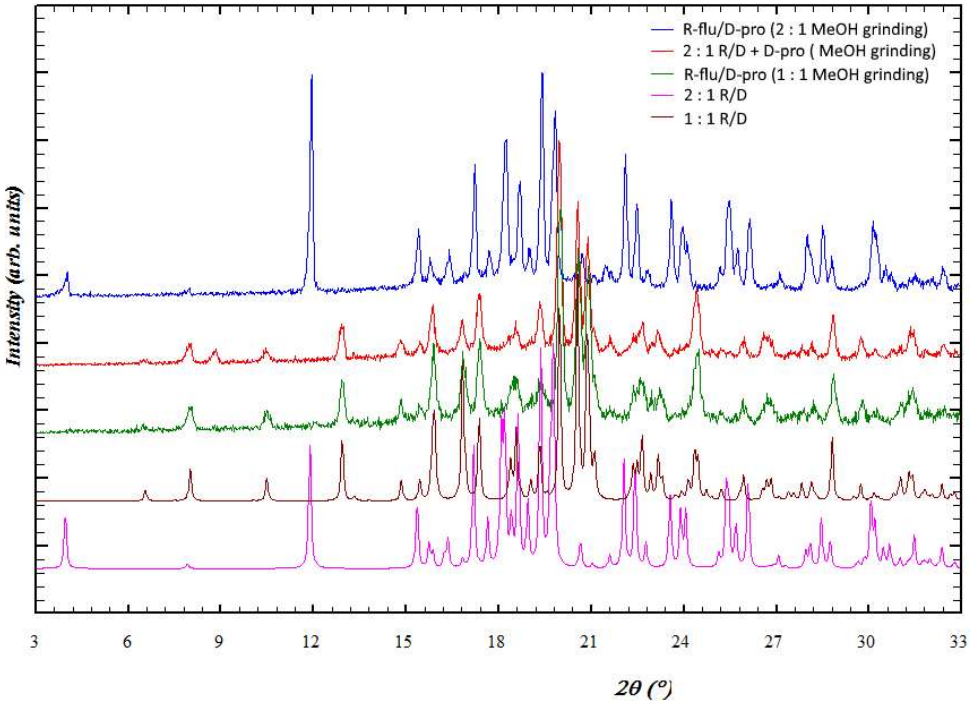


**Figure S35.** Diffraction patterns for the R-flurbiprofen/D-proline samples prepared by methanol-assisted grinding

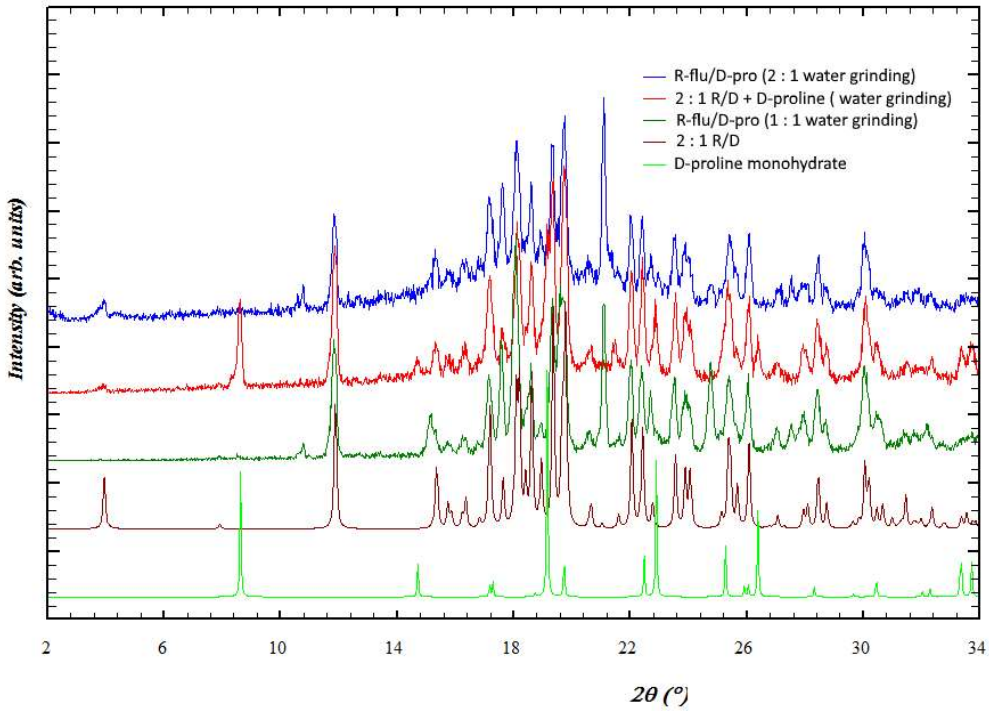


**Figure S36.** Diffraction patterns for the R-flurbiprofen/D-proline samples prepared by water-assisted grinding

R-flurbiprofen/DL-proline

At the first step methanol-assisted grinding (for 60 min) results in the 2 : 1 R/DL cocrystal; the second step (for 60 min) (adding DL-proline, 1 eq. of cocrystal + 1 eq. of DL-proline) leads to the 1 : 1 R/DL cocrystal, which is the same product as from the grinding in the 1 : 1 ratio. The same is observed for other solvents except water, when the reaction stops at the 2 : 1 R/DL phase. Diffraction patterns for the water- and methanol-assisted grinding are presented below.

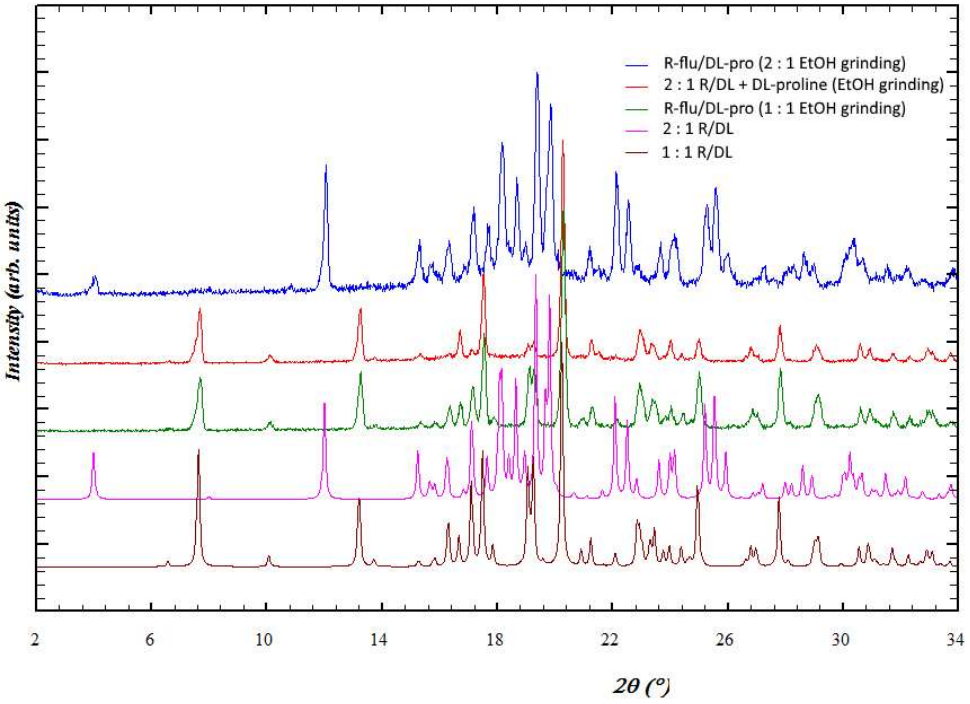


**Figure S37.** Diffraction patterns for the R-flurbiprofen/DL-proline samples prepared by ethanol-assisted grinding

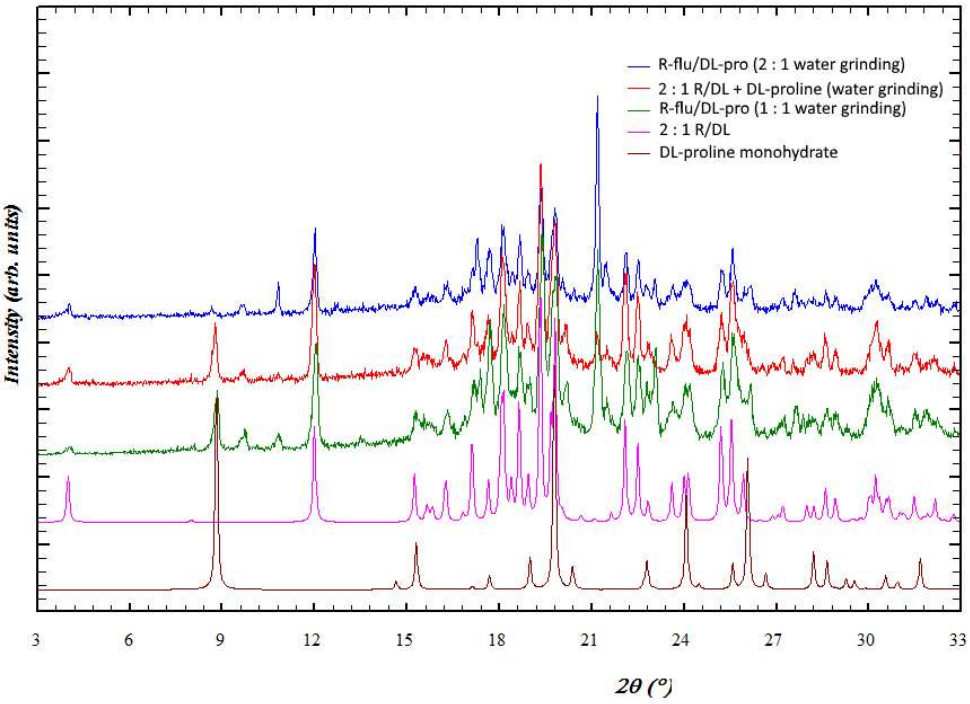


**Figure S38.** Diffraction patterns for the R-flurbiprofen/D-proline samples prepared by water-assisted grinding

RS-flurbiprofen/L-proline

In the case of RS-flurbiprofen/L-proline system, we observed full conversion into the 1 : 1 RS/L pol phase after the second step only in the case of methanol- and ethanol-assisted reactions; this is in agreement with the *in-situ* data, which show that reaction rate strongly depends on the solvent used: 1 : 1 ratio grinding in the presence of some solvents stops at the 2 : 1 phase. Diffraction patterns for methanol-, ethanol-, isopropanol-, and water-assisted reactions are presented below (both steps of grinding were performed for 60 min). The patterns are compared to the simulated ones as well as to those obtained by 1 : 1 grinding.

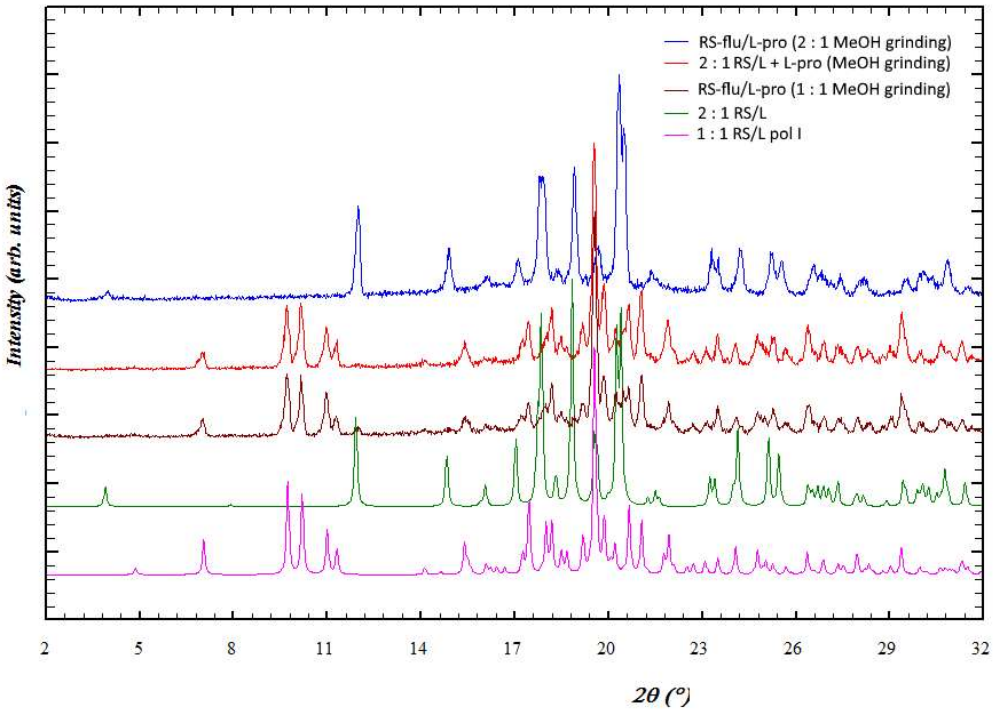


**Figure S39.** Diffraction patterns for the RS-flurbiprofen/L-proline samples prepared by methanol-assisted grinding. At the first step, 2 : 1 RS/L emerges, which after the second step transforms into the 1 : 1 RS/L pol I.

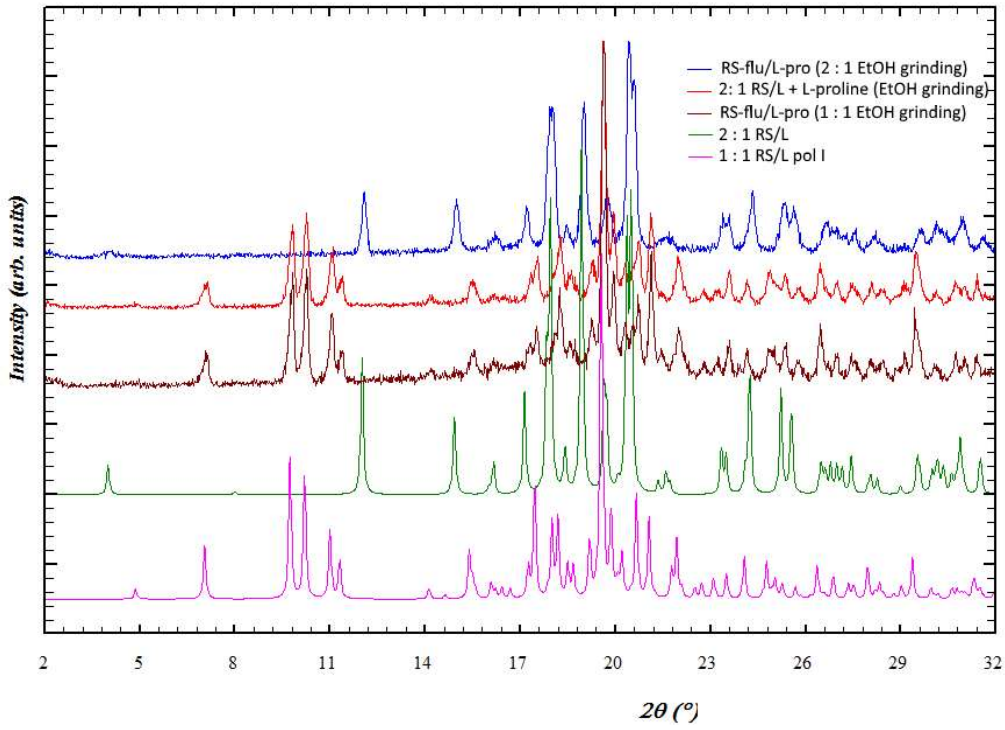


**Figure S40.** Diffraction patterns for the RS-flurbiprofen/L-proline samples prepared by ethanol-assisted grinding. At the first step, 2 : 1 RS/L emerges, which after the second step transforms into the 1 : 1 RS/L pol I.

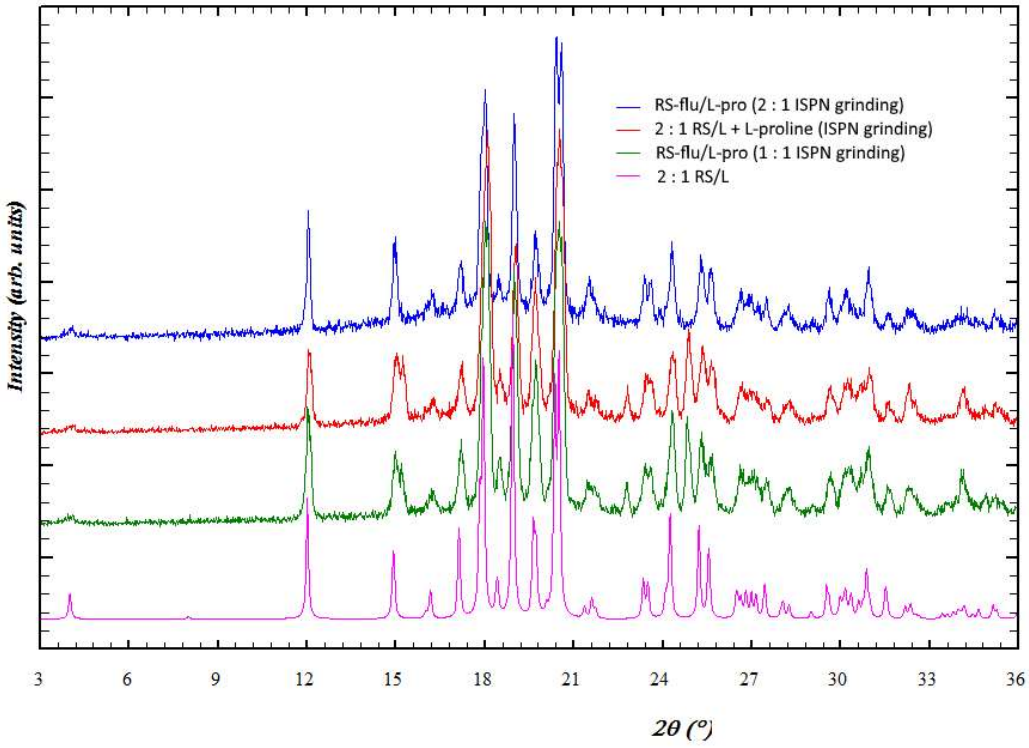


**Figure S41.** Diffraction patterns for the RS-flurbiprofen/L-proline samples prepared by isopropanol-assisted grinding. At the first step, 2 : 1 RS/L emerges and does not convert into the 1 : 1 phase after the second step grinding.

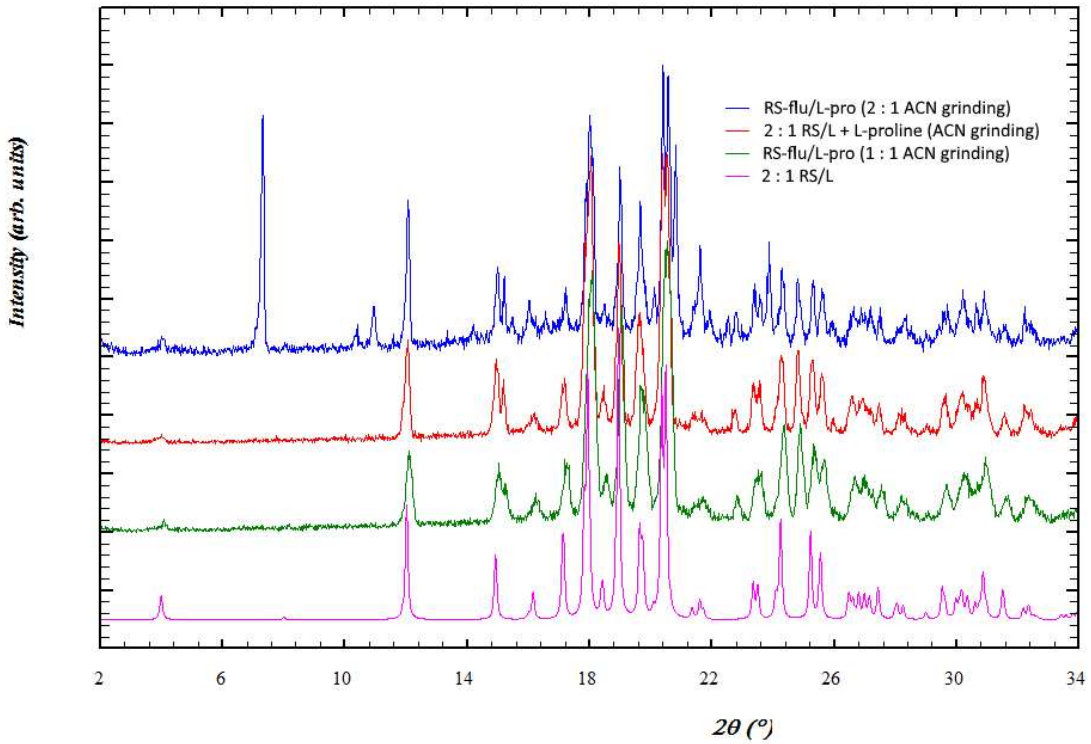


**Figure S42.** Diffraction patterns for the RS-flurbiprofen/L-proline samples prepared by acetonitrile-assisted grinding. At the first step, 2 : 1 RS/L emerges and the sample contains non-reacted RS-flurbiprofen. After the second step, the 2 : 1 form persists.

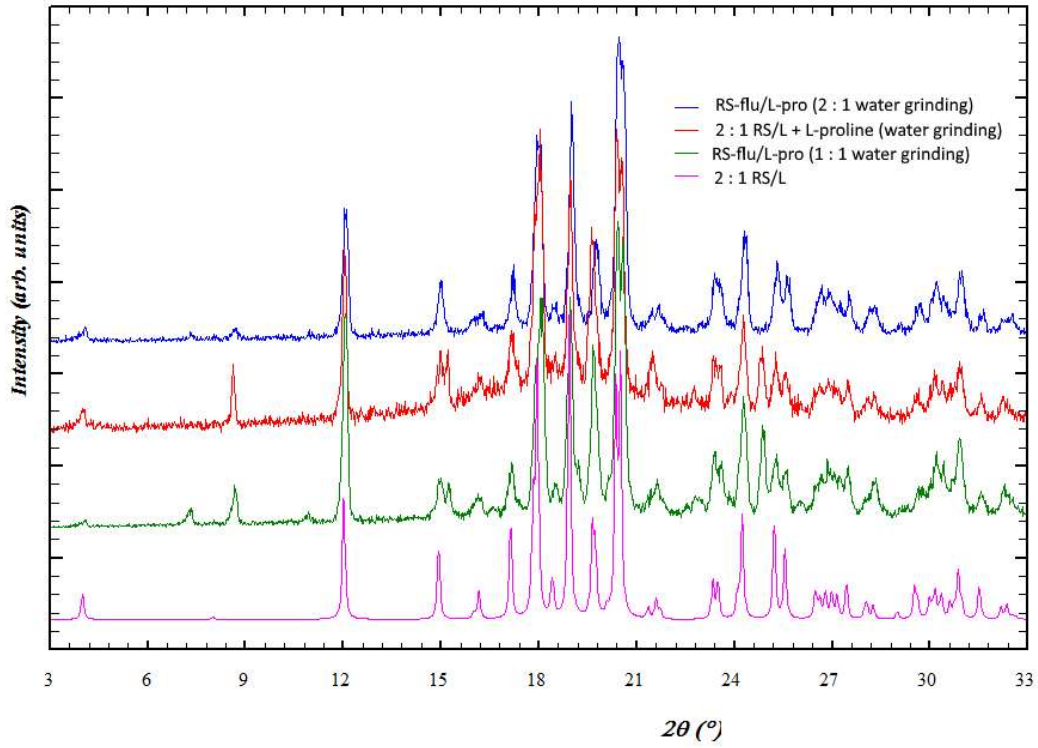


**Figure S43.** Diffraction patterns for the RS-flurbiprofen/L-proline samples prepared by water-assisted grinding. At the first step, 2 : 1 RS/L emerges. After the second step, the 2 : 1 form persists.

RS-flurbiprofen/D-proline

RS-flurbiprofen/D-proline system behaves similarly to the RS-flurbiprofen/L-proline. As example, diffraction patterns for the methanol and isopropanol-assisted reactions are presented below.

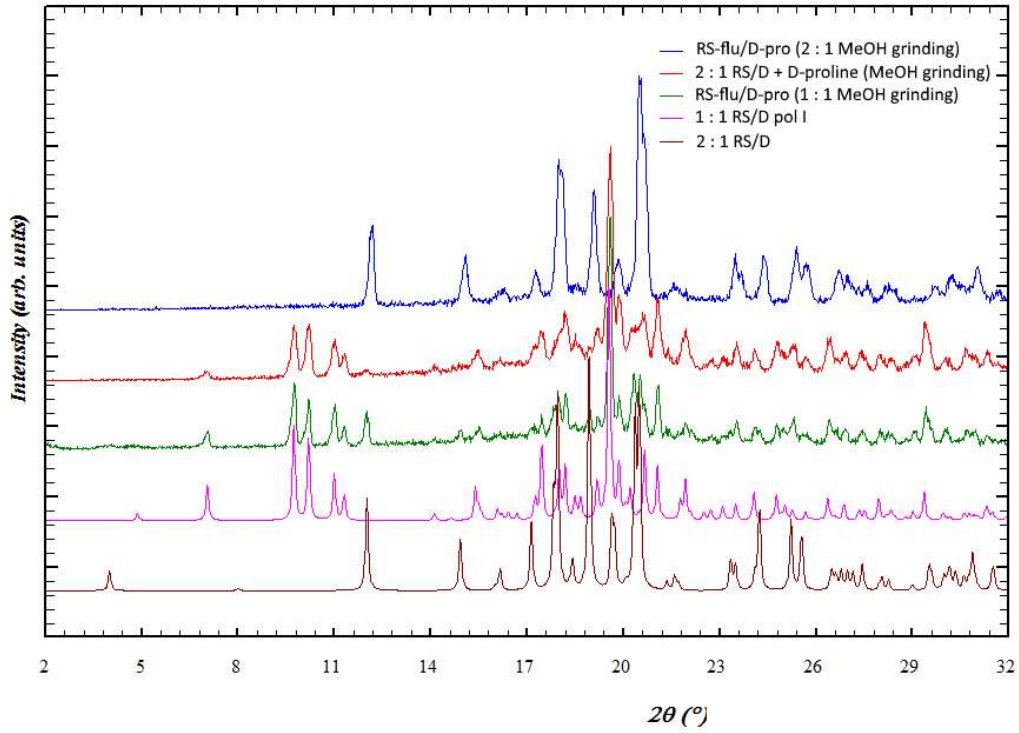


**Figure S44.** Diffraction patterns for the RS-flurbiprofen/D-proline samples prepared by methanol-assisted grinding

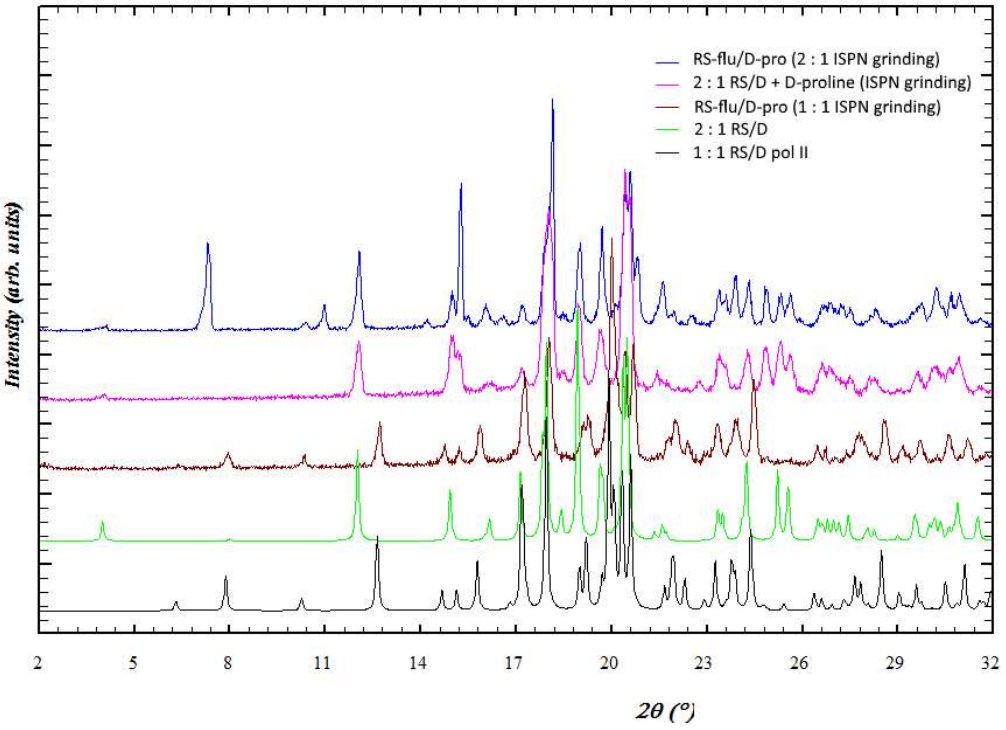


**Figure S45.** Diffraction patterns for the RS-flurbiprofen/D-proline samples prepared by isopropanol-assisted grinding

RS-flurbiprofen/DL-proline

RS-flurbiprofen/DL-proline system exhibits a specific behavior not observed in other systems. Grinding in the presence of ethanol, isopropanol, acetonitrile or water in the 2 : 1 ratio results in a conglomerate (2 : 1 RS/L + 2 : 1 RS/D cocrystals), which upon the second step grinding with an additional amount of DL-proline leads to the 1 : 1 RS/DL cocrystal. However, 2 : 1 methanol-assisted grinding results directly in 1 : 1 RS/DL (the sample contains non-reacted RS-flurbiprofen) without showing conglomerate formation. Each grinding step was performed for 90 min.

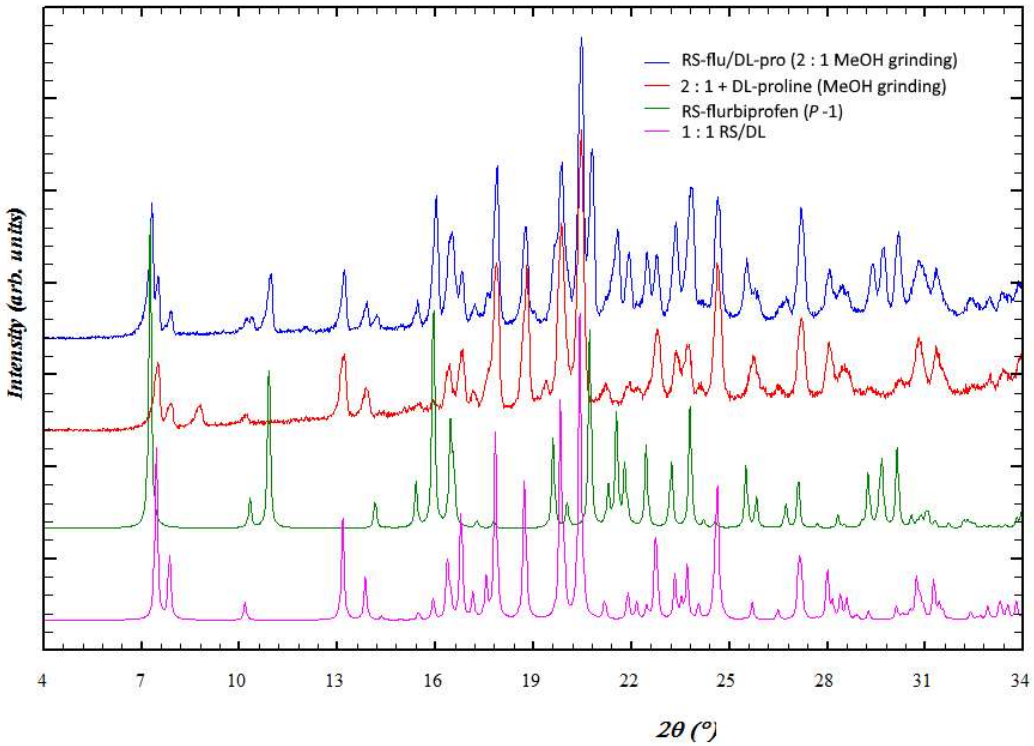


**Figure S46.** Diffraction patterns for the RS-flurbiprofen/DL-proline samples prepared by methanol-assisted grinding

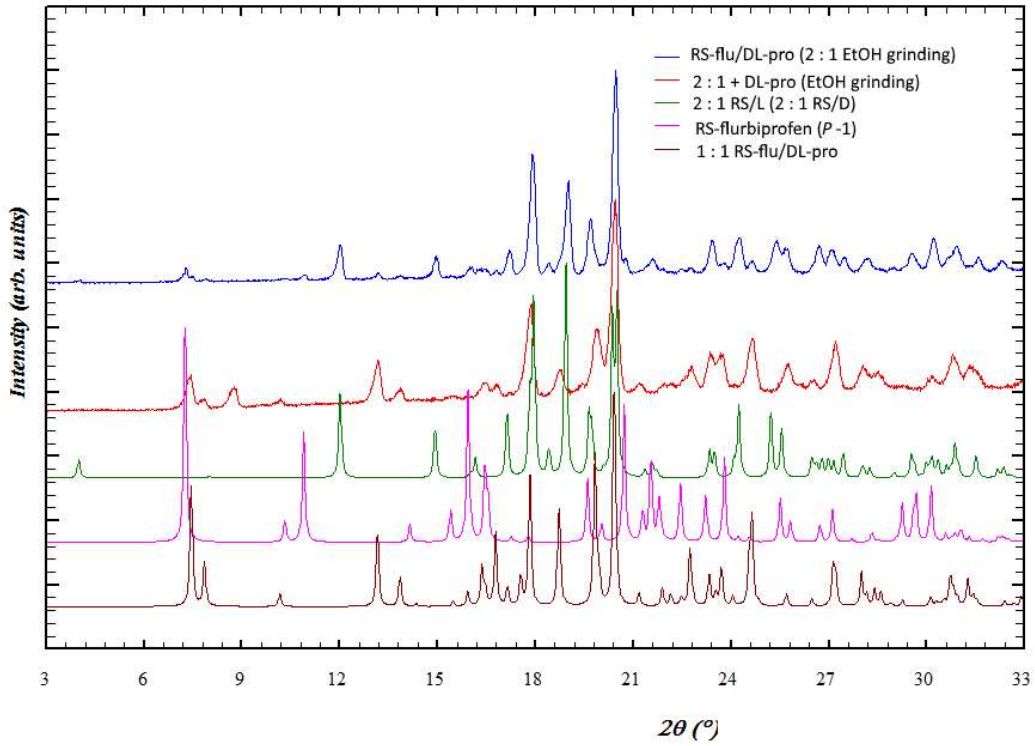


**Figure S47.** Diffraction patterns for the RS-flurbiprofen/DL-proline samples prepared by ethanol-assisted grinding

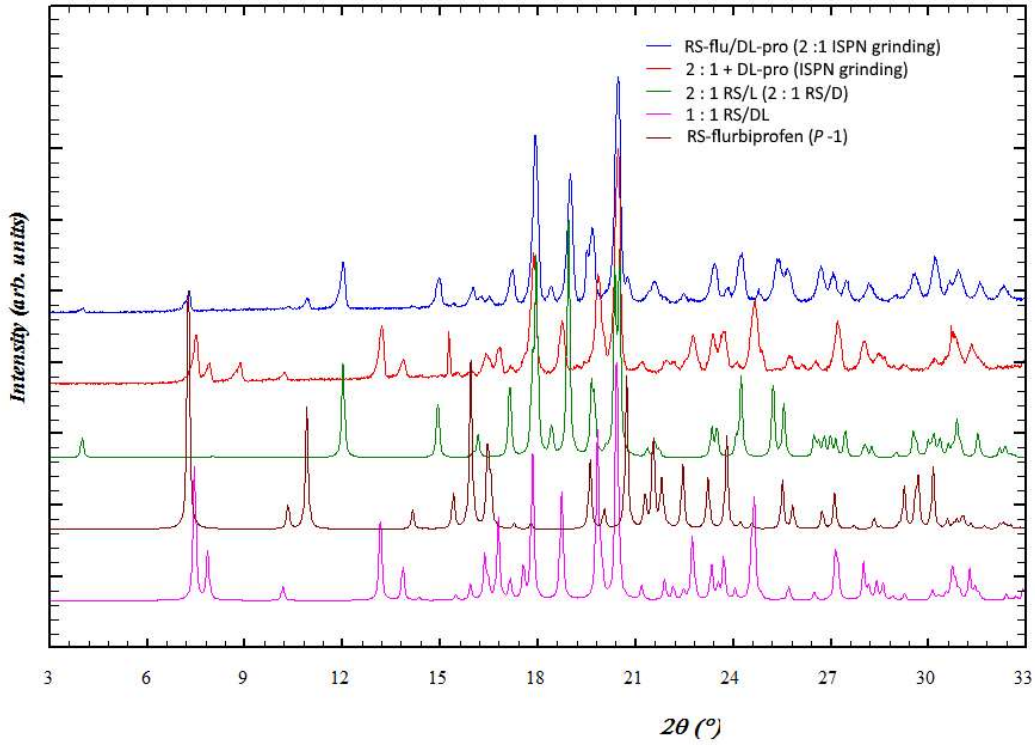


**Figure S48.** Diffraction patterns for the RS-flurbiprofen/DL-proline samples prepared by isopropanol-assisted grinding

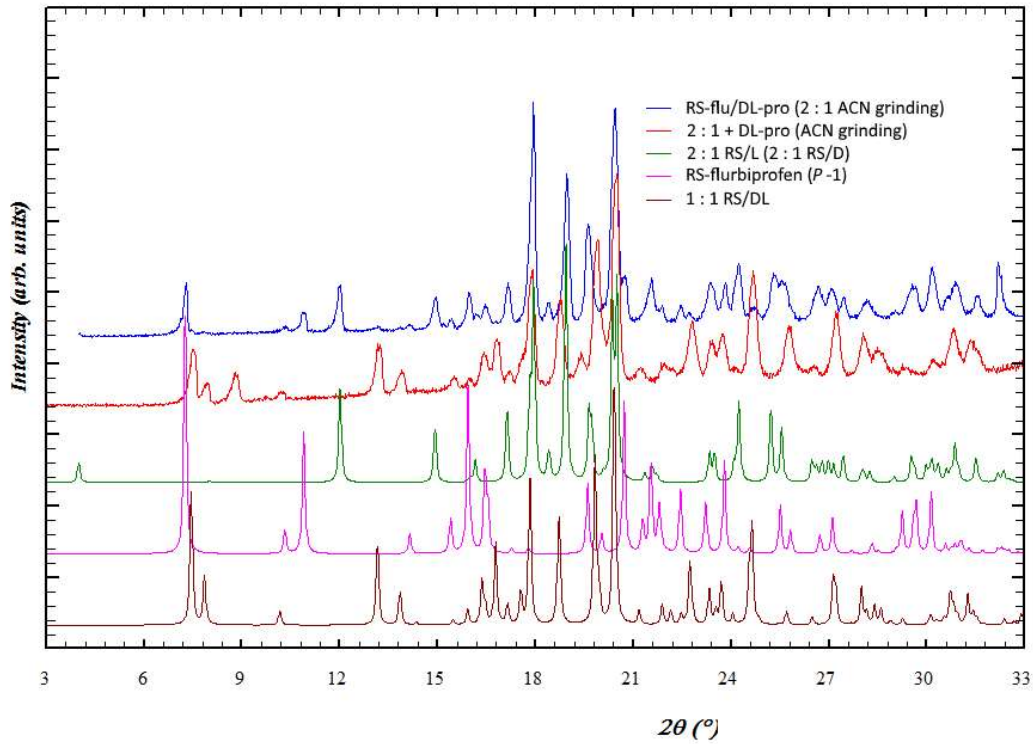


**Figure S49.** Diffraction patterns for the RS-flurbiprofen/DL-proline samples prepared by acetonitrile-assisted grinding

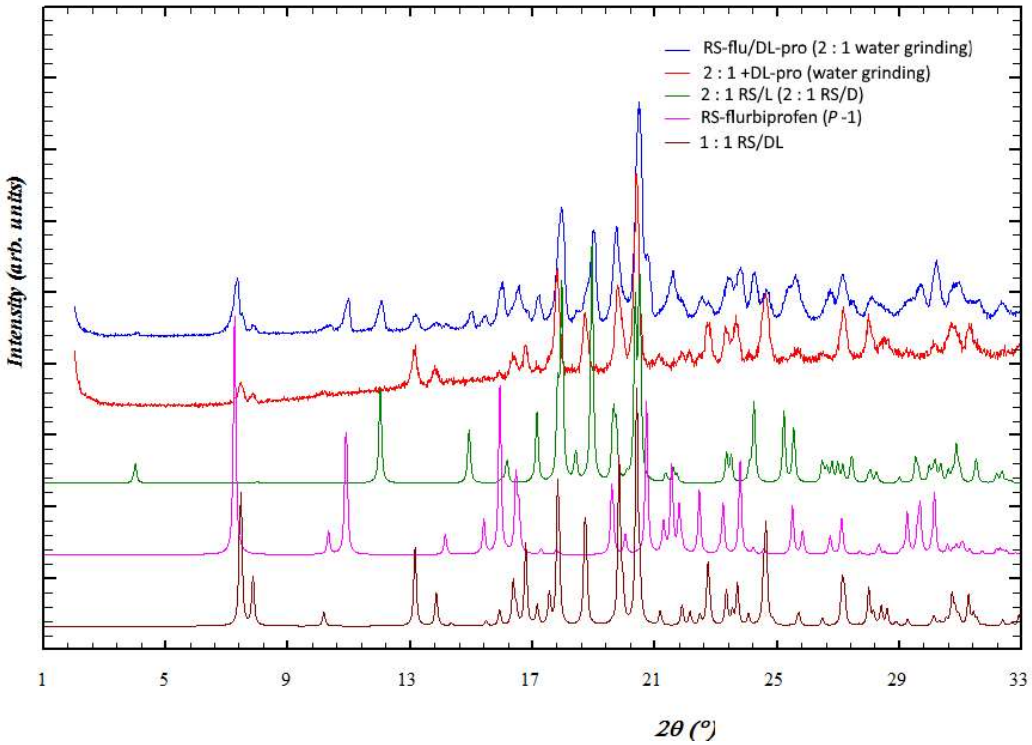


**Figure S50.** Diffraction patterns for the RS-flurbiprofen/DL-proline samples prepared by water-assisted grinding

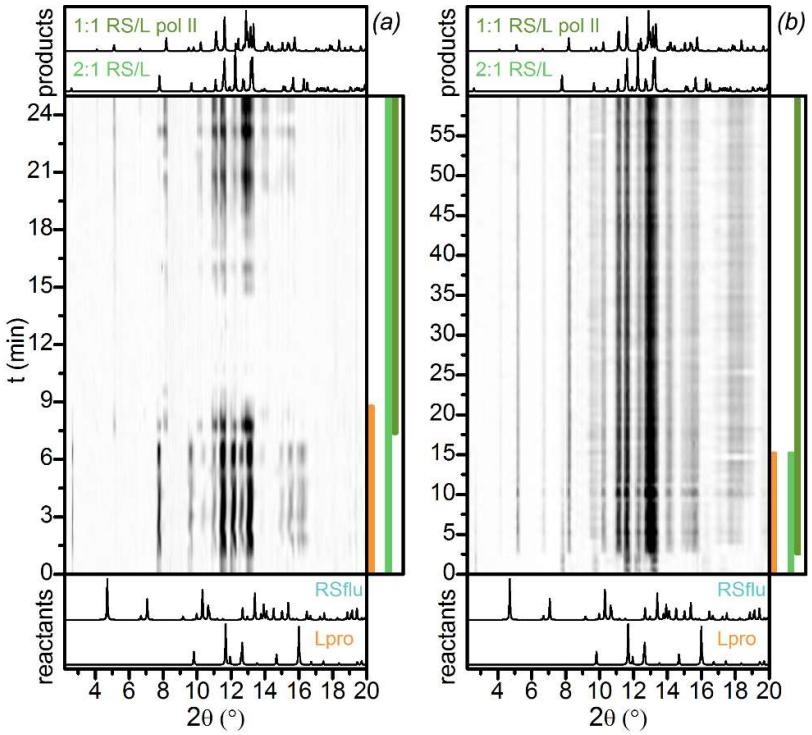


**Figure S51.** *In-situ* ball-milling X-ray diffraction patterns for the RS/L system, methanol-assisted grinding for (*a*) 25 min and (*b*) 60 min

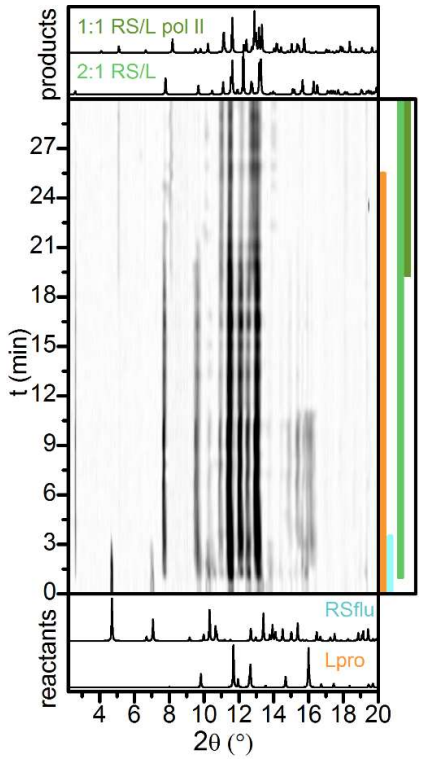


**Figure S52.** *In-situ* ball-milling X-ray diffraction patterns for the RS/L system, acetonitrile-assisted grinding for 30 min

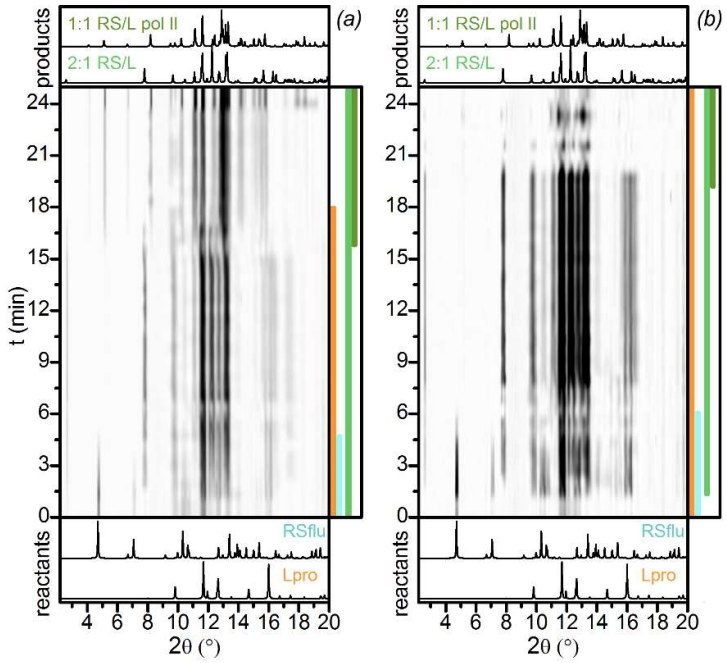


**Figure S53.** *In-situ* ball-milling X-ray diffraction patterns for the RS/L system, isopropanol-assisted grinding for 25 min: (*a*) sample was in contact with solution for 2 h; (*b*) solvent was added right before grinding

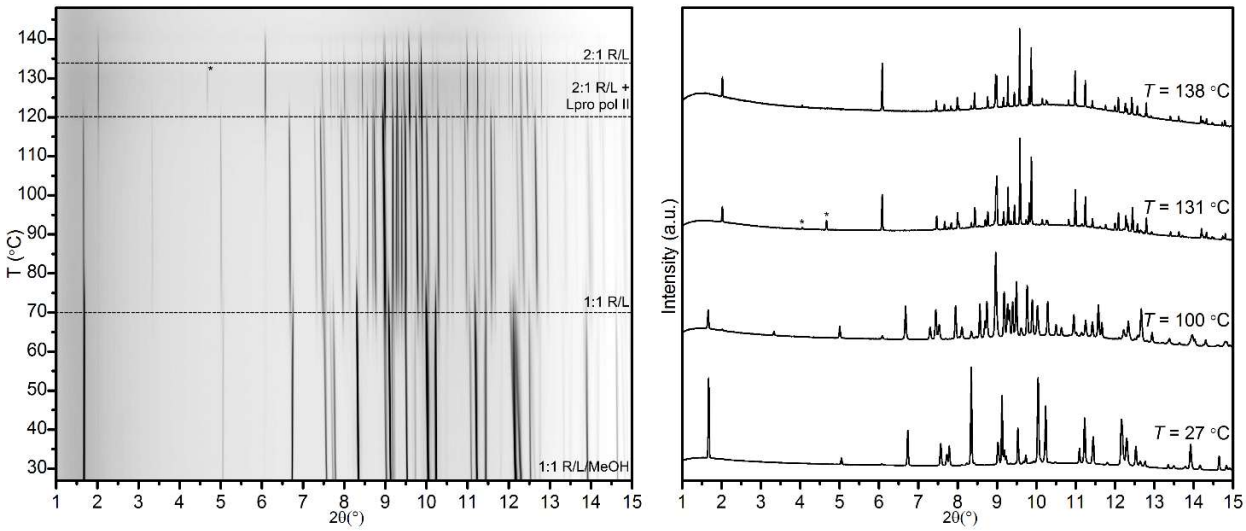


**Figure S54.** Powder X-ray diffraction patterns (λ = 0.77663 Å) measured *in-situ* upon heating from 27 to 148 °C for the R-flurbiprofen/L-proline sample prepared by methanol-assisted grinding in 1 : 1 ratio (sample *2* in Table S3): (left) film representation; (right) diffraction patterns at selected temperatures. *T* = 27 °C – 1 : 1 R/L/MeOH; *T* = 100 °C – 1 : 1 R/L pol I; *T* = 131 °C – a mixture of 2 : 1 R/L and L-proline pol II (marked as '*'); and *T* = 138 °C – 2 : 1 R/L.

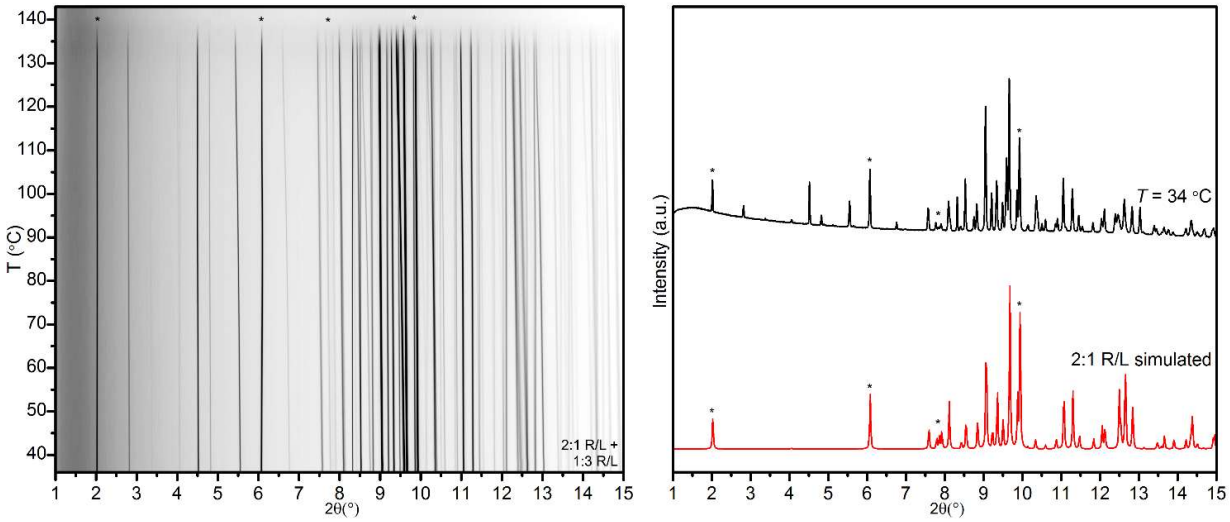


**Figure S55.** Powder X-ray diffraction patterns (λ = 0.77663 Å) measured *in-situ* upon heating from 34°C to 143°C for the R-flurbiprofen/L-proline sample prepared by ethanol-assisted grinding in 1 : 1 ratio, not dried, but measured very shortly after being prepared (sample *6* in Table S3): (left) film representation; (right) the diffraction pattern at 34 °C temperatures and the simulated one for 2 : 1 R/L (major peaks are marked as '*'). *T* = 34 °C – a mixture of 1 : 3 R/L and 2 : 1 R/L.

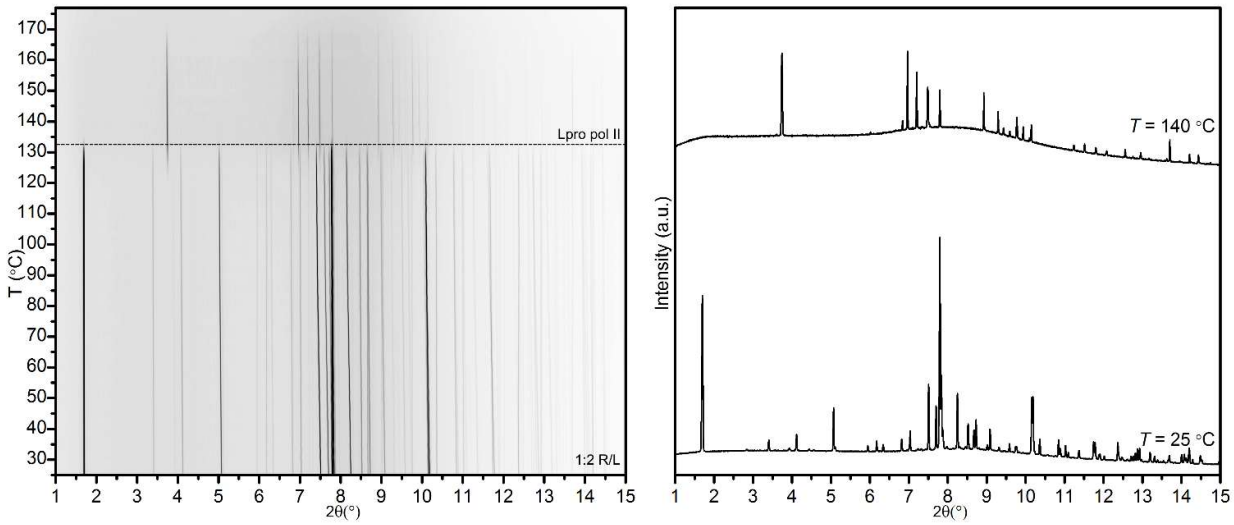


**Figure S56.** Powder X-ray diffraction patterns (λ = 0.62127 Å) measured *in-situ* upon heating from 25°C to 177°C for the R-flurbiprofen/L-proline sample prepared by ethanol-assisted grinding in 1 : 2 ratio, not dried (sample *9* in Table S3): (left) film representation; (right) diffraction patterns at selected temperatures. *T* = 25 °C – 1 : 2 R/L; *T* = 140 °C – L-proline pol II.

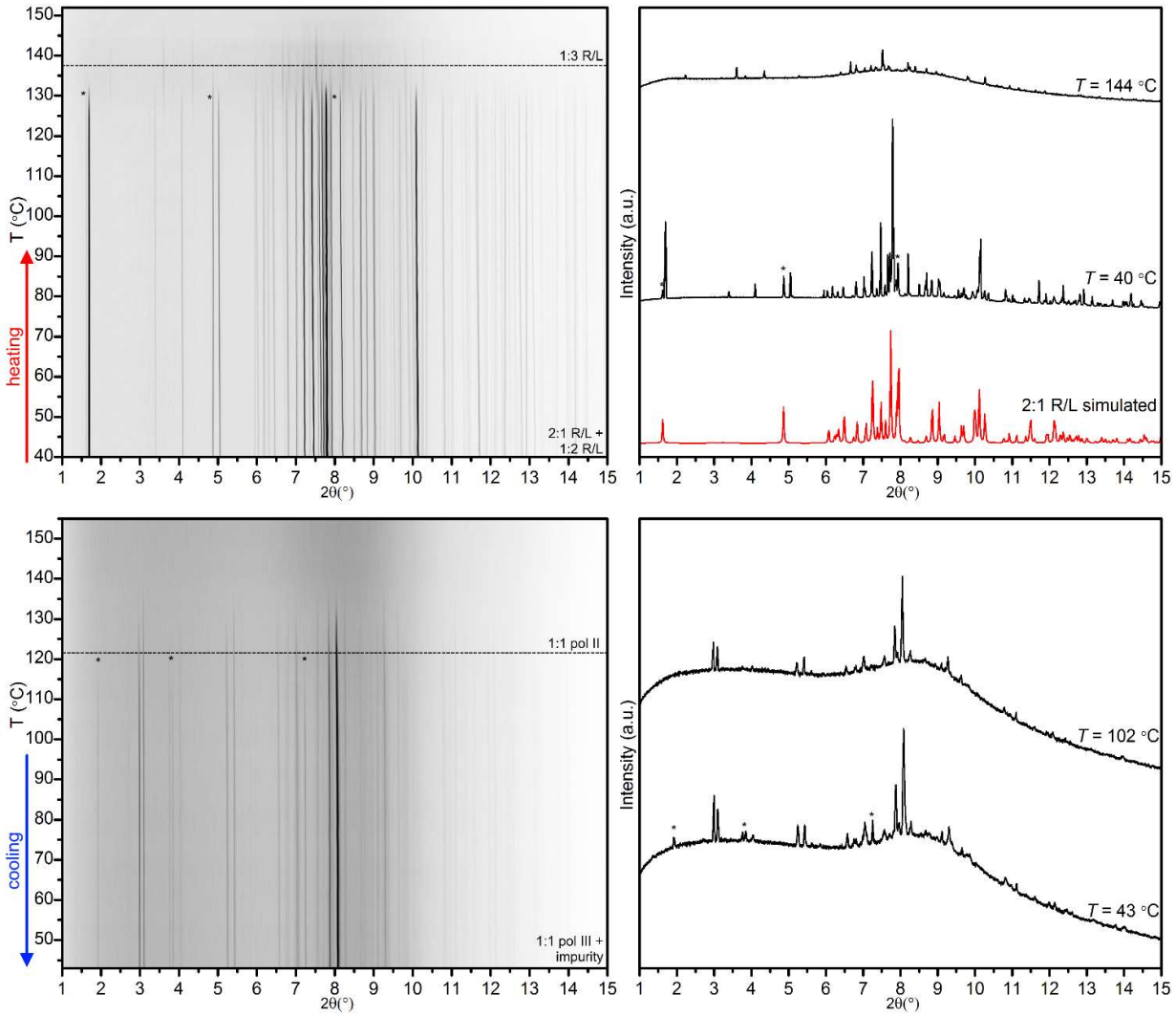


**Figure S57.** Powder X-ray diffraction patterns (λ = 0.62173 Å) measured *in-situ* upon (a) heating from 40°C to 152°C and (b) cooling from 152°C to 43°C for the R-flurbiprofen/L-proline sample prepared by isopropanol-assisted grinding in 1 : 1 ratio (sample *19* in Table S3): (left) film representation; (right) diffraction patterns at selected temperatures and the simulated one for 2 : 1 R/L. (a) $T$ = 40 °C – a mixture of 1 : 2 R/L and 2 : 1 R/L (major peaks are marked as '*'); $T$ = 144 °C – 1 : 3 R/L. (b) $T$ = 43 °C – a mixture of 1 : 1 R/L pol II and a small amount of an impurity (which we were not able to identify due to poor data and only few distinct peaks, marked as '*').

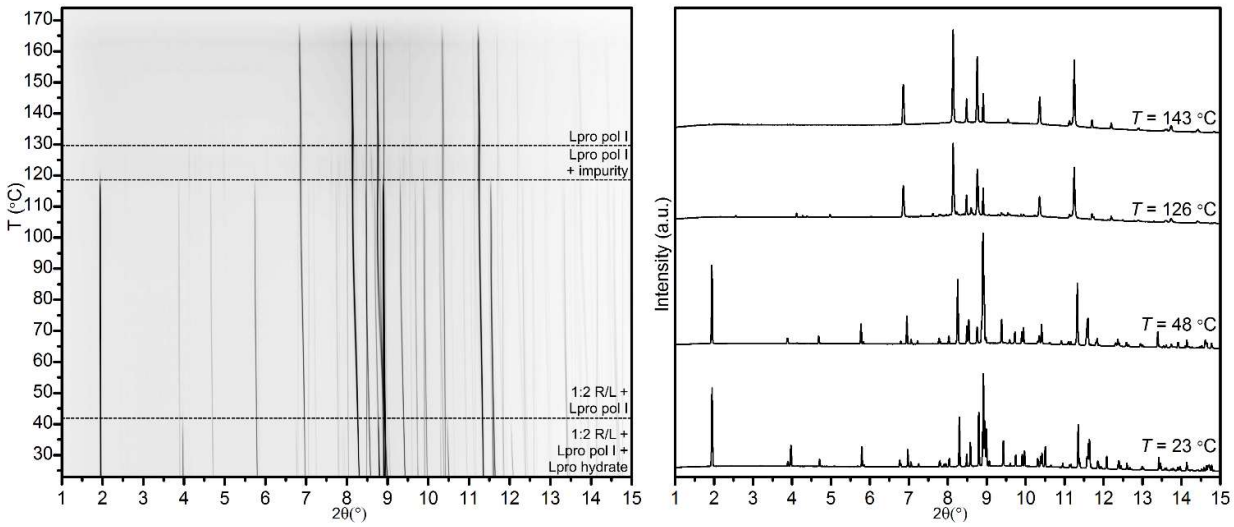


**Figure S58.** Powder X-ray diffraction patterns (λ = 0.708 Å) measured *in-situ* upon heating from 23°C to 174°C for the R-flurbiprofen/L-proline sample prepared by isopropanol-assisted grinding in 1 : 3 ratio, not dried (sample *18* in Table S3): (left) film representation; (right) diffraction patterns at selected temperatures. *T* = 23 °C – a mixture of 1 : 2 R/L, L-proline pol I, and L-proline hydrate; *T* = 48 °C – a mixture of 1 : 2 R/L and L-proline pol I; *T* = 126 °C - a mixture of L-proline pol I and some minor impurity impossible to be identified due to its small amount; *T* = 143 °C – L-proline pol I.

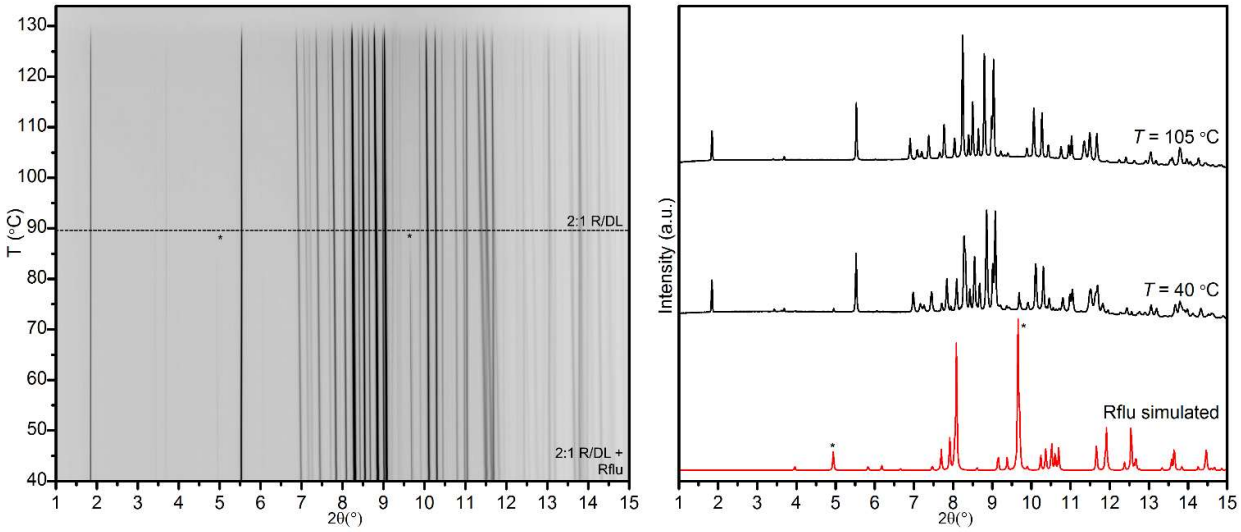


**Figure S59.** Powder X-ray diffraction patterns (λ = 0.708 Å) measured *in-situ* upon heating from 40°C to 134°C for the R-flurbiprofen/DL-proline sample prepared by ethanol-assisted grinding in 2 : 1 ratio (sample *8* in Table S5): (left) film representation; (right) diffraction patterns at selected temperatures and the simulated one for R-flurbiprofen (major peaks are marked as '*'). *T* = 40 °C – a mixture of 2 : 1 R/DL and nonreacted R-flurbiprofen; *T* = 105 °C – 2 : 1 R/DL.

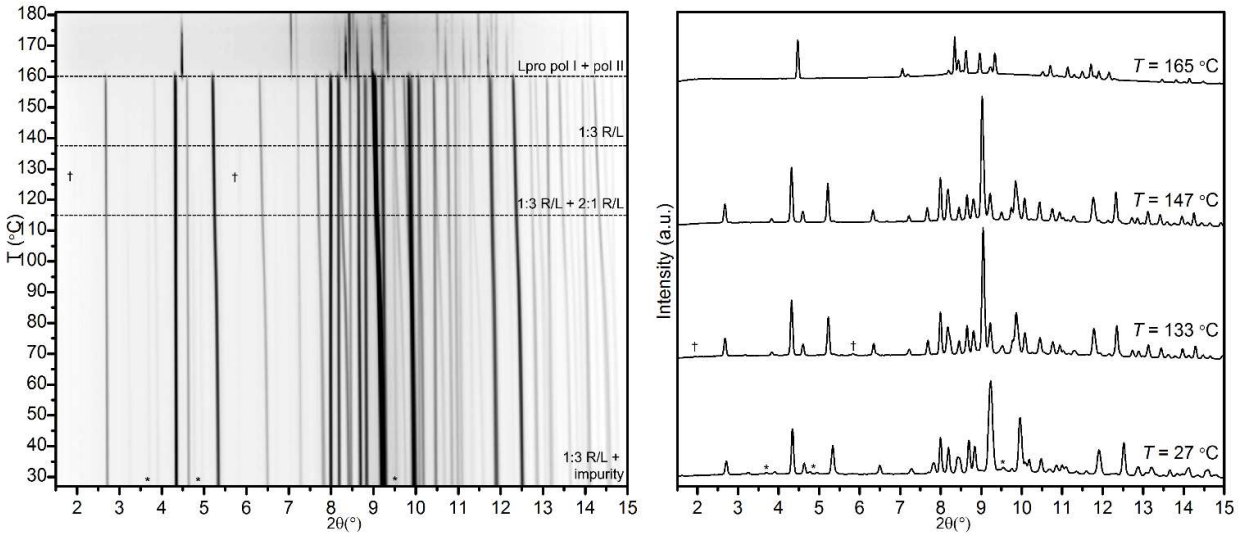


**Figure S60.** Powder X-ray diffraction patterns (λ = 0.7458 Å) measured *in-situ* upon heating from 27°C to 181°C for the R-flurbiprofen/L-proline sample prepared by ethanol-assisted grinding in 1 : 3 ratio (sample *10* in Table S3): (left) film representation; (right) diffraction patterns at selected temperatures: *T* = 27 °C – mainly 1 : 3 R/L and a small amount of impurities (marked as '*'); *T* = 141 °C – a mixture of 1 : 3 R/L and a small amount of 2 : 1 R/L (marked as '†'); *T* = 159 °C – pure 1 : 3 R/L; *T* = 182 °C – a mixture of L-proline polymorph I and L-proline polymorph II.

**COMPARISON OF THE SAME STRUCTURES FOUND FROM POWDER AND SINGLE-CRYSTAL X-RAY DIFFRACTION DATA**

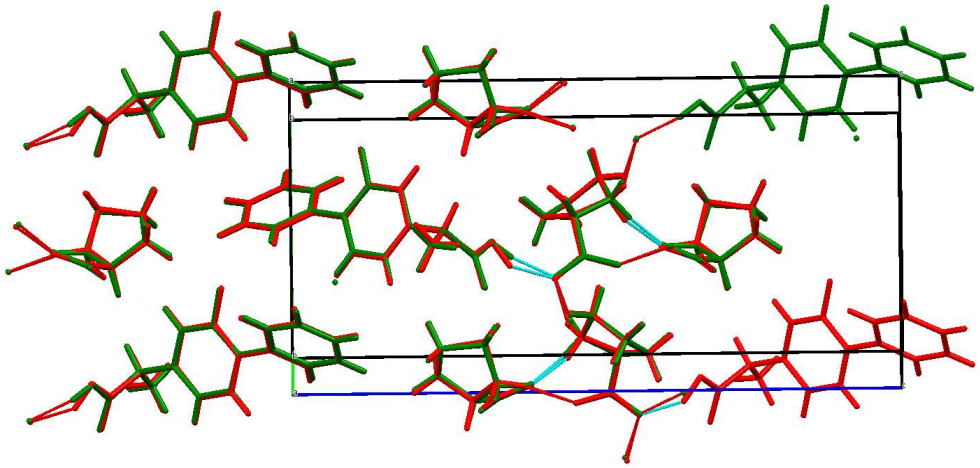

**Figure S61.** Comparison of the structures of 1 : 2 R/L cocrystal found from powder (red, $R_{bragg}$ = 1.5853) and single-crystal (green) X-ray diffraction data. RMSD (root-mean-square distance) calculated using the Mercury software for the packing similarity over 15 molecules is 0.084 Å. Rietveld refinement was done using the TOPAS V5 program (both torsion angles and molecular coordinates were refined)

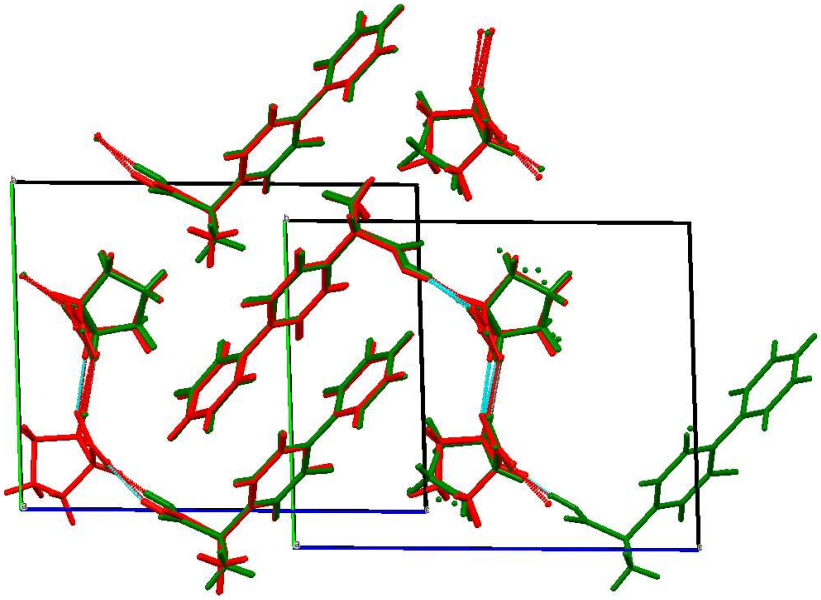

**Figure S62.** Comparison of the structures of 1 : 1 RS/L pol II cocrystal found from powder (red, $R_{bragg}$ = 0.8469) and single-crystal (green) X-ray diffraction data. RMSD calculated using the Mercury software for the packing similarity over 15 molecules is 0.171 Å. The differences are mainly in the orientation of the methyl group of flurbiprofen and the conformation of the proline ring. Rietveld refinement was done using the Topas V5 program (both torsion angles and molecular coordinates were refined)

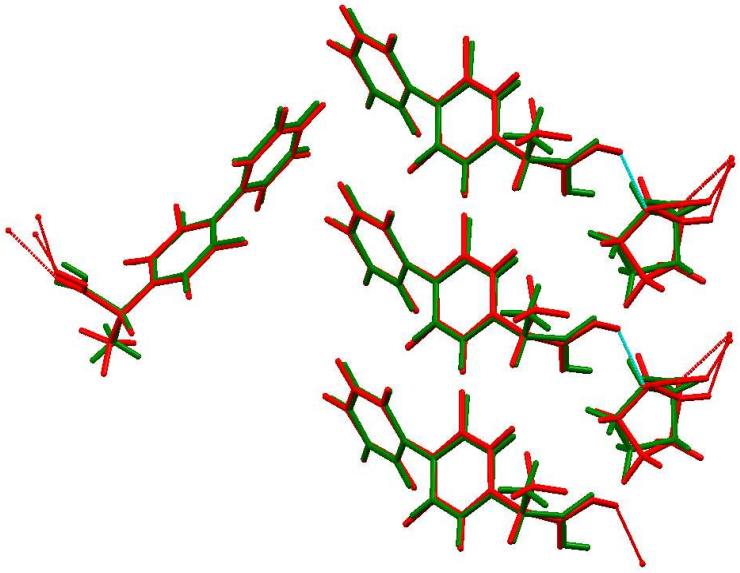

**Figure S63.** Comparison of the structures of 2 : 1 R/D cocrystal found from powder (red, $R_{bragg}$ = 8.6891) and single-crystal (green) X-ray diffraction data. RMS calculated using the Mercury software for the packing similarity over 15 molecules is 0.203 Å. The differences are mainly in the orientation of the methyl group of flurbiprofen and the conformation of the proline ring (Rietveld refinement was done using the Fullprof suite; only molecular coordinates were refined, torsion angles were not refined).

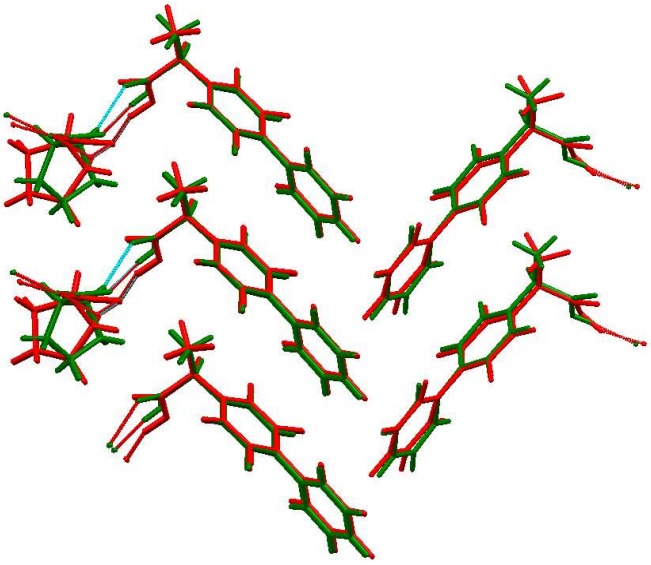

**Figure S64.** Comparison of the structures of 2 : 1 RS/L cocrystal found from powder (red, $R_{bragg}$ = 12.0930) and single-crystal (green) X-ray diffraction data. RMS calculated using the Mercury software for the packing similarity over 15 molecules is 0.438 Å. The differences are mainly in the orientation of the methyl group of flurbiprofen and the conformation of the proline ring (Rietveld refinement was done using the Fullprof suite; only molecular coordinates were refined, torsion angles were not refined).

**ILLUSTRATION OF DISORDER IN PROLINE MOLECULES**

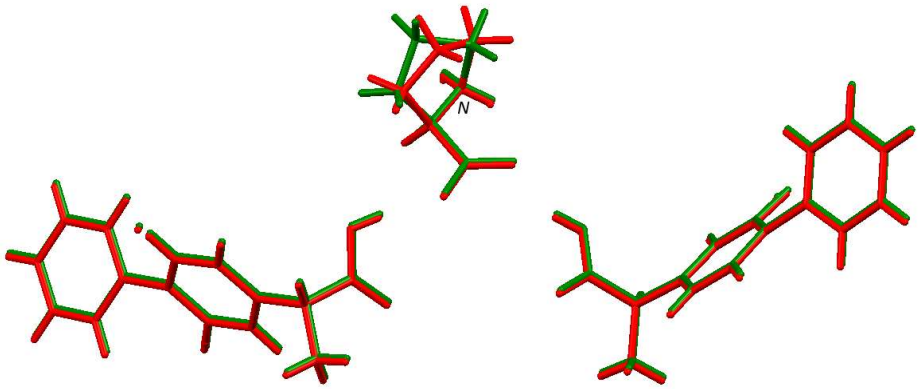


**Figure S65.** Disorder of proline in 2 : 1 R/D cocrystal

**Figure S66.** Disorder of proline in 2 : 1 RS/L cocrystal

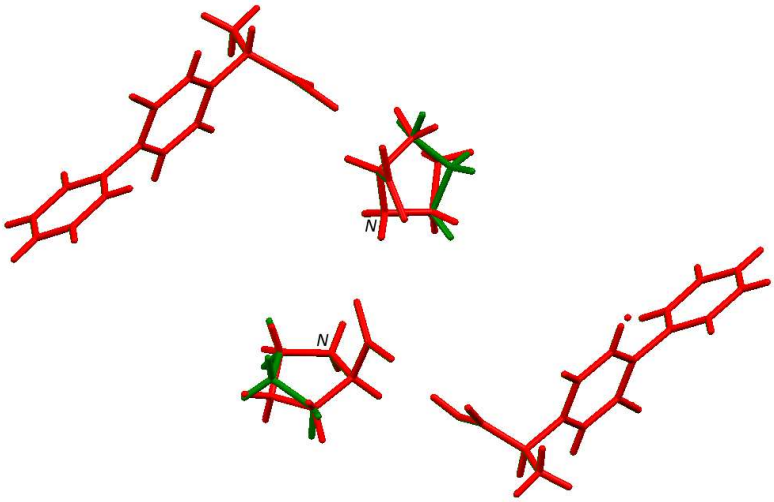


**Figure S67.** Disorder of proline in 1 : 1 RS/L pol II cocrystal

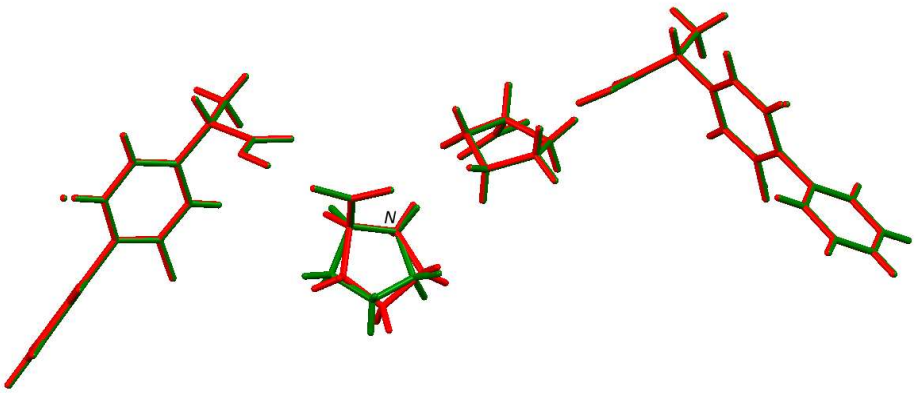


**Figure S68.** Disorder of proline in 1 : 1 RS/L pol IV cocrystal

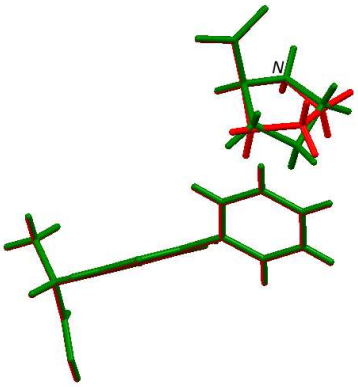


**Figure S69.** Disorder of proline in 1 : 1 RS/DL cocrystal

**STRUCTURAL PECULIARITIES IN 2 : 1 R/DL COCRYSTAL**

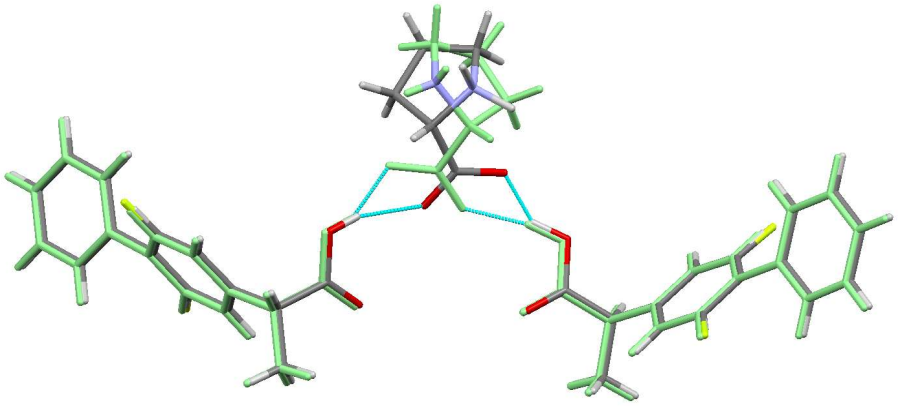

**Figure S70.** Disorder of proline in 2 : 1 R/DL cocrystal

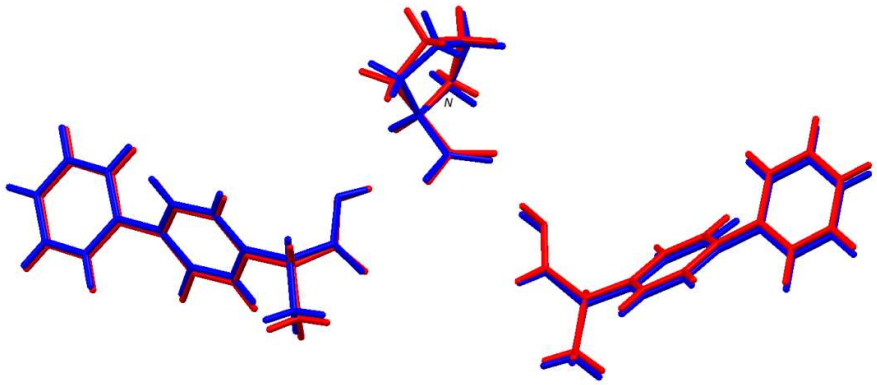

**Figure S71.** Comparison of the R/D fragment of the 2 : 1 R/DL cocrystal with the 2 : 1 R/D cocrystal; red – 2 : 1 R/DL, blue – 2: 1 R/D

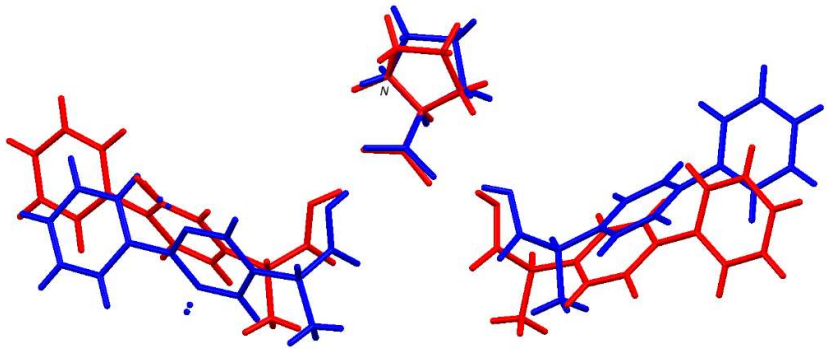

**Figure S72.** Comparison of the R/L fragment of the 2 : 1 R/DL cocrystal with the 2 : 1 R/D cocrystal; red – 2 : 1 R/DL, blue – 2: 1 R/L

**COMPARISON OF DIFFRACTION PATTERNS FOR 2 : 1 COCRYSTALS**

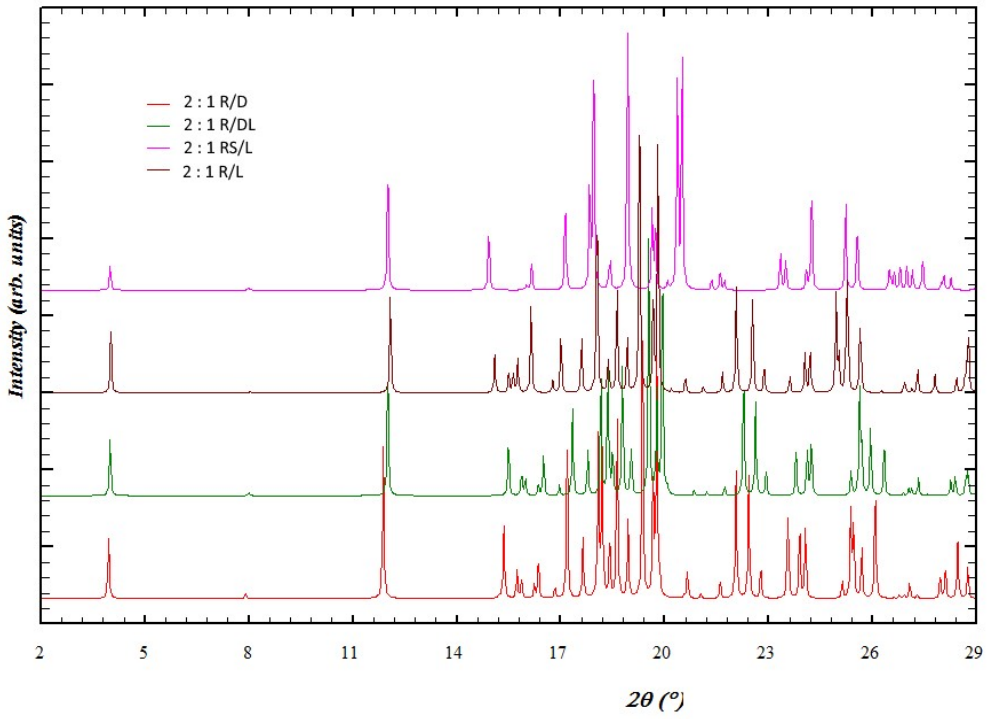


**Figure S73.** Comparison of diffraction patterns for 2 : 1 cocrystals (all cocrystals are at room temperature)

**PACKING IN L-PROLINE POL I AND L-PROLINE POL II**

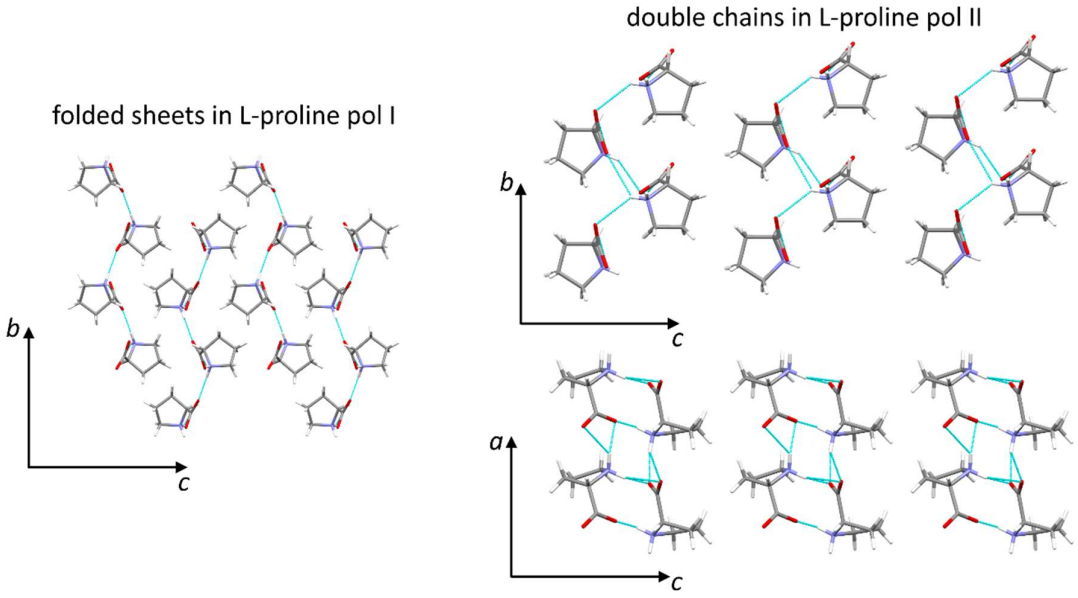


**Figure S74.** Head-to-tail chains in L-proline pol I (right) and L-proline pol II (left). In L-proline pol, head-to-tail chains form folded sheets; in L-proline pol II, double head-to-tail chains form separate layers.

**INCAR file (VASP)**

ALGO = Fast

EDIFF = 0.0001

ENCUT = 520

IBRION = 2

ICHARG = 1

ISIF = 3

ISMEAR = -5

ISPIN = 1

LORBIT = 11

LREAL = Auto

LWAVE = False

NELM = 100

NSW = 500

PREC = Accurate

NPAR = 4

LVDW = TRUE

IVDW = 12

**Table S9.** Crystal lattice parameters converted into *P*1 space group (VASP analyses symmetry itself during minimization procedure) and *k*-point grids used

| Structure | | *a* | *b* | *c* | α | β | γ | Volume | *K*-point grid |
|---|---|---|---|---|---|---|---|---|---|
| 2 : 1 R/L | P1 | 5.785 | 6.19 | 44.639 | 90 | 90 | 110.815 | 1494.206 | 4 4 2 |
| 2 : 1 R/D | P1 | 5.955 | 6.155 | 44.661 | 90 | 90 | 109.156 | 1546.499 | 4 4 2 |
| 2 : 1 RS/L | P1 | 5.8399 | 6.3302 | 22.36 | 95.277 | 95.033 | 108.947 | 772.407 | 4 4 4 |
| 1 : 2 R/L | P1 | 5.99344 | 9.49502 | 20.9123 | 90 | 90.4325 | 90 | 1190.04 | 4 4 2 |
| 1 : 3 R/L | P1 | 5.6866 | 19.677 | 26.317 | 90 | 90 | 90 | 2944.75 | 4 4 2 |
| 1 : 1 R/L pol I | P1 | 5.81938 | 6.3341 | 26.6334 | 88.0448 | 88.312 | 73.664 | 941.338 | 4 4 4 |
| 1 : 1 R/L pol II | P1 | 5.87 | 13.253 | 23.954 | 90 | 90 | 96.287 | 1852.36 | 4 2 2 |
| 1 : 1 R/D | P1 | 5.79 | 14.168 | 22.788 | 85.968 | 82.701 | 78.209 | 1813.298 | 4 4 2 |
| 1 : 1 R/DL | P1 | 5.844 | 13.559 | 21.152 | 90 | 90 | 97.487 | 1819.019 | 4 2 2 |
| 1 : 1 RS/L pol I | P1 | 5.7912 | 17.332 | 18.2738 | 90 | 96.658 | 90 | 1821.83 | 4 2 2 |
| 1 : 1 RS/L pol II | P1 | 5.76337 | 11.2468 | 14.2595 | 91.372 | 100.713 | 92.925 | 906.474 | 4 4 2 |
| 1 : 1 RS/L pol III | P1 | 5.911 | 13.095 | 24.162 | 90 | 90 | 95.667 | 1861.275 | 4 2 2 |
| 1 : 1 RS/L pol IV | P1 | 5.6856 | 6.4145 | 26.4325 | 87.568 | 89.083 | 70.624 | 908.58 | 4 4 2 |
| 1 : 1 RS/DL | P1 | 5.931 | 12.861 | 23.736 | 90 | 90 | 95.425 | 1802.608 | 4 2 2 |
| L-proline pol I | P1 | 5.28018 | 8.8794 | 11.5307 | 90 | 90 | 90 | 540.615 | 8 4 4 |
| L-proline pol II | P1 | 5.21242 | 5.92921 | 9.52184 | 87.8578 | 89.9133 | 87.6845 | 293.832 | 8 8 4 |
| RS-flurbiprofen *P*-1 | P1 | 5.823 | 9.315 | 12.738 | 73 | 83 | 72.8 | 630.711 | 8 8 4 |
| R-flurbiprofen | P1 | 5.6535 | 13.2097 | 16.0709 | 90 | 90 | 90 | 1200.19 | 8 4 4 |
| RS-flurbiprofen $P2_1/n$ | P1 | 5.721 | 5.981 | 38.715 | 90 | 90 | 111.655 | 1231.272 | 4 4 2 |
| DL-proline | P1 | 5.299 | 8.991 | 11.479 | 97.041 | 90 | 90 | 542.699 | 8 4 4 |

**Table S10.** Initial and DFT optimized unit cell parameters

| Structure | | Initial unit cell parameters | | | | | | | DFT optimized unit cell parameters | | | | | | | Volume change, % |
|---|---|---|---|---|---|---|---|---|---|---|---|---|---|---|---|---|
| | Space group | *a* | *b* | *c* | α | β | γ | Volume, Å$^3$ | *a* | *b* | *c* | α | β | γ | Volume, Å$^3$ | |
| 2 : 1 R/L | $P2_1$ | 5.7851 | 44.639 | 6.1901 | 90 | 110.815 | 90 | 1494.21 | 6.2559 | 35.2569 | 6.7896 | 90 | 101.599 | 90 | 1466.96 | -1.86 |
| 2 : 1 R/D | $P2_1$ | 5.9554 | 44.661 | 6.1553 | 90 | 109.156 | 90 | 1546.5 | 6.3773 | 36.0483 | 6.5849 | 90 | 103.4287 | 90 | 1472.42 | -5.03 |
| 2 : 1 RS/L | *P*1 | 5.8399 | 6.3302 | 22.36 | 95.277 | 95.033 | 108.947 | 772.407 | 6.1413 | 6.6602 | 19.1934 | 95.6229 | 93.7037 | 105.728 | 748.612 | -3.18 |
| 1 : 2 R/L | $P2_1$ | 5.99344 | 9.49502 | 20.9123 | 90 | 90.4325 | 90 | 1190.04 | 6.073 | 9.1026 | 20.1602 | 90 | 90.4594 | 90 | 1114.42 | -6.79 |
| 1 : 3 R/L | $P2_12_12_1$ | 5.6866 | 19.677 | 26.317 | 90 | 90 | 90 | 2944.75 | 5.9529 | 21.4486 | 23.6098 | 90 | 90 | 90 | 3014.53 | 2.31 |
| 1 : 1 R/L pol I | *P*1 | 5.81938 | 6.3341 | 26.6334 | 88.0448 | 88.312 | 73.664 | 941.338 | 5.9737 | 7.0699 | 22.0666 | 88.1648 | 84.4567 | 82.9703 | 920.425 | -2.27 |
| 1 : 1 R/L pol II | $P2_1$ | 5.8702 | 23.954 | 13.253 | 90 | 96.287 | 90 | 1852.36 | 6.1448 | 18.7062 | 15.5885 | 90 | 91.8721 | 90 | 1790.88 | -3.43 |
| 1 : 1 R/D | *P*1 | 5.79 | 14.168 | 22.788 | 85.968 | 82.701 | 78.209 | 1813.298 | 5.9917 | 13.3648 | 21.5078 | 88.7733 | 83.5421 | 80.5355 | 1688.07 | -7.42 |
| 1 : 1 R/DL | $P2_1$ | 5.84419 | 23.1523 | 13.5593 | 90 | 97.4871 | 90 | 1819.02 | 6.049 | 20.9212 | 13.5491 | 90 | 98.3155 | 90 | 1696.64 | -7.21 |
| 1 : 1 RS/L pol I | $P2_1$ | 5.7912 | 17.332 | 18.2738 | 90 | 96.658 | 90 | 1821.83 | 6.0011 | 16.8149 | 18.3562 | 90 | 96.9093 | 90 | 1838.83 | 0.92 |
| 1 : 1 RS/L pol II | *P*1 | 5.76337 | 11.2468 | 14.2595 | 91.372 | 100.713 | 92.925 | 906.474 | 6.0051 | 11.193 | 13.0934 | 91.5585 | 98.1387 | 93.4392 | 869.074 | -4.30 |
| 1 : 1 RS/L pol III | $P2_1$ | 5.91137 | 24.1621 | 13.0953 | 90 | 95.667 | 90 | 1861.27 | 6.0832 | 21.4148 | 13.2308 | 90 | 96.9423 | 90 | 1710.95 | -8.79 |
| 1 : 1 RS/L pol IV | *P*1 | 5.6856 | 6.4145 | 26.4325 | 87.568 | 89.083 | 70.624 | 908.58 | 5.9311 | 6.8998 | 22.0613 | 88.8564 | 88.2089 | 74.3758 | 868.976 | -4.56 |
| 1 : 1 RS/DL | $P2_1/n$ | 5.9312 | 23.7365 | 12.8615 | 90 | 95.425 | 90 | 1802.61 | 6.1455 | 21.5023 | 13.4869 | 90 | 112.6843 | 90 | 1644.33 | -9.63 |
| L-proline pol I | $P2_12_12_1$ | 5.28018 | 8.8794 | 11.5307 | 90 | 90 | 90 | 540.615 | 5.3356 | 8.7633 | 11.2835 | 90 | 90 | 90 | 527.588 | -2.47 |
| L-proline pol II | *P*1 | 5.21242 | 5.92921 | 9.52184 | 87.8578 | 89.9133 | 87.6845 | 293.832 | 5.29694 | 5.817558 | 9.502093 | 87.3849 | 91.68731 | 90.1602 | 292.378 | -0.50 |
| RS-flurbiprofen *P*-1 | *P*-1 | 9.315 | 12.738 | 5.823 | 83 | 107.2 | 107 | 630.711 | 6.4006 | 8.7954 | 11.8698 | 77.4954 | 86.0533 | 73.3982 | 625.157 | -0.89 |
| R-flurbiprofen | $P2_12_12_1$ | 5.6535 | 13.2097 | 16.0709 | 90 | 90 | 90 | 1200.19 | 5.8256 | 12.8665 | 15.422 | 90 | 90 | 90 | 1155.96 | -3.83 |
| RS-flurbiprofen $P2_1/n$ | $P2_1/n$ | 5.7214 | 38.715 | 5.9808 | 90 | 111.655 | 90 | 1231.27 | 6.0231 | 30.626 | 7.6874 | 90 | 123.9607 | 90 | 1176.16 | -4.69 |
| DL-proline | $P2_1/c$ | 8.9906 | 5.2987 | 11.4786 | 90 | 97.041 | 90 | 542.699 | 8.8085 | 5.4329 | 11.0468 | 90 | 98.8353 | 90 | 522.379 | -3.89 |

Parameters highlighted by grey color significantly change as compared to the initial values due to a strong thermal effect (see Discussion for further details)

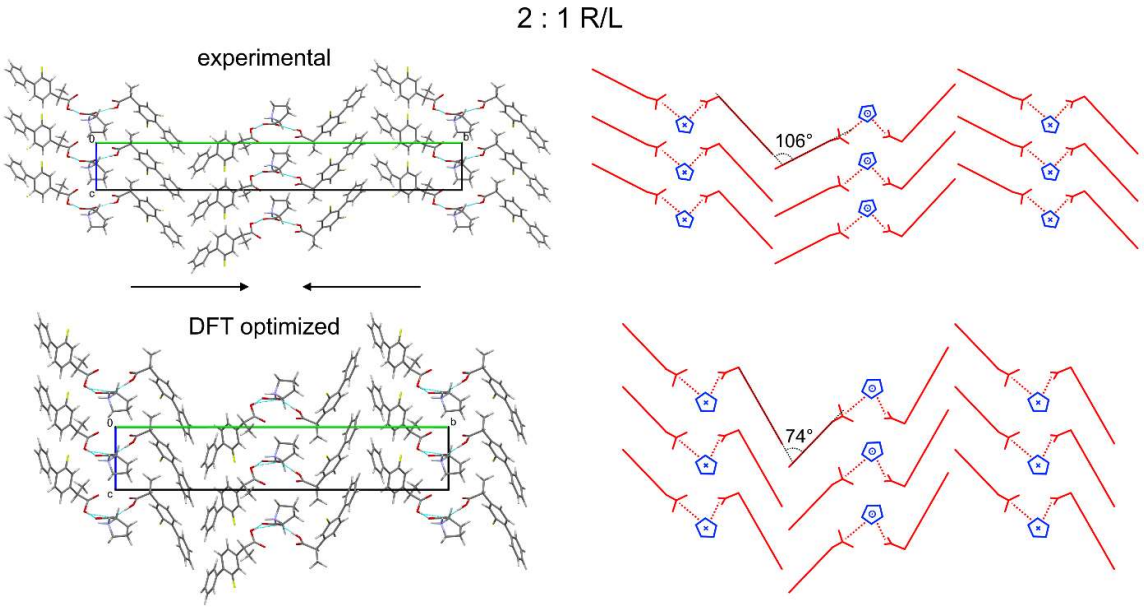


**Figure S75.** Comparison of the initial and DFT optimized structures for the 2 : 1 R/L cocrystal, demonstrating the shrinkage of the structure in a scissor-like manner. All other 2 : 1 structures behave similarly. Arrows in the left part of the figure demonstrate the direction of shrinkage.

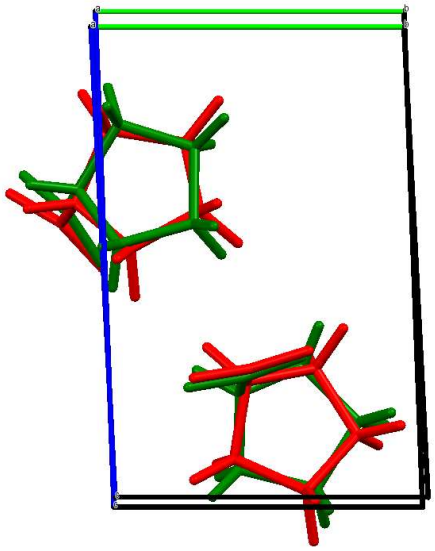

**Figure S76.** Overlap of the initial and DFT optimized structures for L-proline pol II; red corresponds to the DFT optimized and green to the initial structure

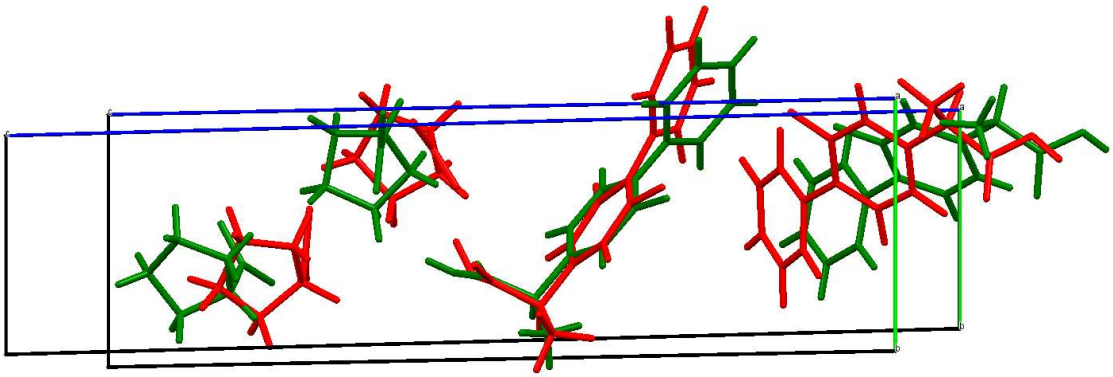

**Figure S77.** Overlap of the initial and DFT optimized structures for 1 : 1 R/L pol I; red corresponds to the DFT optimized and green to the initial structure

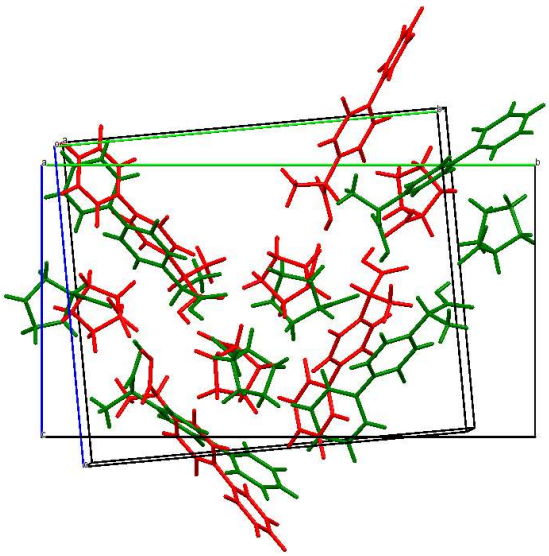

**Figure S78.** Overlap of the initial and DFT optimized structures for 1 : 1 R/L pol II; red corresponds to the DFT optimized and green to the initial structure

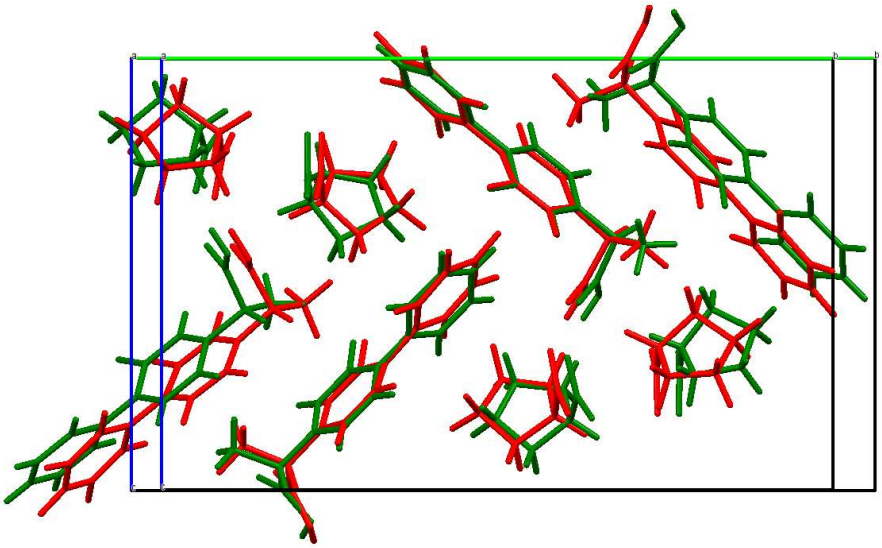

**Figure S79.** Overlap of the initial and DFT optimized structures for 1 : 1 R/DL; red corresponds to the DFT optimized and green to the initial structure

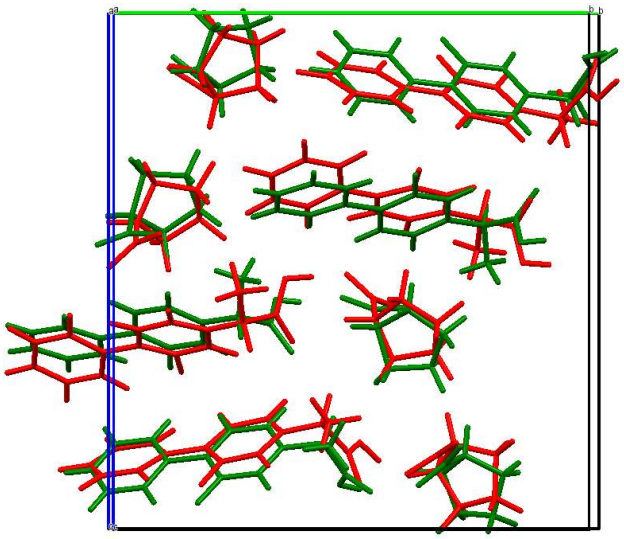

**Figure S80.** Overlap of the initial and DFT optimized structures for 1 : 1 RS/D pol I; red corresponds to the DFT optimized and green to the initial structure

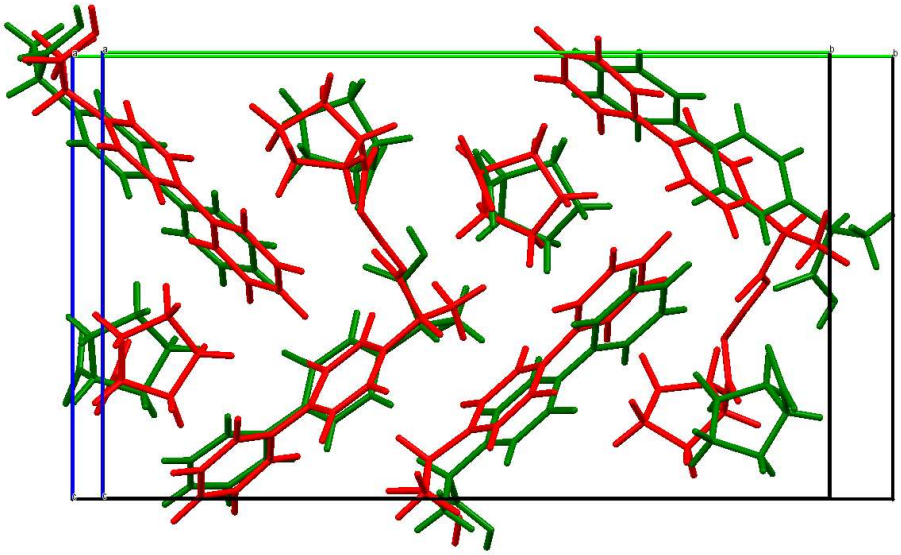

**Figure S81.** Overlap of the initial and DFT optimized structures for 1 : 1 RS/D pol III; red corresponds to the DFT optimized and green to the initial structure

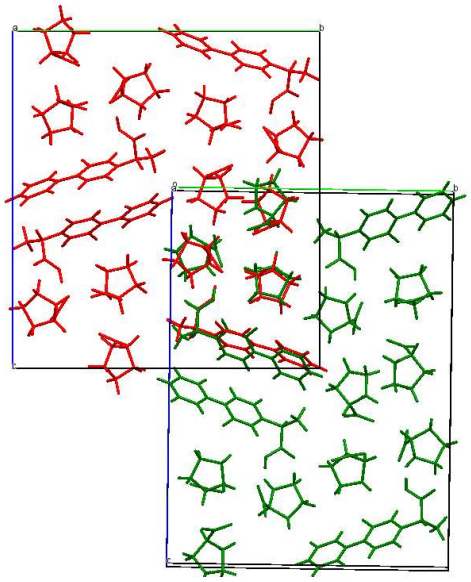

**Figure S82.** Overlap of the initial and DFT optimized structures for 1 : 3 R/L; red corresponds to the DFT optimized and green to the initial structure

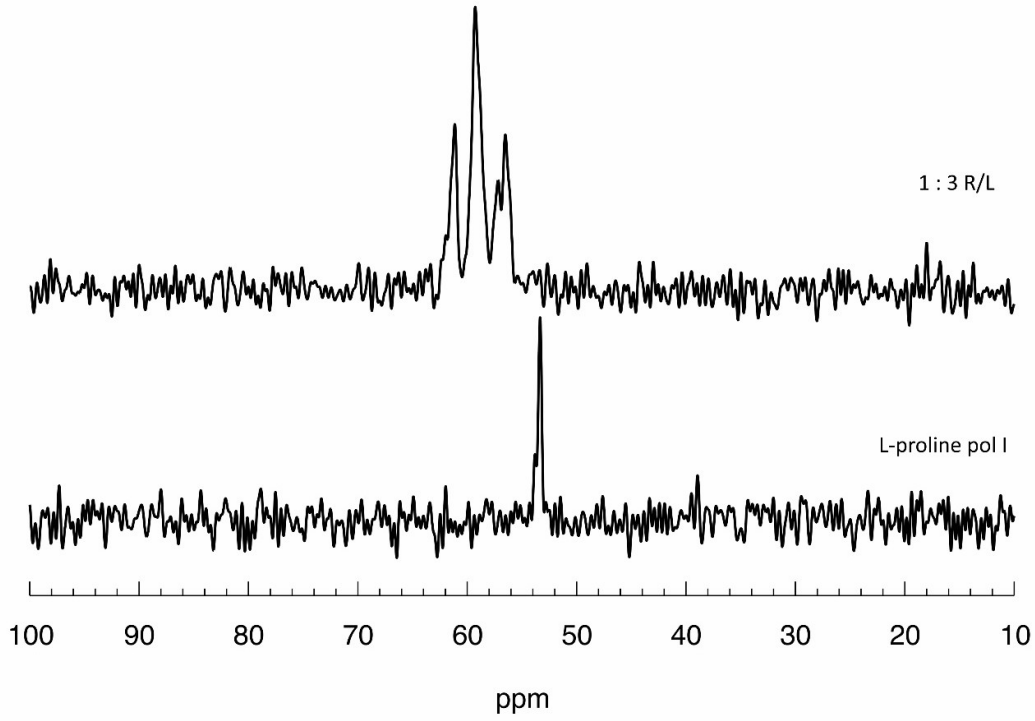


**Figure S83.** 15N NMR spectra for 1 : 3 R/L cocrystal and pure L-proline pol I

**Table S11.** Eigenvalues for the tensor of thermal expansion

| EV1 (*c* axis) | EV2 (*b* axis) | EV3 (*a* axis) | Temperature |
|---|---|---|---|
| $-9.5896 \cdot 10^{-5}$ | $21.438 \cdot 10^{-5}$ | $8.3327 \cdot 10^{-5}$ | 60 °C |
| $-160.81 \cdot 10^{-5}$ | $57.927 \cdot 10^{-5}$ | $58.631 \cdot 10^{-5}$ | 140 °C |
| $-5.5367 \cdot 10^{-5}$ | $11.71 \cdot 10^{-5}$ | $11.204 \cdot 10^{-5}$ | 168 °C |